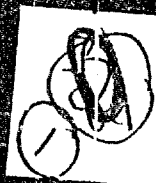


AD-A221 164



UNITED STATES AIR FORCE

AD-A221 164

GRADUATE STUDENT RESEARCH PROGRAM

1989

PROGRAM TECHNICAL REPORT

UNIVERSAL ENERGY SYSTEMS, INC.

VOLUME 2 OF 3

DTIC
S ELECTE
MAY 03 1990
D

PROGRAM DIRECTOR, U. S. A.

RODNEY C. DARRAH

PROGRAM ADMINISTRATOR, U. S. A.

SUSAN K. ESPY

PROGRAM MANAGER, A. F. O. S. R.

LT. COL. CLAUDE CAWENDER

DISTRIBUTION STATEMENT A

Approved for public release
Distribution Unlimited

SUBMITTED TO

AIR FORCE OFFICE OF SCIENTIFIC RESEARCH

ROBBER AIR FORCE BASE

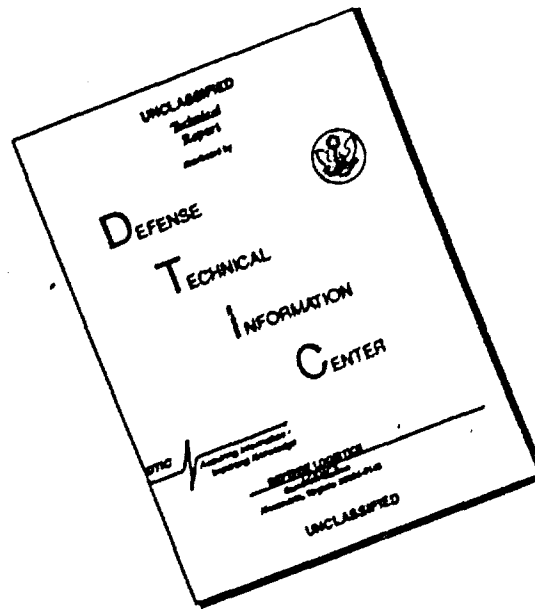
WASHINGTON, DC

DECEMBER 1989

BEST
AVAILABLE COPY

90 05 03 200

DISCLAIMER NOTICE



THIS DOCUMENT IS BEST QUALITY AVAILABLE. THE COPY FURNISHED TO DTIC CONTAINED A SIGNIFICANT NUMBER OF PAGES WHICH DO NOT REPRODUCE LEGIBLY.

PREFACE

The United States Air Force Graduate Student Research Program (USAF-GSRP) is conducted under the United Air Force Summer Faculty Research Program. The program provides funds for selected graduate students to work at an appropriate Air Force facility with a supervising professor who holds a concurrent Summer Faculty Research Program appointment or with a supervising Air Force Engineer/Scientist. This is accomplished by the students being selected on a nationally advertised competitive basis for a ten-week assignment during the summer intersession period to perform research at Air Force laboratories/centers. Each assignment is in a subject area and at an Air Force facility mutually agreed upon by the students and the Air Force. In addition to compensation, travel and cost of living allowances are also paid. The USAF-GSRP is sponsored by the Air Force Office of Scientific Research, Air Force Systems Command, United States Air Force, and is conducted by Universal Energy Systems, Inc.

The specific objectives of the 1989 USAF-GSRP are:

- (1) To provide a productive means for the graduate students to participate in research at Air Force Laboratories/Centers;
- (2) To stimulate continuing professional association among the graduate students and their professional peers in the Air Force;
- (3) To further the research objectives of the United States Air Force;
- (4) To enhance the research productivity and capabilities of the graduate students especially as these relate to Air Force technical interests.

During the summer of 1989, 102-graduate students participated. These researchers were assigned to 23 USAF laboratories/centers across the country. This three volume document is a compilation of the final reports written by the assigned students members about their summer research efforts.

AFCSSR T2 90-0371

AIR FORCE DIVISION OF SCIENTIFIC RESEARCH (AFSC)
RESEARCH REPORT NO. 10-11 TO TRIC
THE REPORT HAS BEEN REVIEWED AND IS
BEING RELEASED TO THE PUBLIC IN ACCORDANCE WITH AFR 190-12.
BY: J. K. KREMER
TECHNICAL INFORMATION DIVISION
Ordn, Technical Information Division

Approved for release
Distribution limited

UNITED STATES AIR FORCE
GRADUATE STUDENT RESEARCH PROGRAM
1989
PROGRAM TECHNICAL REPORT
UNIVERSAL ENERGY SYSTEMS, INC.
VOLUME II of III

Program Director, UES
Rodney C. Darrah

Program Manager, AFOSR
Lt. Col. Claude Cavender

Program Administrator, UES
Susan K. Espy

Submitted to
Air Force Office of Scientific Research
Bolling Air Force Base
Washington, DC

December 1989

Accession	
NTIS	CR 89-1
DTIC	154
Unannounced	
Justification	
By	
Distribution	
Dist	
A-1	

TABLE OF CONTENTS

<u>Section</u>	<u>Page</u>
Preface	i
List of Participants	ii
Participant Laboratory Assignment	xv
Research Reports	xix

PREFACE

The United States Air Force Graduate Student Research Program (USAF-GSRP) is conducted under the United Air Force Summer Faculty Research Program. The program provides funds for selected graduate students to work at an appropriate Air Force facility with a supervising professor who holds a concurrent Summer Faculty Research Program appointment or with a supervising Air Force Engineer/Scientist. This is accomplished by the students being selected on a nationally advertised competitive basis for a ten-week assignment during the summer intersession period to perform research at Air Force laboratories/centers. Each assignment is in a subject area and at an Air Force facility mutually agreed upon by the students and the Air Force. In addition to compensation, travel and cost of living allowances are also paid. The USAF-GSRP is sponsored by the Air Force Office of Scientific Research, Air Force Systems Command, United States Air Force, and is conducted by Universal Energy Systems, Inc.

The specific objectives of the 1989 USAF-GSRP are:

- (1) To provide a productive means for the graduate students to participate in research at Air Force Laboratories/Centers;
- (2) To stimulate continuing professional association among the graduate students and their professional peers in the Air Force;
- (3) To further the research objectives of the United States Air Force;
- (4) To enhance the research productivity and capabilities of the graduate students especially as these relate to Air Force technical interests.

During the summer of 1989, 102-graduate students participated. These researchers were assigned to 23 USAF laboratories/centers across the country. This three volume document is a compilation of the final reports written by the assigned students members about their summer research efforts.

LIST OF 1989 PARTICIPANTS

NAME/ADDRESS

DEGREE, SPECIALTY, LABORATORY ASSIGNED

Ben Abbott
Vanderbilt Univ.
Electrical Eng. Dept.
Nashville, TN 37240
(615) 322-6588

Degree: BS
Specialty: Computer Science
Assigned: Arnold Engineering Development
Center

Sudarkodi Alagarsamy
Trinity University
715 Stadium
San Antonio, TX 78284
(512) 736-7011

Degree: BS
Specialty: Biochemistry
Assigned: School of Aerospace Medicine

Julie Albertson
Washington State Univ.
Sloan 201
Pullman, WA 99164
(509) 335-8654

Degree: MS
Specialty: Mechanical Eng.
Assigned: Frank J. Seiler Research Lab.

David Alden
Cincinnati, Univ. of
408A Rhodes Hall
Cincinnati, OH 45221
(513) 556-3701

Degree: MS
Specialty: Metal. Engineering
Assigned: Materials Laboratory

Darren Allen
Middle Tennessee State Univ.
Dept. of Mathematics
Murfreesboro, TN 37132
(615) 898-2669

Degree: MS
Specialty: Mathematics
Assigned: Arnold Engineering Development
Center

Mojdeh Anderson
Cornell University
Phillips Hall
Ithaca, NY 14853
(607) 255-1445

Degree: BS
Specialty: Physics
Assigned: Frank J. Seiler Research Lab.

David Andreshak
Illinois, Univ. of
101 Transportation Bldg.
Urbana, IL 61801
(217) 333-2651

Degree: BS
Specialty: Aerospace Engineering
Assigned: Weapons Laboratory

Fred Arnold
Michigan, University of
Rackman Graduate School
Ann Arbor, MI 48109
(318) 764-4437

Degree: BS
Specialty: Physics
Assigned: Aero Propulsion Laboratory

John Baker
Kentucky, Univ. of
3200 Lochness Dr.
Lexington, KY 40503
(606) 439-1296

Degree: BS
Specialty: Mechanical Eng.
Assigned: Flight Dynamics Laboratory

John Bambery
Indiana Univ. at Penn.
Rm. 25 Weyanot Hall
Indiana, PA 15705
(412) 357-2611

Degree: BS
Specialty: Physics
Assigned: Avionics Laboratory

Rosemary Barbaro
Dayton, Univ. of
300 College Park Drive
Dayton, OH 45432
(513) 254-4444

Degree: BS
Specialty: Biology
Assigned: Harry G. Armstrong Aerospace
Medical Research Laboratory

Brian Bennett
Middle Tennessee State Univ.
Computer Sci. Dept.
Murphreesboro, TN 37132
(615) 898-2397

Degree: BS
Specialty: Electrical Eng.
Assigned: Arnold Engineering Development
Center

Robert Bolton
Texas A&M Univ.
EDG Area
College Station, TX 77843
(409) 845-0588

Degree: MS
Specialty: Civil Eng.
Assigned: Weapons Laboratory

Darwin Boyd
Kent State Univ.
Smith Laboratory of Physics
Kent, OH 44242
(216) 672-2880

Degree: MS
Specialty: Physics
Assigned: Materials Laboratory

Marcia Boyle
New Hampshire, Univ. of
PO Box LL
Durham, NH 03824
(603) 868-3107

Degree: BS
Specialty: Mechanical Eng.
Assigned: Materials Laboratory

John Butemeyer
Texas A&M Univ.
Dept. of Psychology
College Station, TX 77843
(409) 845-0483

Degree: MS
Specialty: Psychology
Assigned: Human Resources Laboratory:
Manpower & Personnel Division

Eric Byrne
Kansas State Univ.
1225 Claflin Rd. #6
Manhattan, KS 66502
(913) 537-8647

Degree: MS
Specialty: Computer Sci.
Assigned: Avionics Laboratory

Paul Calvo
Scranton, Univ. of
Biology Dept.
Loyola Hall
Scranton, PA 18510
(717) 961-6117

Degree: BS
Specialty: Biology
Assigned: School of Aerospace Medicine

Keith Carroll
Oregon Instit. of Tech.
3201 Campus Dr.
Klamath Falls, OR 97601
(503) 882-6321

Degree: BS
Specialty: Electronical Eng.
Assigned: Electronic Systems Division

Kerry Christopher
West Florida, Univ. of
11000 University Parkway
Pensacola, FL 32514
(904) 474-2150

Degree: BS
Specialty: Physical Science
Assigned: Flight Dynamics Laboratory

J. Clemens
Wright State Univ.
Chemistry Dept.
Dayton, OH 45431
(513) 873-2855

Degree: BS
Specialty: Chemistry
Assigned: Harry G. Armstrong Aerospace
Medical Research Laboratory

Scott Coffin
Oklahoma, Univ. of
5530 Willowcliff
Oklahoma City, OK 73122
(405) 325-4721

Degree: BS
Specialty: Physics
Assigned: Rome Air Development Center

Bradley Combs
Wichita State Univ.
1845 Fairmont
Wichita, KS 67208
(316) 689-3120

Degree: BS
Specialty: Biochemistry
Assigned: Frank J. Seiler Research Lab.

Michael Costarella
Wright State Univ.
Dept. of Computer Sci.
Dayton, OH 45435
(513) 879-2491

Degree: BS
Specialty: Computer Science
Assigned: Avionics Laboratory

Duane Daddis
Buffalo, Univ. of
PO Box 554
Buffalo, NY 14209
(716) 884-1993

Degree: BS
Specialty: Mechanical Engineering
Assigned: Aero Propulsion Laboratory

Brian Davis
Meharry Medical College
1005 D.B. Todd Blvd.
Nashville, TN 37212
(615) 297-2763

Degree: BS
Specialty: Biology
Assigned: School of Aerospace Medicine

Vincent Dimiceli
Texas A&M Univ.
407 A Tauber St.
College Station, TX 77840
(409) 846-5874

Degree: MS
Specialty: Applied Mathematics
Assigned: Harry G. Armstrong Aerospace
Medical Research Laboratory

Judy Dye
Alabama, Univ. of
Box 870350
Tuscaloosa, AL 35487
(205) 348-1970

Degree: MS
Specialty: Applied Mathematics
Assigned: Arnold Engineering Development
Center

Nancy Faulkner
Central State Univ.
110 Jenkins Tech. Bldg.
Wilberforce, OH 45384
(513) 376-6435

Degree: BS
Specialty: Manufacturing Eng.
Assigned: Flight Dynamics Laboratory

Dagmar Fertl
Texas A&M Univ.
Wildlife & Fisheries Sci.
College Station, TX 77843
(409) 845-1261

Degree: BS
Specialty: Biology
Assigned: School of Aerospace Medicine

Michael Findler
Arizona State Univ.
Dept. of Computer Sci.
Tempe, AZ 85287
(602) 965-3190

Degree: MS
Specialty: Computer Science
Assigned: Avionics Laboratory

Patrick Fitzpatrick
Texas A&M Univ.
Heaton Hall
College Station, TX 77843
(409) 845-1003

Degree: BS
Specialty: Meteorology
Assigned: Geophysics Laboratory

Lawrence Fleischer
Texas A&M University
347 Zachry Eng. Center
College Station, TX 77843
(409) 845-5531

Degree: MS
Specialty: Industrial Engineering
Assigned: Harry G. Armstrong Aerospace
Medical Research Laboratory

Bryan Foos
Ohio State Univ.
2070 Neil Ave.
Columbus, OH 43201
(614) 292-2771

Degree: BS
Specialty: Civil Engineering
Assigned: Flight Dynamics Laboratory

Robert Gabruk
Virginia Poly. Instit.
400 A Houston St.
Blacksburg, VA 24061
(703) 552-3434

Degree: BS
Specialty: Mechanical Engineering
Assigned: Aero Propulsion Laboratory

Ellen Goldey
Miami Univ.
Dept. of Zoology
Oxford, OH 45056
(513) 529-3184

Degree: MS
Specialty: Zoology
Assigned: Harry G. Armstrong Aerospace
Medical Research Laboratory

Charles Gray
Wright State Univ.
Dept. of Chemistry
Dayton, OH 45435
(513) 873-2855

Degree: BS
Specialty: Chemistry
Assigned: Materials Laboratory

Stuart Harbert
Texas A&M Univ.
2500 A Tabor Rd.
Bryan, TX 77803
(409) 845-1251

Degree: MS
Specialty: Mechanical Engineering
Assigned: Weapons Laboratory

David Harper
Bowling Green State Univ.
Dept. of Psychology
Bowling Green, OH 43402
(419) 372-2301

Degree: BS
Specialty: Psychology
Assigned: Harry G. Armstrong Aerospace
Medical Research Laboratory

Bradley Herman
Tennessee Tech. Univ.
201 West 13th Apt. 2
Cookeville, TN 38501
(615) 528-5032

Degree: BS
Specialty: Electrical Engineering
Assigned: Electronic Systems Division

Randall Hodgson
Alabama-Huntsville, Univ. of
4402-A Myrtlewood Cir.
Huntsville, AL 35816
(205) 895-6276

Degree: BS
Specialty: Applied Physics
Assigned: Armament Laboratory

Dean Hofmann
Dayton, Univ. of
Dept. of Materials and
Chemical Engineering
Dayton, OH 45469
(513) 229-2627

Degree: BS
Specialty: Chemical Engineering
Assigned: Materials Laboratory

Deborah Hollenbach
Ohio State Univ.
1803 Gerrard Ave.
Columbus, OH 43212
(614) 481-0986

Degree: MS
Specialty: Biology
Assigned: Harry G. Armstrong Aerospace
Medical Research Laboratory

Alice Horton
Northern Colorado, Univ. of
2725-20th St. #1
Greeley, CO 80631
(303) 351-8344

Degree: BS
Specialty: Mathematics
Assigned: Human Resources Laboratory:
Manpower & Personnel Division

Genevieve Huston
Ohio Univ.
9 S. Congress St.
Athens, OH 45701
(614) 594-7315

Degree: BS
Specialty: Electrical Engineering
Assigned: Flight Dynamics Laboratory

Matthew Jacobson-Carroll
Boston College
Devlin Hall Rm. 209
Chestnut Hill, MA 02167
(617) 552-3640

Degree: BS
Specialty: Geology
Assigned: Geophysics Laboratory

Neal Jähren
Minnesota-Duluth, Univ. of
371 Marshall W. Alworth Hall
Duluth, MN 55812
(212) 726-8568

Degree: BS
Specialty: Philosophy
Assigned: Materials Laboratory

William Jefferson
South Carolina, Univ. of
Marine Science Program
Columbia, SC 29208
(803) 777-3943

Degree: BS
Specialty: Biology
Assigned: Occupational and Environmental
Health Laboratory

Terrance Jorden
Meharry Medical College
944 21st Ave. N. #515
Nashville, TN 37208
(615) 321-5657

Degree: BS
Specialty: Biology
Assigned: Wilford Hall Medical Center

George Kim
Trinity Univ.
715 Stadium Dr.
San Antonio, TX 78284
(512) 736-7231

Degree: BS
Specialty: Biology
Assigned: School of Aerospace Medicine

Christopher Kocher
Southern Illinois Univ.
Carbondale, IL 62901
(618) 536-7525

Degree: BS
Specialty: Engineering
Assigned: Astronautics Laboratory

John Lafferty
Miami, Univ. of
Dept. of Chemistry
Coral Gables, FL
(305) 284-5842

Degree: BS
Specialty: Mathematics
Assigned: Wilford Hall Medical Center

David Lapioli
Penn State Univ.
51A Hammond Bldg.
University Park, PA 16802
(814) 865-0396

Degree: BS
Specialty: Aerospace Engineering
Assigned: Astronautics Laboratory

Teresa Lee
Western Illinois Univ.
Dept. of Sociology
Macomb, IL 61455
(309) 298-1056

Degree: BS
Specialty: Western Literature
Assigned: School of Aerospace Medicine

Patricia Liu
California, Univ. of
2404 Cedar St.
Berkeley, CA 94708
(415) 644-8394

Degree: BS
Specialty: Materials Engineering
Assigned: Astronautics Laboratory

Jon Longtin
Cincinnati, University of
Mechanical Eng. Dept.
Cincinnati, OH 45238
(513) 451-4136

Degree: BS
Specialty: Mechanical Engineering
Assigned: Aero Propulsion Laboratory

Lester Lynd
Vanderbilt Univ.
612 Watts Circle
Nashville, TN 37209
(615) 356-3632

Degree: BS
Specialty: Electrical Engineering
Assigned: Arnold Engineering Development Center

Diana Major
Southwestern Louisiana,
University of
PO Box 70504
Lafayette, LA 70504
(318) 231-6702

Degree: MS
Specialty: Physics
Assigned: Avionics Laboratory

Randal Mandock
Georgia Instit. of Tech.
PO Box 37122
Atlanta, GA 30332
(404) 894-3503

Degree: MS
Specialty: Atmospheric Science
Assigned: Rome Air Development Center

Toby Martin
Illinois, Univ. of
1010 W. Illinois St.
URH 126 TW
Urbana, IL 61801
(217) 332-4006

Degree: BS
Specialty: Aerospace Engineering
Assigned: Weapons Laboratory

Timothy Mavor
Worcester Poly. Instit.
100 Institute Rd.
Worcester, MA 01609
(508) 831-5730

Degree: BS
Specialty: Mathematics
Assigned: Rome Air Development Center

Walter McCarter
North Carolina State Univ.
2501 Kilgore Ave.
Raleigh, NC 27607
(919) 755-1541

Degree: MS
Specialty: Physics
Assigned: Weapons Laboratory

Stephen McClain Cornell Univ. Phillips Hall Ithaca, NY 14853 (607) 255-1445	<u>Degree:</u> MS <u>Specialty:</u> Physics <u>Assigned:</u> Frank J. Seiler Research Lab.
John McCord Murray State Univ. Dept. of Chemistry Murray, KY 42071 (502) 762-4490	<u>Degree:</u> BS <u>Specialty:</u> Chemical Engineering <u>Assigned:</u> Aero Propulsion Laboratory
Paula Mellon New York University Washington Square East New York, NY 10003 (212) 998-4730	<u>Degree:</u> PhD <u>Specialty:</u> Psychology <u>Assigned:</u> Wilford Hall Medical Center
Douglas Melton Ohio State Univ. 205 Dreesse Lab Columbus, OH 43210 (614) 292-2906	<u>Degree:</u> MS <u>Specialty:</u> Electrical Engineering <u>Assigned:</u> Avionics Laboratory
Cynthia Moorhead Texas A&M Univ. 1907 Dartmouth #206 College Station, TX 77843 (409) 845-3381	<u>Degree:</u> BS <u>Specialty:</u> Economics <u>Assigned:</u> School of Aerospace Medicine
Lisa Newberg Eastern Washington Univ. Mathematics Dept. Cheney, WA 99004 (509) 458-6200	<u>Degree:</u> BS <u>Specialty:</u> Mathematics <u>Assigned:</u> Occupational and Environmental Health Laboratory
William Newbold Florida, Univ. of 231 Aerospace Bldg. Gainesville, FL 32611 (904) 392-0961	<u>Degree:</u> BS <u>Specialty:</u> Aerospace Engineering <u>Assigned:</u> Armament Laboratory
Randy Nguyen San Jose State University San Jose, CA 95117 (408) 244-9743	<u>Degree:</u> BS <u>Specialty:</u> Mechanical Engineering <u>Assigned:</u> Astronautics Laboratory

Mary Nickels
New Mexico, Univ. of
Clark Hall
Albuquerque, NM 87131
(505) 277-6655

Degree: BS
Specialty: Chemistry
Assigned: Weapons Laboratory

William Patience
Ohio Univ.
21 1/2 S. Court St.
Athens, OH 45701
(614) 594-2468

Degree: BS
Specialty: Electrical Engineering
Assigned: Rome Air Development Center

Douglas Pederson
Oregon Instit. of Tech.
Electronics Dept.
Klamath Falls, OR 97601
(503) 882-6321

Degree: BS
Specialty: Electrical Engineering
Assigned: Electronic Systems Division

Hao Pham
California State Univ.
1250 Bellflower Blvd.
Long Beach, CA 90840
(213) 985-1524

Degree: BS
Specialty: Mechanical Engineering
Assigned: Frank J. Seiler Research Lab.

Betty Pipes
Middle Tennessee State Univ.
Computer Science Dept.
Murfreesboro, TN 37132
(615) 898-2397

Degree: BS
Specialty: Mathematics
Assigned: Arnold Engineering Development Center

Laura Pytel
Ohio University
428 Sargent Hall
Athens, OH 45701
(614) 597-5663

Degree: BS
Specialty: Mechanical Engineering
Assigned: Harry G. Armstrong Aerospace Medical Research Laboratory

George Ramlow
Oregon Instit. of Tech.
PO Box 2297
Klamath Falls, OR 97601
(503) 882-6524

Degree: BS
Specialty: Electrical Engineering
Assigned: Electronic Systems Division

Lionel Ramos
Texas-San Antonio, Univ. of
Div. of Engineering
San Antonio, TX
(512) 691-5518

Degree: BS
Specialty: Electrical Engineering
Assigned: School of Aerospace Medicine

Rex Ramsier
Akron, Univ. of
Dept. of Physics
Akron, OH 44325
(216) 375-6054

Degree: BS
Specialty: Physics
Assigned: Materials Laboratory

Joseph Rea
Texas-San Antonio, Univ. of
Dept. of Electrical Eng.
San Antonio, TX 78285
(512) 691-4011

Degree: BS
Specialty: Electrical Engineering
Assigned: School of Aerospace Medicine

Ernest Rho
Illinois Instit. of Tech.
3300 S. Federal
Chicago, IL 60616
(312) 567-3400

Degree: BS
Specialty: Electrical Engineering
Assigned: Rome Air Development Center

James Sago
Missouri-Rolla, Univ. of
B-19 McNutt Hall
Rolla, MO 65401
(314) 341-6461

Degree: BS
Specialty: Metal. Engineering
Assigned: Materials Laboratory

John Salinas
Meharry Medical College
1005 D.B. Todd Blvd.
Nashville, TN 37208
(615) 327-6204

Degree: MS
Specialty: Biochemistry
Assigned: Wilford Hall Medical Center

David Sanborn
Lowell, Univ. of
Box 2559N
Lowell, MA 01854
(508) 452-5000

Degree: MS
Specialty: Electrical Engineering
Assigned: Geophysics Laboratory

Sonja Schillmoeller
Illinois Univ. of
Urbana, IL 61801
(217) 328-6638

Degree: BS
Specialty: Aero. Engineering
Assigned: Astronautics Laboratory

Royce Simpson
Alabama, Univ. of
Box 870348
Tuscaloosa, AL 35487
(205) 348-1934

Degree: BS
Specialty: Psychology
Assigned: Human Resources Laboratory:
Operations Training Division

Janet Slifka
Dayton, Univ. of
300 College Park Ave.
Dayton, OH 45469
(513) 229-3611

Degree: MS
Specialty: Electrical Engineering
Assigned: Harry G. Armstrong Aerospace
Medical Research Laboratory

Richard Souder
Vanderbilt Univ.
612 Watts Circle
Nashville, TN 37209
(615) 356-3632

Degree: BS
Specialty: Electrical Engineering
Assigned: Arnold Engineering Development
Center

Richard Swift
Notre Dame, Univ. of
Dept. of Aero. and Mech. Eng.
Notre Dame, IN 46556
(219) 239-7666

Degree: BS
Specialty: Aeronautical Engineering
Assigned: Flight Dynamics Laboratory

Lynda Tomlinson
Syracuse Univ.
111 Link Hall
Syracuse, NY 13244
(315) 443-4415

Degree: MS
Specialty: Electrical Engineering
Assigned: Rome Air Development Center

George Tompkins
Kansas State Univ.
M-27 Jardine Terrace
Manhattan, KS 66502
(913) 776-5691

Degree: BS
Specialty: Industrial Engineering
Assigned: Materials Laboratory

Mona Toms
Wright State Univ.
Applied Behavior Sci.
Dayton, OH 45435
(513) 873-2310

Degree: BS
Specialty: Psychology
Assigned: Human Resources Laboratory:
Logistics & Human Factors

Robert Tramel
Tennessee Space Instit.
Dept. of Mathematics
Tullahoma, TN 37388
(615) 455-0631

Degree: BS
Specialty: Physics
Assigned: Arnold Engineering Development
Center

Scott VanDam
Central Florida, Univ. of
PO Box 2500
Orlando, FL 32816
(407) 275-2416

Degree: MS
Specialty: Electrical Engineering
Assigned: Aero Propulsion Laboratory

Ronald VanEtten
Illinois State Univ.
Normal, IL 61761
(309) 452-6529

Degree: BS
Specialty: Education
Assigned: Human Resources Laboratory:
Manpower & Personnel Division

John Wagon
Oklahoma State Univ.
2001 N. Perkins #M135
Stillwater, OK 74075
(405) 743-3750

Degree: BS
Specialty: Electrical Engineering
Assigned: Rome Air Development Center

Glenn Waguespack
Louisiana State Univ.
736 Dentation Dr.
Baton Rouge, LA 70808
(504) 766-1271

Degree: BS
Specialty: Mechanical Engineering
Assigned: Armament Laboratory

Matthew Westerheide
Missouri-Rolla, Univ. of
Thomas Jefferson Hall
Room 729
Rolla, MO 63138
(314) 341-5740

Degree: BS
Specialty: Electrical Engineering
Assigned: Astronautics Laboratory

John Williamson
Texas A&M Univ.
Dept. of Psychology
College Station, TX 77843
(409) 845-2581

Degree: BS
Specialty: Psychology
Assigned: Human Resources Laboratory:
Training Systems

Raymond Wolfe
Scranton, Univ. of
423 Madison Ave.
Scranton, PA 18510
(717) 342-3402

Degree: BS
Specialty: Biology
Assigned: School of Aerospace Medicine

Jon Zern
Florida, Univ. of
Box J-125
Gainesville, FL 32610
(904) 392-2381

Degree: BS
Specialty: Biology
Assigned: Engineering Services Center

Joseph Ziegler
Florida, Univ. of
Dept. of Civil Eng.
Gainesville, FL 32611
(904) 392-3261

Degree: BS
Specialty: Civil Engineering
Assigned: Engineering Services Center

PARTICIPANT LABORATORY ASSIGNMENT

C. PARTICIPANT LABORATORY ASSIGNMENT (Page 1)

1989 USAF/UES GRADUATE STUDENT RESEARCH PROGRAM

AERO PROPULSION LABORATORY (WRDC/APL)

(Wright-Patterson Air Force Base)

- | | |
|------------------|-----------------|
| 1. Fred Arnold | 4. Jon Longtin |
| 2. Duane Daddis | 5. John McCord |
| 3. Robert Gabruk | 6. Scott VanDam |

ARMAMENT LABORATORY (ATL)

(Eglin Air Force Base)

1. Randall Hodgson
2. William Newbold
3. Glenn Waguespack

HARRY G. ARMSTRONG AEROSPACE MEDICAL RESEARCH LABORATORY (AAMRL)

(Wright-Patterson Air Force Base)

- | | |
|-----------------------|-----------------------|
| 1. Rosemary Barbaro | 6. David Harper |
| 2. J. Matthew Clemens | 7. Deborah Hollenbach |
| 3. Vincent Dimiceli | 8. Laura Pytel |
| 4. Lawrence Fleischer | 9. Janet Slifka |
| 5. Ellen Goldey | |

ARNOLD ENGINEERING DEVELOPMENT CENTER (AEDC)

(Arnold Air Force Base)

- | | |
|------------------|-------------------|
| 1. Ben Abbott | 5. Lester Lynd |
| 2. Darren Allen | 6. Betty Pipes |
| 3. Brian Bennett | 7. Richard Souder |
| 4. Judy Dye | 8. Robert Tramel |

ASTRONAUTICS LABORATORY (AL)

(Edwards Air Force Base)

- | | |
|-----------------------|------------------------|
| 1. Christopher Kocher | 4. Randy Nguyen |
| 2. David Lapioli | 5. Sonja Schillmoeller |
| 3. Patricia Liu | 6. Matthew Westerheide |

AVIONICS LABORATORY (Avionics Laboratory)

(Wright-Patterson Air Force Base)

- | | |
|-----------------------|--------------------|
| 1. John Bambery | 4. Michael Findler |
| 2. Eric Byrne | 5. Diana Major |
| 3. Michael Costarella | 6. Douglas Melton |

ELECTRONIC SYSTEMS DIVISION (ESD)

(Hanscom Air Force Base)

- | | |
|-------------------|---------------------|
| 1. Keith Carroll | 3. Douglas Pederson |
| 2. Bradley Herman | 4. George Ramlow |

ENGINEERING AND SERVICES CENTER (ESC)

(Tyndall Air Force Base)

1. Jon Zern
2. Joseph Ziegler

C. PARTICIPANT LABORATORY ASSIGNMENT (Page 2)

FLIGHT DYNAMICS LABORATORY (FDL)

(Wright-Patterson Air Force Base)

- | | |
|----------------------|---------------------|
| 1. John Baker | 4. Bryan Foos |
| 2. Kerry Christopher | 5. Genevieve Huston |
| 3. Nancy Faulkner | 6. Richard Swift |

FRANK J. SEILER RESEARCH LABORATORY (Frank J. Seiler Research Lab.)

(USAF Academy)

- | | |
|--------------------|--------------------|
| 1. Julie Albertson | 4. Stephen McClain |
| 2. Mojdeh Anderson | 5. Hao Pham |
| 3. Bradley Combs | |

GEOPHYSICS LABORATORY (Geophysics Laboratory)

(Hansom Air Force Base)

1. Patrick Fitzpatrick
2. Matthew Jacobson-Carroll
3. David Sanborn

HUMAN RESOURCES LABORATORY

(Brooks, Williams and Wright-Patterson Air Force Bases)

- | | |
|-------------------|---------------------|
| 1. John Butemeyer | 6. Mona Toms |
| 2. Alice Horton | 7. Ronald Van Etten |
| 3. Royce Simpson | 8. John Williamson |

MATERIALS LABORATORY (ML)

(Wright-Patterson Air Force Base)

- | | |
|-----------------|--------------------|
| 1. David Alden | 6. Neal Jahren |
| 2. Darwin Boyd | 7. Rex Ramsier |
| 3. Marcia Boyle | 8. James Sago |
| 4. Charles Gray | 9. George Tompkins |
| 5. Dean Hofmann | |

OCCUPATIONAL AND ENVIRONMENT HEALTH LABORATORY (OEHL)

(Brooks Air Force Base)

1. William Jefferson
2. Lisa Newberg

C. PARTICIPANT LABORATORY ASSIGNMENT (Page 3)

ROME AIR DEVELOPMENT CENTER (Rome Air Development Center)
(Griffiss Air Force Base)

- | | |
|---------------------|--------------------|
| 1. Scott Coffin | 5. Ernest Rho |
| 2. Randal Mandock | 6. Lynda Tomlinson |
| 3. Timothy Mavor | 7. John Wagon |
| 4. William Patience | |

SCHOOL OF AEROSPACE MEDICINE (School of Aerospace Medicine)
(Brooks Air Force Base)

- | | |
|-------------------------|---------------------|
| 1. Sudarkodi Alagarsamy | 6. Teresa Lee |
| 2. Paul Calvo | 7. Cynthia Moorhead |
| 3. Brian Davis | 8. Lionel Ramos |
| 4. Dagmar Fertl | 9. Joseph Rea |
| 5. George Kim | 10. Raymond Wolfe |

WEAPONS LABORATORY (Weapons Laboratory)
(Kirtland Air Force Base)

- | | |
|--------------------|--------------------|
| 1. David Andreshak | 4. Toby Martin |
| 2. Robert Bolton | 5. Walter McCarter |
| 3. Stuart Harbert | 6. Mary Nickels |

WILFORD HALL MEDICAL CENTER (Wilford Hall Medical Center)
(Lackland Air Force Base)

- | | |
|--------------------|-----------------|
| 1. Terrance Jorden | 3. Paula Mellon |
| 2. John Lafferty | 4. John Salinas |

RESEARCH REPORTS

RESEARCH REPORTS

1989 GRADUATE STUDENT RESEARCH PROGRAM

Technical
Report
Number

Title

Graduate Researcher

Volume I

Armament Laboratory

- | | | |
|---|--|------------------|
| 1 | Laser Polarimeter Development | Randall Hodgson |
| 2 | Euler Solutions to Transonic Flow Past
an Ogive-Cylinder Body with Wraparound
Fins | William Newbold |
| 3 | Observations and Improvements of
Ballistic Stress Analysis Techniques | Glenn Waguespack |

Arnold Engineering Development Center

- | | | |
|----|---|----------------|
| 4 | Distributed and Parallel Image and
Signal Processing
*** Same Report as Dr. Wilkes *** | Ben Abbott |
| 5 | Latin Hyper-Cube Sampling with Regression
Analysis for Prediction of Engine
Infrared Observables | Darren Allen |
| 6 | A General Purpose Two Dimensional
Plotting Program | Brian Bennett |
| 7 | Matrix Inversions of Candidate
Geometries for Application of CT
Emission Techniques to Broad Band
Radiative Transfer | Judy Dye |
| 8 | Distributed and Parallel Image and
Signal Processing
*** Same Report as Dr. Wilkes *** | Lester Lynd |
| 9 | A Survey of the Personal Computer
Environment at Arnold Engineering
Development Center | Betty Pipes |
| 10 | Distributed and Parallel Image and
Signal Processing
*** Same Report as Dr. Wilkes *** | Richard Souder |
| 11 | A Nonlinear Filter and an Odd/Even
Iteration for Inviscid Fluid Flow Equations | Robert Tramel |

Astronautics Laboratory

- | | | |
|----|--|---------------------|
| 12 | The Effects of Elevated Temperature Exposure on the Strength and Microstructure of 2-D Carbon-Carbon | Christopher Kocher |
| 13 | Vibration Control of a Cantilevered Beam Using a Distributed Actuator | David Lapioli |
| 14 | Using the STM to Characterize the Effects of Surface Treatments on the Surface Morphology of Carbon Fibers | Patricia Liu |
| 15 | Finite Element Model for Astrex | Randy Nguyen |
| 16 | Modeling of Combustion Instability in Solid Rocket Motors | Sonja Schillmoeller |
| 17 | State Variable Control of a Flexible Grid Structure | Matthew Westerheide |

Electronic Systems Division

- | | | |
|----|---|------------------|
| 18 | Carrier Free Radar
*** Same Report as Beryl Barber *** | Keith Carroll |
| 19 | Analysis of Testability Concepts and its Application to RSIP
*** Same Report as Dr. S. Natarajan *** | Bradley Herman |
| 20 | Carrier Free Radar
*** Same Report as Dr. Beryl Barber *** | Douglas Pederson |
| 21 | Carrier Free Radar
*** Same Report as Dr. Beryl Barber *** | George Ramlow |

Engineering and Services Center

- | | | |
|----|--|----------------|
| 22 | Effects of Jet Aircraft Noise on Domestic Goats | Jon Zern |
| 23 | Contaminant Flux Reduction Through In Situ Solubility Modification
*** Same Report as Dr. Kirk Hatfield *** | Joseph Ziegler |

Frank J. Seiler Research Laboratory

- | | | |
|----|---|-----------------|
| 24 | An Investigation of Dynamic Stall Vortex Characteristics
*** Same Report as Dr. Troutt *** | Julie Albertson |
|----|---|-----------------|

Frank J. Seiler Research Laboratory (continued)

- | | | |
|----|--|-----------------|
| 25 | Second Harmonic Generation in Optical
Fibers
*** Same Report as Dr. Hillman ** | Mojdeh Anderson |
| 26 | Transition State Analysis:
Gluconolactone by MOPAC | Bradley Combs |
| 27 | Second Harmonic Generation in Optical
Fibers
*** Same Report as Dr. Hillman *** | Stephen McClain |
| 28 | Modeling of a Structure-Actuator
System with Structure-Borne
Reaction-Mass Actuators with Optimal
Design of Passive Vibration Absorbers
*** Same Report as Dr. Hung Vu *** | Hao Pham |

Geophysics Laboratory

- | | | |
|----|---|-----------------------|
| 29 | Adaptation of the Axisymmetric TASS
Model for Hurricane Simulations | Pat Fitzpatrick |
| 30 | Estimating Characteristics of Chemical
Explosions in New England and Eastern
Kazakhstan Using Local and Regional
Seismic Data
*** Same Report as Dr. Alan Kafka *** | Matt Jacobson-Carroll |
| 31 | Final Summary of Research Effort
*** 1988 Participant *** | Thomas Kimble |
| 32 | Comparative Analysis of Various
Atmospheric Modelling Techniques | David Sanborn |

Rome Air Development Center

- | | | |
|----|--|------------------|
| 33 | Characterization of a Spatial Light
Modulator for Optical Filtering | Scott Coffin |
| 34 | Adaptive Beamforming Software for
the Digital Beam Steering Antenna | Randal Mandock |
| 35 | A Study of Interacting Tunneling
Units with Possible Application to
High Temperature Superconductors
*** Same Report as Dr. Klein *** | Timothy Mavor |
| 36 | A Simplified Method of Determining
Noise Parameters of High Frequency
MESFETs | William Patience |

Rome Air Development Center (continued)

- | | | |
|----|--|-----------------|
| 37 | Study of a Communication Receiver
for Spread Spectrum Signals
*** Same Report as Dr. Donald Ucci *** | Ernest Rho |
| 38 | A Computer for Temporal Frequency
Spectrum of Vegetation Clutter Return
*** Same Report as Dr. Jay Lee *** | Lynda Tomlinson |
| 39 | Neural Networks and Parallel Computation
of Fourier Transforms | John Wagnon |

Weapons Laboratory

- | | | |
|----|--|-----------------|
| 40 | An Experimental Protocol for Line-
of-Sight Slewing, Optical Alignment
of AFT Body Station Keeping Control
Emulation
*** Same Report as Dr. Thomas Dwyer *** | David Andreshak |
| 41 | Scattering of Elastic Waves in a
Random Inhomogeneous Soil Media
*** Same Report as Dr. Duane Sanders *** | Robert Bolton |
| 42 | Modeling the Response of Pressurized
Composite Cylinders to Laser Damage
*** Same Report as Dr. Harry Hogan *** | Stuart Harbert |
| 43 | An Experimental Protocol for Line-
of-Sight Slewing, Optical Alignment
of AFT Body Station Keeping Control
Emulation
*** Same Report as Dr. Thomas Dwyer *** | Toby Martin |
| 44 | GPS Time Synchronization | Walter McCarter |
| 45 | Preliminary Guidelines on Tunable
Diode Laser Use | Mary Nickels |

Volume II

Wright Research Development Center
Aero Propulsion Laboratory

- | | | |
|----|---|---------------|
| 46 | A Study of J_c in High T_c Superconductors
Using a Magnetic Induction Method | Fred Arnold |
| 47 | Design of an LDV Data Analysis System | Duane Daddis |
| 48 | Preparation of a Dump Combustor for
IDA Measurements | Robert Gabruk |

Aero Propulsion Laboratory (continued)

- | | | |
|----|---|--------------|
| 49 | Flow Limitations in Micro Heat Pipes
*** Same Report as Dr. Frank Gerner *** | Jon Longtin |
| 50 | Laser Induced Fluorescence Probe of
CH Radical | John McCord |
| 51 | Examination and Application of a One
Dimensional Thermionic Energy
Converter (TEC) Code | Scott VanDam |

Avionics Laboratory

- | | | |
|----|--|--------------------|
| 52 | Band Diagram Subroutine and Band
Bending in the Spike Layer for the
BICFET | John Bambery |
| 53 | Software Design Recovery: A Case
Study | Eric Byrne |
| 54 | Toolbox for Image Processing using
Distributed Computing
*** Same Report as Dr. Larry Crum *** | Michael Costarella |
| 55 | Neural Networks and Machine Learning | Michael Findler |
| 56 | A Theoretical Resolution of Multiple
Frequencies
*** Same Report as Dr. Choate *** | Diana Major |
| 57 | An Implementation of an Objective
Measure of Speech Intelligibility | Douglas Melton |

Flight Dynamics Laboratory

- | | | |
|----|---|-------------------|
| 58 | Radiation Hypersonic Aerodynamics:
Numerical Simulation of Hypersonic
Flows Past Slender Wedges Near the
Continuum Limit | John Baker |
| 59 | Validation Schemes for Accelerated
Crazing Tests and X3D - A Finite
Element Analysis Code | Kerry Christopher |
| 60 | Neural Networks and their Role in
Visual Object Recognition
*** Same Report as Augustus Morris *** | Nancy Faulkner |
| 61 | Damage in Graphite/Epoxy Plates
Subjected to Low Velocity Impact
(1988 Participant) | Bryan Foos |

Flight Dynamics Laboratory (continued)

- | | | |
|----|---|------------------|
| 62 | Strain Distribution in Composite Coupons in Tension
*** Same Report as Dr. W. Wolfe *** | Bryan Foos |
| 63 | Control System Design Modeling | Genevieve Huston |
| 64 | Accessing the Computer Automated Design Database (CADDB) Through CADS- A Computer Aided Design System | Richard Swift |

Materials Laboratory

- | | | |
|----|---|-----------------|
| 65 | Dislocations in Rene' N4+ with Respect to Orientation and Temperature | David Alden |
| 66 | An Approximate Analytical Solution of the Nonlinear Diffusion Equation and a Preliminary Investigation of Nonlinear Optics | Darwin Boyd |
| 67 | Investigation of the Thermomechanical Response of a Titanium Aluminide Metal Matrix Composite Using a Viscoplastic Constitutive Theory
*** Same Report as Dr. James Sherwood *** | Marcia Boyle |
| 68 | Synthesis of Model Benzothiazoles | Charles Gray |
| 69 | State of the Art Sensors for In-Situ Monitoring of Composite Cure | Dean Hofmann |
| 70 | Data Reduction of Photoreflectance from Capped Aluminum Gallium Arsenide Structures | Neal Jahren |
| 71 | Scanning Tunneling Microscopy and and Ballistic-Electron-Emission Spectroscopy | Rex Ramsier |
| 72 | Evaluation of CR-SI Alloys for Aerospace Structural Applications
*** Same Report as Dr. Joseph Newkirk *** | James Sago |
| 73 | An Intelligent Neural Model for Recognition of Input/Output Patterns for a Molecular Beam Epitaxy Process | George Tompkins |
| 74 | High Resolution Scanning Electron Microscopy of Pitch-Based Carbon Fiber
(1988 Participant) | Deborah Vezie |

Volume III
Human Systems Divisions Laboratories
Harry G. Armstrong Aerospace Medical Research Laboratory

75	Research into Semen Analysis as a Sensitive Indicator of Neurotoxicity	Rosemary Barbaro
76	The Metabolism of 2-Methylheptane in Fischer 344 Rats	J. Matthew Clemens
77	Harness Belt Task *** Same Report as Dr. Szucs ***	Vincent Dimiceli
78	A Study of Transport Delay Using an Aircraft Simulator: Pilot Study	Lawrence Fleischer
79	Maternal Transfer of Hexachlorobenzene in the Rat	Ellen Goldey
80	Effects of Data Error on Problem-Solving Heuristics *** Same Report as Dr. Bonnie Walker ***	David Harper
81	The Physiological Effects of Dobutamine on the Cardiovascular System	Deborah Hollenbach
82	Investigation of a Selspot II Molten Analysis System Response to Impact Conditions	Laura Pytel
83	Speech Coding and Feature Recognition with a Backpropagation Neural Network	Janet Slifka

Human Resources Laboratory

84	Career Progression in Air Force Enlisted Personnel: An Examination of Two Alternate Criterion Measures *** Same Report as Dr. David Woehr ***	John Butemeyer
85	Investigation of Color Appearance within Low Light Levels *** Same as Prof. Douglas Mandra (1988) ***	Patricia Cooper
86	Working Memory and Cognitive Structure *** Same as Dr. Kathryn Cochran ***	Alice Horton
87	Evaluation of Air-Intercept Performance: Observer Reliability Issues *** Same Report as Dr. Tomporowski ***	Royce Simpson
88	Integral Displays in Interactive Dynamic Environments	Mona Toms

Human Resources Laboratory (continued)

- | | | |
|----|---|------------------|
| 89 | Software Development to Support Data Collection and Analysis of Cognitive Task Analysis Studies | Ronald Van Etten |
| 90 | An Evaluation of Stereoscopic 3D Computer Displays | John Williamson |

Occupational and Environmental Health Laboratory

- | | | |
|----|--|-------------------|
| 91 | Biological Analysis of Three Ponds at Peterson AFB, Colorado Springs, CO
*** Same Report as Dr. Zagursky *** | William Jefferson |
| 92 | Statistical Analyses of Data Pertaining to Ground Water Contamination and Laboratory Quality Control
*** Same Report as Dr. Barbara Alvin *** | Lisa Newberg |

School of Aerospace Medicine

- | | | |
|-----|--|----------------------|
| 93 | Investigation of the Release of Glutamate and Dynorphin A(1-8) by Hippocampal Mossy Fiber Synaptosomes Through Chemical and Electrical Stimulation | Sudarkodi Alagarsamy |
| 94 | Investigation of Picosecond Pulses from a CW Q-Switched Active Mode-Locked Laser
(1988 Participant) | John Barnaby |
| 95 | PCR Analysis and in situ Detection of Ureaplasma urealyticum and Microplasma hominis
*** Same Report as Dr. DelVecchio *** | Paul Calvo |
| 96 | Glutamate Involvement in the Photic Entrainment of Activity Rhythms in Hamsters | Brian Davis |
| 97 | Magnetodetection by Animals | Dagmar Fertl |
| 98 | Cryopreserving Chlamydomonas reinhardtii at -70°C by the Two-step Cooling Method | George Kim |
| 99 | Statistical Models in Social Dynamics | Teresa Lee |
| 100 | A Research Opportunity at Brooks Air Force Base: A Multi-Faceted Experience | Cynthia Moorhead |

School of Aerospace Medicine (continued)

- | | | |
|-----|---|---------------|
| 101 | System and Signal Analysis of VEP
Data and Joystick Error Analysis
*** Same Report as Dr. Longbotham *** | Lional Ramos |
| 102 | System and Signal Analysis of VEP
Data and Joystick Error Analysis
*** Same Report as Dr. Longbotham *** | Joseph Rea |
| 103 | PCR Analysis and in situ Detection
of Ureaplasma urealyticum and
Microplasma hominis
*** Same Report as Dr. Delvecchio *** | Raymond Wolfe |

Wilford Hall Medical Center

- | | | |
|-----|---|-----------------|
| 104 | Dental Materials | Terrance Jorden |
| 105 | Temperature Effects on Erythrocyte
Sedimentation Rates in Whole Blood
and on Erythrocyte and Platelet
Volumes
*** Same Report as Dr. Drost-Hansen *** | John Lafferty |
| 106 | Collecting Data and Occurrence of
AIDS-Related Symptoms: Longitudinal
Study of HIV U.S. Air Force
Personnel | Paula Mellon |
| 107 | Comparison of Thromboelastography (TEG)
versus Standard Hematologic Parameters
to Predict Hemorrhage after Cardiopulmonary
Bypass (CPB) | John Salinas |

1989 USAF-UES Summer Faculty Research Program

Graduate Student Research Program

Sponsored by the

Air Force Office of Scientific Research

Conducted by the

Universal Energy Systems, Inc.

Final Report

A Study of J_c in High T_c Superconductors Using a Magnetic Induction Method

Prepared by: Fred Arnold B.S.

Academic Rank: Graduate student

Department and University: Polymer Science, University of Akron

Research Location: WRDC/APL, Wright Patterson AFB

USAF Researcher: Dr. Charles Oberly

Date: August 21, 1989

Contract No.: F49620-88-C-0053

A Study of Jc in High Tc Superconductors Using a Magnetic Induction Method

by

Fred Arnold

Abstract

When a high Tc superconductor is cooled below its transition temperature, its resistance drops essentially to zero. By using a non-contact method in studying the electrical properties of these ceramic superconductors, we can avoid the large contact resistance associated with a probe method. The critical current density (Jc) of a material is a measure of how well it can transport current. A magnetic induction method will be used to determine Jc. Jc will be measured at 4K and at 77K. The dependence of Jc on the cross sectional area of the specimen will also be determined as well as the effect of adding silver (Ag) to the 1-2-3 (YBa₂Cu₃O_{7-x}) material.

Acknowledgements

I wish to thank Universal Energy Systems for giving me the opportunity to work under Dr. Charles Oberly at the APL/WPAFB. It was a worthwhile and enriching experience to work with Dr. Oberly and Dr. Gregory Kozlowski. I would also like to thank Bob Leese, Fernando Rodriguez, and Lt. Russ Spyker for their help during my stay at the APL.

Introduction

On April 17, 1986, the era of high T_c superconductors was born. Previously the highest transition temperature recorded was around 23K compared to the new ceramic superconductors which have a T_c range of between 30 and 125K. The discovery of compounds with a T_c above 77K is of great importance. Previously liquid helium had to be used to induce superconducting properties, but now it is possible to use liquid nitrogen which has the value of a higher boiling point and is relatively inexpensive.

The objective of the Air Force high temperature superconducting SDIO program is to develop high current density ceramic superconductors with low loss electrical power for use in high power devices. The program now concentrates on processing the ceramic powders into component forms and testing their quality on a small scale.

One of the program's objectives is to create superconductors with good superconducting properties by increasing the amount of oxygen in the material. The control of oxygen in bulk materials is essential for producing a good superconductor. Oxygen can diffuse into the material with a rate controlled sintering process. This is accomplished by sintering the sample at various temperatures and then cooling the superconductor back to room temperature. During the cooling process, the oxygen is added to the material. Silver can be added to the 1-2-3 material ($YBa_2Cu_3O_{7-x}$) in an attempt to strengthen the mechanical properties. The problem with the addition of Ag is finding the equilibrium between strengthening the mechanical properties

without significantly diminishing the superconducting properties.

One of the problems with these new high T_c superconductors is the difficulty in producing bulk materials with high O_2 concentrations. The rate controlled sintering process has produced O_2 concentrations of 6.92 at a 3mm depth in 99.3% dense 1-2-3 material. This is a very important accomplishment because we now have a process that can diffuse oxygen into the material, penetrating the surface.

Research Effort

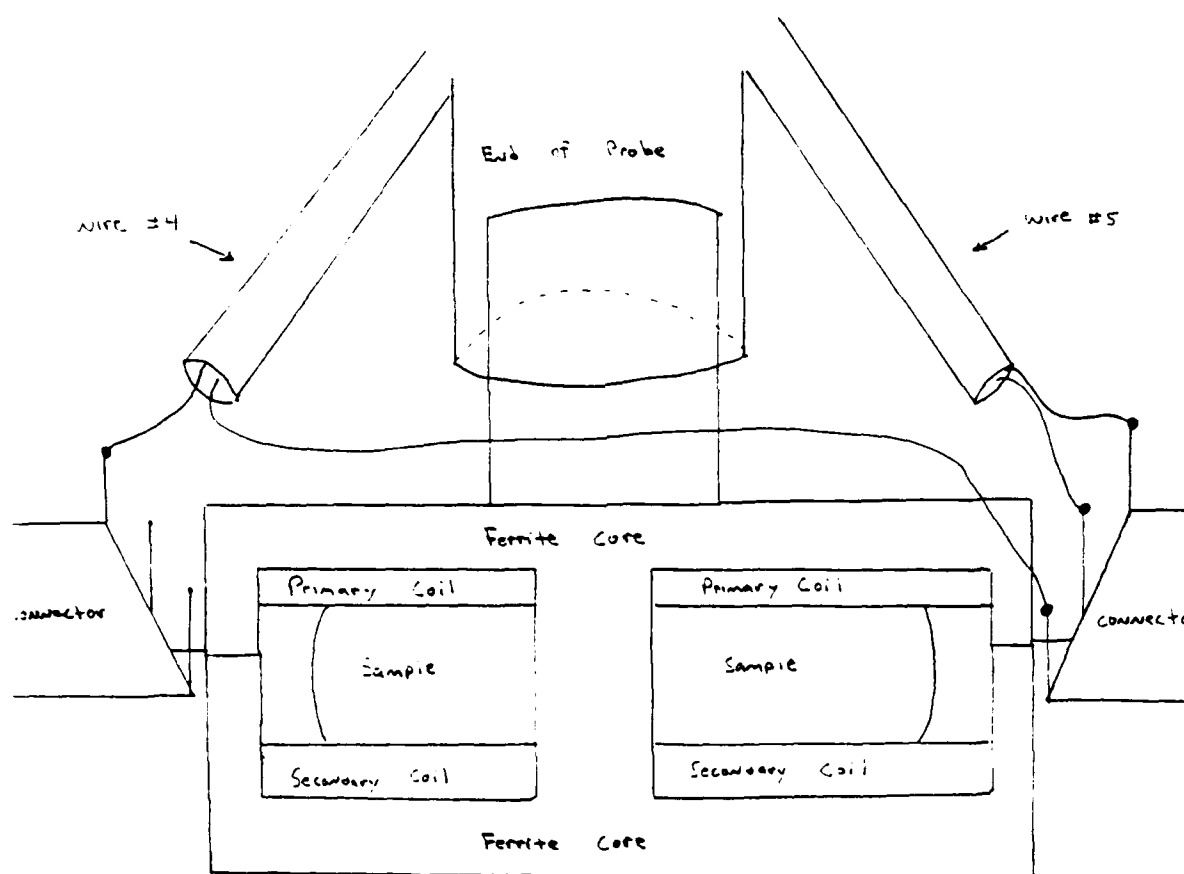
My assignment as a participant as a Summer Graduate Research Fellow was to set up a device that could measure the J_c of a superconductor. By using the principle of magnetic induction, a non-contact method for measuring the electrical properties of a high T_c superconductor has been developed. Without contacts this method avoids the problem of the resistance at the point of contact. The familiar four probe method presents problems due to the large contact resistance associated with the probes.

Two copper coils are created and put inside a ferrite core. The coils consist of sixty-five turns of wire, gauge number thirty-four. The sample has a $\frac{5}{16}$ th hole drilled through the center and is placed within the ferrite core between the primary and secondary coils (diagram). A diamond core drill must be used to create the ring sample due to the brittle nature of the material.. It is also very important to take into account the resistance of the coils in nitrogen and helium compared to room temperature.

The material ferrite is used as the core material because it enhances the inductance between the two coils. The flux linking the sample to the two coils (primary and secondary) is concentrated in the core, giving a flux linkage of about 100%. It also has a "screening effect" which keeps the magnetic field experienced by the sample to a minimum. This is very important since the critical current density of a superconductor ($YBa_2Cu_3O_{7-x}$) is greatly reduced in the presence of a magnetic field.

There is an inductance "M" which relates the flux in the

CORE SPECS



Core number 18118 3037
Primary secondary turns: 65
Wire gauge number: 34
Sample size 2mm thick
Size of hole $\frac{1}{8}$ inch (diameter)

core with the total current circulating around it. The flux within the sample has a similar relationship except a little flux will by-pass the core.

$$\Phi_c = M(N_1 i_1 + i_c) \quad \text{flux of core} \quad \text{(Harris)}$$

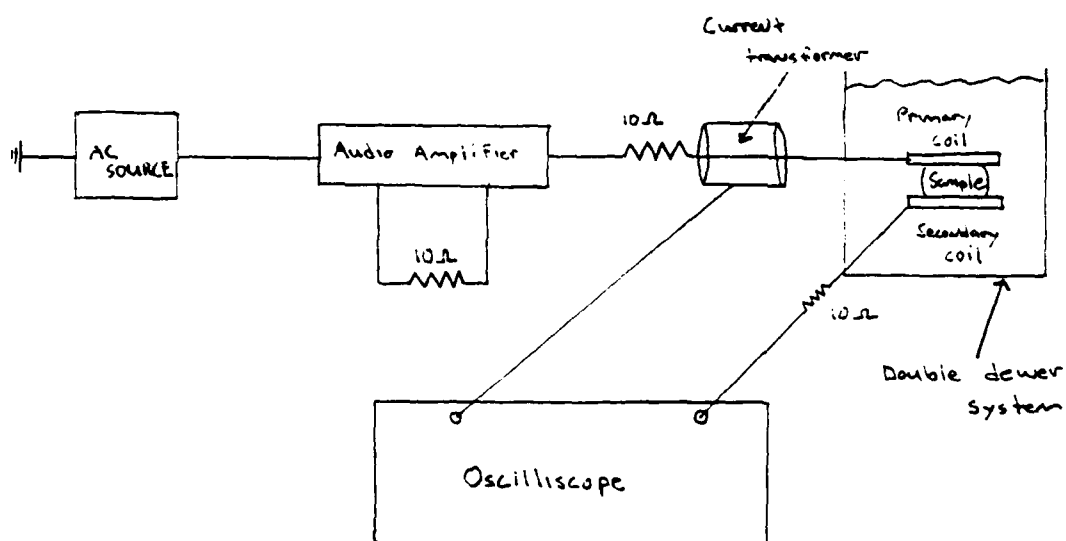
$$\Phi_s = M N_1 i_1 + L i_s \quad \text{flux of sample}$$

$$L = M(1 + \epsilon)$$

According to Harris the value of ϵ is about 2×10^{-3} . This figure is the sinusoidal background noise which is $\frac{\pi}{2}$ radians out of phase with the applied current.

The mechanics of this induction system begin with an applied current to the primary coil from some variable AC source. Thus current induces a voltage across the secondary coil (V_2). The primary and secondary coils basically form a one to one transformer. When the sample is placed between the two coils, the voltage (V_2) in the secondary coil is measured using an oscilloscope. When the system is cooled through T_c , the measured voltage (V_2) should drop to zero, excluding noise. The absence of the voltage indicates that a super current " i_s " has been induced equal but opposite to the applied current. When the input current is increased beyond a distinct threshold, tiny bumps will appear on the scope (diagram). The value of the current at which this phenomena begins is the critical current of the superconductor. The height of these blips is independent of the frequency. The critical current density (J_c) is obtained

Experimental Set-up Specs



AC Source: Wavetek Model 148A

Amplifier: Audio Amp Carver Model M-1.5

Max output 10A

Current Transformer: 1 Volt per 1 Amp

Oscilloscope: Model #7633

Double Dewers: Glass with an applied vacuum to the outer dewer

by dividing the critical current by the smallest cross sectional area of the ring.

$$I_c = \mu_c (I_{coil}) \quad \text{critical current}$$

$$J_c = I_c / A_{cs} \quad \text{critical current density}$$

The value of J_c will increase dramatically as the temperature of the superconductor is lowered further past T_c . The relationship between J_c and temperature is linear.

The preparation of $YBa_2Cu_3O_{7-x}$ depends heavily on the temperature of the furnace being very stable. A box furnace is preferred due to the stability of the temperature fluxuation. To make the $YBa_2Cu_3O_{7-x}$ material, we first mix the reagents Y_2O_3 , $BaCO_3$ and CuO in the following ratio, 1:3.5:2.1, and then grind them into a fine powder. The powder is then placed into the box furnace, sintered for twenty-four hours, removed and ground into a powder. At this point the powder should be a dark black color, similar to the grace powder. The powder is put back into the furnace, allowed to sinter for twenty-four hours at a temperature of $920^\circ C$, removed and ground back into powder form. The black powder is put back into the furnace for twenty-four hours at $940^\circ C$, removed and ground into powder form. At this point pellets can be found, and a comparison to the grace powder can be executed. After pellets are made, they are sintered for 24 hrs. at which time they should possess superconducting properties. The 4.0g pellet that was made possessed these properties before the annealing process with dry O_2 .

To strengthen the mechanical properties of $YBa_2Cu_3O_{7-x}$, Ag

can be added.

<u>% Ag</u>	<u>ρ_{comp} [Ω/cm^2]</u>
0	6.38
10	6.77
15	7.00
25	7.41
30	7.62

A full analysis of the effect of silver was not possible due to the limited number of samples that were successfully drilled. The J_c of a 15% Ag 1-2-3 superconductor with a cross sectional area of $.0279 \text{ cm}^2$ at 77K was found to be 221.5 A/cm^2 and 4193.5 A/cm^2 at 4.2K. The increase in J_c from 77K to 4.2K is expected since the dependence of J_c on T_c is a linear relationship with J_c becoming larger as the temperature is decreased further below T_c . J_c was also measured for the two remaining samples of 25% Ag 1-2-3 and 30% Ag 1-2-3, but they were found not to be superconducting. A pure 1-2-3 sample as well as a 10% Ag 1-2-3 sample were destroyed upon attempting to drill a hole through the center.

An analysis of the cross sectional area dependence of J_c was conducted using a 15% ag 1-2-3 specimen. It was observed that J_c increased as the cross sectional area was decreased until the ring became too thin to support a superconducting current. This was probably the result of the destruction of the tiny grains in which the current is carried.

<u>Area (cm^2)</u>	<u>I_{c11} (mA)</u>	<u>I_c (A)</u>	<u>J_c (A/cm^2)</u>	<u>σ</u>
.0279	95.0	6.18	221.5	-
.0212	98.0	6.37	300.4	$\pm 5 \text{ mA}$
.0194	78.8	5.12	263.9	$\pm 4.8 \text{ mA}$

<u>Area (cm²)</u>	<u>I_{crit} (mA)</u>	<u>I_c (A)</u>	<u>I_c (A/cm²)</u>	<u>σ</u>
.0180	75.0	4.88	271.1	—
.0171	65.0	4.23	247.4	—
.0143	50.8	3.27	228.6	$\pm .5mA$
.0100	—	—	—	—

Recommendations

A full analysis for the research above wasn't possible due to the limited number of samples. A diamond core drill would make it possible to turn out a great number of samples which is necessary in order to derive solid conclusions. Another useful apparatus would be a variable temperature cryostat so we could develop a better quality control of superconductors that are produced inhouse. The amplifier used at the present time can only put out about eight amps which will not be sufficient with high quality pure 1-2-3 material. A more powerful amplifier is required for highly pure 1-2-3 material.

References

Bransky and J. Bransky, "Dependence of Transport Critical Current Density on Sample Size for Ceramic $\text{RBa}_2\text{Cu}_3\text{O}_{7-x}$ ($\text{R}=\text{Y}, \text{Ho}, \text{Gd}$)," Systran Corporation, Dayton, Ohio

G. Ferguson, K. O'Grady, A. Briggs, and I. A. Denton, "Magnetic Measurements of Critical Currents in High T_c Superconductors," Critical Currents in High T_c Superconductors, Birmingham UK, 16 May 1988

E.A. Harris, J. E. L. Bishop, R. L. Havill, and P. J. Ward, "Critical and Supercritical Current Measurements by a Magnetic Induction Method," Critical Currents in High T_c Superconductors, Birmingham UK, 16 May 1988

Poole, Datta, and Farach, Copper Oxide Superconductors, Columbia, South Carolina, Wiley-Interscience Publications, 1988

1989 USAF-UES SUMMER FACULTY RESEARCH PROGRAM/
GRADUATE STUDENT RESEARCH PROGRAM

Sponsored by the
AIR FORCE OFFICE OF SCIENTIFIC RESEARCH

Conducted by the
Universal Energy Systems, Inc.

FINAL REPORT

DESIGN OF AN LDV DATA ANALYSIS SYSTEM

Prepared by:	Duane Daddis
Academic Rank:	Masters Degree Candidate
Department and	Mechanical and Aerospace Engineering
University:	State University of New York at Buffalo
Research Location:	WRDC/POPT
	Aero Propulsion Laboratory
	Wright-Patterson AFB, OH 45433
USAF Researcher:	Abdollah S. Nejad, Ph.D.
Date:	September 1, 1989
Contract No:	F49620-88-C-0053

DESIGN OF AN LDV DATA ANALYSIS SYSTEM

by

Duane Daddis

ABSTRACT

The bulk of this report is a users guide and technical reference manual for a data analysis system. This system was developed in order to extract useful information from raw LDV data. This report deals specifically with the structure of the analysis system. A theoretical description of the methods used in the analysis can be found in the final report "Large Scale Motion and Coherent Structures In Axisymmetric Swirling Flow of a Dump Combustor", written by B. Lieber.

The first section of the manual provides the user with a quick reference for operating the analysis package. This section contains the the information necessary to obtain a power spectra of the velocity field in predetermined points.

The second section provides a detailed technical description of the analysis package. The methods used in the computer codes that make up the system are also described.

ACKNOWLEDGEMENTS

For their sponsorship of this research effort, I thank the Air Force Systems Command and the Air Force Office of Scientific Research. I thank Universal Energy Systems for allowing me the opportunity to apply and expand my knowledge.

I wish also to thank all of the group at WRDC/POPT, and my supervising professor, Dr. Baruch Lieber. It was certainly an enlightening experience working with these people. Special thanks are in order for Ken Schwartzkopf, Doug Rabe, Marty Marcum, and Brian Peffley. Without their assistance in computer programming and computer operating, this research effort would not have been as successful.

I INTRODUCTION

Complex turbulent flowfields such as the type found in a dump combustor or ramjet/turbojet engine present the researcher with a difficult problem. These flows do not lend themselves to accurate modeling by conventional analytical or numerical methods. As a result, difficulties arise when attempting to predict the behavior or performance of such devices. Experimentally however, the laser doppler velocimeter provides the means to measure the velocities in complex flows with high resolution in time and space. Experimental data measured by LDV can be used to create sophisticated turbulence models needed for numerical simulation of these flows. The problem then becomes one of extracting useful information from this data. This is a challenging task, as the data measured by LDV require extensive analysis in order to extract the information necessary to construct a turbulence model.

The author of this report is presently pursuing a degree with specialization in the the area of fluid and thermal sciences at the State University of New York, Buffalo. His research interests are in the areas of turbulence and convective heat transfer. He was introduced to UES GSRP by Dr. B. Lieber, his supervising professor, who also participated in this research effort.

II OBJECTIVES OF RESEARCH EFFORT

The goal of this research effort is to develop an analysis system for LDV obtained data. The system incorporates many state of the art analysis techniques such as spectral transformations, conditional sampling, and phase conditioning. These techniques enable the decomposition of flowfield variables into different physical categories. Results from this analysis package will ultimately aid in the construction of sophisticated turbulence models. These models will provide computational fluid mechanitians with a useful tool for modeling turbulent velocity fields.

III

U S E R S G U I D E & T E C H N I C A L

R E F E R E N C E M A N U A L

for

L D V D A T A A N A L Y S I S P A C K A G E

BY: Duane Daddis &
Barruch Lieber

FORWARD

The objective of this package is to obtain the power spectrum of velocity fluctuations in a turbulent velocity field. This is accomplished with a series of FORTRAN programs. There are three main programs that make up this system. The first program reads raw LDV data from magnetic storage tapes and creates files on a storage disk so they may be more easily accessed for analysis. The second program creates an equally-spaced data array from the raw data file. This is necessary for subsequent analysis. The final program calculates the power spectrum of the data.

The first section of this manual provides the user with a quick reference for operating the package. This contains all the information necessary to obtain a power spectrum at a desired point in a velocity field.

The second section gives a detailed technical description of the package. The theory that was used to develop the FORTRAN code in the subroutines is presented here. This section is intended for the user who wishes to further develop the system, or wishes to check the validity of the calculations.

PART I QUICK USERS REFERENCE

Logon Procedure:

To logon to the VAX 8650 VMS from a VT-340 terminal, the following procedure must be executed.

- 1) Type CTRL A for menu.
- 2) Type .POMIS to choose VMS VAX.
- 3) Type NEJADAS for user name.
- 4) Type DADDISED for password.

Tape Mounting Procedure:

The package is currently set up to read data from tapes that were recorded on the MODCOMP computer system. The following tapes are on file with the system operators, ready to be mounted.

- NEJ TAPE 1 - swirl#-0.3, axial position- 1 in
- NEJ TAPE 2 - swirl#-0.3, axial position- 2 in
- NEJ TAPE 3 - swirl#-0.3, axial position- 3 in
- NEJ TAPE 4 - swirl#-0.3, axial position- 6 in
- NEJ TAPE 5 - swirl#-0.3, axial position- 4 in

To read a tape the user must follow this procedure:

- 1) Choose tape to look at.
- 2) Call system operator at 54972.
- 3) Ask to have tape mounted on VMS VAX.

Allow several minutes for the tape to be mounted then continue with the following procedure.

Tape Read Procedure:

To read the tape that has just been mounted, type the following command at the VAX \$ prompt.

RUN READTAPE

This starts the program READTAPE that reads the tapes. The program takes about 30 seconds to read the first file, then gives the user several options for control of the tape. The options are:

TYPE 0 TO SAVE FILE ON DISK: If a zero is typed here the program will then ask for a file name to store the data in. The user should type in a file name here. A file will then be created.

TYPE 1 TO SKIP THIS FILE: This allows the user to continue on to the next data file without storing data from the current file.

TYPE 2 TO QUIT: This allows the user to stop the tape read procedure, and exit the READTAPE program.

TYPE 3 TO REWIND: This allows the user to rewind back to the first file on the tape.

TYPE 4 TO AVERAGE FILE: This option allows the user to determine the average velocities at the different radial positions on the tape, in order to construct an average velocity profile. If the user chooses this option, the profile data are stored in the file PROFILE.DAT.

Possible Errors:

The following are several errors that may occur while running this program.

1) Exceeded storage in account. The data files on the tapes require large disk space to store. If the user tries to store many files at once he will surpass the limit set on the account. This

may be overcome by reading in only several files at a time and completing processing of these files. These files can then be deleted and the next files can be read in, and processed.

2) No header returned: This means that the end of the tape has been reached. Type either 2 to quit, or 3 to rewind.

Equally-Space Data:

Once there are several raw data files in the directory, the analysis programs can be run. The first program is the equal-spacing routine. To start this, type at the VMS prompt \$:

RUN LDV

The program will ask for the name of the file that was saved from the tape that is to be equally-spaced. The user should type in the file name excluding the extension.

Next the program will remove the bad points from the data. The user must type in the number of standard deviations from the mean that he considers the limit for good data. A typical input is 3 to 5 standard deviations.

Now the program will start the equal-spacing procedure. The average sampling rate is output to the screen, and the user is prompted to choose an equal-spacing method. The choices are:

TYPE 1 FOR A LINEAR INTERPOLATION: It is the authors recommendation to use this method.

TYPE 2 FOR SAMPLE AND HOLD: This method is well accepted however, it has not been tested to the authors satisfaction.

TYPE 3 FOR SLOTTED TIME WINDOW: The authors caution against using this method due to the fact that it has not been made fully

compatible with the system. Also, the power spectrum program will not run with the output of this routine.

Next, the system will ask for the desired sampling rate of the equally-spaced data. If the user uses either of the first two choices above, he is warned to use a sampling rate that is $1/2$ or smaller than the original average sampling rate. If the user selects choice 3 above, he should use a sampling rate that is about $1/10$ of the raw data average sampling rate, and a window width in the range of 0.0 to 0.5.

After the operator inserts the desired data rate, the system performs the equally-spacing procedure. It then requires the input of a file name for the equally-spaced data file. The data array is stored in the directory under this file name, and the equally-spacing procedure is complete.

Calculate Power Spectrum:

To enter the program that calculates the power spectrum, type:

RUN SPAN

at the \$ prompt. The program will ask for the name of the equally-spaced data file. Input the file that was made from the LDV program. The program then asks the user to input the number of points per block (for ensemble averaging) to be used in the power spectrum estimates. The maximum number is 1024, and it must be an integer power of 2. The author suggests the use of 1024 points per block unless the data record is shorter than 12,000 points. The next requirement is the input of the autoregressive (AR) model order. The range is any integer from $1/16$ to $1/2$ the number of

points per block input above. For example, with a block size of 1024, an model order of 80-100 yields a good AR spectrum estimate. After these parameters are chosen, the program calculates the fast fourier transform (FFT), and the autoregressive model spectra. The program then asks for input of the file names, where the FFT and AR data is to be stored. These files each consist of two columns one half the number of points per block in length. The left column contains the logarithm or linear(specified by the user) frequency (x axis), and the right column contains the spectral magnitude in dB (y axis). The user may then plot these files using the plotting system of his choice.

PART II REFERENCE MANUAL

Structure of Raw Data File

The following is a description of how the input file (raw data) is set up in order to be compatible with the data analysis system. It should be noted here that due to the installation of a new data acquisition system at the aero propulsion laboratory where this research was done, there is an inconsistency in the way in which data is recorded. The new data acquisition system creates files with a different structure than the files this analysis package is set up to read. Therefore, the system must be modified in order to read the data files created by the the new acquisition system.

As the system is now set up, the input file must be in binary form. The first line of the file contains the number of data points in the file. The second line of the file must contain information on the time, and date that the data was recorded. This line should be recorded as character data. The third and all following lines contain the velocity data. Recorded are the time, axial velocity component, and tangential velocity component.

Removal of Inaccurate Data

In an array of turbulence data recorded with an LDV, there are some points where the velocity varies greatly from the mean (± 5 standard deviations). It is thought that these points can not represent an actual measurement of the velocity, and must be in error (Srikantaiah 1985). Therefore, these "bad" points must be

removed from the data record. The following is the procedure used by this system in order to remove these points.

First, the raw data file must be averaged in order to find the mean value of the velocity (axial or tangential). For data recorded with an LDV (data with unequal intervals between points), the following equation is used:

$$XBAR = \frac{1}{T} \sum_{i=1}^n \left[\frac{V_{i+1} + V_i}{2} \right] \times (t_{i+1} - t_i) \quad \text{eq 1}$$

The mean velocity is XBAR. T represents the total length of time the data was accumulated over. T can be found by summing up all the individual time intervals between points, or it is also the difference between the last and first recorded times in the data file. V(i) and t(i) represent the instantaneous velocity and time respectively.

The standard deviation of the velocity SD, is calculated by:

$$SD = \left[\frac{1}{n} \sum_{i=1}^n (V_i - XBAR)^2 \right]^{1/2} \quad \text{eq 2}$$

In this equation, n represents the number of recorded data points.

With the standard deviation calculated, the system prompts the user to specify the number of standard deviations from the mean, A (A is the notation used in the FORTRAN programs) he considers the limit for good data. When this is input, points are removed if they fall outside the range $XBAR \pm A * SD$. To remove a bad point the system eliminates the point from the record as if it were never recorded.

Equally-Spacing The Data In Time

It is necessary to have equal time intervals between the data points, in order to perform certain operations on the data. Most data analysis programs are designed for this type of input. Some examples are the fast fourier transform (FFT), and the digital filters. Turbulence detection techniques (conditional sampling) such as variable interval time averaging (VITA) may require this also.

The analysis package is set up with three different methods for equal spacing data. The option of choosing which of the three methods to use is given to the user. The author finds it necessary to provide this option for user preference, and it is a convenient way to check the results.

The first method is one which uses a linear interpolation between points to create the equally spaced data. This is a newer method which is recently beginning to see use. The method estimates the value of the velocity between two points as a straight line connecting the points. This in effect, makes a continuous signal of the data. The system then requires the user to input the data rate for the equally spaced data file. An array of equally spaced data is then interpolated from the series of straight lines. Note that in order to comply with the Niquist criteria, this data rate should be no more than $1/2$ the average data rate from the raw data.

The second method is the sample and hold technique. This method is similar, but less sophisticated than the previous method. Instead of creating a continuous signal from the data by interpolation, this technique assumes a constant value for the

velocity between points. Again, the user should not use a data rate greater than $1/2$ the average rate of the raw data.

The third method is the slotted time window method. This method has been developed by the researchers at WRDC/POPT. It equally spaces data by having a user specified window to find points that are within a certain range of where an equally spaced point should be. The average raw data rate must be very high compared to the desired equally spaced data rate to use this method (possibly 10X higher). If this is not the case, the new equally-spaced data file will have many "holes" where no data points at all were found within a window. Steps have been taken by the author to alleviate the problems associated with this method, but at this time it is not compatible with the proceeding spectral analysis methods in this package.

Spectral Analysis

This system provides the user with two different methods of computing a power spectrum from velocity data; the fast fourier transform (FFT) and autoregressive modeling (AR). For technical information on these methods, the user is referred to the final report by B. Lieber, " Large Scale Structures and Coherent Structures in Axisymmetric swirling Flow of a Dump Combustor ".

IV RECOMMENDATIONS

The reduction of LDV data to information necessary to construct advanced turbulence models requires extensive analysis. This research effort, though significant, constitutes only a first step in providing this large scale analysis. This researcher suggests that the data analysis system designed here, be further developed. The many conditional sampling, spectral transformation, and filtering techniques should be combined into one large general LDV data analysis package. This system should also be integrated with the proper graphics to provide convenient presentation of results.

The author also recommends that a detailed study be made on turbulence models such as large eddy simulation, that are constructed with information available from techniques mentioned herein. Ultimately, the author envisions a close tie between the data analysis package and a numerical model, thus enabling the prediction of the nature and behavior of certain complex flow fields.

V REFERENCES

Srikantaiah, D.V. and Coleman, H.W., "Turbulence Spectra From Individual Realization Laser Velocimetry Data", Experiments in Fluids 3, 1985, pp 35-44.

Lieber, B.B., "Large Scale Motion and Coherent Structures in Axisymmetric Swirling Flow of a Dump Combustor". Final Report submitted to Universal Energy Systems Inc. Sept., 1989. Contract # F49620-88-C-0053

1989 USAF-UES SUMMER FACULTY RESEARCH PROGRAM

GRADUATE STUDENT RESEARCH PROGRAM

SPONSORED BY THE

AIR FORCE OFFICE OF SCIENTIFIC RESEARCH

CONDUCTED BY THE

UNIVERSAL ENERGY SYSTEMS, INC.

Preparation of a Dump Combustor for IDA Measurements

FINAL REPORT

PREPARED BY:	ROBERT S. GABRIK
ACADEMIC RANK:	MASTERS OF SCIENCE STUDENT
DEPARTMENT AND	MECHANICAL ENGINEERING
UNIVERSITY:	VIRGINIA TECH
RESEARCH LOCATION:	WRDC/POPT
	WRIGHT-PATTERSON AFB
	DAYTON, OH 45433
USAF RESEARCHER:	ABDOLLAH NEJAD
DATE:	20 SEPT 89
CONTRACT NO.:	F49620-88-C-0053

Preparation of a Dump Combustor for

LDA Measurements

by

Robert S. Gabruk

ABSTRACT

To examine the effects of combustion on the flowfield of a ramjet engine, a water-cooled, stainless steel dump combustor model was developed. Two main goals had to be met before any flowfield data could be obtained. First of all, the combustor had to be configured to operate in an acceptably stable mode. Stability was identified by the pressure spectra obtained under various running conditions using piezoelectric pressure transducers wired to a spectrum analyzer. Operational parameters such as fuel composition, fuel injection location, acoustic configuration, and equivalence ratio were varied until instabilities were minimized. The optimal configuration ran with upstream fuel injection (premixed mode) with propane as the fuel. Injection occurred near the centerline of the inlet duct with an equivalence ratio of 0.65. An orifice plate was installed to change the acoustic character of the duct and to enhance fuel-air mixing.

After the combustor was configured to run in an acceptable mode of operation, the data acquisition system (NEFF 470) was updated as to correctly measure and calculate inlet and combustion conditions. Furthermore, a user's help manual was written to simplify the process of learning the system.

Acknowledgements

First of all, I wish to thank the Air Force Systems Command and the Air Force Office of Scientific Research for sponsoring such a beneficial program. U.E.S also deserves a great deal of appreciation for providing me with all of the information necessary for a comfortable and productive research session.

My experience would not have been as enriching without the support of Abdollah Nejad. He provided me with all of the tools needed to carry out my obligations as well as providing me with the encouragement I needed when things were not running as smoothly as expected. Further, I wish to extend my gratitude to Saad Ahmed and Charles Smith for all of their assistance throughout the program.

I. INTRODUCTION:

The study of a dump combustor (sudden expansion) flowfield can be of significant value in the aerospace industry. Dump combustors are characteristic of the widely used ramjet engine. Therefore, if one is able to characterize the flowfield of a particular dump combustor, the information can be used in the future design of larger, usable (in aircraft) ramjet engines. This can save significant time and money that would be otherwise used in testing these larger models.

Of particular interest is the effect of combustion on the flowfield. To examine the effect of combustion, cold flow data will be compared to that of the hot (combusting) flow. The cold flow data has already been well documented, therefore, only hot flow data acquisition is necessary. However, to do so, a stable running combustor had to be configured. This is what the summer research concentrated on. That is, modifying as already constructed rig (as well as the attached data acquisition system) to run with minimal instabilities.

My research interests are in the area of internal flows, both with and without combustion. This summer provided me with my first real research effort.

II. OBJECTIVES OF THE RESEARCH EFFORT:

My incoming objectives were to document the effects of heat release on the flowfield of a dump combustor and to provide a quality set of data that could be used in the development of numerical codes. Although these goals still exist, others arose during the research program.

My first (and most important) objective was to assist in the determination of a stable running condition for the combustor. Two pressure transducers (at two locations along the inlet duct to the combustor) were wired to a Nicolet spectrum analyzer to aid in the resolution of the most stable running condition. Various operational parameters were changed in order to realize the most stable mode.

My second objective of the research period was to study and document a newly implemented data acquisition system. This system would provide us with necessary information such as combustion and inlet conditions. I needed to learn the system as well as document how it worked so that anyone could use system without wasting valuable time reading the complicated user's manual.

III.

a. As stated previously, quality baseline data for non-reacting flow through a dump combustor has already been obtained. These results have been acquired using a plexiglass dump combustor model with an area ratio of 2.25. A two-component, frequency-shifted, backscatter LDA system was used to obtain mean velocity and turbulence data. TiO_2 particles were used as the seeder. Typical validation rates in each LDA channel ranged from 5000 to 10000/sec, while stored data rates ranged from 2000 to 6000/sec (using a 20 μsec coincidence window requirement). Samples were collected to calculate mean velocities, rms fluctuations, and Reynold's stresses. The inlet velocity at the dump plane was 16 m/s, which corresponds to a Reynolds number of 1.03×10^5 .

For the reacting case, a stainless steel, water-cooled dump combustor was constructed. It is shown in figure 1. The design has the same characteristic dimensions as the plexiglass model and has a high-quality quartz window for optical access to the flowfield. The original design called for downstream fuel injection at the inlet duct walls, with ethylene being used as the fuel. An orifice plate was not initially installed.

As originally constructed, the combustor ran very unstable, with significant low frequency vibrations. Quality LDA measurements could not be obtained under these conditions. So, the first priority was to have the dump combustor running with an acceptable mode of stability. Variable parameters were fuel type, fuel injector location (axially and radially), equivalence

ratio, and acoustic configuration. Piezoelectric pressure transducers (mounted in the duct upstream of the dump) were wired to a Nicolet 660 A dual-channel FFT analyzer. The pressure spectra from the FFT helped identify instabilities. Desirable characteristics included a low operating temperature, low pressure fluctuations, a non-predominance of specific frequencies, and a minimum of very low frequency component. In the baseline configuration, light-off occurred with a large detonation, and frequent flashback and low-frequency oscillations were produced during operation. The flashback was believed to have occurred in the low velocity regions near the wall of the inlet duct. Therefore, the fuel was changed from ethylene to propane - a fuel with a lower flame speed and smaller quenching distance. Although the flashback was eliminated, the combustor still ran unstable. The coherent output power spectrum of the baseline configuration (with propane) is shown in figure 2. (Coherent output power indicates the output power of one input channel that is linearly related to the other. It is a good indication of the acoustic power due solely to system response.) The total rms pressure level was 0.296 in the duct interior. The equivalent value for the nonreacting case was 0.0228 psi.

The next step was to change the axial position of the fuel injectors. With the fuel injectors located downstream (just upstream of the dump plane), it was believed that a flame that was diffuse in nature was being created. Further, this diffusion flame had constantly changing fuel-rich zones which contributed

to the instability of the system. Therefore, the fuel injection was moved far upstream, far enough to create a premixing of the air and fuel. The fuel injectors consisted of four 0.125 in. diameter tubes located 11 ft. upstream of the dump. Each tube entered the duct radially, had an orifice of 0.065 in. diameter located in the side, and allowed for injection at various radial distances from the duct centerline. Although a decrease in instability was achieved, the combustor was not running in an acceptable mode. Spectral data was not obtained since the combustor would not run under an equivalence ratio of 0.8. This means that the system would only run under unacceptably hot conditions.

Further, an orifice plate was implemented just upstream of the new fuel injection location. A 2.00 in. diameter plate was installed in the 4.00 in. diameter inlet duct. It was believed that the plate would reduce airflow-coupled instabilities, isolate the reaction region from the large resonant contribution of the settling chamber, and provide acoustic tuning. The coherent output power of the system with the orifice plate and downstream fuel injection is shown in figure 3. In comparing figures 2 and 3, one can see significant improvement. Note the magnitudes on the vertical axis. Although the pressure fluctuations are still dominated by narrow bandwidth signals, the total levels decreased by over an order of magnitude.

Considerable improvement was observed when the fuel injection was moved back to the upstream location while the orifice was in

place. Further, even more improvement was discovered as the fuel injection was moved radially inward (at the upstream location). Figure 4 shows the coherent power output versus the radial location of the injection. The fuel injectors were moved radially from the recirculation region (caused by the orifice), through the high shear regions of the orifice flowfield, and into the high-speed core near the duct centerline. The curve in figure 4 demonstrates yet another benefit of adding the orifice plate - enhancing mixing. As can be seen from the curve, the coherent power output decreases as the fuel injectors are moved through the recirculation region, flattens out near the shear region, and drops off further as they moved through the core region. The lower coherent output power acknowledges the fact that better mixing is occurring in the high-speed core. Note that the coherent output power levels are close to two orders of magnitude lower than that of figure 2. The combustor was now running with an acceptable amount of instability.

The next problem was determining what equivalence ratio to operate with. It is important to run at a low equivalence ratio (while maintaining stability) in order to keep combustion temperatures down. Equivalence ratios were varied from 0.575 to 0.8. The results are shown in figure 5. At the higher fuel flows, the coherent output power varies directly with fuel flow, as would be expected from thermoacoustic efficiency arguments. However, below 0.6, the power increases as the thermoacoustic energy release decreases. This was accompanied by unstable operation

and a shift to low frequency dominant peaks in the power spectrum.

Based on these results, it was decided to continue the research effort under the conditions of premixed combustion with an equivalence ratio of 0.65 and fuel injection near the inlet duct centerline. Figure 6 shows the coherent power output spectrum for this configuration. Compared to the initial configuration (figure 2), it can be seen that the spectrum is broadened, shifted to higher frequencies, and the power levels are lower by two orders of magnitude. The rms average pressure was 0.065 psi, which is 15% of the original configuration.

b. Decreasing the instabilities of the dump combustor to an acceptable level was only part of the necessary preparatory steps. The learning of the data acquisition system was also a very significant part. After all, the research effort is meaningless unless there is a way of obtaining data. The system implemented here was the NEFF model 470. A good deal of time was spent studying this system and preparing an "easy-to-read" user's manual. Since this manual applies only to those interested in this particular acquisition system, it is not included in the body of the report. See the appendix for a copy of the manual.

IV. RECOMMENDATIONS

a. Increasing the combustion stability of an experimental rig can be of major concern in preliminary testing. In order to acquire quality flowfield data, the combustor must be running in

a stable mode. The best way of deciding upon an appropriate configuration is by applying some engineering sense. One must first identify all of the possible variable parameters and then decide which of these are most likely to influence stability. Power spectra may then be used to help identify the instabilities. By comparing the power spectra for each operating condition, one can recognize trends that can help in determining a suitable combustor configuration. For the dump combustor studied here, it was shown that the best configuration called for premixed combustion with an equivalence ratio of 0.65 with fuel injection near the inlet duct centerline, immediately following an orifice plate.

b. The NEFF data acquisition system is fairly complex, however, it is easy to use upon proper instruction. The attached manual should simplify the process of learning the NEFF and implimenting some of its programs.

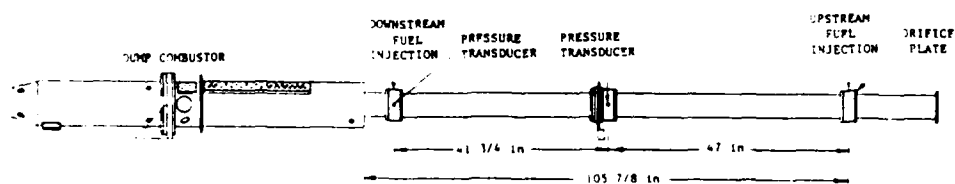


FIG. 1. SCHEMATIC OF DUMP COMBUSTOR SYSTEM

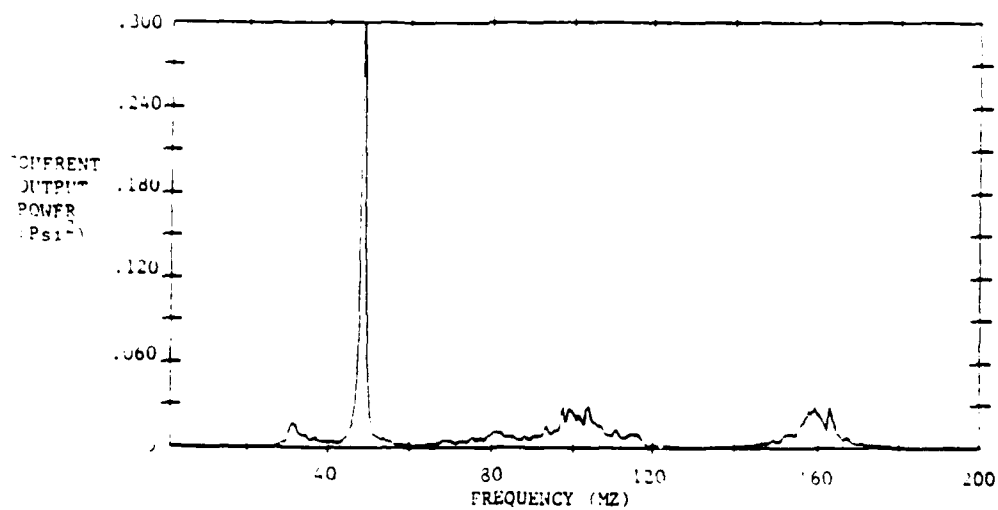


FIG. 2. COHERENT OUTPUT POWER VS. FREQUENCY FOR DOWNSTREAM FUEL INJECTION WITH NO ORIFICE PLATE

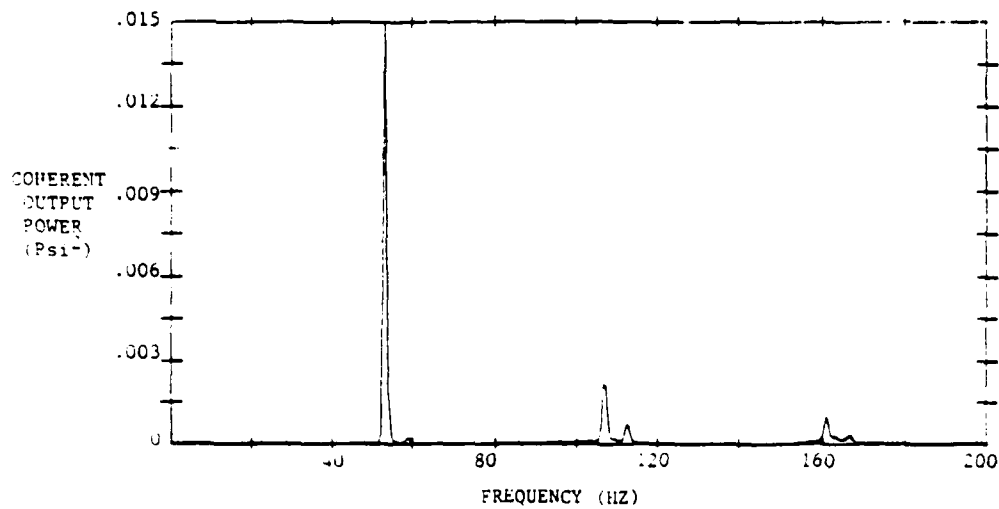


FIG. 3. COHERENT OUTPUT POWER VS. FREQUENCY
FOR DOWNSTREAM FUEL INJECTION WITH ORIFICE PLATE

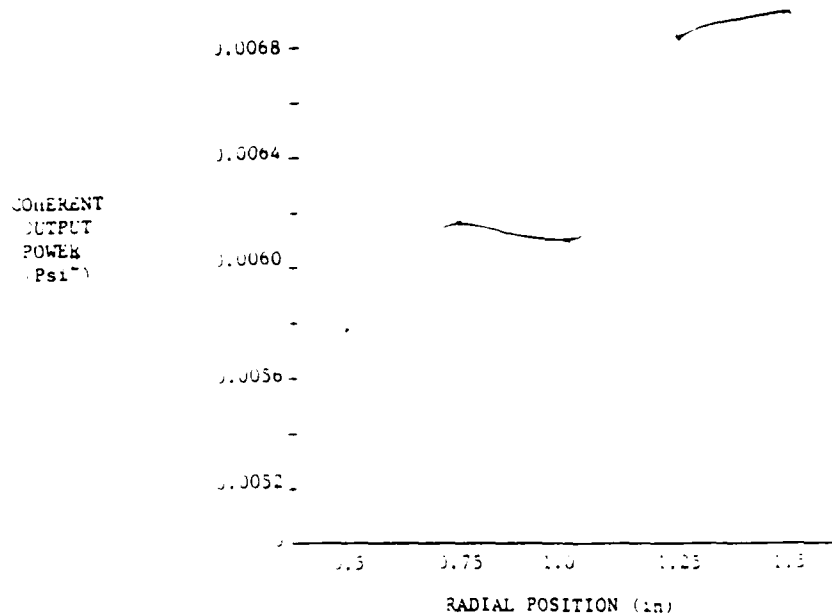


FIG. 4. COHERENT OUTPUT POWER VS. RADIAL
POSITION OF UPSTREAM FUEL INJECTORS
(EQUIVALENCE RATIO = 0.77)

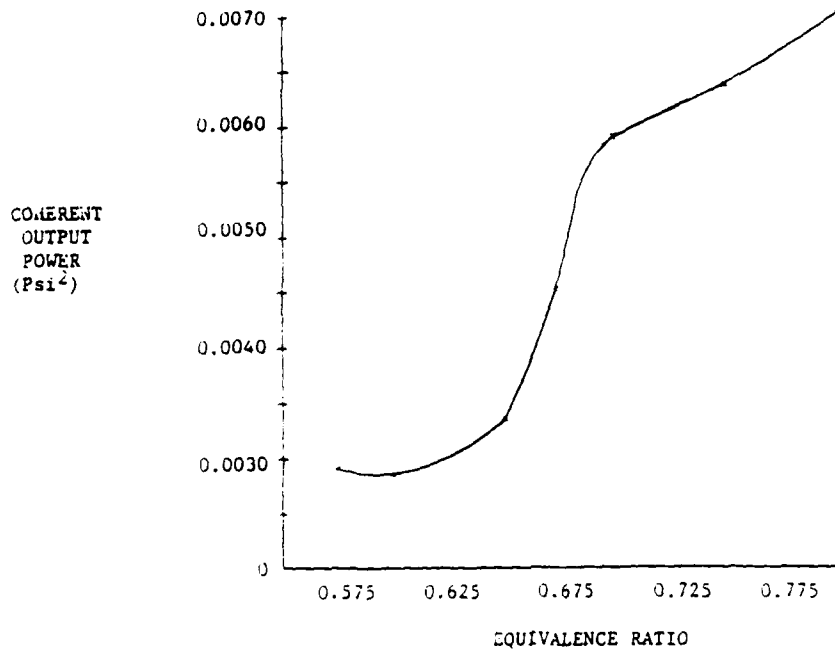


FIG. 5. COHERENT OUTPUT POWER VERSUS
EQUIVALENCE RATIO
(FUEL INJECTOR RADIAL POSITION = 0.5 in)

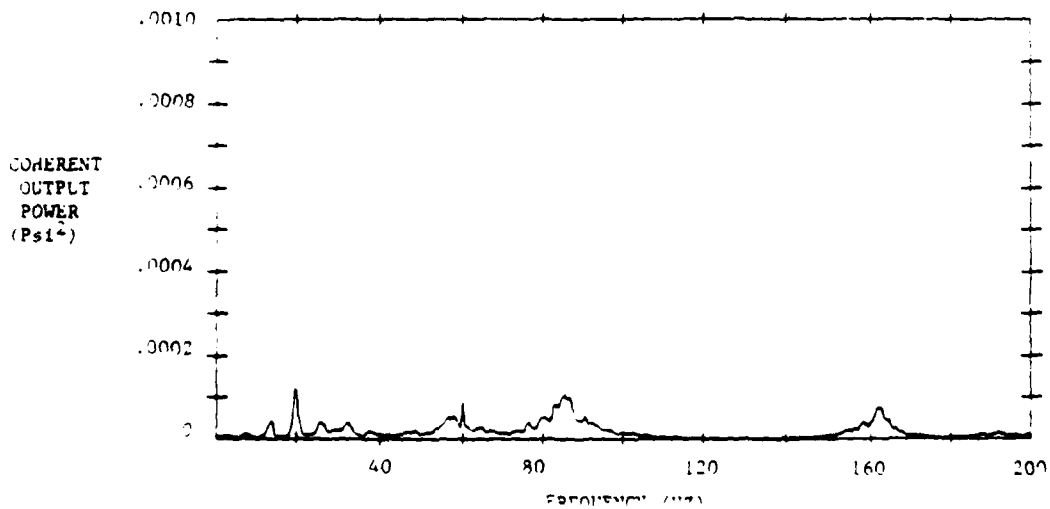


FIG. 6. COHERENT OUTPUT POWER VS. FREQUENCY
FOR UPSTREAM FUEL INJECTION WITH ORIFICE PLATE

REFERENCES

Favaloro, S.C., Nejad, A.S., Ahmed, S.A., Miller, T.J., and Vanka, S.P., "An Experimental and Computational Investigation of Isothermal Swirling Flow in an Axisymmetric Dump Combustor," AIAA 89-0620, 1989.

Reardon, F.H., "An Examination of Some Possible Mechanisms of Combustion Instability in Liquid-Fuel Ramjets," AFWAL F33615-81-C-2078, 1986.

Roe, L.A., Gabruk, R.S., Nejad, A.S., and Favaloro, S.C., "Stability Characterization of a Dump Combustor," Paper no. 77, Eastern Section of the Combustion Institute, Albany NY, 1989.

APPENDIX MAY BE OBTAINED
FROM AUTHOR OR
UES

1989 USAF-UES SUMMER FACULTY RESEARCH PROGRAM

GRADUATE STUDENT RESEARCH PROGRAM

Sponsored by the
AIR FORCE OFFICE OF SCIENTIFIC RESEARCH

Conducted by the
Universal Energy System, Inc.

FINAL REPORT

FLOW LIMITATIONS IN MICRO HEAT PIPES

Prepared by:	Frank M. Gerner, Ph.D. <u>Jon P. Longtin</u> , Graduate Student
Academic Rank:	Assistant Professor
Department and University:	Department of Mechanical and Industrial Engineering University of Cincinnati
Research Location:	Aero Propulsion and Power Laboratory Wright Research and Development Center Wright-Patterson AFB, OH 45433
USAF Researcher:	Won S. Chang
Date:	8 Sept., 1989
Contract No:	F49620-88-C-0053

Same Report As
Prof. Frank Gerner
(Report # 92)

1989 USAF-UES SUMMER FACULTY RESEARCH PROGRAM/
GRADUATE STUDENT RESEARCH PROGRAM

Sponsored by the
AIR FORCE OFFICE OF SCIENTIFIC RESEARCH
Conducted by the
Universal Energy Systems, Inc.

FINAL REPORT

LASER INDUCED FLUORESCENCE PROBE OF CH RADICAL

Prepared by:	John E. McCord
Academic Rank:	Graduate Student
Department and	Chemistry Department
University:	Murray State University
Research Location:	Aero-Propulsion Laboratory Building 450, Lab D-193 Wright-Patterson Air Force Base
USAF Supervisor:	Dr. Peter Bletzinger
Date:	11 September 1989
Contract No:	F49620-88-C-0053

LASER INDUCED FLUORESCENCE OF CH RADICAL

by

John E. McCord

ABSTRACT

The capability for laser excited fluorescence detection of radical species (primarily CH) has been developed for Dr. Peter Bletzinger's laboratory in room D-103, building 450 at Wright-Patterson AFB. It is intended that this technique be used to measure diffusion and loss rates of deposited radicals in frozen rare gas matrices at various matrix temperatures.

I. INTRODUCTION:

Methylidyne radicals (CH) are being evaluated at the Wright Research and Development Center (WRDC) at the Wright-Patterson Air Force Base as a potential high energy density material. A neutralized ion beam apparatus has been constructed by Bletzinger and Ruark (1989) to selectively deposit CH radicals in a frozen argon matrix.

Evaluation of matrix storage of CH radicals requires the measurement of diffusion and loss rates of the deposited CH radicals. The diagnostic technique that was selected for this study is laser excited fluorescence spectroscopy using a tunable dye laser.

The existing excimer-pumped dye laser in the laboratory, which was intended for fluorescence probing of the radicals, was not operating up to desired specifications. For future CH laser induced fluorescence (LIF) experiments, it would be necessary for this laser system to function properly. It would also need to have an optical system capable of collecting the fluorescence light from the matrix-isolated radicals.

My research experience has been with excimer and diode lasers used in photolysis and absorption probes respectively. I have also had experience in the design and development of optical systems used for the collection of

signals resultant from laser probes. This technical experience contributed to my assignment in Dr. Bletzinger's laboratory along with dye laser specialist Dr. David A. Dolson from Wright State University.

II. OBJECTIVES OF THE RESEARCH EFFORT:

My overall assignment as a participant in the 1989 Graduate Student Research Program (GSRP) was to aid in the establishment of quantitative procedures involving tunable dye laser fluorescence spectroscopy for the analysis of free radicals (primarily CH) deposited in frozen gas matrices. A correlation of fluorescence signal strengths with time-integrated ion currents would provide a basis for this work. If successful, these procedures would then provide the capability to investigate spatial diffusion rates of the matrix-isolated CH radicals. It was planned that an existing residual gas analyzer would be used to assist in these measurements by sampling the gaseous species desorbing from the cryostat as it was warmed.

In achieving this overall goal, I would also have to evaluate and test the existing excimer-pumped dye laser. Eventually, this system would be tuned in the 380 nm - 435 nm spectral region in order to excite fluorescence from CH radicals, using the B-X and A-X electronic transitions. I

would also help design the optical system that would be used to collect fluorescence light from the matrix-isolated radicals.

As stated, the initial objective was to extend the fluorescence observations to CH radicals deposited in a rare gas matrix; however, the matrix deposition apparatus was undergoing modifications when Dr. Dolson and I were ready to proceed. After consultation with Dr. Bletzinger, we decided to further pursue laser excited fluorescence detection of gas phase CH radicals. It was felt that this experience would be valuable in optimizing the fluorescence collection optics and in estimating the CH detection limits. Moreover, it would develop the technique for subsequent use in future studies of the importance of CH in the growth of diamond-like carbon films in plasma environments.

III. APPROACHES AND RESULTS:

Much of my preliminary work involved the alignment of the existing dye laser so that it would operate near the original specifications (approximately 16 mJ/pulse at 30 Hz rep rate). Shortly after this, we successfully obtained the laser excited fluorescence spectrum of CH radicals in an atmospheric pressure methane/oxygen flame. The reproduction of this simple experiment, first done by Garland and Crosley

(1985), served as the initial test of our abilities.

As for the optical system designed for our experiments, fluorescence was collected with an f/3.5 lens, and detection was accomplished with a sensitive photomultiplier tube (PMT). The amplified signal from the PMT was large enough so that a gated integrator could be used to analyze the photomultiplier output and to enhance the signal-to-noise-ratio (S/N).

In accordance with our decision to further pursue LIF detection of gas phase CH radicals, Dr. Dolson and I assembled a fast-flow tube apparatus in which CH radicals in the ground electronic state were produced by collisions of helium metastable atoms with methane or acetylene molecules. CH radicals in the excited state have been studied previously by Chang and Setser (1978). This apparatus underwent several modifications, all of which have led to the generation of quite acceptable CH fluorescence excitation spectra. The CH spectrum in Figure 1. is a portion of the R-branch of the 0-0 band of the A-X transition. It was obtained by scanning the laser wavelength while detecting the emitted light through a 10 nm bandpass filter centered at 430 nm. In this example the CH was generated from $\text{He}^* + \text{methane}$. The spectral positions of the vibrational and rotational peaks have been assigned according to Moore and Broida (1959). The presence of

rotational lines of the 1-1 band enables the measurements from which vibrational state distributions may be determined.

Observations of fluorescence intensity as a function of laser power indicated that a linear relationship existed only up to laser pulse energies of 0.2 mJ on the stronger lines. The weaker lines showed no indication of saturation below 1 mJ pulse energy. In order to ensure linearity all spectra were obtained with ≤ 0.2 mJ pulse energy. Preliminary examination of spectra obtained after 500 μ s contact time with hydrocarbon concentrations ranging from 1×10^{12} to 1×10^{13} cm^{-3} gave no evidence of vibrational relaxation. This absence of measurable relaxation suggests that the observed vibrational energy distribution is the nascent distribution of CH radicals in the ground electronic state.

Further analysis of the spectra through Boltzmann plots showed that the nascent vibrational populations of CH generated from acetylene could be described by a "temperature" of approximately 2600 K, and that the rotational level populations were in equilibrium at a temperature of approximately 390 K (See FIGURES II and III). Preliminary evaluation of the CH spectrum indicates that the vibrational "temperature" of CH generated from methane was somewhat less (2400 K) than that of CH from acetylene.

At present, the rotational energy temperature profile of the flame generated in our fast-flow cell is being determined. Overall, our major accomplishment is that we have been able to develop the capability for this laboratory to carry out laser excited fluorescence detection of radical species. It is likely that the completed analysis of the data will lead to a short publication of the nascent CH vibrational distribution from helium metastable reactions with acetylene and methane.

IV. RECOMMENDATIONS

I have two suggestions that could be implemented when the time has come for probing the CH radicals deposited in frozen rare gas matrices.

One concerns the way in which the CH radicals are actually put into the frozen matrices. The current laboratory method used by Bletzinger and Ruark involves generating the CH radicals with an ion gun, neutralizing the radicals in a charge exchange chamber, and then depositing CH and argon on the cold finger of a cryostat. Instead of processing the CH through this intricate system, an aperture could be put on the helium-methane discharge exit end of the fast-flow glass cell. Then, CH radicals could simply be leaked out onto a cooled surface with argon gas. Although

this technique would be capable of more rapid deposition of higher quantities of CH, it lacks the elegant selectivity of the neutralized ion beam deposition. In fact, the parent hydrocarbon concentration is likely to be one or two orders of magnitude higher than that of the radical species.

My other suggestion concerns a way in which to check whether or not CH does indeed fluoresce in a frozen matrix. This check could be done by depositing CH₄/argon or C₂H₂/argon in a matrix and then exposing the matrices to vacuum ultra-violet radiation to generate CH radicals by photolysis. This study would determine if CH was made (along with other molecules) from the precursor suspended in the matrix.

ACKNOWLEDGEMENTS

I wish to thank the Air Force Systems Command and the Air Force Office of Scientific Research for sponsorship of this research. I also wish to thank Universal Energy Systems for again giving me the opportunity to participate in this research program.

My research experience this past summer was very rewarding, as well as very educational. Dr. David A. Dolson is always supportive of my efforts, and I welcomed the opportunity to work with him again. The technical assistance provided by Mr. Bob Knight on this project was invaluable. Many thanks to the father and son glassblowing team of Jimmy and Mike Ray for their quick turnaround on our glass cell designs. A very special thanks is extended to Dr. Peter Bletzinger, who is chiefly responsible for my being brought aboard on this research project. The availability of his laboratory facilities and the friendly and encouraging atmosphere he maintained were very conducive to the progress made during this endeavor.

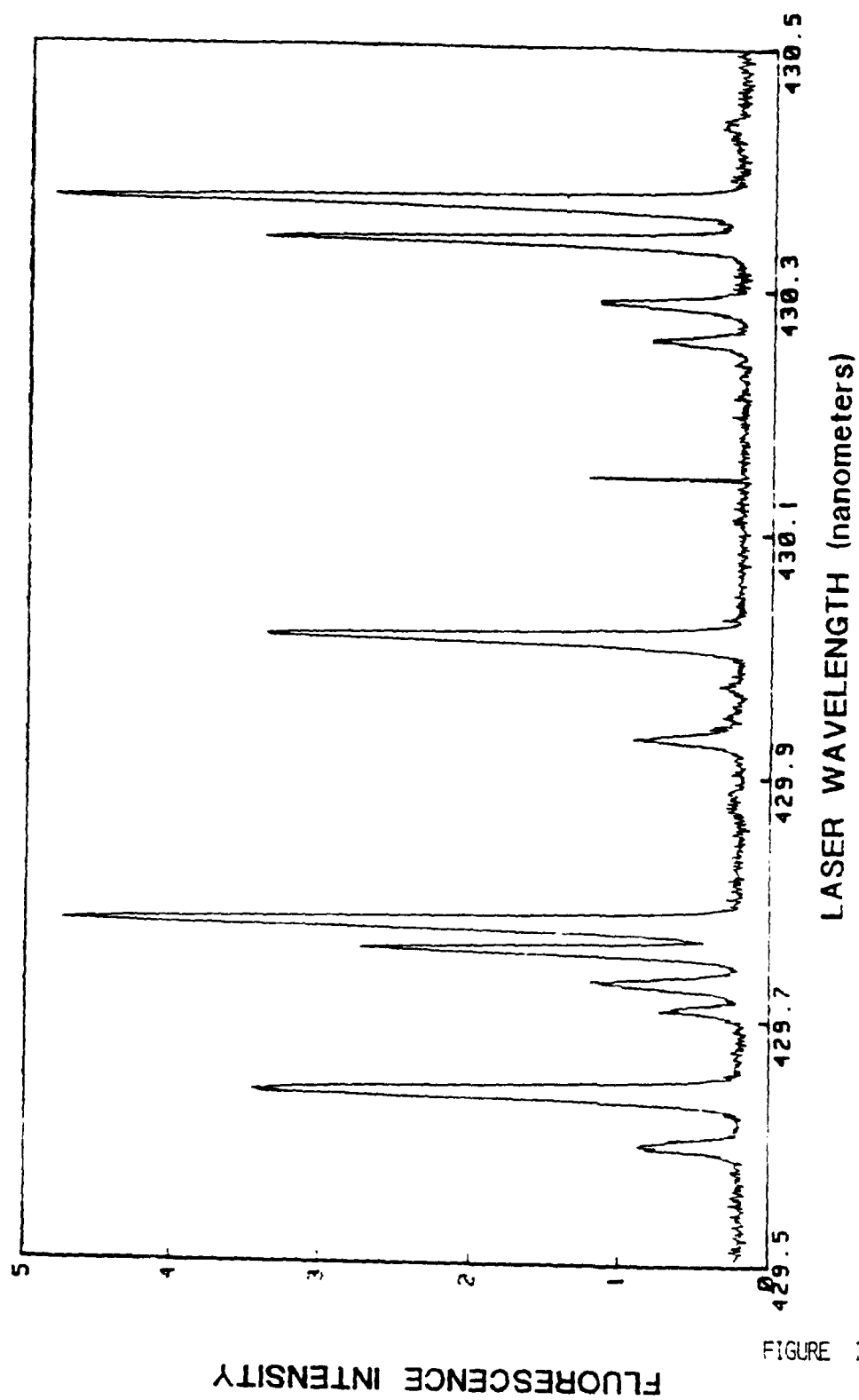
REFERENCES

Bletzinger, P., M.E. Ruark., Production of the CH Radical with an Ion Gun. 1989 HEDM Contractors Conference, Atlanta, GA.

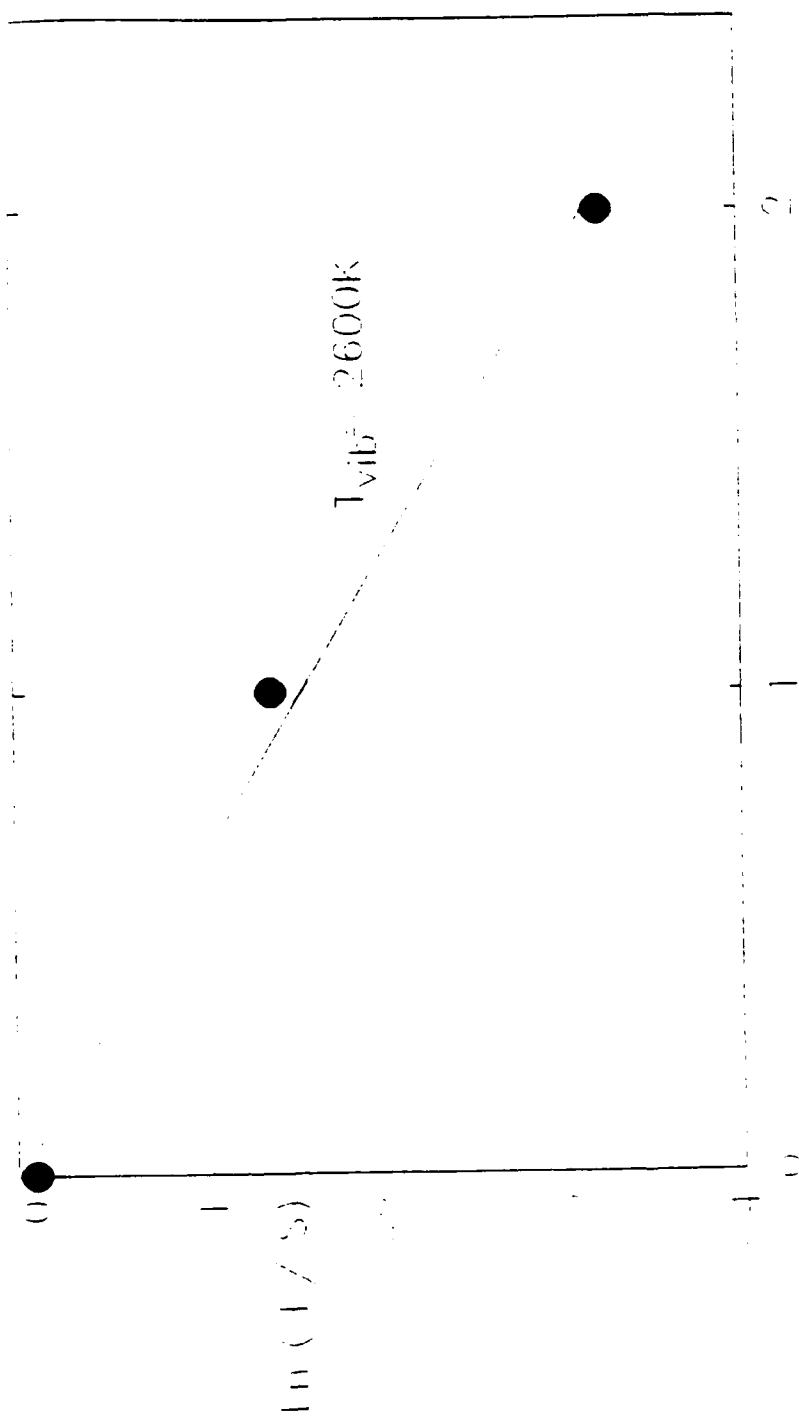
Garland, N.L., D.R. Crosley., Energy Transfer Processes in CH $A^2\Delta$ and $B^2\Sigma^-$ in an Atmospheric Pressure Flame. Applied Optics. 1985, Vol. 24, pp. 4229-37.

Chang, R.S.F., D.W. Setser., Assignment of Rate Constants to Exit Channels from Quenching of He(2^3S) Metastable Atoms. Chemical Physics. 1978, Vol. 25, pp. 201-14.

Moore, C.E., H.P. Broida., CH in the Solar Spectrum. J. Research NBS.-A. Phys. and Chem. 1959, Vol. 63A, pp. 19-53.

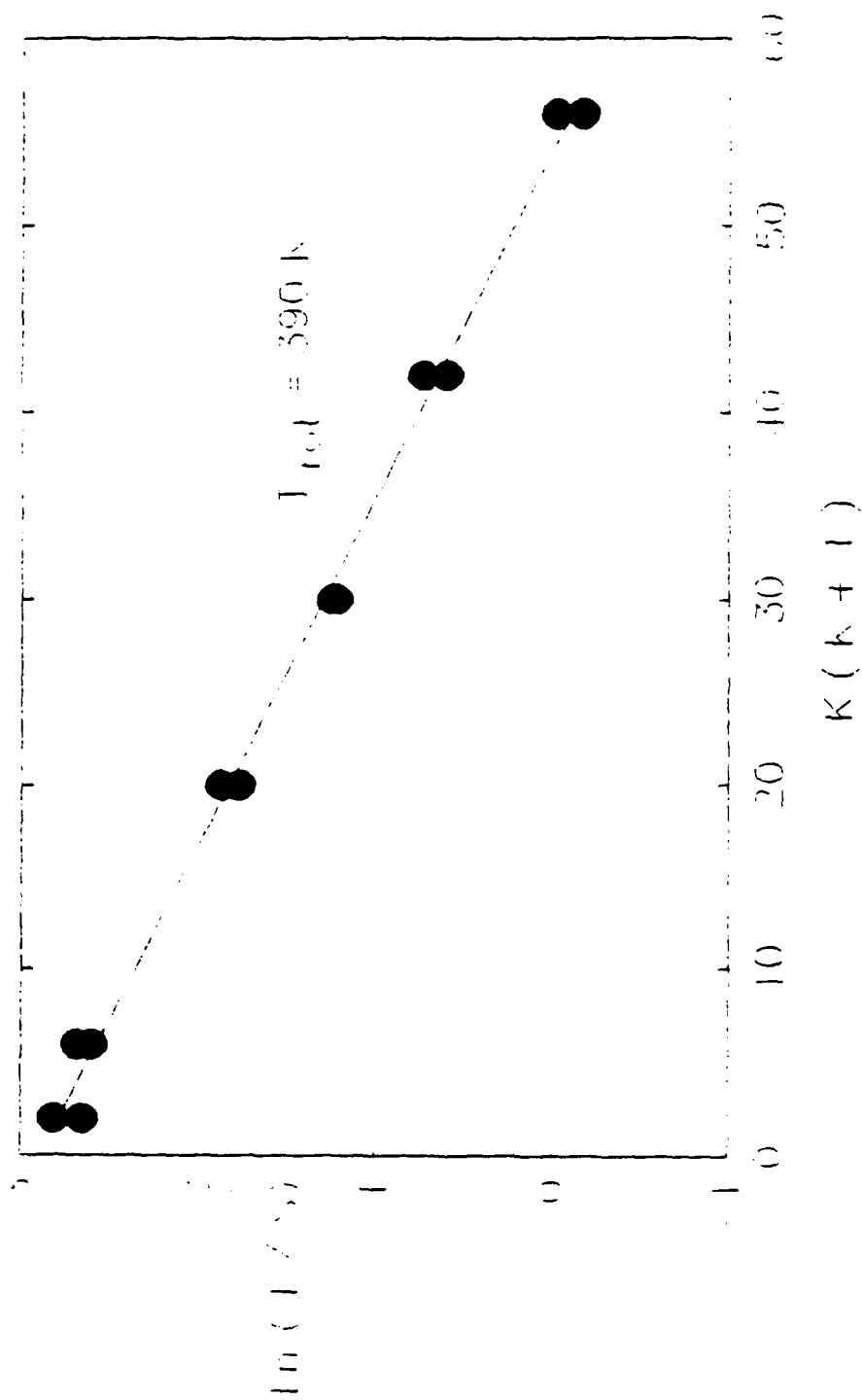


CH RADICAL FLUORESCENCE EXCITATION SPECTRUM



VIBRATIONAL QUANTUM NUMBER
 A GRAPH OF VIBRATIONAL BOLEZMAN PLOT

FIGURE II



CH RADICAL ROTATIONAL BOLZMANN PLOT

FIGURE III

1989 USAF-UES SUMMER FACULTY RESEARCH PROGRAM/
GRADUATE STUDENT RESEARCH PROGRAM

Sponsored by the
AIR FORCE OFFICE OF SCIENTIFIC RESEARCH
Conducted by the
Universal Energy Systems, Inc.

FINAL REPORT

Investigation and Application of a One Dimensional
Thermionic Energy Converter (TEC) Device

Prepared by: Scott A. Frazier, M.S., P.E.
Academic Rank: Ph.D. student
Department and Mechanical Engineering
Institution: University of Central Florida
Research Location: WFO/PCN
 Wright-Patterson AFB
 Dayton, OH 45433-3563
USAF Researcher: Dr. Bob Kerr

Date: 15 September, 1989
Contract No: A49620-80-3-0053

Examination and Application of a One Dimensional
Thermionic Energy Converter (TES) Code

by

Scott A. Vandam

ABSTRACT

A one dimensional thermionic energy converter computer code was examined and utilized to provide a theoretical basis of comparison for experimentally derived data obtained from a lanthanum-hexaboride (LaB_6) cesium vapor thermionic diode. Although the code-generated characteristics were not in precise agreement with the experimental results, they do provide a basis for establishing the validity of the experimental data from an analytical perspective. Certain discrepancies were thus identified and attempted to be accounted for in terms of possible code inadequacies and/or experimental error.

Auxiliary programs were written and used in conjunction with the original TES code to generate both general and simulated LaB_6 diode current density vs. output voltage (J-V) characteristics. The effects of changing the emitter and collector work functions, as well as the operating cesium vapor pressure, were investigated for both codes. The results are displayed and analyzed in terms of their respective J-V characteristic curves.

ACKNOWLEDGEMENTS

I wish to thank the Air Force Systems Command and the Air Force Office of Scientific Research for sponsorship of this research. Universal Energy Systems must also be mentioned for their concern and help to me in all administrative and directional aspects of the program and for selecting me for this research opportunity. Furthermore, the Aero-Propulsion Laboratory of Wright Patterson Air Force Base must be thanked for allowing the use of their facilities.

Finally, this work could not have been completed without the assistance and comments provided by Dr. J. L. Cain of the Georgia Institute of Technology and Dr. H. L. Hall of Universal Energy Systems. Dr. L. A. Anderson of the University of Cincinnati also provided many helpful suggestions.

I. INTRODUCTION:

Thermionic energy conversion has recently received renewed impetus as the result of increased efforts focused toward nuclear space power utilization. The Aero-Propulsion Lab (APL) of Wright Patterson Air Force Base (WPAFB) has become a focal point for some of this research. Computer codes can expedite the characterization and performance determination of such diode/converter designs by providing initial approximations based on the known underlying fundamental physical equations. In the future, computer modeling is likely to be extended via multi-dimensional codes to entire converter systems.

My personal research interests have been in the area of improving the efficiency and power capability of energy conversion systems (such as thermionics). My work record in energy conversions, both academic and industrial, as well as my work in power systems during my M.S. thesis writing, contributed to my being selected for a summer fellowship in the thermionics lab of the APL at WPAFB.

In the following pages, the goals of the research activity are established and the methods and conclusions derived therefrom are presented. Finally, a list of references is included after the recommendations.

II. OBJECTIVES:

Presently, not a great deal of correlation has been established between experimental diode tests and theoretical diode code results. The research direction, then, has been an attempt to begin filling the gap between the diode empirical response and theoretically predicted diode behavior. These objectives were carried out in two ways:

The first approach was that of obtaining the results of a specific TUC code. Those obtained were displayed in the typical diode J-V characteristic curve and compared to that which would be expected from a strictly phenomenological approach.

In the second approach, the same code was run with the diode operating parameters set according to those used in the experimental laboratory tests. The results were compared to the experimental diode characteristic obtained from those experimental tests. (The diode used was the L-3 diode which has been covered thoroughly in detail in previous studies and thus merits continued investigation in thermionic code research).

III.

A. The code utilized was a time-dependent analysis code which computed the TEB diode plasma conditions over discrete time intervals. Additional codes were written and run in tandem with the TEB code to produce the required J-V characteristics. If run to a sufficient number of iterations, in some cases, a convergence was achieved; the plasma ignited and a "steady-state" condition of the diode was observed.

B. The transient nature of the TEB diode J-V characteristic was established and is shown in Figure 1 where the TEB code operating parameters were set arbitrarily. As time advances, the characteristic shifts to the left, approaching a converged, ignited mode of operation. Initially, at low current densities, the unignited, space charge mode of operation can be identified. But as the number of iterations, N , is increased, ignition eventually occurs and the Boltzmann slope becomes pronounced. Ignition is best demonstrated by the $N=1000$ curve in the figure. The apparent "knee" at the top of the Boltzmann portion of the curve is least well understood.

THEORETICAL OUTPUT SIMULATION CHARACTERISTIC

(One dimensional code)

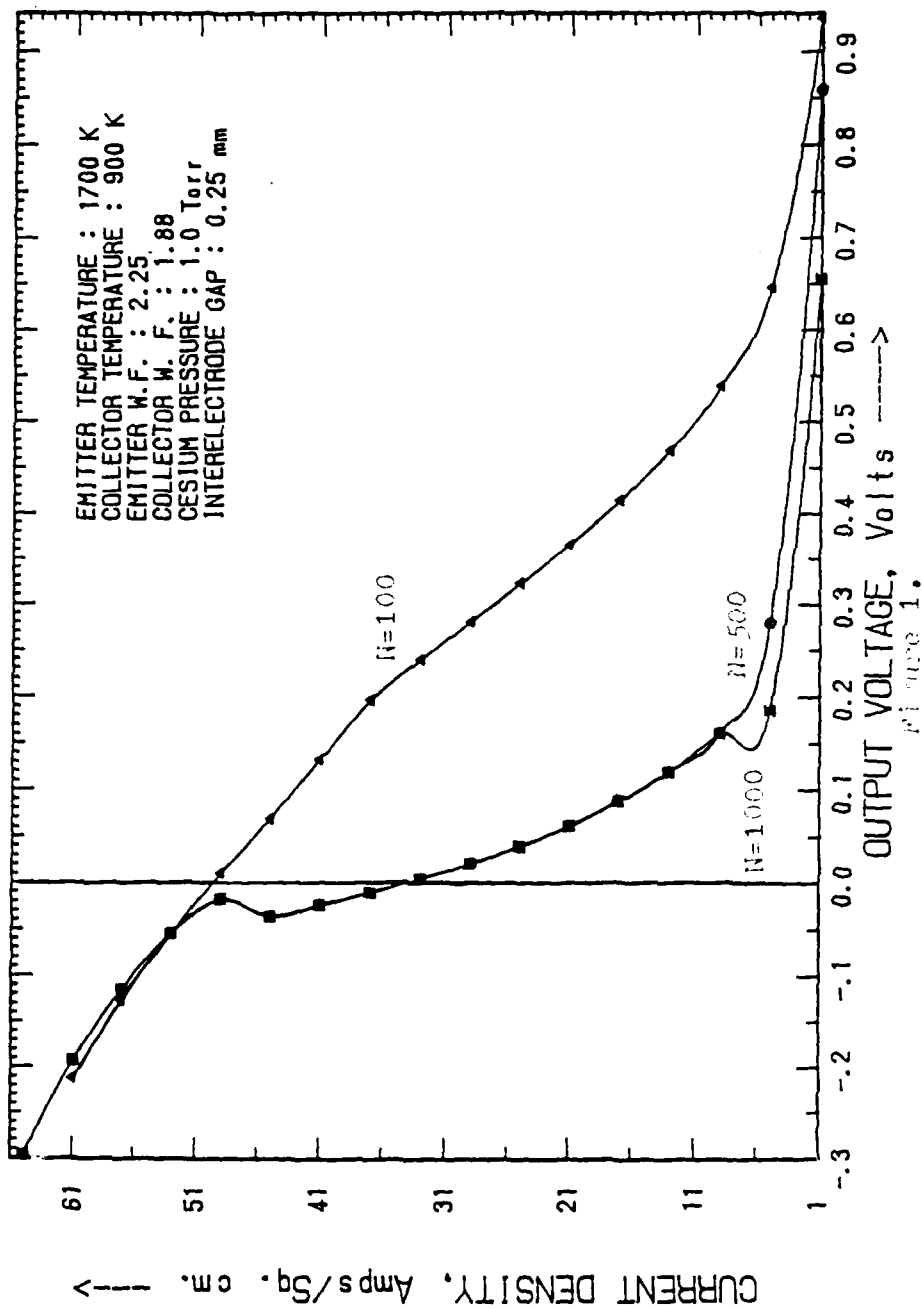


Figure 2 is similar to that of figure 1 except that it was produced for half the cesium vapor pressure of figure 1. It becomes apparent that low pressures can produce unwarranted results after many iterations (evidenced by the $N = 2000$ characteristic). Notwithstanding, all curves are seen to converge at the highest current density shown in the figure. As in figure 1, the TSD diode operates not fully ignited for the $N=100$ curve. Here, the relatively short characteristic time has probably not allowed the ions time to achieve sufficient concentration resulting in a significantly higher inter-electrode potential.

Figure 3 is again similar to figures 1 and 2 except that it represents a further reduction in cesium vapor pressure to only one-tenth torr. Again, the current density is seen to decay over time (with increasing numbers of iterations). The $N=2500$ near characteristic in figure 3 indicates that finally occurs after a relatively long time period. It seems for the continued apparent increase in the slope of these lower pressures that be due to inaccurate modeling of electron collision cross-section or possibly the neglect of ion inertia in the conservation of momentum equations. Also, longer mean free paths associated with lower inter-electrode pressures are less easily modeled precisely, particularly using the necessary statistical methods within the code.

THEORETICAL OUTPUT SIMULATION CHARACTERISTIC

(One dimensional code)

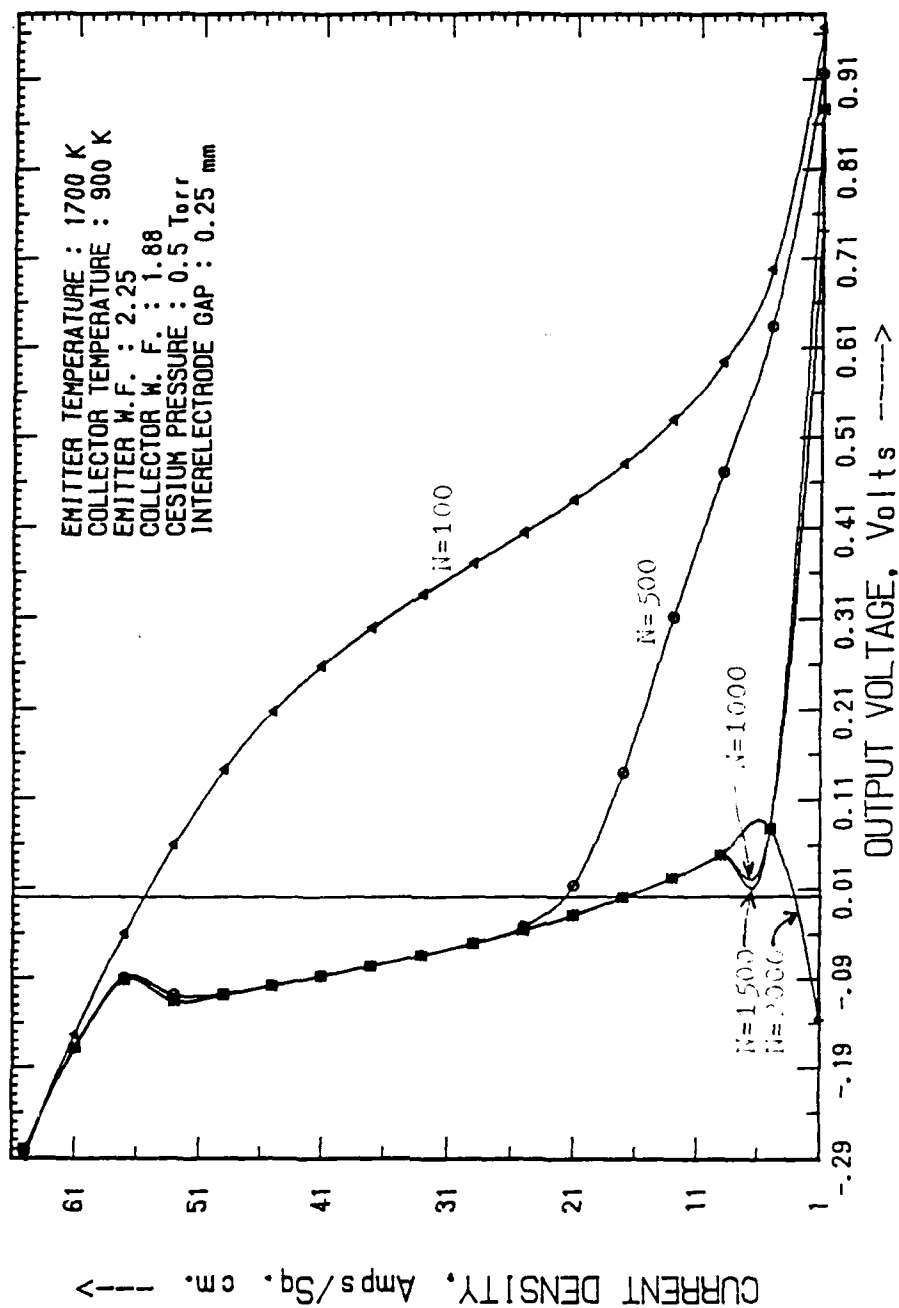
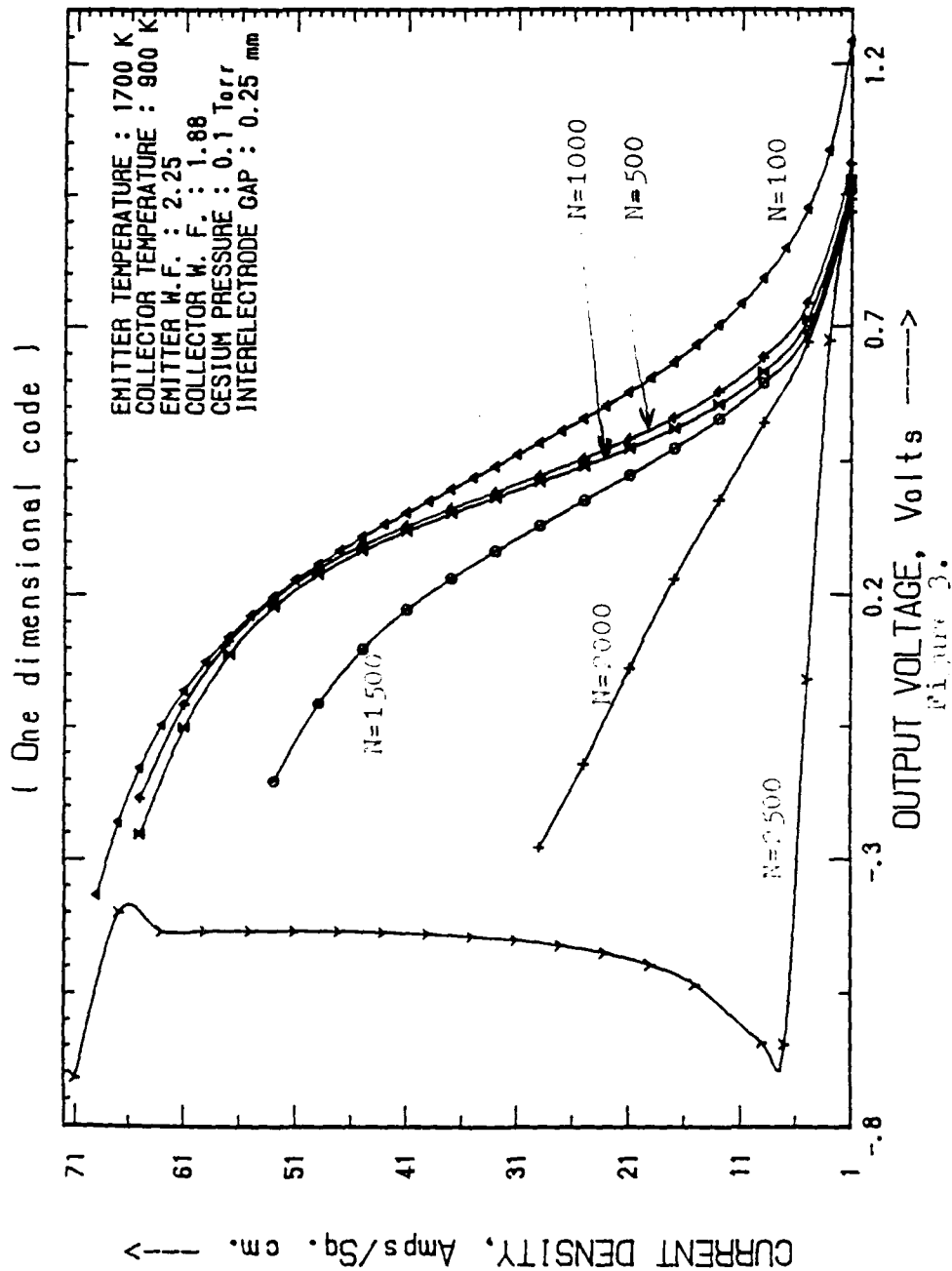


Figure 2.

THEORETICAL OUTPUT SIMULATION CHARACTERISTIC



In Figure 4, TEG diode operation under varied emitter temperature conditions is characterized by the curve. As would be expected, large variations in current density with modest changes in emitter temperature are observed. The squared T in the Richardson-Dushman equation verifies the appropriateness of the result:

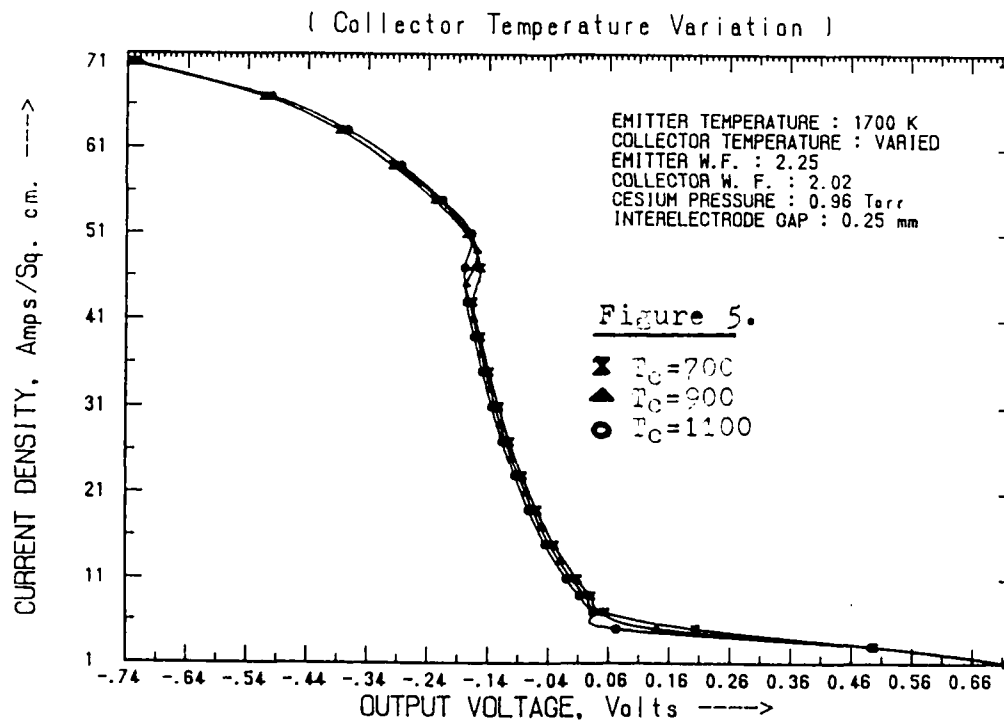
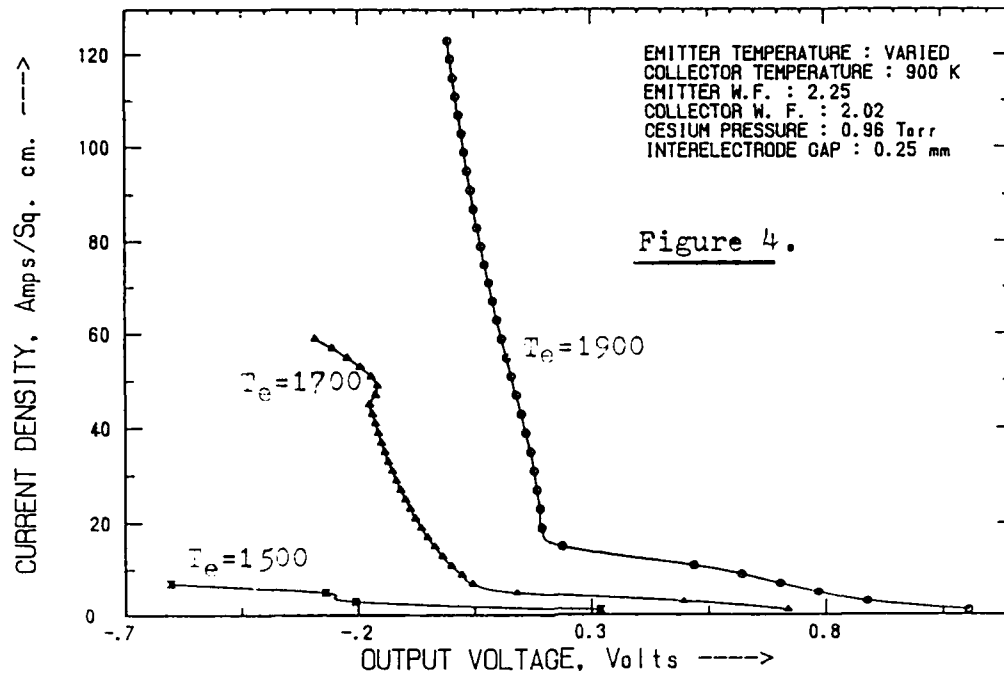
$$J = AT^2 \exp\left(-\frac{\phi}{kT}\right) \quad (1)$$

where J = saturated electron current density
 A = constant
 T = temperature of emitter
 ϕ = work function
 k = Boltzmann's constant

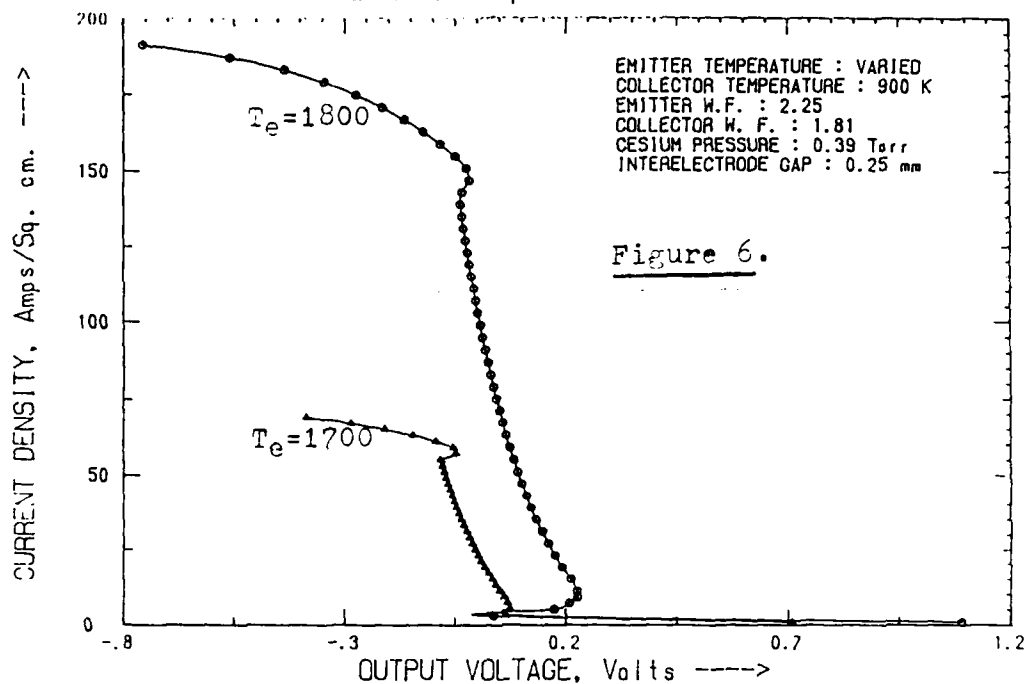
Conversely, Figure 5 was generated from a series of similar pressure but varying collector temperature. Even so, using the characteristic, it is apparent that similar relative collector temperature variations, in this case, cause only minor variations in current density.

Similar to Figure 4, Figure 6 shows the results of varied emitter temperature but under lower pressure conditions. In this case, the current density curves are in slight but expected, with a seemingly greater proportion to increase at the higher temperature than that observed previously in Figure 4. Furthermore, ignition discontinuities are shown to be more pronounced in Figure 6 than when they were barely noticeable in the higher pressure characteristics of Figure

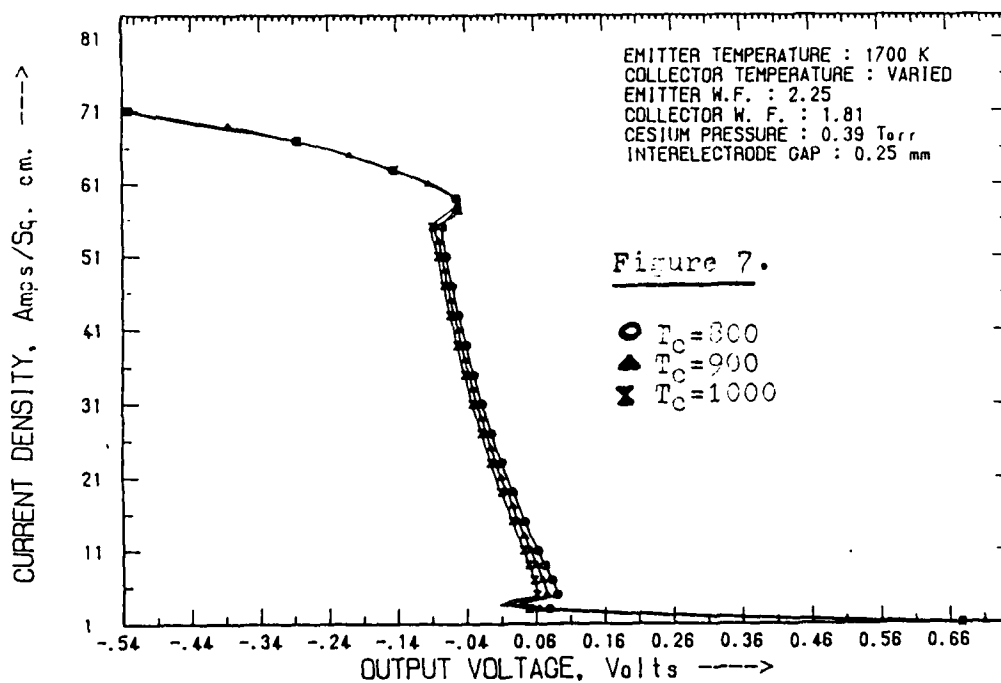
THEORETICAL OUTPUT SIMULATION CHARACTERISTIC (Emitter Temperature Variation)



THEORETICAL OUTPUT SIMULATION CHARACTERISTIC (Emitter Temperature Variation)



(Collector Temperature Variation)



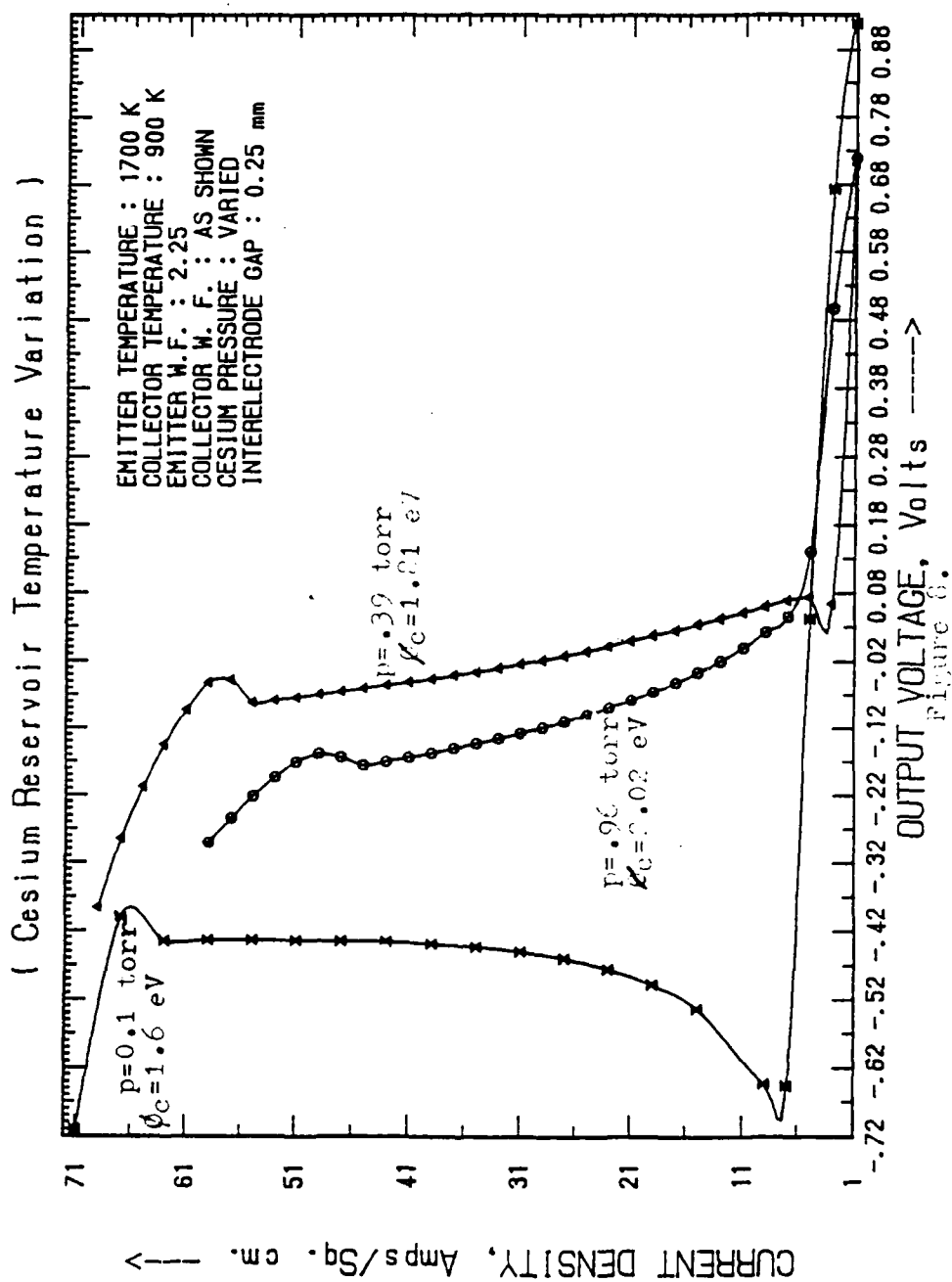
4. Finally, Figure 7 again verifies the code's results as in figure 5 for collector temperature variations except at cesium vapor pressures corresponding to that of figure 6. As before, only small changes in the characteristic are produced as the result of relatively large variations in collector temperature.

IV.

A. The second approach taken was that of comparing the results of the code with those of experimental tests. A composite plot was thus generated for several diode conditions and is shown in figure 8.

The code was able to approximate the experimental curves by employing approximated emitter and collector work functions. The diode operating parameters used were the same as those used during the experiment 1 tests. The LaSg emitter work function was approximated as 2.25 volts or 1.5 eV based on the magnitudes and slopes of the J-V characteristics from previous work. Similarly, the LaB₆ collector work function was approximated between 1.31 and 2.02 volts based on the various zero-voltage intersects determined from other similar LaB₆ characteristics. A collector work function approximation calculation follows:

THEORETICAL OUTPUT SIMULATION CHARACTERISTIC



Assuming the electrode output voltage (V) is greater than or equal to the difference between the emitter and collector work functions, the previous equation (1) can be written as

$$J = A T_E^2 \exp\left(-\frac{\phi_c + V}{k T_E}\right) \quad (2)$$

where J = saturated emitter to collector current density
 T_E = emitter temperature
 ϕ_c = collector work function
 and the other variables were defined previously

Rearranging (2) and allowing for coulombic resistance:

$$\phi_c = k T_E \ln\left[\frac{A T_E^2}{J}\right] - V - [(R_c)(d)(J)] \quad (3)$$

where R_c = coulombic resistance
 d = inter-electrode spacing

Making appropriate variable substitutions and simplifying:

$$\phi_c = 0.14655 \ln\left[\frac{3.468 \times 10^8}{J}\right] - V - (.75)(.025)(J) \quad (4)$$

where $T_E = 1700$, $k = 8.62 \times 10^{-5}$
 $A = 120$, $d = .025$
 and $R_c = .75$ from J-V slope measurements

Using corresponding J and V values from other appropriate LaB_6 characteristics resulted in an average ϕ_c of 1.01 eV.

3. Figure 8 shows variations of the J-V characteristic with respect to deviations in several parameters. Notably, as the cesium vapor pressure is decreased, the Boltzmann slope portion of the curve is seen to become less negative

and even approach infinity for the $p = 0.1$ torr case. Furthermore, the height of the "knee" portion of the curve is shown to decrease as the pressure is diminished.

In comparing the results to those observed experimentally, it was determined that the $p = 0.39$ characteristic was most similar, closely approximating the slope and initial ignition type of response. The $p = 0.26$ torr case did not reveal ignition initially, but this may be due in part to the programmed current density spacing. Least similar was the $p = 0.1$ torr plot where the slope was found to be totally askew and the curve remained continuously in the negative voltage region following ignition.

The equipment used in the experimental tests discussed above for the measurement of the "knee" portion (higher current densities); hence, these portions of the characteristics are found lacking of any of local comparison.

In the next section, additional results are presented and conclusions and recommendations are discussed accordingly.

V. RECOMMENDATIONS:

A. The TEC code J-V characteristic results were significant in their use as a comparison for actual characteristics generated experimentally. In addition, they were useful in demonstrating the transient nature of the characteristics that elapse over time.

B. Figure 1 at a pressure of 600 torr corresponded approximately to what might be expected under different conditions. The "knee" in the curve, however, was not evident from the experiments and might be due to a different rate of decay of the plasma or to a different rate of rise for the region between the two curves. The transition portions of the curves. Other results from the TEC code include the $N = 2500$ curve in Figure 2 and the $N = 2500$ curve in Figure 3. Although the TEC code in plasma ignition characteristics were generated, other code-generated characteristics are not available. The character of plasma ignition is such that many necessary assumptions (i.e. mean free path, ionization, etc.), it is expected that a large error could result for this portion of the curve might be involved.

C. The IES program used demonstrates the capability of an existing code to produce significant results and provide reasonably accurate IES diode characteristics. With more advanced computational facilities, it is expected that this and possibly other codes will be further improved, thereby providing continued insight and increased analytical corroboration of experimental work in thermionics.

Potential areas for possible improvement in the mentioned code examined include improved modeling accuracy at relatively low pressures and better ignition/definition definition. Close attention must also be paid to the "noise" portion of the characteristic. Finally, several routines within the code might be reformulated to allow for a better program execution time. The code might also be recompiled to run on more powerful minicomputers.

REFERENCES

1. Main, G.L., "Emitter Sheath Effects on Thermionic Converter Performance," Dissertation, Princeton University, Princeton, New Jersey, October 1964.
2. Lawless, Jr., J.L. and J.H. Lam, "The Plasmasdynamics and Ionization Kinetics of Thermionic Energy Conversion," Dept. of Mechanical and Aerospace Engineering, Princeton University, Princeton, New Jersey, February 1962.
3. Ramalingam, R.L. and M. Morgan, "Optimization of Lanthanum Hexaboride Electrodes for Maximum Thermionic Power Generation," IAF Space Power Conference, Cleveland, Ohio, June 1969.
4. Morris, J.F., "High Efficiency, Low Temperature Carbon Diodes with Lanthanum Hexaboride Electrodes," NASA TM-71549; International Conference on Plasma Science, IEEE, Knoxville, Tennessee, May 1974.
5. Kroeger, E.L., V.L. Bair, and J.F. Morris, "Diinodiode Thermionic Energy Conversion with Lanthanum-Hexaboride Electrodes," NASA TM-78877; International Conference on Plasma Science, IEEE, Monterey, California, May 1978.

1989 USAF-UES SUMMER FACULTY RESEARCH PROGRAM/
GRADUATE STUDENT RESEARCH PROGRAM

Sponsored by the
AIR FORCE OFFICE OF SCIENTIFIC RESEARCH

Conducted by the
Universal Energy Systems, Inc.

FINAL REPORT

Band Diagram Subroutine and Band Bending in the
Spike Layer for the BICFET

Prepared by: John Bambery
Academic Rank: Graduate Student
Department and Physics Department
University: Indiana University of Pennsylvania
Research Location: WPAFB, Wright Research and Development Center,
Electronic Technology Laboratory,
Device Research Group
USAF Researcher: Dennis Whitson and Gary McCoy
Date: November 4, 1989
Contract No: F49620-88-C-0053

Band Diagram Subroutine and Band Bending in the
Spike Layer for the BICFET

by

John Bambery

ABSTRACT

The BAND subroutine was added to the analytical program for the BICFET so that one may visualize the band structure of the device.

The GAASEQ subroutine was modified to take into account the band bending which occurs in the highly doped spike layer under equilibrium conditions. The structure of GAASEQ was modified to accomodate changes more easily, while still solving the charge balance equation through the use of a bisection routine.

ACKNOWLEDGMENTS

I would like to thank the Air Force Systems Command and the Air Force Office of Scientific Research for the sponsorship of my research effort. The Electronic Technology Laboratory of Wright Patterson Air Force Base has an Environment quite conducive to scientific research. I would also like to thank the ELRD group and Gary McCoy for the support and encouragement which made the summer both productive and enjoyable.

Special thanks go to Ben Carroll for his help in using the computer system and his exemplary patience in answering any questions concerning the VAX machines.

In addition, acknowledgement should go to Dr. Dennis Whitson whose guidance was an essential part of this project.

I. INTRODUCTION

The tasks for which I took responsibility were oriented toward computer programming and basic theoretical calculations. My understanding of basic FORTRAN programming concepts stem mainly from an independant study project concerning the determination of an average index of refraction for HgCdTe samples. This study was performed under the guidance of Dr. Larry Freeman at Indiana University of Pennsylvania. My familiarity with the VAX systems comes from work performed at Wright-Patterson Air Force Base under the direction of Dr. Dennis Whitson during the summer of 1988.

A basic understanding of the BICFET program and my direction throughout both summer research periods came from Dr. Dennis Whitson. Difficult theoretical tasks and any conceptual difficulties were explained by him. Dr. Whitson has been on leave from Indiana University of Pennsylvania under the auspices of the AFOSR Resident Research Program. He first came to WPAFB in the summer of 1986 under the faculty component of the summer program sponsored by UES. He was involved with a research program concerned with modelling heterojunction devices such as the BICFET and resonant tunneling diodes. The methods included analytical modelling and finite difference numerical techniques.

I will continue work with the BICFET at IUP as part of my M.S. research, also under Dr. Whitson.

II. OVERVIEW

No changes were made in the basic structure of the BICFET program. The main program, BIC reads data from an input deck, INPUT. BIC then enters a series of driver loops which generate data for several 1-dimensional arrays. The subroutine GAASPAR is then called from within these loops in order to determine several material parameters of the AlGaAs material. The three additional subroutines called from within the driver loops are as follows: GAASEQ, GAASNEQ and BAND. Normally, one would not generate data in the subroutines mentioned while stepping through the driver loops. The output files become much too large. Therefore, several warnings are printed to the screen and the program is stopped if necessary.

The summer's research effort focused on several changes and additions to GAASEQ, extensive changes in the GAASNEQ subroutine and the addition of the BAND subroutine. GAASEQ solves the charge balance equation when the device is in an equilibrium state, while GAASNEQ is used to determine the solution when the BICFET is subjected to nonequilibrium conditions (when the device is under bias).

The various regions of the BICFET are referred as regions 1-4 where region 1 corresponds to the emitter, region 2 to the semi-insulator, region 3 to the highly doped spike layer and region 4 to the semiconductor. This is shown diagrammatically in figure 1.

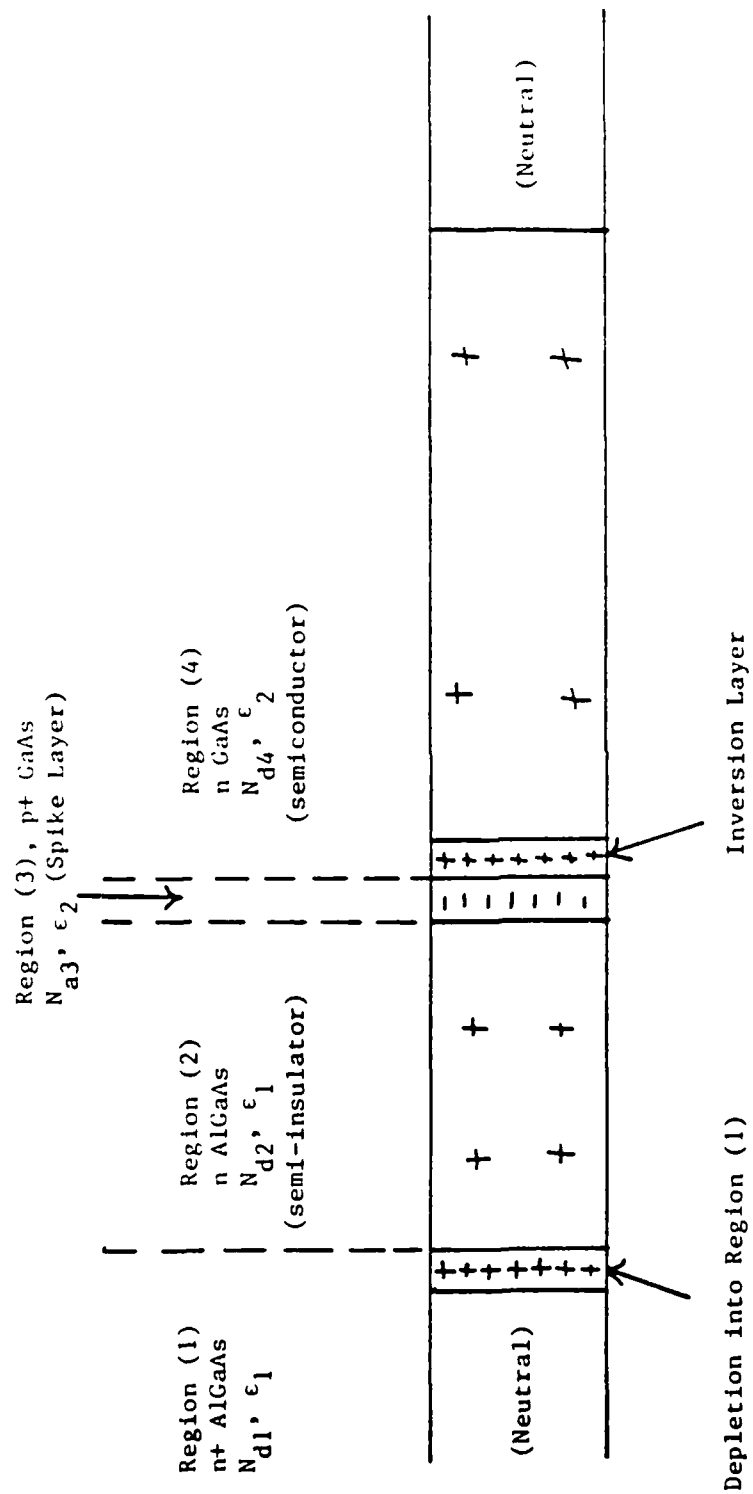


FIGURE 1. Space charge distribution in the NPN BICFET with the assumption of ohmic contact to and space charge in the semi-insulator. Not drawn to scale.

III. BAND SUBROUTINE

The bulk of the summer was spent working on the BAND subroutine. Using BAND, one may calculate and display the energy levels and electric field strength as a function of position through the device. Under equilibrium conditions, the Fermi level is calculated using Boltzmann statistics,

$$E_{F-0122} = KT \ln(N_{d1}/N_{c1}) \quad (1)$$

where N_{d1} is the donor concentration in region one, and N_{c1} is the concentration of electrons in the conduction band in the first region. For the equilibrium case, the Fermi level will be constant throughout the device.

After calculating the Fermi level, the width (in cm) of regions one and four are calculated. Let $D1$ ($D4$) denote the width of region 1 (region 4), then

$$D1 = \sqrt{\left| \frac{2 \epsilon_1}{\rho_1} V_{b1} \right|} \quad (2)$$

and

$$D4 = \sqrt{\left| \frac{2 \phi_4 \epsilon_4}{q N_{d4}} \right|} \quad (3)$$

Definitions for the variables used may be found in appendix I.

Next, the conduction band discontinuity is determined between region 1 and region 2. For an AlGaAs emitter, there is no discontinuity, while the GaAs emitter causes a discontinuity DELEC across the junction, which is a material parameter calculated in GAASPAR. The logical variables used are ALGAEM and GAASEM. Values for several more variables are then determined to be used in the potential and electric field loops.

The structure of BAND is such that data is collected

for each region as a function of position, starting with the emitter and moving through the device to the semiconductor collector. A DO loop is used to step through each region. Calculations are made for both the potential and the electric field strength across a particular region and the output is sent to a data file named BAND.OUT. The format of the output file is simply a numeric list which may be used with several different plotting/graphing packages.

The emitter is the first region to be considered. The expression for the potential in the emitter is determined using the depletion approximation. That is, the depletion width calculated earlier defines a region in which all the electrons which have been excited to the conduction band have been drawn away. The result is a region of positive charge due to the ionized donors. A gradient is expected for the charge concentration, but the step function which results from the depletion approximation is sufficient to get at the physics. The potential at the junction between the emitter and the semiconductor material of region 2 is V_{b1} .

In the semiconductor, region 2, the same calculations are made for the electric field and the potential. However one needs to be aware of the placement of the spike layer. The spike layer is a thin layer grown either in the semiconductor collector or the semi-insulator, in which there is a high concentration of acceptors (10^{19}). The choice of placement is made with the logical variables SPIKESC and SPIKESI. SPIKESC places the spike layer in the semiconductor and SPIKESI places it in the semi-insulator. The electric field and potential are then calculated through the spike layer.

Region 4 is designated the collector and is made of the semiconducting material GaAs. In the collector we also assume that depletion of the conduction band electrons occurs over a width, D_4 . The electric field and potential are again calculated as a function of position using the appropriate boundary conditions.

The BAND subroutine uses data generated by the GAASEQ subroutine when plotting the band structure under equilibrium conditions. The SPIKESC/SPIKESI option was incorporated into the GAASEQ subroutine and the original charge balance equation was modified in such a way as to ease corrections and future changes. GAASEQ uses a bisection analysis routine to converge on a value of Q_e , the emitter charge, from which several additional variables were evaluated. The only equation present in the loop was the charge balance equation solved in terms of Q_e . The approach used currently, determines equilibrium values for V_{b1} , V_i , ϕ_{is} , $DEL-E_i$, P_o , Q_c and Q_3 . These variables are then used in the new form of the charge balance equation. A bisection routine is still used to determine a value of Q_e , but the variables mentioned above are now incorporated into that loop.

Using the Gauss law, one may determine an expression for the electric field as a function of position along the physical symmetry axis of the device. Poisson's equation is then used to obtain an expression for the electrostatic potential as a function of position throughout the device.

The charge per unit area for the emitter is determined in the depletion approximation by multiplying the concentration of donor atoms in the depleted region by the electronic charge, Q ($=1.6022 \times 10^{-19}$ coulomb). The

depletion approximation assumes that any free carriers in a specified region will be swept away in the presence of an electric field.

The Gauss law for the emitter region follows

$$\frac{dE}{dx} = \begin{matrix} 0 & 0 < x < d \\ \frac{qNa_1}{\epsilon_1} & d < x < d_{regl} \end{matrix} \quad (4)$$

where $(d_{regl} - d)$ is the width of the depletion region.

A single integration gives the result:

$$E(x) = \frac{qNa_1}{\epsilon_1} x - \frac{qNa_1}{\epsilon_1} d \quad (5)$$

for the boundary condition

$$E(x) = 0 \quad \text{for} \quad 0 < x \leq d \quad (6)$$

Poisson's equation then follows for $x > d$,

$$-\frac{dV}{dx} = \frac{qNa_1}{\epsilon_1} x - \frac{qNa_1}{\epsilon_1} d \quad (7)$$

Integrating and recognizing that $V(x=d) = 0$ and

$V(x=d_{regl}) = V_{b1}$ leads to

$$V(x) = \frac{qNa_1}{2\epsilon_1} (x-d_{regl})^2 + \frac{qNa_1}{\epsilon_1} d (d_{regl} - x) + V_{b1} \quad (8)$$

where V_{b1} has been determined in the GAASNEQ subroutine.

The calculation of the electric field through region two proceeds in the same manner. The constant of integration is determined by forcing the electric displacement vector to be constant across the boundary. This condition must hold for either GAASEM or ALGAEM. The result is

$$E(x) = \frac{qNa_2}{\epsilon_2} x + (\epsilon_1/\epsilon_2) E_1 \quad (9)$$

where E_1 is the value of the electric field at the junction

in the emitter and $x=0$ is defined at the junction in region 2. The potential is then found,

$$V(x) = \frac{-qNd_2}{2\epsilon_1} x^2 - (\epsilon_1/\epsilon_2) E_1 x + V_{b1} \quad (10)$$

recognizing that the potential is constant across the junction.

The expressions for the electric field and the potential in the spike layer depend upon its placement. For SPIKESI = .TRUE., the spike layer is in the semi-insulator and the following equations hold:

$$E(x) = \frac{-qCNA3}{\epsilon_2} x + \frac{qNd_2}{\epsilon_2} (D2-D3) + \frac{Q_e}{\epsilon_1} \quad (11)$$

$$V(x) = \frac{qCNA3}{2\epsilon_2} x^2 - \frac{qNd_2}{\epsilon_2} (D2-D3)x + \frac{Q_e}{\epsilon_1} x + V_{b1} + V_{i2} \quad (12)$$

Again, the displacement vector and the potential are continuous across the boundary, thereby allowing one to determine the constants of integration. For SPIKESC = .TRUE., the expressions for the electric field and the potential follow:

$$E(x) = \frac{Q(P3-CNA3)}{\epsilon_4} x - \frac{q(P3-CNA3)}{\epsilon_4} D3 - \frac{Q_c}{\epsilon_4} \quad (13)$$

$$V(x) = \frac{-q(P3-CNA3)}{2\epsilon_4} x^2 + \frac{q(P3-CNA3)}{\epsilon_4} D3 x - \frac{Q_c}{\epsilon_4} x + V_{b1} + V_{i2} \quad (14)$$

In equations 11-14, V_{i2} represents the change in potential across that portion of the semi-insulator included in region 2 which does not include the highly doped spike layer.

The collector region is treated in the same manner as region 1 in that a depleted region is defined by d_4 , through which the charge concentration is constant. Outside the depleted region, the charge concentration is zero. Following the same procedure as for the other regions

leads to the expressions:

$$E(x) = \frac{q N_0 d}{\epsilon_1} x - \frac{q N_0 d}{\epsilon_1} D_1 \quad (15)$$

$$V(x) = \frac{-q N_0 d}{2 \epsilon_1} x^2 + \frac{q N_0 d}{\epsilon_1} D_1 x + V_3 \quad (16)$$

IV. GAASEQ SUBROUTINE

The original GAASEQ subroutine ignored the effect of band bending in the spike layer. The changes made in the GAASEQ subroutine were oriented largely toward accomodating this band bending. The main function of this subroutine is still the determination of a solution to the charge balance equation, Q_e . However, several modifications have been made. In order to create a logical flow, the lengthy expression which resulted from writing the charge balance equation in terms of Q_e has been replaced by several equations written in terms of familiar variables. The forms of the various equations depend heavily on the placement of the highly doped spike layer as will become evident.

Consider the case where the spike layer is placed in the semiconductor. The charge balance equation is then written

$$0 = Q_e^* + Q_{N42} D_2 + Q_c^* + Q_3^* + q_{03} P_0^* \exp(-\beta E_i^*) \quad (17)$$

In order to determine Q_e through the use of a bisection routine, values must be determined for all terms except Q_e . A value for Q_e is assumed at the start of each iteration. The second term in the above expression, $Q_{N42} D_2$ is the charge in the semi-insulator. All the values are known and a numerical value is calculated. The charge in region 3 is then given by $Q_3^* + q_{03} P_0^* \exp(-\beta E_i^*)$, where the hole concentration is taken into account by the second term. Q_3 is then given by the following

$$Q_3 = \frac{-q C_{NA3} D_3}{1 + q \exp(\beta * (\epsilon_p - \Delta E_i^* + E_i^*))} \quad (18)$$

Finally, the charge in the collector (region 4) is determined by the following expression:

$$Q_c^* = \sqrt{2q\epsilon_4 [\kappa_T P_o^* + N_{d4} \phi_s^*]} \quad (19)$$

Definitions for the remaining variables dependant upon Q_e follow:

$$P_o^* = N_v \exp(-\beta \Delta E_i^*) \quad (20)$$

$$\Delta E_i^* = E_{g4} + \kappa_T \ln(N_{d4}/N_{c4}) - \phi_s^* \quad (21)$$

$$\phi_s^* = \kappa_T \ln(N_{c1}/N_{d1}) + \frac{Q_e^2}{2qN_{d1}\epsilon_1} + \kappa_T \ln(N_{d4}/N_{c4}) - V_s^* \quad (22)$$

$$V_s^* = \frac{-qN_{d2}Dz^2}{2\epsilon_2} - \frac{Q_e Dz}{\epsilon_2} \quad (23)$$

$$V_{bi}^* = \frac{-Q_e^2}{2q\epsilon_1 N_{d1}} \quad (24)$$

If the spike layer is placed in the semi-insulator, the equations must be changed accordingly. There will be no hole contribution in the charge balance equation from the spike layer. The resultant form of the charge balance equation is then

$$0 = Q_e^* + Q_{N_{d2}(O2-O3)} + Q_c^* + Q_s^* \quad (25)$$

The second term accounts for the charge in that part of the semi-insulator excluding the highly doped spike layer. The charge in the spike layer is given by

$$Q_s^* = \frac{-qCNA3 O3}{1 + q \exp[\beta(\epsilon_p - \Delta E_i^* + E_i^* - \Delta E_v^*)]} \quad (26)$$

Again, the equations dependant upon Q_e follow:

$$P_o^* = N_v \exp(-\beta \Delta E_i^*) \quad (27)$$

$$\Delta E_i^* = E_{g4} + \kappa_T \ln(N_{d4}/N_{c4}) - \phi_s^* \quad (28)$$

$$\phi_s^* = kT \ln(N_A/N_{D1}) - V_{bi}^* + kT \ln(N_A/N_{C4}) - V_i^* + \Delta E_{C1} - \Delta E_C \quad (29)$$

$$V_i^* = \frac{-q N_A Z D_2^2}{2 \epsilon_2} - \frac{Q_e}{\epsilon_2} D_2 + \frac{Q(N_{D1} Z + C N_A Z)}{2 \epsilon_2} D_3^2 \quad (30)$$

$$V_{bi}^* = \frac{-Q_e^2}{2 \times q \epsilon_1 \times N_{D1}} \quad (31)$$

V. BAND DIAGRAMS

Following are two examples of the output which may be generated using the BAND subroutine. Data files are generated and used in conjunction with one of several graphing packages. The plots included with this report were constructed using RS/1.

When viewing the plots, please ignore the dashed lines. They correspond to the electric field but are not quite correct. Two different calculations were made but both contain rather large discontinuities which should not occur. The horizontal dashed line represents the constant Fermi level throughout the device under equilibrium conditions, while the solid curves represent the conduction and valence bands through the device.

The first graph is plotted with the logical variables FERMI, GAASEM and SPIKESC all set true and the second graph was produced with ALGAEM and SPIKESC set true. Region 4 has been scaled by a factor of 100 so as to include the entire diagram. The scaling option will be improved when time permits and will probably be included in region 3.

Band Structure of the BICFET
Equilibrium Conditions
ALGAEM and SPIKESC = TRUE
FERMI = FALSE

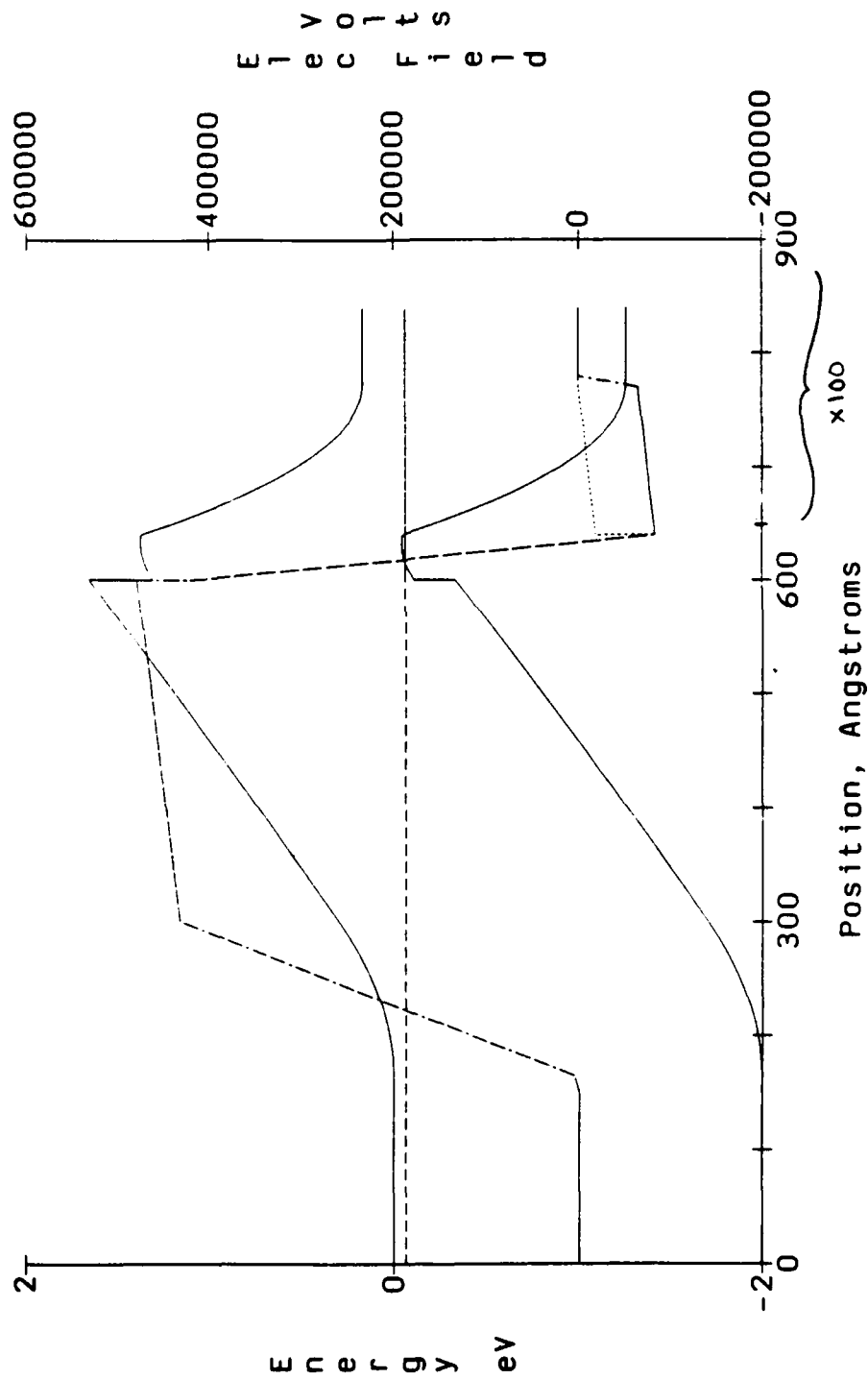


FIGURE 2

Band Structure of the BICIET
Equilibrium Conditions
FERMI, GASEM and SPIKESI

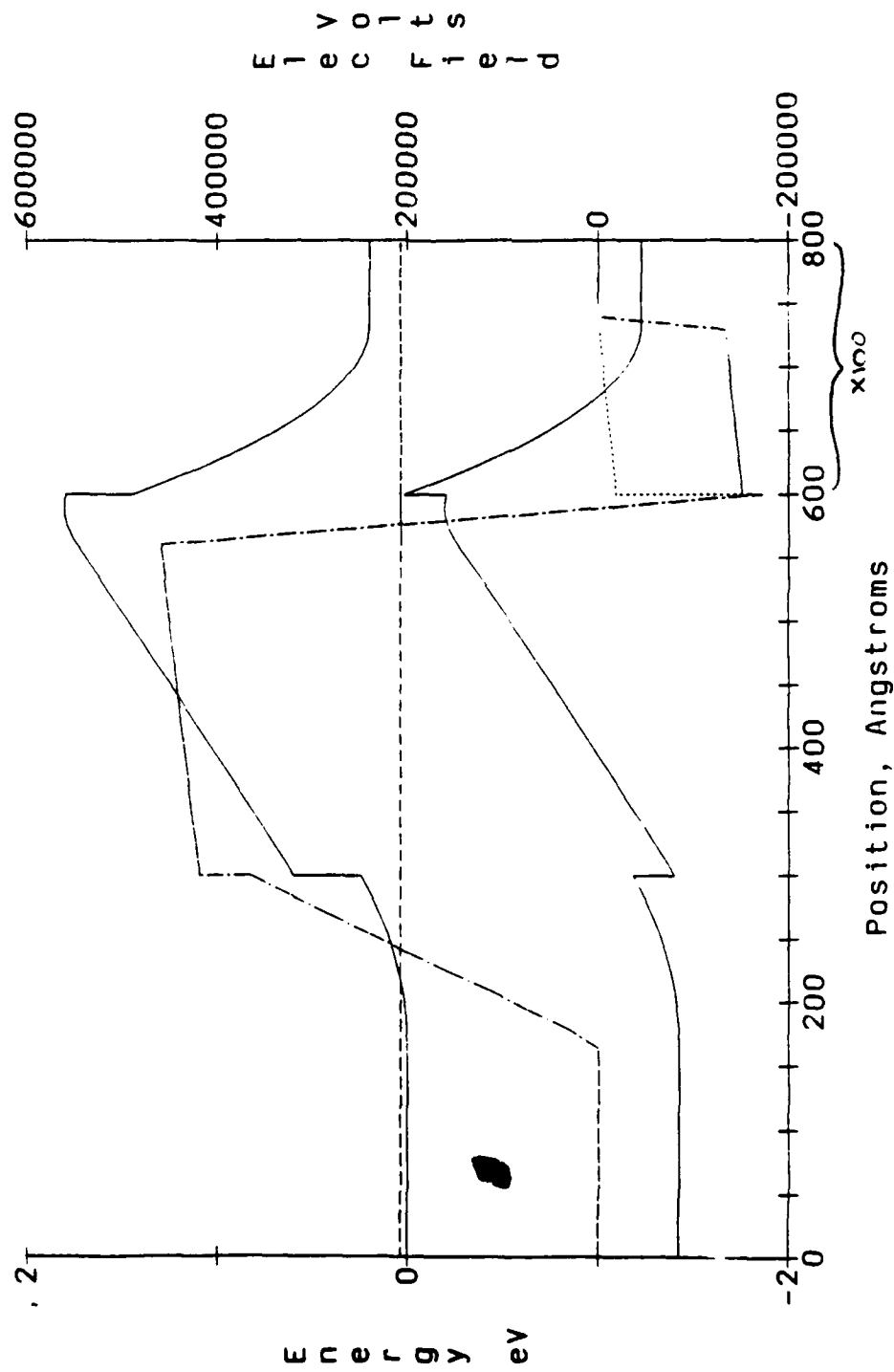


FIGURE 3

VI. CONCLUSION

The GAASNEQ subroutine received a great deal of attention during the last two weeks, but the changes were not completed. Work will continue on this subroutine in order that the BAND subroutine may be used for the nonequilibrium case. Several effects have been considered, including the effect of band banding in the spike layer and those effects resulting from recombination of electron-hole pairs in the device. Also to be considered are Si impurity levels. Several equations have been developed by Dr. Whitson, but remain to be incorporated into the program.

Appendix 1 Variable Definitions

β	= $1 / kT$
CNA3	= Concentration of acceptors in region 3
d	= Width of depleted region in emitter
D1 - D4	= Width of regions 1 - 4
dreg1 - 4	= Defines width of regions 1 - 4 inside counter loops of BAND subroutine
$\Delta E_c, \Delta E_{c1}$	= Conduction band discontinuity between semi-insulator and semiconductor (emitter and semi-insulator)
ΔE_i	= Position of Fermi level with respect to semiconductor valence band
ΔE_v	= Valence band discontinuity between semi-insulator and semiconductor
E(x)	= Electric field
Ef-bltz	= Fermi level calculated using the Boltzmann statistics
Eg1 - Eg4	= Band gap in regions 1 - 4
Ei	= Position of semiconductor Fermi level
ϵ_p	= Acceptor level energy above valence band
$\epsilon_1 - \epsilon_4$	= Dielectric constant in regions 1 - 4
g	= Fermi factor
k	= Boltzmann constant
Nc1, Nc4	= Density of states in conduction band of regions 1 - 4
Nd1 (2,4)	= Donor concentration in region 1 (2,4)
Nv	= Density of states in valence band
Po	= Hole concentration at semiconductor surface
P3	= Hole concentration in region 3

ϕ_s	= Band bending in semiconductor
q	= Electronic charge
Q_c	= Collector charge
Q_e	= Emitter charge
Q_3	= Charge in region 3
ρ_1	= Charge density in region 1
T	= Absolute temperature
$V(x)$	= Electrostatic potential
V_{b1}	= Band Bending in emitter (depleted region)
V_i	= Potential drop across semi-insulator
V_{i2}	= Potential drop across region 2
V_3	= Potential at region 3 - region 4 boundary

1989 USAF_UES SUMMER RESEARCH PROGRAM/
GRADUATE STUDENT RESEARCH PROGRAM

Sponsored by the
AIR FORCE OFFICE OF SCIENTIFIC RESEARCH

Conducted by the
Universal Energy Systems, Inc.

FINAL REPORT

Software Design Recovery: A Case Study

Prepared by:	Eric J. Byrne
Academic Rank:	PhD Student
Department and	Computing and Information Science
University:	Kansas State University
Research Location:	Software Concepts Group WRDC/AAAF-3 Wright-Patterson Air Force Base Dayton, Ohio
USAF Researcher:	Otheus Jackson
Date:	August 10, 1989
Contract No:	F49620-88-C-0053

Software Design Recovery: A Case Study

by

Eric J. Byrne

ABSTRACT

The "dusty deck" problem refers to old programs that are still useful. Such programs usually are undocumented, difficult to understand, maintain, and/or modify. There exists a large body of software that could benefit by being re-structured and/or rewritten using modern techniques and programming languages. Computer aided software engineering (CASE) tools promise to help in the development and maintenance of new software, but often are not helpful with older software. Many CASE tools for design and development can not work with software not initially developed using these tools. A solution is to recover the design of older software and record it in a CASE environment. This allows older programs to be re-developed using modern structured techniques. The result is that useful software is given new life, is better structured, well documented, and easier to maintain. This paper reports on a design recovery effort and the experiences gained.

ACKNOWLEDGEMENTS

I wish to thank the Air Force Systems Command and the Air Force Office of Scientific Research for sponsorship of this research. Universal Energy Systems must also be thanked for their role in administrating this program.

I also wish to thank the staff of the Software Concepts Group for their support and interest in this work. James Williamson who was kind enough to suggest a project in my area of interest. Otheus Jackson deserves thanks for all his help and assistance. Also, Kenneth Littlejohn for his expertise with Ada.

1. INTRODUCTION

The "dusty deck" problem refers to old programs that are still useful, but may be undocumented, difficult to understand, maintain, and/or modify. Tools to assist maintenance programmers have been developed [1]. Modern software development has moved from an art-form activity to an engineering activity. Software designers now have a set of useful and successful techniques and methodologies that can be used to produce software that is well structured, understandable, easier to maintain, contains fewer errors, and is well documented. To assist designers in their task, computer implemented tools (CASE) that help perform these tasks are becoming popular. However, CASE tools often can only operate on software developed using these tools.

There is a large body of older useful programs that could benefit by being re-designed and implemented using modern techniques and CASE environments. One approach is to develop an abstraction of program functionality and transform the abstraction into a source code language [2,3]. Another approach is to recover program information and maintain it in a CASE environment. Such information can be low-level program information [4] or higher level design information [5,6]. Such activity is called "reverse engineering." Reverse engineering involves

abstracting code to a specification level such that the specifications can be modified and revised code can be generated. Translating source code from one language to another is a simpler form of reverse engineering.

Design recovery is a more complex process that uses not only source code, but also comments in the code, existing documents, maintenance history and experience, and knowledge about a program's application domain. Design recovery attempts to provide information that fully explains a program. This information should allow a person to understand what a program does (specification), how it does it (design), why it does it, etc. Tools to help with this task have also been proposed [7].

The Avionics Laboratory's Software Concepts Group (WRDC/AAAF-3) is concerned with researching, evaluating, and transitioning new software technologies. As part of their mission they evaluate CASE tools to determine their suitability for work done within the group and to determine the appropriateness and usability of the tools with respect to other DoD organizations. Design recovery and the use of CASE tools are topics of interest to the Software Concepts Group and were explored as part of this research.

2. OBJECTIVES OF THE RESEARCH EFFORT

Design recovery is a demanding activity that forces the person performing the recovery to collect every available piece of information and analyze it for useful facts. Very little design information is encoded in source code. Recovering an equation from a procedure is a simple task, understanding what the equation does and why it is important requires much more effort.

CASE tools are available to support most activities in the software life cycle. CASE tools for software requirements analysis and design are useful in the early phases of software development and are needed as software is modified.

Two objectives were defined for this research effort. The first objective was to perform design recovery on an application program to identify issues involved with design recovery. The second, was to select a CASE tool, supporting software requirements analysis and design activities, and use it to record the recovered design. Entering the recovered design into the tool would serve as a means of evaluating the tool.

3. CASE TOOL EVALUATION

The Software Concepts Group had previously selected the

CASE tool "Software through Pictures" (StP) for evaluation. Software through Pictures (1) is an integrated set of editors and utilities that support structured analysis/structured design. The tool set includes editors for data/control flow diagrams, structure charts, data structure diagrams, E-R diagrams, state transition diagrams, control specifications, and object annotations. StP also provides a document preparation system [8].

The evaluation of StP was concerned with its ability to support the specification and design of real-time software. Other issues of concern were its ease-of-use, range of capabilities, customizability, integration level, quality, and overall support for software design activities.

StP performed very well overall and was successfully used to record the recovered design. This report discusses the design recovery effort. The StP evaluation is reported in [9].

1 Software through Pictures is marketed by Interactive Development Environments, Inc.

595 Market Street, 12th Floor,
San Francisco, California 94105
1-800-888-IDE1 or 1-415-543-0900

4. DESIGN RECOVERY PROCEDURE

To identify issues involved with design recovery an application program was selected and its design recovered. The application selected was a software model of the Air Data Computer (ADC) used in F-16 A/B Block 15S1 aircraft. The model software is a real-time application that runs as part of a distributed simulation environment used to test the F-16 Fire Control Computer. The source code for the application was written in Fortran.

The remainder of this section explains the procedure used to conduct the design recovery experiment. The next section presents experiences and issues identified.

Step one: Collect all possible information about the ADC model. Sources of information included the Fortran source code, one detailed design document, and documentation for system calls and external functions. Personnel experienced with the ADC software were also identified.

Step two: The person performing the recovery read the source code and began to build an understanding of the software, its structure, and how the program worked.

Step three: The structure of the software was recovered and entered into the StP environment. This involved

identifying who called which routines and parameters passed. This step resulted in a set of structure charts that showed the detailed design of the software. Information about all variables, common blocks, etc., was recorded and entered in the data dictionary.

Each module in the structure charts corresponded to a subroutine in the source code. The Fortran code for each subroutine was translated manually into a generic program design language (PDL). The PDL representation used generic operations and was not source language dependent. The purpose was to attempt to remove language dependent features from the design. The PDL was associated with the corresponding module to show the processing performed by that module. Information about data declarations was similarly recorded using generic data types instead of using source language specific declarations.

Step four: The source code was analyzed and the functionality of the software components was identified. This information was used to develop a data flow model. StP uses structured analysis techniques similar to those given in [10] to represent system functionality.

Step Five: The source code was analyzed and the control structure was identified. This does not refer to low-level control that is part of the functionality, but to

high-level control that affects the overall operation of the software. The ADC software runs in a distributed environment. It interacts with other programs and the control related to that interaction had to be modeled. StP uses techniques taken from [11] to represent control specifications.

Step Six: At this point the design was reviewed for consistency with available information. Incomplete items were identified and an attempt was made to collect the needed information.

Step Seven: Having recovered the design, the final step was to use the design to develop an implementation of the ADC model in Ada. This step is not part of design recovery but is a natural task that follows a design recovery effort. By performing this task, the suitability of the design representation could be evaluated. This in turn would provide information about the adequacy of the recovered design.

StP does not support source code generation. StP does support the capability to generate Ada style data declarations. The PDL for the modules was printed using an Ada style procedure declaration template and was then manually translated into Ada code.

5. EXPERIENCES

This section discusses the experiences encountered while performing the design recovery. The recovery took seven weeks. Part of that time was spent learning StP and dealing with the StP evaluation aspect of this effort.

The first step was to collect information. Several pieces of information were not available or did not exist. The ADC software used signals and shared memory to communicate with other processes. Fortran common blocks were mapped onto the shared memory locations to access the information stored there. Descriptions of the information passed, ranges of values, and significance was not documented. The origin of the ADC model was not available and the equations used were not explained.

The second step was to become familiar with the program, its structure, and how it worked. The person doing the recovery becomes familiar with the system and forms a mental model. This is the first real step in recovering the design. This mental model is developed as understanding of the system grows.

The third step was to recover the detailed design from the source code. This involved showing the calling hierarchy, information about parameters passed, and processing done within each module. Information about data

items was also recorded.

Several problems were encountered at this step. First, the source code contained debugging statements. Was this part of the design? Probably not, but it was part of the operational capabilities of the software. Talks with the maintenance staff revealed that debugging statements were never used. Therefore, these statements were not recovered. The code contained conditional compilation code. How should this be recovered and represented? This issue was not resolved. The next question was how to handle Fortran common blocks? All information was passed in common blocks. No parameters were passed between subroutines in the software. Common blocks mapped to shared memory needed to be kept intact. Common blocks used internally to the model were another question. Was this an implementation detail? Finally, it was decided to treat the common blocks elements as global data. Modules were shown to read from and write to global data variables. Their implementation as common blocks was not recovered. The fact that these variables had been contained in common blocks did have an effect on the detailed design recovered. Another problem was recognizing implementation details that should not be recovered as part of the design. Language specific details were hard to detect also.

Information about system functions and externally defined subroutines was recovered. Information about the purpose of each routine and parameters passed in/out was recorded. This information included data type, range of values (if known), significance, intended usage, etc. The purpose of an argument may not be recoverable if it is not documented. An understanding of the application domain can help recover the purpose in some cases. The name of an argument can provide a hint.

Finally, recovering the detailed design forced a hard look at the source code and software documentation. One error in the source code was discovered. Comments that were incorrect or outdated were also detected. The documentation was found to be outdated and 44 errors were found. Documentation errors consisted of errors in the document and discrepancies between documentation and the source code. Due to the errors in the documentation some information could not be trusted and this eliminated one source of information about the software and its design.

The fourth step was to identify functionality performed in the software and develop a data flow model. Structured design gives heuristics for transforming data flow diagrams into structure charts. To some extent, this process can be reversed. However, not all software is well designed. A single subroutine can contain more than

one function or parts of several functions. Subroutines do not map directly into processes in a dataflow diagram. Functionality performed must be identified. The flow of data between functions can then be recovered.

One problem encountered was identifying low-level control structures that served as part of a function and high-level control structures that served to control the software operation. The former should be included as part of the functionality recorded in a process specification, the latter should be recorded in a control flow diagram and its control specification.

Finally, each function performed in the software should become a process in the data flow diagram. Each process must be given a specification (pspec). A pspec should be more abstract than the PDL used in the structure charts, recording what the process should do, without specifying how it should be implemented. The intent of each process should be learned if possible. It is not enough just to say that process X does step Y. The reason for doing step Y should be learned and expressed.

The fifth step was to identify the control structure of the software. Actually, this is partially done during step four. What remained was to specify the control structure and explain its purpose.

The sixth step is important. The recovered design must be reviewed for completeness and accuracy. Missing information should be identified and an effort made to recover it. It is not possible to recover a design completely. The reasons for doing something, or its significance, may be lost with the original design.

The final step was to take the design and use it to develop an Ada implementation. This step provided some very good insight into representing the design. Further, is raised the issue of abstracting the design from the source code and how much does the original code affect the recovered design.

The design represented should not be source language dependent. The representation should be such that the new implementation will agree with the design. Items of concern are variable names, data types, and efficiency issues that can contort the code structure. It is important that the design represent the intent of the operations as well as the operations to be done. It was found that the recovered design was strongly influenced by the original character of the Fortran code.

Here is an example. The Fortran code contained a call to a system function that returned as status value when completed. The calling interface of the function was

recovered. The data type of the status variable was "integer" and the fact that the variable was used to hold status information was recorded. In Ada, the same system function had a different name and interface. It was no longer a function, but a procedure and the status variable was passed as a parameter. The status variable no longer had a type of integer. Its Ada type was "COND_VALUE_TYPE." In addition, the value of the status variable was checked in several IF-statements. The conditional clause in these statement had to be changed in the Ada version as well.

The design recovered was influenced strongly by the original Fortran code. It pointed out that data type information should be represented in an abstract way that emphasizes the purpose of the data as much as its range of values.

Another issue that arose is when should re-structuring be done? When transforming the source code into PDL? When developing the data flow and control flow specifications? One solution is that after the data flow and control flow is identified and documented that should serve as a restructuring point. Structure based on the source code should be rejected in favor of a structure that represents the true functionality of the software. Recognizing what structure is necessary and what is an

artifact from the code can be difficult.

One mistake made in this experiment is that the recovered structure charts and PDL was used to develop the Ada version. Once the specification of the software had been recovered and represented in dataflow and control diagrams, then the specification should have been studied for possible improvements. Then the structure charts and PDL should have been redeveloped from the specification.

6. RECOMMENDATIONS

This experiment in design recovery has revealed several interesting issues and identified several areas for future research. The first issue is that the original source code can strongly affect the recovered design. Part of this problem arises from the mental model that the person doing the recovery builds. This mental model is biased by the code and unconsciously affects the design recovered. Rules and heuristics must be developed to help in the design recovery activity. Such rules will only become known as experience in this activity is gained. We need guidelines to help identify sections of code that are affected either by the source code language or the operating constraints placed on the original software by the operating system and hardware. We need guidelines to differentiate between low-level and high-

level control operations.

Tools to help recover structure information are already available. However, source code only contains surface information. To understand and recover the design, deeper information is needed. An understanding of the application domain can aid the recovery of information about the purpose of a function and why it is needed. Such domain knowledge could be built into a tool to help analyze the source code and documentation. Keywords could be identified and their significance explained.

When to re-structure the design for improvements is another issue. The best time seems to be after the specification has been recovered. The detailed design information should be re-generated once the specification has been re-worked. If a new version of the software is to be produced, it can then be developed using modern techniques and programming languages. This will result in a system that is better structured, documented, and maintained than the previous version. Thus, design recovery will prove to be useful in extending the life of older programs.

REFERENCES

- [1] Foster, John R., Muneo, Malcolm., "A Documentation Method Based on Cross-Referencing," Conference on Software Maintenance, Austin Texas, September 21-24, 1987, pp. 181-185.
- [2] Boyle, James M., Muralidharan, Monagur N., "Program Reusability through Program Transformation," IEEE Trans. Soft. Eng., Vol. SE-10, No. 5, (September 1984), pp. 574-588.
- [3] Waters, Richard C., "Program Translation via Abstraction and Reimplementation," IEEE Trans. Soft. Eng., Vol. 14, No. 8, (August 1988), pp. 1207-1228.
- [4] Benedusi, P. Antonini., Cantone, G., Cimitile, A., "Maintenance and Reverse Engineering: Low-Level Design Documents Production and Improvement," Conference on Software Maintenance, Austin Texas, September 21-24, 1987, pp. 91-100.
- [5] Arango, Guillermo., et al., "Maintenance and Porting of Software by Design Recovery," Conference on Software Maintenance, 1985, pp. 42-49.
- [6] Sneed, Harry M., Jandrasics, Gabor., "Inverse Transformation of Software From Code to Specifica-

tion," Conference on Software Maintenance, Phoenix Arizona, October 24-27, 1988, pp. 102-109.

- [7] Biggerstaff, Ted J., "Design Recovery for Maintenance and Reuse," IEEE Computer, Vol. 22, No. 7., (July 1989), pp. 36-49.
- [8] Software through Pictures User Manual by Interactive Development Environments, Release 4.1.
- [9] Byrne, Eric J., "Software through Pictures : A CASE Tool Evaluation," WRDC/AAAF-3, Wright-Patterson AFB, August 1989.
- [10] Yourdon, Edward., Constantine, Larry L., Structured Design : Fundamentals of a Discipline of Computer Program and Systems Design, Prentice-Hall, 1979.
- [11] Hatley, Derek J., Pirbhai, Imtiaz A., Strategies for Real-Time System Specification, Dorset House Publishing, 1987.

1989 AFOSR SUMMER FACULTY RESEARCH PROGRAM

GRADUATE STUDENT RESEARCH PROGRAM

Toolbox for Image Processing using
Disbtributed Computing

Sponsored by the

AIR FORCE OFFICE OF SCIENTIFIC RESEARCH

Conducted by the

Universal Energy Systems, Inc.

FINAL REPORT

Prepared by:	Larry A. Crum, Ph.D.	Michael A. Costarella
Academic Rank:	Professor	Graduate Student
Department:	Computer Science & Engineering	Computer Science & Engineering
University:	Wright State University	Wright State University

Research Location: Wright Avionics Laboratory
Wright-Patterson AFB
Dayton, Ohio

USAF Researcher: Louis Tamburino, Ph.D.

Date: 11 Nov 89
Contract No: F9620-88-C-0053

Same Report as
Dr. Larry Crum
Report # 101

1989 USAF-UES SUMMER FACULTY RESEARCH PROGRAM/

GRADUATE STUDENT RESEARCH PROGRAM

Sponsored by the

AIR FORCE OFFICE OF SCIENTIFIC RESEARCH

Conducted by the

Universal Energy Systems, Inc.

FINAL REPORT

Neural Networks and Machine Learning

Prepared by:	Michael J. Findler
Academic Rank:	Candidate for Ph.D.
Department and	Computer Science Department,
University:	Arizona State University
Research Location:	Wright Research and Development Center WRDC/AART-2 Wright-Patterson AFB, OH 45433-6543
USAF Researcher	Dr. Timothy D. Ross
Date:	4 August 1989
Contract No.:	F49620-88-C-0053

Neural Networks and Machine Learning

by

Michael J. Findler

ABSTRACT

Survey of machine learning literature, with emphasis on pattern based learning techniques. Expert systems are reviewed and discarded as being too "brittle." Then adaptive systems are reviewed. Different assumptions are examined and current learning models are reviewed. Neural networks are contrasted to expert rule-based systems. Some of the advantages and disadvantages of neural networks are described. Finally, we present a light overview of Gail Carpenter and Stephen Grossberg's Adaptive Resonance Theory (ART) neural network topology.

Acknowledgements

I wish to thank the Air Force Systems Command and the Air Force Office of Scientific Research for sponsorship of this research. Universal Energy Systems must be mentioned for their concern and help to me in all administrative and directional aspects of this program.

My experience was rewarding and enriching because of many different influences. Dr. Tim Ross provided me with the support, encouragement and expert guidance to make this a truly enjoyable work experience. John Jacobs provided the perfect working environment. Numerous discussions with Mike Noviskey, Devert Wicker and Dave Gadd were invaluable to completing this project. Dr. Leon Winslow of the University of Dayton gave me confidence in my abilities and inspiration. I would like to thank Ms. Teri Miller for her support. The other summer hires, Chris Vogt, John Langenderfer and Tina Normand, served as a constant source of stimulation.

I. Introduction -- Military Applications of Machine Learning

The success of a military mission often depends upon the intelligent exploitation of sensed information and the intelligent allocation of offensive resources. There are a variety of functional, operational and logistical penalties associated with using people as the exclusive source of intelligence in military aircraft. Therefore the requirement to automate intelligent functions within military aircraft systems is both strongly and widely recognized. Of the several abilities that go together to make up intelligence, learning certainly plays a central role.

"For the medieval Scholastic Thomas Aquinas, seeing was a matter of 'grasping' the form of a thing" [Pratt]. This type of philosophy still permeates the thinking of those studying knowledge acquisition. Nobody has been able to scientifically define how to "grasp the form of a thing." We will be looking at why some of this has been so difficult.

II. Expert Systems

A major problem with expert systems has to do with what [Holland] calls "brittleness". Brittleness is a "fuzzy" description of the robustness of an expert system. An expert system is powerful only in its very limited domain. If a question is requested outside of this limited domain, the expert system's solution is either not very good or nonsense. In other words, a rule-based learning system is not very flexible in unknown environs. There are methods to make an expert system less brittle such as the "genetic" and "bucket brigade" algorithms in conjunction.

A genetic algorithm is used to create new rules -- by splicing old rules together, like a geneticist would do with chromosomes. Which rules are chosen is dependent on its "strength," defined as the measure of credit a rule receives for supporting the correct solution. This algorithm has a very Darwinian approach to rule survival and generation -- when the rule base is fully populated with rules, the weaker rules die out and the stronger rules generate new rules. It is truly a "survival of the fittest" world.

Generally, there are three methods of "genetically" splicing old rules to create new rules: **crossover**, **mutation** and **inversion**. The most important being **crossover** -- simply exchanging a randomly selected segment between rule pairs chosen on basis of their individual strength factors. Some of the new rules thus generated will share the strong characteristics of their parent rules without their individual weaknesses. These new rules will gain strength in turn and be chosen in the next evolutionary round. **Mutation** and **inversion** are mainly used to de-emphasize the sole use of crossover.

As stated earlier, a pair of rules is chosen for the genetic algorithm based upon its strength. Typically, strength credit is given for a correct solution in an expert system to just the rule(s) that fired that solution. This does not give credit to the rule(s) that fired the rule(s) that gave the correct answer, and so on In other words, additional strength is not given to the "building blocks" of the rule base.

In a knowledge acquisition expert system, this failure to give credit to the "building blocks" can lead to a type of brittleness, the strength of a "building block" may be overshadowed by a later, newer rule's strength. A bucket brigade algorithm causes each node to act as its own middleman. If rule "is paid" strength credit for a supporting a correct solution from

rules it generated, then it must also "pay" those rules that generated it from its "pocket."

[Holland] claims the genetic and bucket brigade algorithms used together can make an expert system non-brittle. The combination of these algorithms allows an expert system to expand its specific domain into a more general domain. However, it does not make the domain very general and therefore the system is still brittle.

III. Adaptive Systems

When one speaks of adaptive systems (neural networks being a special case), several assumptions are made:

- The samples are of a valid format. We do not know how these samples were brought about, but they are there. This further assumes prior knowledge of what the samples should look like. "If we observe our own actions under similar conditions, we note that not all possible methods are subject to consideration. First, we separate those methods that have nothing to do with the problem from those that may provide some leads." [Bongard]
- Whatever we are looking for must be measurable and observable. This seems like a silly statement until one examines it closer. For example, theoretically a type II supernova was considered to originate only from red giant stars. This could not be proved or disproved until 1987. That was when the world was lucky enough to observe a type II supernova and

discovered its origin to be a blue giant star.

- There exists some "primer" sample to get the process of learning started. This sample is found by a "mechanism" (probably a human being) that recognizes the sample to be valid and of the correct form. In addition, information that is not necessary to the problem is deemed unimportant and not supplied to a mechanical algorithm. So far, only human beings seem to be able to discover what is the correct form.
- For biological learning there exists some feedback loop essential to the mental health of the subject. (Refer to studies in isolation and sensory deprivation.) This feedback can be considered to provide either positive (reward) or negative (punishment) stimuli.
- The chicken and the egg problem -- which came first: the problem or the recognition of a problem. This is the ultimate challenge, in order for a solution to a problem to exist the problem must be recognized to exist. If there exists a problem and nobody knows of its existence then there will exist no solution.

In the field of adaptive systems, five models of learning are prevalent:

- learn from example,
- learn by practice,
- learn by analogy,
- learn from pleasure feedback, and

-- learn inductively.

These learning models are usually considered distinct, but they tend to overlap. Some of the rules of one model are very similar to another.

Learn by example can be divided into positive and negative examples. Positive examples induce generalizations and negative examples rule out certain overgeneralizations [Berwick]. As an example, if a program was to learn the letters 'a', 'b' and 'c' by only positive example, then only 'a', 'b' and 'c' would be input into the program. If the letter 'd' was introduced after the learning cycle had completed, the program would have difficulty categorizing the letter. Restricting samples to positive examples makes learning more difficult because of the tendency to overgeneralize. If one assumes the ability of ordering our hypothesis such that knowledge acquisition can be described as analogous to an onion's layered skin. In [Berwick's] words, "What is the Subset Principle? Intuitively, it is a strategy of 'timid acquisition': If possible guesses can be arranged in a subset relationship, then the learner should make the smallest possible guess about what it should learn consistent with the evidence it has seen so far." [Kodratoff] uses the intuitive notion of "conceptual distance" to bring about the same results. "A generalization of two examples, as well as the process of obtaining this generalization" is a measure of the conceptual distance between the examples. This conceptual distance is minimized, to guarantee the smallest step toward completely general.

If negative examples were allowed, then during the learning cycle the letter 'd' could be learned as a not (a), not (b) and not (c). Or if another unlearned letter, say 'e', was introduced, a valid response could be not (a or b or c). "Positive examples force the boundary of the 'specific descriptions' frontier toward more general descriptions, and

negative examples force the boundary of the 'maximally general descriptions' toward more specific descriptions." [Berwick]

Learn by practice is physically doing something. The feedback is given to the learner in a very tactile way. For example, one needs to throw a football many times to learn to throw it in what is considered an aesthetically pleasing way. If a person had never held a football, he/she would probably not throw it well the first time. (Many of the new robot multi-digit hand manipulators are taught by practice: a user wears a feedback glove and performs the motions the robot should perform. The robot will mimic the movements the user is performing and finally be able to perform adequately without guidance.)

However, if an adult had learned to kick a soccer ball as a child and then was asked to kick a football, he/she would probably not perform badly. The adult might make an good correlation between the two sports kicking styles. This is an example of **learn by analogy**. It assumes prior knowledge of a similar field and the ability to "make the connection" between the known field and the unknown field.

"When encountering a new problem situation, a person is reminded of past situations that bear strong similarity to the present problem (at different levels of abstraction). This type of reminding experience serves to retrieve behaviors that were appropriate in earlier problem-solving episodes, whereupon past behavior is adapted to meet the demands of the current situation." [Michalski]

In the **learn by induction** model, People create theorems based on a small data sample and then test these new theorems for validity against new situations. These theorems do not have to be "perfect" solutions, just "good" solutions. If a new situation invalidates an old theorem, a feedback mechanism is used to redefine the old theorem into a new theorem

that also handles the new situation. The old theorem is not thrown away. According to [Berwick], people tend to expand their knowledge base slowly -- preferably by a minimal amount. A radical shift in perspective is thus avoided. Children tend to overgeneralize [MacWhinney] probably because of a lack of samples. In more formal terms, the ability to learn an assigned algorithm without complete information about it is learning by induction.

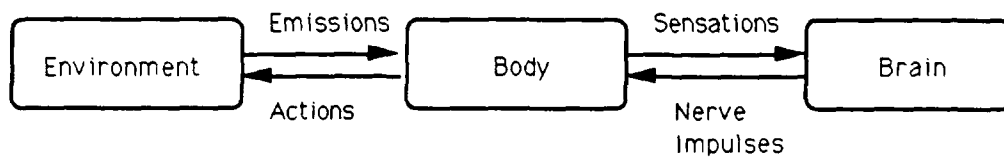


Figure 1

Perhaps the most intriguing model (to me) was the **Learning Based on Pleasure** model proposed by [Fritz]. In this model, the amount of (mechanical or biological) learning accomplished is directly proportional to the perceived pleasure level derived during the learning experience. This model is an offshoot of the Maslow's "Hierarchy of Needs" theory¹.

[Fritz] claims the brain is not directly affected by the environment, but rather indirectly (refer to Figure 1). He claims the body is the intermediary directly interacting with the world environment for any given situation. The body sends coded information to the brain via nerve sensations. The brain reacts to these sensations and transmits nerve impulses back to the body to attain the highest pleasure level. The body does the actions the nerve impulses have requested. Afterwards, the body must react to this new situation. "Reward and punishment calibrate whether the action has or has not satisfied internal needs, . . . in

machine applications [these] include a wide variety of internal cost functions." [Carpenter]

(For mechanical learning, the feedback loop was what decided the "pleasure" level. The program written on an IBM PC in BASIC not only had to learn from its experiences, it had to "forget" irrelevant memories. The IBM PC memory limitations required the need to forget.)

Little or no generalization takes place unless prior information about the algorithm is introduced to the neural network. [Anshelevich] draws a direct correlation between the number of possible algorithms a process can identify and general learning.

IV. Neural Nets

At this time, it might be interesting to contrast the neural network approach and the expert system's rule based approach:

- The knowledge of a neural network lies in its inter-unit connections and their weights. In contrast, much of an expert system lies in its rules.
- A Neural network is driven by the activation that passes from units to other units. In contrast, an expert system is driven by symbols generated as a consequence of rule-firing.
- When a neural network solves a problem, it cannot explain what logical steps were needed to solve it. Its magic! Rule based systems can usually

step through its logic process to explain the reasoning behind a recommended solution.

The most important concept of neural networks is the holistic approach regarding the nets. Each net is considered macroscopically as a whole, without regard to the inner workings of the individual nodes. It is fairly safe to say that how a neural network works is not fully understood. It just works!

Neural networks were originally developed to model the human brain. Some of the side effects to this is neural networks do not handle numbers well, especially if you need them fast and accurate. Deductive logic, accuracy and computational power are not their strongest abilities -- just like the human brain. However, once trained and implemented on hardware, there is no faster method for classification than neural networks. When a problem is solved by a neural network, it can not tell you how the problem was solved. "What any particular network can do is dependent on its structure and the computational properties of its component elements" [Rummelhart]. In other words, no network can learn anything that it is not capable of doing in theory. Since neural networks are modelling the human brain, whatever the human limits are, so follows the neural network limits.

Using [Rummelhart's] definition, the basic components of a "typical" neural network are:

- Start with a set of nodes that are all the same except for some randomly distributed parameter which makes each of them respond slightly differently

to a set of input patterns.

- Limit the "strength" of each node.
- Allow the nodes to compete in some way for the right to respond to a given subset of inputs.

The result of correctly applying these three components is the individual nodes "learn" to specialize on sets of similar patterns. The nodes start to discriminate between different classes of patterns by discovering features unique to each class. These unique features are not known by the neural network prior to the learning procedure.

Each neural network is made up of many, many nodes². A neural net is constructed of an input layer, an output layer and one or more hidden layers. These hidden layers are poorly understood [Touretzky]. Each hidden node is to simulate the human neuron cell. As such, it does not do much by itself, but in conjunction with the other hidden nodes, they create a very powerful, dynamic system. A simulated neuron has four important components: an input connections, a summation (product) function, a threshold function and an output connections. [Jones]

Neural networks lend themselves to certain styles of learning methods. If the number of hidden nodes is relatively small compared to the number of input nodes, the network will emulate the learn by induction method. It is a classifier. All neural networks tend to learn by positive examples. The function "discovered" by a neural network is essentially a least squares function to minimize the cost (error) function.

The most popular area in neural network research for pattern recognition is the use of back propagation during the training mode to correct any errors encountered. The back propagation is a method of implementing [Berwick's] Subset Principle. That is, based on the error calculated from the differences between the actual output and the expected output, make the smallest possible step towards lowering the error. This method of back propagation works, but it requires a tremendous amount of training time and it has all the problems of a gradient search (local minima, local maxima, etc.).

Another problem a neural network has is it does not always learn a temporally stable code in response to an arbitrary input environment. "The network's adaptability . . . enables prior learning to be washed away by more recent learning in response to a wide variety of input environments." [Carpenter] The problem results from characteristics that when combined, on the surface, seem so admirable: its ability to learn from experience and its ability to categorize several patterns into a compact internal representation.

[Carpenter] and [Grossberg] have proposed using Adaptive Resonance Theory (ART) to overcome these obstacles. Their neural network comes in two models: ART-1 and ART-2. ART-1 can only process binary input patterns; whereas, ART-2 can process gray scale input data.

"ART was introduced in 1976 to show how to embed a competitive learning model into a 'self-regulating control structure' whose autonomous learning and recognition proceed stably and efficiently in response to an arbitrary sequence of input patterns." [Carpenter] This is achieved by using a positive feedback loop allowing more stable output pattern

recognition. That is, "older experiences" are not lost to newer input experiences. Again, [Berwick's] Subset Theorem is employed to update the "learned" experiences database.

V. Conclusion

Military success on the field is depending more and more on sophisticated machinery in complicated situations. The massive amount of information flooding the pilot in a battle situation is overwhelming. Depending solely on a human pilot to decipher this barrage of data is, to say the least, foolhardy. There are many places where a pattern recognition intelligent system would benefit the military mission.

For instance, during an air-to-air "dogfight" a fighter pilot has should not have to identify friend or foe. A multi-tracking aircraft classifier should tell the pilot what and where the most immediate threat is, and at the same time target that system, based on the other aircraft's "pattern" and his own aircraft configuration. A possibility that has civilian and military applications would be a couple of pattern recognition systems for aircraft controller's. One system would recognize potentially dangerous flight congestion patterns and the other could identify hazardous wind shear conditions.

Using pattern recognition machines will greatly reduce the burden of data analysis these battlefield leaders must currently wade through. The machines should be autonomous learners, with the ability to be easily updated and reprogrammed in the field. Current research in the neural network field is quickly approaching this desired ability.

Endnotes

¹Maslow's "Hierarchy of Needs" theory basically states: a person must satisfy certain basic needs (such as food and water) before any higher, more esoteric need (such as religion and social approval) must be satisfied.

²The simplest "true" neural network contains 6 nodes: 2 input, 2 output and 2 hidden layer. This network can describe the logical XOR function. The same network without the hidden layer cannot perform this function.

Bibliography

GOVERNMENT PUBLICATIONS

Ross, T. D., "Definition and Realization in Pattern Recognition System Design." Air Force Wright Aeronautical Laboratories (AFWAL/AART-2), IEEE SMC Conference, 1987.

Ross, T. D., "Elementary Theorems in Pattern Theory." [Dissertation] AFIT/DS/ENC/88-01.

Ross, T. D., Lair, A. and Gadd, D., "A Generalized Development of the Combinatorial Implications for Computibility." [Internal Memo No. 9] Wright Research and Development Center (WRDC/AART-2), 27 February 1989.

BOOKS

Andrews, H. C., Introduction to Mathematical Techniques in Pattern Recognition. John Wiley and Sons, Inc., 1972.

Bongard, M., Pattern Recognition. Spartan Books. 1970.

Devijver, P. A. and Kittler, J., Pattern Recognition: A Statistical Approach. Prentice / Hall International, 1982.

Fu, K. S., Syntactic Pattern Recognition and Applications. Prentice / Hall International, 1982.

McClelland, J. L., et al., Parallel Distributed Processing. Vol 2: Psychological and Biological Models. MIT Press, 1986.

Michalski, R. S., et al., Machine Learning -- an Artificial Intelligence Approach, Vol. II. Morgan Kaufman Publishers, Inc., 1986.

Chapter 20: Holland, J. H., "Escaping Brittleness: The possibilities of General-Purpose Learning Algorithms Applied to Parallel Rule-Based Systems."

Chapter 21: Berwick, R. C., "Learning From Positive-Only Examples: The Subset Principle and Three Case Studies."

Pratt, V., Thinking Machines. Basil Blackwell, Ltd. 1987.

Rumelhart, D. E., et al., Parallel Distributed Processing, Vol 1: Foundations. MIT Press, 1986.

Chapter 5: "Feature Discovery by Competitive Learning," Rumelhart, D. E. and Zipser, D.

Chapter 7: "Learning and Relearning in Boltzmann Machines," Hinton, G. E. and Sejnowski, T. J.

JOURNALS

Alkon, D. L., "Memory Storage and Neural Systems." Scientific American. Vol. 261, No. 1, pp. 42 - 50. July 1989.

Anshelevich, V. V., et al., "On the Ability of Neural Networks to Perform Generalization by Induction." Biological Cybernetics. Vol. 61, pp. 125 - 128. July 1989.

Baim, P. W., "A Method for Attribute Selection in Inductive Learning Systems." IEEE Transactions on Pattern Analysis and Machine Intelligence. Vol. 10, No. 6, pp. 888 - 896. November 1988.

Barhen, J., et al., "Neural Learning of Constrained Nonlinear Transformations." Computer (IEEE). Vol. 22, pp. 67 - 76. June 1989.

Carpenter, G. A. and Grossberg, S., "The ART of Adaptive Pattern Recognition by a Self-Organizing Neural Network." *Computer (IEEE)*. Vol. 21, pp. 77 - 88. March 1988.

Caudill, M., "Neural Nets Primer, Part VIII." *AI Expert*. pp. 61 - 73. August 1989.

Fritz, W. et al., "The Autonomous Intelligent System." *Robotics and Autonomous Systems*. Vol. 5, No. 2, pp. 109 - 126. July 1989.

Greiner, R., "Learning By Understanding Analogies." *Artificial Intelligence*. Vol. 35, pp. 81 - 125. August 1988.

Grossberg, S., "Competitive Learning: From Interactive Activation to Adaptive Resonance." *Cognitive Science*. Vol. 11, pp. 23 - 63. 1987.

Hopfield, J. J. and Tank, D. W., "Computing with Neural Circuits: A Model." *Science*. Vol. 233, pp. 625 - 633. 8 August 1986.

Jones, W. P. and Hoskins, J., "Back-Propagation: A Generalized Delta Learning Rule." *Byte*. pp. 155 - 162. October, 1987.

Kodratoff, Y. and Tecuci, G., "Learning Based on Conceptual Distance." *IEEE Transactions on Pattern Analysis and Machine Intelligence*. Vol. 10, No. 6, pp. 897 - 909. November 1988.

Levine, D. S., "Neural Networks: Growth Field for the 1990s." *SIAM NEWS*. pp. 8 - 10, July 1988.

Lippmann, R. P., "An Introduction to Computing with Neural Nets." *IEEE ASSP Magazine*. pp. 4 - 21. April 1987.

MacWhinney, B. et al., "Language Learning: Cues or Rules?" *Journal of Memory and Language*. Vol. 28, No. 3, pp. 255 - 277. June 1989.

Obermeier, K. K. and Barron, J. J., "Time to Get Fired Up." Byte Magazine. Vol. 14, No. 8, pp. 217 - 224, August 1989.

Tank, D. W. and Hopfield, J. J., "Collective Computation in Neuronlike Circuits." Scientific American. pp. 104 - 114. December 1987.

Touretzky, D. S. and Pomerleau, D. A., "What's Hidden in the Hidden Layers?" Byte Magazine. Vol. 14, No. 8, pp. 227 - 233, August 1989.

Waibel, A. and Hampshire, J., "Building Blocks for Speech." Byte Magazine. Vol. 14, No. 8, pp. 235 - 242, August 1989.

1989 USAF-UES SUMMER FACULTY RESEARCH PROGRAM

GRADUATE STUDENT SUMMER SUPPORT PROGRAM

Sponsored by the
AIR FORCE OFFICE OF SCIENTIFIC RESEARCH

Conducted by the
Universal Energy Systems, Inc.

FINAL REPORT

A THEORETICAL RESOLUTION OF MULTIPLE FREQUENCIES

Prepared by:	Dr. David B. Choate <u>and Diana Major</u>
Academic Rank:	Assistant Professor
Department and	Science Division
University:	Transylvania University
Research Location:	Air Force Avionics Laboratory, Electronic Support Measure Group WPAFB, Ohio
USAF Researcher:	Dr. James Tsui
Date:	August 15, 1989
Contract No.	F49620-88-C-0053

Same Report As
Prof. David Choate
(Report # 99)

1989 USAF-UES SUMMER FACULTY RESEARCH PROGRAM/

GRADUATE STUDENT RESEARCH PROGRAM

Sponsored by the
AIR FORCE OFFICE OF SCIENTIFIC RESEARCH

Conducted by the
Universal Energy Systems, Inc.

FINAL REPORT

An Implementation of an Objective
Measure of Speech Intelligibility

Prepared by:	Douglas E. Melton
Academic Rank:	Graduate Student
Department and	Electrical Engineering
University:	The Ohio State University
Research Location:	WRDC/AAAI-4, Wright Patterson AFB
USAF Researcher:	2nd Lt Glenn Nead
Date:	August 21, 1989
Contract No:	F49620-88-C-0053

An Implementation of an Objective
Measure of Speech Intelligibility

by

Douglas E. Melton

ABSTRACT

A method of calculating the Speech Transmission Index (STI) was implemented in software to measure the intelligibility over a voice communication system. A FORTRAN program was developed to generate speech-like test signals that replace speech sources in a voice communication system. The STI is evaluated at the receiver by a second program. The speech intelligibility measurement system was tested using test signals that had been corrupted by stationary bandlimited noise at various signal to noise ratios. Appropriate signal to noise ratios were first determined from informal listening tests.

Acknowledgments

I am grateful to the Air Force Systems Command and the Air Force Office of Scientific Research for sponsoring this effort. I consider myself fortunate to have worked with the WRDC/AAAI-4 group. All of the members of the group were helpful and provided a truly enjoyable working atmosphere. I appreciate their contributions to this project. In particular, Cpt. Ted Riffle and Lt. Glenn Nead's participation was invaluable.

I greatly appreciate the encouragement and direction from my advisor, Dr. Ashok Krishnamurthy.

I: INTRODUCTION:

The evaluation of intelligibility over a voice communication system is a difficult measurement because intelligibility is a subjective property of speech. Many factors contribute to intelligibility including acoustic noise, semantic context, syntactic context, and the psychological and physiological condition of the listener.

The Communication Analysis and Evaluation Group of the Wright Research and Development Center is particularly concerned with the intelligibility of speech. The group's task is to evaluate the performance characteristics of avionic communication systems to serve as a reference standard or to determine the system's susceptibility to jamming or other interference. Integrated Communication, Navigation, Identification Avionics (ICNIA) is a recent effort to integrate several independent avionic communication systems. A large portion of the Communication and Analysis Group's work is geared to the analysis of ICNIA. Four of the sixteen systems contained in ICNIA are for voice communication. Therefore, a means of evaluating intelligibility would be of great use in analyzing ICNIA and other voice communication systems.

Intelligibility measures may be separated into two general classes. The first class includes all measures that incorporate human listeners. This class is known as the subjective measures. The subjective measures are usually

implemented by asking listeners to indicate what was heard in a controlled test. The results are then statistically evaluated to provide a measure of intelligibility. The second class of measures known as the objective measures do not incorporate human listeners in the process of determining intelligibility. Instead, the objective measures generally evaluate distortion related to intelligibility. One such measure is the STI developed by Steenken and Houtgast [1].

The STI is calculated by transmitting a speech-like signal over a voice communication system and then evaluating a particular type of distortion that is directly related to intelligibility. A test signal is created by sinusoidally varying the intensity within a band of frequencies in an otherwise stationary noise signal. Typically, the noise signal is spectrally shaped to represent the long term average spectrum of speech. The bands are chosen at one-octave widths to approximate the concentration of critical bands at low frequencies. The intensity of a single band is sinusoidally modulated at a fixed frequency between 0.625 Hz and 12 Hz to reflect the intensity modulation rate found in natural connected speech. The composite signal is used as a source in a communication speech. At the receiver, the signal is bandpass filtered to retain only the modulated band. Next, a waveform representing intensity is derived from the signal. The modulation index of the intensity waveform is computed and adjusted for the masking from lower frequency bands to replicate the effects of masking in the critical bands.

The adjusted modulation index is converted to SNR and normalized from -15 to 15 dB to a number in the interval $[0,1]$. This number is known as the Transmission Index (TI). The procedure is repeated to get a TI for each band. The TI's are weighted and summed to yield the STI. Figure 1 shows a sinusoidally modulated band and the corresponding waveform for the intensity in each band at the transmitter and at the receiver.

The STI measures the combined effects of additive noise, time dispersion and frequency dispersion on a modulated signal. Additive noise decreases the percent modulation of the intensity by adding an offset to the sinusoidal variation in intensity. Time dispersion decreases the modulation index by redistributing the energy over time, found in systems which include reverb or automatic gain control. Inter-band frequency dispersion is characterized by band crosstalk. Energy transfer from unmodulated bands to modulated bands results in a reduction of the modulation index. Thus several types of distortion contribute to the reduction of the modulation index.

My research interests have been in a variety of speech applications. I am currently working as a Graduate Research Associate at The Ohio State University in the areas of speech coding, speech applications of neural networks, speech recognition and intelligibility measures.

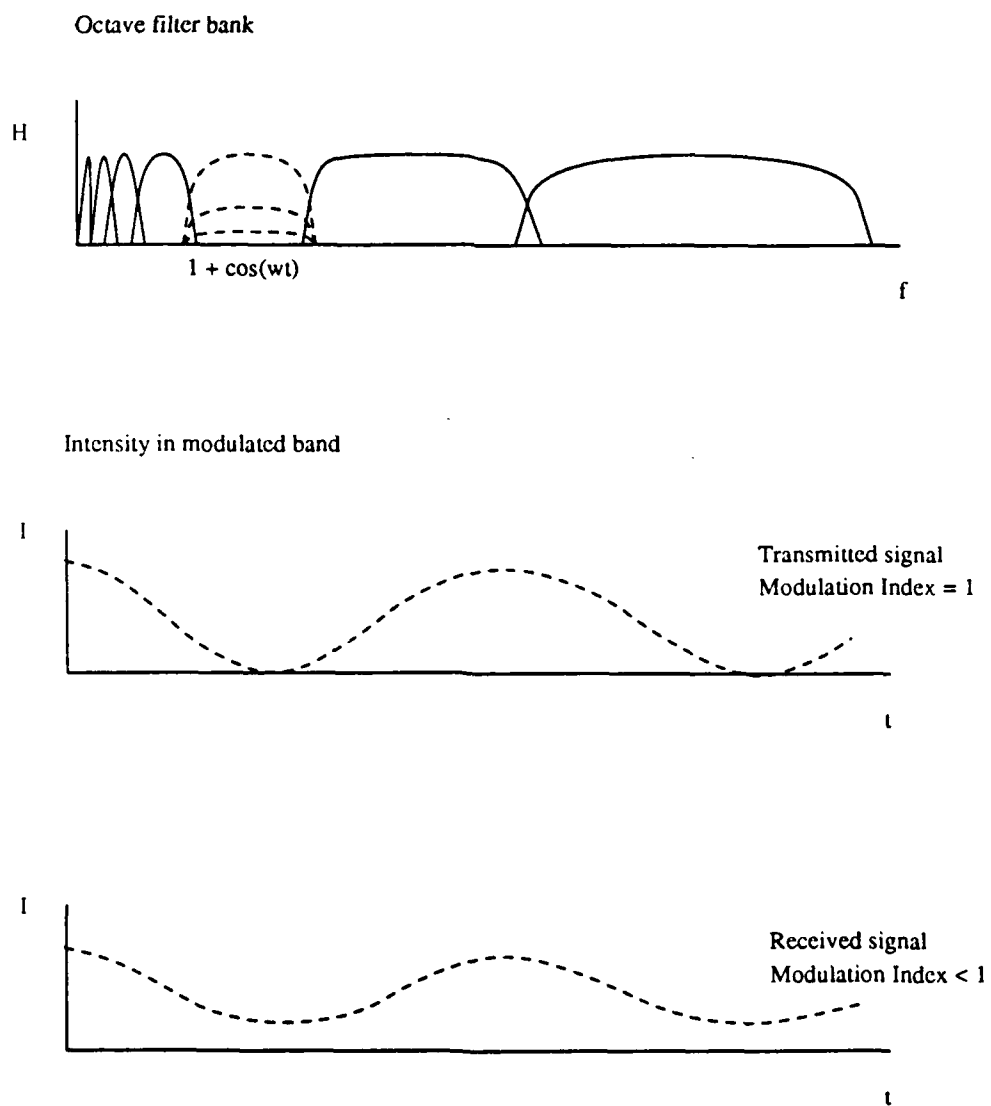


Fig. 1 STI Signals Used in TI Measurement

II: OBJECTIVES OF THE RESEARCH EFFORT:

Currently, the Analysis and Evaluation Group does not have a method of analyzing the performance of voice communication systems in terms of intelligibility. Communication systems are characterized in terms of bit error rate or signal to noise ratio (SNR). These measures have the disadvantage of being indirectly related to intelligibility.

As a participant in the 1989 Graduate Student Research Program, my assignment was to implement a means of measuring intelligibility over a communication channel. It was decided that the Speech Transmission Index (STI) was to be implemented in software. The measurements from the STI would be compared to subjective measurements of intelligibility. The tests would involve the use of simulated communication systems and a radio test set that is typical of avionics communication equipment. A description of the suggested method of measuring intelligibility was to be provided to the Analysis and Evaluation Group.

III:

a. Implementation, Programs and Methods

A FORTRAN program called "generate" was developed to produce the STI measurement test signal. It reads a set of configuration files named "stigen.cfg", "LPF.cfg", "HPF.cfg" to configure the filters and parameters used in the signal generation process. The file named "stigen.cfg" contains the sampling frequency f_s , the length of the test sequence in samples per band, the modulating frequency f_m , and the initial phase offset ϕ of the modulation $1 + \cos 2 * \pi * f_m * t + \phi$ for modulation, and a scaling factor.

The sampling frequency should be set to accommodate the frequency range that is to be analyzed. The sequence length should be chosen to be greater than to 2^N where N is equal to the number of bands. The modulating frequency is typically from 0.625Hz to 12.5Hz and should be a integer multiple of the sampling frequency divided by the length in samples,

$$f_m = k * \frac{f_s}{\text{length}}. \quad (\text{III} : .1)$$

The scaling factor should be chosen from the interval of 0.0 to 1.0. The factor indicates the maximum fraction of the available range for quantization. The range of quantization is fixed at -32767 to 32767 to accommodate 16-bit ADC/DAC. The scaling factor may be used to control the amplitude of the test signal. However, to retain full maximum resolution in the digital

to analog conversion, it is recommended that the scaling factor be kept at 1.0. Signal levels should be controlled by adjusting other gains in a test setup.

The development of the "generate" program required a noise sequence to be generated and split into frequency bands that might be individually modulated and recombined to form the test signal. A pink noise sequence is synthetically generated using the pseudo-random number generator in VAX extended FORTRAN. The sequence consists of independent random numbers, uniformly distributed over the interval $[-1,1]$.

The initial implementation of the "generate" program used a bank of $1/2$ octave digital filters to separate the pink noise signal into bands. A typical sampling frequency of 20480 Hz required a high resolution in the low frequency bands. The smallest bandwidth filter in the octave set had a bandwidth of 47 Hz. Some experimentation showed that the resolution required by the filters created a problem even when the filters were implemented using double precision floating point operations.

A solution was developed using upsampling and downsampling to avoid the high resolution requirements of the filters. Because the bands are arranged in octaves, it was possible to use a single lowpass filter and highpass filter in the construction of a test signal. The coefficients for the lowpass FIR filter are read from the configuration file "LPE.cfg". The coefficients for the highpass FIR filter are read from the file "HPF.cfg". A pink noise

sequence is generated with a length that corresponds a fraction of the total length of the test sequence per band. The appropriate length is found by dividing total length of the test sequence per band by $2^{(N-M)}$ where M is the index of the band being modulated (assuming the bands are numbered with the lowest frequency band as 1 and the highest as N). The noise sequence is lowpass filtered and highpass filtered. The highpass signal is modulated with the specified modulating frequency and added to the low-pass signal. Next, the signal is upsampled by a factor of 2. The remainder of the unmodulated bands are included in the composite signal by generating noise sequences of the correct length, high pass filtering, summation and upsampling until all bands are included. The composite signal is stored in a binary file called "stigen.dat". This method of generating a test signal allows the user to select high order FIR filters with low leakage, nearly eliminating crosstalk.

A program called "evaluate" was developed to analyze a test signal which may have been distorted by a communication system or by the introduction of synthetic noise. The program first reads a file called "stieva.cfg" to configure parameters including the sampling frequency, sequence length per band and modulating frequency. The parameters should be chosen to match the test signal. It then reads the file "stinoi.dat" which contains the signal in a binary format. The modulated band is separated by repeatedly downsampling and lowpass filtering the signal until the modulated band

may be extracted by high pass filtering. Rather than squaring the rectified signal filtered at 50Hz to obtain the intensity, as suggested by Steeneken and Houtgaust [1], a moving window is used to calculate the intensity waveform by forming a moving average of energy. A Gaussian shaped window was selected. The window shape is a function of the modulating frequency and the window overlap is fixed at 50 percent. This method of generating the intensity waveform requires less computation than digitally implementing the method described by Steeneken and Houtgaust. The correlation between the intensity waveform and sine and cosine at the modulating frequency are used to calculate the modulation index. The modulation index is converted to SNR and normalized from $[-15\text{dB}, +15\text{dB}]$ to $[0.0, 1.0]$ to obtain the TI. The hard limits of 0.0 and 1.0 are used for SNR's outside of the $[-15\text{dB}, +15\text{dB}]$ range. The TI's are found for each band, weighted and summed to form the STI.

A program called "addnoise" was developed to corrupt the test signal with synthetic additive noise. The program first reads a parameter file "stinoi.cfg" which specifies the type of additive noise, either Gaussian or uniformly distributed, the desired SNR, and the coefficients of a FIR/IIR digital filter to spectrally shape the noise. The sequence of data in the file "stigen.dat" is read and added to a noise sequence. The noisy sequence is stored in the file "stinoi.dat".

b. Data Collection Using Synthetic Noise

An informal study was conducted to determine an approximate threshold of intelligibility. Single word tokens were corrupted with Gaussian pink noise using the "addnoise" program. Three listeners unfamiliar with the tokens were asked to identify the tokens as each was presented, increasing the SNR each time. The listeners were also asked to identify the SNR level at which they first perceived speech even if it was unintelligible. The SNR at which the listeners indicated the presence of unintelligible speech was typically between -10dB and -15dB. The listeners typically first identified the token correctly at SNR's between -3dB and 3dB. The results of this study were used to determine a range of SNR's that would be used in data collection. The results also support the normalization step in the STI analysis procedure. Speech with a SNR -15dB roughly corresponds to the limit of the perception of speech. These conclusions are only valid for pink noise. Since the study was only used as a starting point in data collection, no attempt was made to generalize the tests to other noise spectra, or types of noise.

A fixed set of weights is used to produce the STI from the TI's. Steeneken and Houtgast list the weights they used to form the STI from a set of TI's. However, because of the differences in the methods of calculating the STI, it was unclear whether the weights would be appropriate for this imple-

mentation.

Ideally, the STI should be force to represent a subjective measure of intelligibility by using a set of weights that optimally correlate intelligibility with the STI over a large number of cases. Unfortunately, neither the time or resources were available to conduct such a study. The programs described above were configured to evaluate the seven octave bands used in standard STI measurements. In lieu of a alternate optimization criterion that would correlate the weights to a meaningful quantity, each band was weighted equally. Subsequent experiments with noisy data yielded results that seemed satisfactory.

c. Proposed Method of Measuring the STI

The measurement of the STI over a voice communication system at the CSEL laboratory will be conducted using the programs that have been described above. A proposed test setup is shown in Figure 2. The test arrangement will include a PC-AT equipped with a DSP-16 Ariel ADC/DAC board and a hard disk drive. The PC will be used to store several test signals with different modulating frequencies produced by the "generate" program on the MicroVax. The DSP-16 board and software will enable the PC to simultaneously provide a test signal source for the voice communication transmitter and digitize a noisy signal from the voice communication receiver. After the noisy signal is stored on the PC's disk, it will be trans-

ferred to the MicroVax and analyzed using the "evaluate" program.

IV: RECOMMENDATIONS

Several recommendations follow the investigation and implementation of the STI measure. The current method of measuring STI uses a flat pink noise spectrum. The STI method in Steeneken and Houtgast requires that the spectrum be shaped to represent the long term average spectrum of speech. It is believed that the effect on the ability of the STI measurement to characterize intelligibility is not greatly affected by the difference between the two methods. However, it may be desirable to compare the methods to verify this assumption.

To capture time-domain distortion such as the effects of reverb or automatic gain control, it is necessary to average the STI measurements at various modulating frequencies. In addition, because the STI measurement is based on noise processes, several measurements under identical conditions are suggested to obtain an average STI.

If subjective tests and STI measurements are to be performed simultaneously, the file "tilog.dat" should be used to record the TI's. After the subjective tests have been compiled, this data may be used to find an optimal set of weights that minimize the error between the subjective data

and the STI. For example, the difference between the STI and the fraction of correctly identified tokens may be used to find an optimal set of weights in a least squares sense.

The addition of bands to the STI warrants further investigation. The critical bands in the ear are known to be spaced in approximately $1/3$ octave widths. The implementation of the STI measurement currently uses seven bands. Increasing the STI measurement to include twenty-one bands would increase the bandwidth resolution to roughly the same as found in the ear.

As an alternative to the software implementation, the STIDAS-II is a hardware device to perform the STI measurement. Its current price is approximately \$18,000 and is available from the TNO Institute for Perception, Soesterberg, The Netherlands. This system is primarily implemented in analog hardware, thus reducing computational requirements.

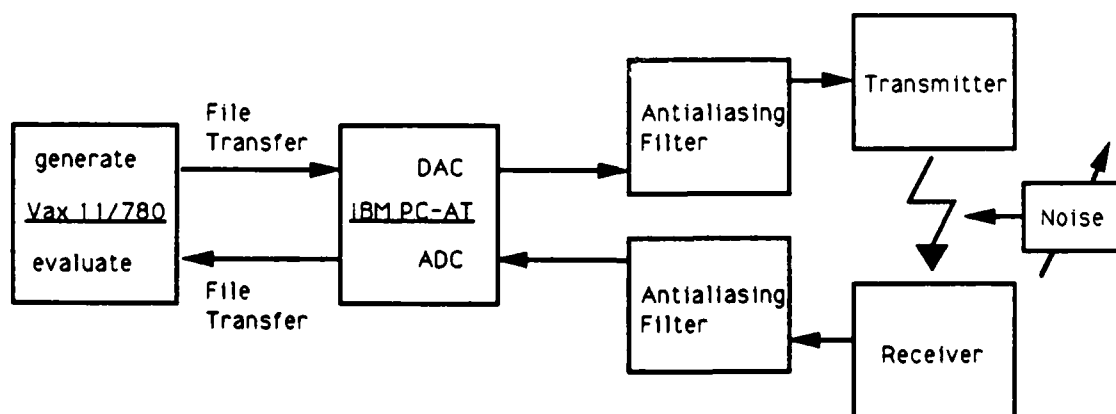


Figure 2. Test Setup for STI Measurement

Appendix

The following represent suggested configuration files.

stigen.cfg

20480	Sampling frequency in Hz
131072	Length in samples per band
5.0	Modulation frequency in Hz*
0.0	Initial phase of modulation in radians

* for extensive testing choose a variety of modulating frequencies, e.g.

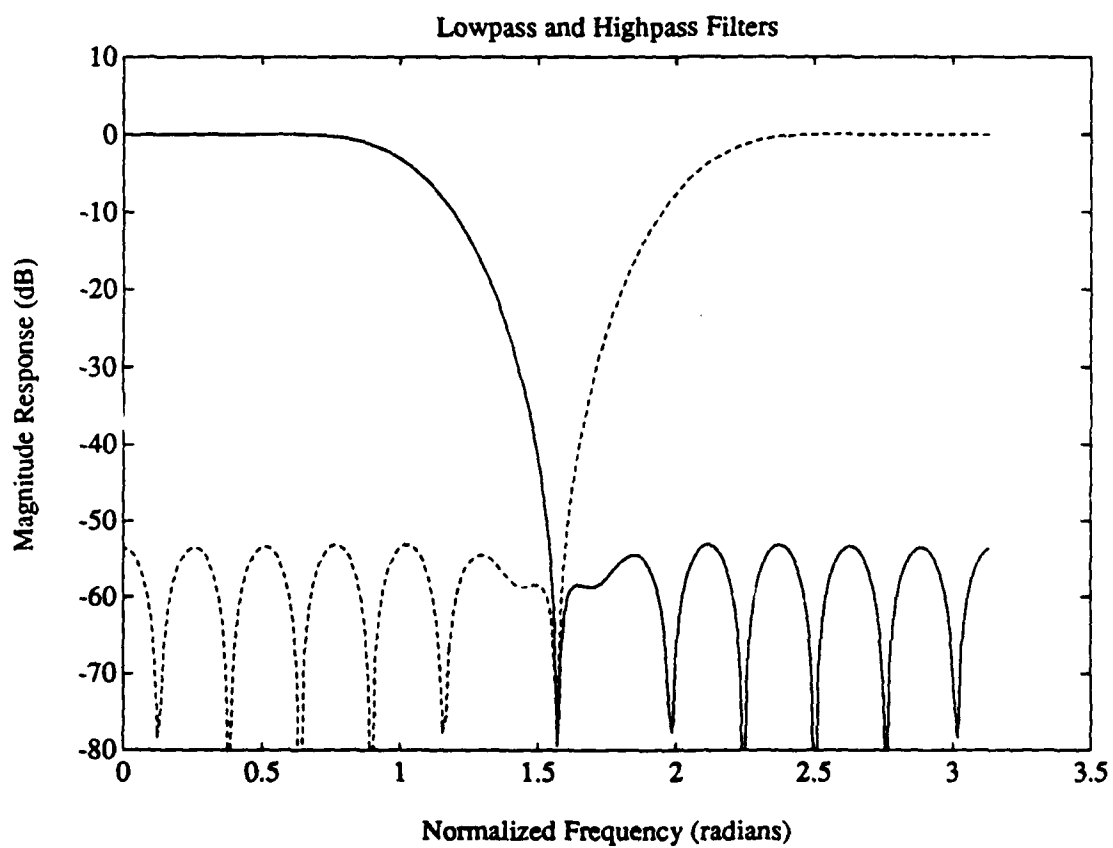
0.625Hz, 1.25Hz, 2.5Hz, 5.0Hz, 10.0Hz

stieva.cfg

20480	Sampling frequency in Hz
131072	Length in samples per band
5.0	Modulation frequency in Hz*

* should match modulation frequency in stigen.cfg

LPF.cfg and **HPF.cfg** configure the lowpass and highpass filters. The transform functions for the currently configured filters are shown below.



References

- [1] Steeneken, H.J.M. and Houtgast, T., "A physical measure for measuring the quality of speech transmission channels," J. Acoust. Soc. Am. 67, 318.

1989 USAF-UES SUMMER FACULTY RESEARCH PROGRAM/
GRADUATE STUDENT RESEARCH PROGRAM

Sponsored by the
AIR FORCE OFFICE OF SCIENTIFIC RESEARCH

Conducted by the
UNIVERSAL ENERGY SYSTEMS, INC.

FINAL REPORT

Radiation Hypersonic Aerodynamics: Numerical Simulation of
Hypersonic Flows Past Slender Wedges Near the Continuum
Limit

Prepared by:	John Baker
Academic Rank:	Graduate Student
Department and	Department of Mechanical Engineering
University:	University of Kentucky
Research Location:	WRDC/FIMM W.P.A.F.B. Dayton, OH 45433-6553
USAF Researcher:	Joseph S. Shang
Date:	04 August 1989
Contract No:	F49620-88-C-0053

Radiation Hypersonic Aerodynamics: Numerical Simulation of
Hypersonic Flows Past Slender Wedges Near the Continuum
Limit

by
John Baker

ABSTRACT

A survey of literature dealing with hypersonic flows, numerical techniques for describing hypersonic flows, radiative transfer, and approximations to the Radiative Transfer Equation is presented. The problem of hypersonic flow in a slightly rarefied medium past a slender wedge is formulated using an explicit MacCormack finite difference scheme, the Navier-Stokes equations, and the Maxwellian velocity slip and temperature jump boundary conditions. Preliminary results are presented for the no slip case of a 2° half-angle wedge. No conclusions are drawn since the research effort is still in the initial stages of finding convergent (steady-state) solutions of the Navier-Stokes equations for slightly rarefied flow past slender wedges.

ACKNOWLEDGEMENT

I wish to thank the Air Force Systems Command, the Air Force Office of Scientific Research, and Universal Energy Systems for allowing me the opportunity to spend a very challenging and worthwhile summer at the Flight Dynamics Laboratory, Wright-Patterson Air Force Base, Dayton, Ohio. I would also like to thank Dr. Shiva N. Singh for bringing this program to my attention.

My experience this summer was fulfilling because of many different influences. Joe Shang provided me with guidance, support, and encouragement. My discussions with Dr. Shang were very helpful in my overall understanding of computational fluid dynamics. The help of Don Rizzetta and Miguel R. Visbal was invaluable in overcoming many of the technical problems I faced, and their interest in my project often served as a source of motivation. The assistance I received from Gerald Trummer, Raymond E. Gordnier, and Steve Sherr with the various computer systems was greatly appreciated. Eswar Josyula must be mentioned, not only for his contribution of a number of high informative articles, but also for his helpful advice throughout the summer. I would like to thank Capt. Gary Huband and Kervyn Mach for their help and encouragement. My discussions with Phil Webster, Mike Stanek, Capt. Paul Boyles, and Datta Gaitonde greatly contributed to the summer's success. Though rarely technical, these discussions were always memorable.

Finally, I would like to thank Wladimiro Calarese for the fencing lesson.

I. INTRODUCTION

Hypersonic aerodynamics is conventionally defined as those flows where the Mach number is greater than 5. It is near this Mach number that various physical flow phenomena; viscous interactions, vorticity interactions, thin shock layers, and high temperature effects, become increasingly more important. Since most hypersonic flight vehicles will operate at high altitudes, low-density effects are also important in an analysis of hypersonic flows.

The Computational Aerodynamics Group of the Wright Research and Development Center's Flight Dynamics Laboratory at Wright-Patterson Air Force Base is primarily concerned with the application of finite difference techniques in the analysis of various flow fields. A number of researchers in the Computational Aerodynamics Group have extensive experience with the explicit MacCormack finite difference method and its application to hypersonic flow fields. The group also has access to excellent computational facilities ranging from a Cray 2, at Kirtland Air Force Base, and a Cray X/MP, at Wright-Patterson Air Force Base, to three Iris workstations in the lab itself.

My research interests have been in the field of computational fluid dynamics as applied to low-density hypersonic flows and the thermal radiation effects in such flows. My thesis advisor, Professor Shiva N. Singh of the University of Kentucky, has been closely associated with the Computational Aerodynamics Group for the past few years. My association with Dr. Singh was how I initially learned of the Graduate Student Research Program and contributed to my assignment to the Computational Aerodynamics Group.

II. OBJECTIVES OF THE RESEARCH EFFORT

The Navier-Stokes equations, which are based on a continuum assumption, yield increasingly unacceptable results as the Knudsen number, defined as the ratio of molecular mean free path to the characteristic length, approaches unity. It has been shown, as will be detailed in the next section, that the introduction of Maxwellian velocity slip and temperature jump boundary conditions, on the solid surface of a flat plate, can increase the range of Knudsen numbers for which the Navier-Stokes equations are valid. If this technique can be shown effective for other flow field configurations, the Navier-Stokes equations can be used instead of the complex Boltzmann equations as a means of effectively predicting flow field characteristics in the hypersonic slip-flow regime.

My assignment as a participant in the 1989 Graduate Student Research Program (GSRP) was to begin a study on the effectiveness of the Navier-Stokes equations, with slip boundary conditions, for predicting characteristics of slightly rarefied hypersonic flow past slender wedges. The research effort may be broken into three parts: 1) a survey of literature relating to hypersonic flows, numerical techniques used to model hypersonic flows, thermal radiative transfer, and approximations to the Radiative Transfer Equation (RTE), 2) modification of an existing algorithm to include the slip boundary conditions and the effects of radiative transfer, and 3) a comparison of the no-slip, slip, and slip plus radiation numerical results with experimental results to determine the validity of the numerical results.

Due to time considerations, it was decided that the literature survey and the modifications to the computer codes, JSTEST and FDL2D.JOB, should take precedent during my stay at Wright-Patterson Air Force Base. Efforts to achieve convergent solutions being attempted during the later portion of the GSRP and continuing at the University of Kentucky upon my return.

III. LITERATURE SURVEY

During the late 1950s and early 1960s, a great deal of work was done in the field of hypersonic flow. A number of texts were published which dealt exclusively with hypersonic flow theory [1,2,3,4,5]. Also at this time, at least two review articles were published [6,7]. However, during the 1970s, research in the hypersonic flow regime dwindled. It has only been in the last 5 to 7 years that hypersonic flows have once again gained interest. Evidence of this interest can be seen in recent review articles [8,9,10,11]. This renewed effort to examine hypersonic flow is generally attributed to plans for a number of hypersonic flight vehicles [12].

The most common method of predicting characteristics of hypersonic flow fields is the integration of the Navier-Stokes equations over a particular flow field. A variety of methods have been developed to accomplish this. The most popular being finite difference methods. In 1970, Davis [13] used a finite difference method to solve the hypersonic viscous shock layer equations, while in 1968, Rudman and Rubin [14] used finite difference to solve for hypersonic viscous flows over slender bodies. In 1971, Erdos and Zakkay [15] used a Lax-Wendroff finite difference method to model wakes behind slender bodies. A version of the Lax-Wendroff method, the MacCormack method [16,17,18,19], has been used to model a number of flow fields, both supersonic and hypersonic. Rizzetta and Mach [20] compared four differencing schemes and found that the MacCormack method performed well in the hypersonic regime. Two excellent texts for an overview of finite differencing techniques have been written by Anderson, Tannehill, and Pletcher [21] and Oran and Boris [22]. Another popular approach is the Monte Carlo method. This method has proved very effective for both equilibrium and nonequilibrium flows [23,24,25,26,27]. Recently, Woronowicz and McDonald [28] used a modified version of the Direct Simulation Monte Carlo Method which takes advantage of the vector architecture supercomputers to model wedge flows near the continuum limit.

As mentioned previously, low density effects, while not caused by hypersonic flow, will likely exist for most hypersonic flight regimes [12]. A great deal of experimental [29,30,31,32] and computational [33] work has been done to examine low density hypersonic flows. From a computational standpoint, this usually entails solving the Boltzmann equations. Further information on the kinetic theory of gases may be found in reference [34,35]. However, for slightly rarefied flows, $0.03 < Kn < 0.2$ [12], it has been shown that the Navier-Stokes equations, with slip boundary conditions, can provide acceptable result for certain flow fields [36,37]. A discussion of slip effects and the slip boundary conditions may be found in [38,39,40,41,42].

One final note before discussing thermal radiative transfer. Equilibrium conditions will rarely exist in actual hypersonic flows. A number of papers have been presented which examine the nonequilibrium effects in hypersonic flows [42,43,44].

The interaction of radiation, conduction, and convection in boundary-layer flows as well as thermal boundary layers is well documented [45, 46,47,48,49,50]. Texts by Seigel and Howell [51] and Özişik [52] contain chapters dealing with multimode heat transfer. Pai [53] has written a text which deals exclusively with radiation interactions with flow fields. A number of researchers have examined the effect of thermal radiation on a hypersonic flow field [54,55]. The difficulty in an analysis of thermal radiation is the complex nature of the Radiative Transfer Equation (RTE). Available approximation techniques are discussed in the review paper by Mengüç and Viskanta [56]. The most popular approximation is the Rosseland, or optically thick, approximation [57,58,59,60,61, 62]. Other approximation techniques are the optically thin approximation [63], the grey gas approximation [64,65], the Milne-Eddington approximation [66,67], spherical harmonics [68,69,70], the moment method [71], and the Monte Carlo method [72].

IV. NOMENCLATURE

Re	Reynolds number
M	Mach number
Kn	Knudsen number
Pr	Prandtl number
C_f	Skin friction coefficient
C_p	Coefficient of pressure
a	Speed of sound
λ	Molecular mean free path
$\vec{U}, \vec{F}, \vec{G}$	Vector fluxes
t	Time
x, y	Cartesian coordinates (physical plane)
ξ, η	Transformed coordinates (computational plane)
ρ	Density
μ	Viscosity
τ	Optical thickness
$\tau_{xx}, \tau_{yy}, \tau_{xy}$	Viscous stress components
e	Specific internal energy
k	Molecular heat conduction
u, v	velocity components (cartesian coordinates)
c_v	Specific heat (constant volume)
p	Static pressure
q	Heat transfer flux term
ϵ	Emissivity coefficient
β	Absorption coefficient
I	Radiation intensity
γ	Specific heat ratio
θ	Wedge half-angle
<u>Subscript</u>	
∞	Free stream condition
w	Wall Condition
<u>Superscript</u>	
r	Radiative terms
i, j	Coordinate index

V. GOVERNING EQUATIONS AND BOUNDARY CONDITIONS

The compressible, time-dependent, two-dimensional Navier-Stokes equations, in cartesian coordinates without body forces, may be represented as [21, 36]

$$\frac{\partial \bar{U}}{\partial t} + \xi_x \frac{\partial \bar{F}}{\partial \xi} + \eta_x \frac{\partial \bar{G}}{\partial \eta} + \eta_y \frac{\partial \bar{G}}{\partial \eta} = 0 \quad (1)$$

where \bar{U} , \bar{F} , and \bar{G} are defined as

$$\bar{U} = \begin{bmatrix} \rho \\ \rho u \\ \rho v \\ \rho e \end{bmatrix} \quad (2)$$

$$\bar{F} = \begin{bmatrix} \rho u \\ \rho u^2 + p - \tau_{xx} \\ \rho uv - \tau_{xy} \\ (\rho e + p)u - u\tau_{xx} - v\tau_{xy} + q_x + q_x^R \end{bmatrix} \quad (3)$$

$$\bar{G} = \begin{bmatrix} \rho v \\ \rho uv - \tau_{xy} \\ \rho v^2 + p - \tau_{yy} \\ (\rho e + p)v - u\tau_{xy} - v\tau_{yy} + q_y + q_y^R \end{bmatrix} \quad (4)$$

and where

$$\tau_{xy} = \tau_{yx} = \mu \left(\frac{\partial u}{\partial y} + \frac{\partial v}{\partial x} \right) \quad \tau_{yy} = \frac{2}{3} \mu \left(2 \frac{\partial v}{\partial y} - \frac{\partial u}{\partial x} \right) \quad (5), (6)$$

$$\tau_{xx} = \frac{2}{3} \mu \left(2 \frac{\partial u}{\partial x} - \frac{\partial v}{\partial y} \right) \quad q_x = -k \frac{\partial T}{\partial x}, \quad q_y = -k \frac{\partial T}{\partial y} \quad (7), (8), (9)$$

The radiation flux terms, q_x^r and q_y^r , will be defined in the next section. μ is defined by Sutherland viscosity formula [21,73,74]. The definition of the thermal conductivity may be found in [17,21]. By assuming the perfect gas relations for the equations of state, a constant Prandtl number, and a constant specific heat, the above system is formally closed. The boundary conditions used for the numerical analysis are found in table 1. See figure 2 for definition of the surfaces. For more information concerning the slip boundary conditions see references [36,37,74].

Table 1: Boundary Conditions for Hypersonic Wedge Flows.

Surface	No slip	Slip
solid surface 1	$u=0$ $v=0$ $T_w = T_\infty$	$u(0) = \frac{2-\epsilon}{\epsilon} \gamma \left(\frac{\partial u}{\partial y} \right)_0$ $v(0) = 0$ $T(0) - T_w = \frac{2-\epsilon}{\epsilon} \frac{2\gamma}{\gamma+1} \frac{T}{Pr} \left(\frac{\partial T}{\partial y} \right)_0$
2,3	$u=u_\infty \cos\Theta$ $v=u_\infty \sin\Theta$ $T_w = T_\infty$	same as for no slip
4	$u(x,y)=u(x+1,y)$ $v(x,y)=v(x+1,y)$ $T(x,y)=T(x+1,y)$	same as for no slip

VI. RADIATION HEAT TRANSFER

The RTE for a semi-infinite, nonscattering, absorbing, and emitting media is defined as [36,52]

$$\mu \frac{\partial I(r, \xi, \mu)}{\partial r} + I(r, \xi, \mu) = I_b [T(r, \xi)] \quad (10)$$

where

$$\begin{aligned} I(0, \xi) &= \int_0^1 I(0, \xi, \mu) d\mu \\ &= \epsilon_w I_b [T_w(\xi)] + 2(1 - \epsilon_w) \int_0^1 I(0, \xi, -\mu') d\mu' \end{aligned} \quad (11)$$

The radiative flux terms, q_x^r and q_y^r , are defined as [52]

$$q^r(r, \xi) = 2\pi \int I(r, \xi, \mu) \mu d\mu \quad (12)$$

The derivation of the formal solution of the heat flux terms are beyond the scope of this report. A complete discussion of the RTE and the formal solution of the radiative heat flux term may be found in [51,52].

VII. NUMERICAL ANALYSIS

For the analysis of the flow field, an explicit MacCormack finite difference method was used [16,17,18,19,21,75]. Applied to equation (1), the following algorithm results

Predictor:

$$\begin{aligned} \bar{U}_{i,j}^{n+1} = & \bar{U}_{i,j}^n - \Delta t(((\Delta \eta / \Delta x)(\bar{F}_{i,j+1}^n - \bar{F}_{i,j}^n) + (\Delta \eta / \Delta y)(\bar{G}_{i,j+1}^n - \bar{G}_{i,j}^n)) \\ & (1/\Delta \eta) + ((\Delta \xi / \Delta x)(\bar{F}_{i+1,j}^n - \bar{F}_{i,j}^n) + (\Delta \xi / \Delta y)(\bar{G}_{i+1,j}^n - \bar{G}_{i,j}^n))(1/\Delta \xi)) \end{aligned} \quad (13)$$

Corrector:

$$\begin{aligned} \bar{U}_{i,j}^{n+1} = & 0.5[\bar{U}_{i,j}^n + \bar{U}_{i,j}^{n+1} - \Delta t(((\Delta \eta / \Delta x)(\bar{F}_{i,j}^{n+1} - \bar{F}_{i,j-1}^{n+1}) + \\ & (\Delta \eta / \Delta y)(\bar{G}_{i,j}^{n+1} - \bar{G}_{i,j-1}^{n+1}))(1/\Delta \eta) - ((\Delta \xi / \Delta x)(\bar{F}_{i,j}^{n+1} - \bar{F}_{i,j-1}^{n+1}) + \\ & (\Delta \xi / \Delta y)(\bar{G}_{i,j}^{n+1} - \bar{G}_{i-1,j}^{n+1}))(1/\Delta \xi))] \end{aligned} \quad (14)$$

The scheme is second order accurate in both space and time. An empirical expression for the time step is given by [21]

$$\Delta t \leq \frac{\sigma (\Delta t)_{CFL}}{(1 + \frac{2}{Re_\Delta})} \quad (15)$$

where $\sigma \approx 0.9$ and $(\Delta t)_{CFL}$ is given by

$$(\Delta t)_{CFL} \leq \left\{ \frac{|u|}{\Delta x} + \frac{|v|}{\Delta y} + a \sqrt{\left(\frac{1}{\Delta x^2} + \frac{1}{\Delta y^2} \right)} \right\}^{-1} \quad (16)$$

Re is the minimum mesh Reynolds number. An initial guess of ambient conditions for the entire flow field grid begins the iterative process by which an asymptotic steady-state solution is found.

VIII. RESULTS AND CONCLUSIONS

Figure 1 is a schematic diagram of the actual flow field configuration. Figure 2 is a diagram of a typical numerical grid of the physical plane used in the current flow field configuration. The spacing is constant in the streamwise direction and exponentially stretched in the normal direction [76]. The solid surface is defined as surface 2. Figures 3, 4, 5, and 6 represent preliminary data from the first convergent solution. The parameters used in this solution were; no slip, 2° wedge half angle, $T_\infty = 74.292^\circ\text{R}$, $T_w = 576.048^\circ\text{R}$, $M = 21.9$, $Re = 370/\text{in.}$, $CFL = 0.02$, and the medium was assumed to be air. The solution was ran to 30000 iterations. I am still unsure as to why the CFL requirement was so small. Figures 3, 4, 5, and 6 are not presented to show any quantitative comparison. They are presented to show that even with the no slip condition the Navier-Stokes equations yield a qualitative picture of the flow field. For instance, notice the shape of the temperature profile, figure 6. The effect of viscous dissipation is clearly shown in the increase in temperature as one moves away from the wall followed by a sharp decrease to ambient temperature beyond a certain y/RL , where RL is the reference (1 ft.).

At this point in the research effort, no conclusions can be drawn as to the effectiveness of the Navier-Stokes (N-S) equations, with slip boundary conditions, in the slip flow regime for flow past slender wedges. I am; however, optimistic. All the literature seems to indicate that the N-S equations, with slip conditions, will be effective and I feel that the slip conditions should not affect the stability of the MacCormack scheme. The radiative transfer may cause problems with the algorithm, but at this point, there is no evidence to indicate that this will happen.

REFERENCES

1. Truitt, R.W., Hypersonic Aerodynamics, Ronald Press, New York, 1959.
2. Cox, R.N. and Crabtree, L.F., Elements of Hypersonic Aerodynamics, Academic Press, New York, 1965.
3. Chernyl, G.G., Introduction to Hypersonic Flow, (trans. by R.F. Probst), Academic Press, New York, 1961.
4. Hayes, W.D. and Probst, R.F., Hypersonic Flow Theory, Academic Press, New York, 1959.
5. Dorrance, W.H., Viscous Hypersonic Flow, McGraw-Hill Book Company, New York, 1959.
6. Cheng, H.K., "Recent Advances in Hypersonic Flow Research," AIAA J., v.1, n.2, Feb. 1963, pp.295-310.
7. Zhigulev, V.N., Romishevskii, Ye. A., and Vertushkin, V.K., "Role of Radiation in Modern Gas Dynamics," AIAA J., v.1, n.6, June 1963, pp. 1473-1485.
8. Singh, S.N., "Radiation Hypersonic Aerodynamics," AFWAL-TM-87-197-FIMM, 1987.
9. Nagamatsu, H.T. and Sheer, R.E., Jr., "Hypersonic Gas Dynamics," AIAA Paper 85-0999, 1985.
10. Holden, M.S., "A Review of Aerothermal Problems Associated with Hypersonic Flight," AIAA Paper 86-0267, 1986.
11. Bird, G.A., "Low-Density Aerothermodynamics," AIAA Paper 85-0994, 1985.
12. Anderson, J.D., Jr., Hypersonic and High Temperature Gas Dynamics, McGraw-Hill Book Company, New York, 1989.
13. Davis, R.T., "Numerical Solution of the Hypersonic Viscous Shock-Layer Equations," AIAA J., v.8, n.6, June 1969, pp.1099-1109.
14. Rubin, S.G. and Rudman, S., "Hypersonic Viscous Flow over Slender Bodies with Sharp Leading Edges," AIAA J., v.6, n.7, July 1971, pp.1287-1293.
15. Erdos, J.I. and Zakkay, V., "Inviscid Solution of the Steady, Hypersonic Near Wake by a Time-Dependent Method," AIAA J., v.9, n.7, July 1971, pp.1287-1293.

16. MacCormack, R.W. and Baldwin, B.S., "A Numerical Method for Solving the Navier-Stokes Equations with Application to Shock Boundary-Layer Interactions," AIAA Paper 75-1, 1975.
17. MacCormack, R.W. and Hung, C.M., "Numerical Solutions of Supersonic and Hypersonic Laminar Flows over a Two-Dimensional Compression Corner," AIAA Paper 75-2, 1975.
18. Shang, J.S., Hankley, W.L., Jr., and Law, C.H., "Numerical Simulation of Shock Wave-Turbulent Boundary-Layer Interaction," AIAA J., v.14, n.10, Oct. 1976, pp. 1451-1457.
19. Shang, J.S. and Hankley, W.L., Jr., "Numerical Solution of the Navier-Stokes Equations for a Three-Dimensional Corner," AIAA J., v.15, n. 11, Nov. 1977, pp.1575-1582.
20. Rizzetta, D. and Mach, K., "Comparative Numerical Study of Hypersonic Compression Ramp Flows," AIAA Paper 89-1877, 1989.
21. Anderson, D.A., Tannehill, J.C., and Pletcher, R.H., Computational Fluid Mechanics and Heat Transfer, Hemisphere Publishing Corp., New York, 1984.
22. Oran, E.S. and Boris, J.P., Numerical Simulation of Reactive Flows, Elsevier, New York, 1987.
23. Vogenitz, F.W., Bird, G.A., Broadwell, J.E., and Rungaldier, H., "Theoretical and Experimental Study of Rarefied Supersonic Flows about Several Simple Shapes," AIAA J., v.6, n.12, Dec. 1968, pp. 2388-2394.
24. Gupta, R.N. and Simmonds, A.L., "Hypersonic Low-Density Solutions of the Navier-Stokes Equations with Chemical Nonequilibrium and Multi-component Surface Slip," AIAA Paper 86-1349, 1986.
25. Gökçen, T. and MacCormack, R., "Nonequilibrium Effects for Hypersonic Transitional Flows using Continuum Approach," AIAA Paper 89-0461, 1989.
26. Cheng, H.K., Lee, C.J., Wong, E.Y., and Yang, H.T., "Hypersonic Slip Flows and Issues on Extending Continuum Model Beyond Navier-Stokes Level," AIAA Paper 89-1663, 1989.
27. Bird, G.A., "Aerodynamic Properties of Some Simple Bodies in the Hypersonic Transition Regime," AIAA J., v.4, n.1, Jan. 1966, PP. 55-60.
28. Woronowicz, M.S. and McDonald, J.D., "Application of a Vectorized Particle Simulation in High-Speed Near-Continuum Flow," AIAA Paper 89-1665, 1989.

29. Vidal, R.J. and Wittliff, C.E., "Hypersonic Low Density Studies of Blunt and Slender Bodies," Rarefied Gas Dynamics, (J.A. Laurmann, ed.), suppl. 2, Academic Press, New York, 1963, pp.343-378.
30. Vidal, R.J. and Bartz, J.A., "Experimental Studies of Low-Density Effects in Hypersonic Wedge Flows," Rarefied Gas Dynamics, (J.H. de Leeuw, ed.), v.1, Academic Press, New York, 1965, pp.467-486.
31. Chow, W.L. and Eiler, R.E., "Hypersonic Low-Density Flow Past Slender Wedges," AIAA J., v.6, n.1, Jan. 1968, pp.177-179.
32. Vidal, R.J. and Bartz, J.A., "Surface Measurements on Sharp Flat Plates and Wedges in Low-Density Hypersonic Flows," AIAA J., v.7, n.6, June 1969, pp.1099-1109.
33. Chung, Chan-Hong, Jeng, Duen-Ren, DeWitt, Kenneth J., and Keith, Theo G., Jr., "Flow of Rarefied Gases over Two-Dimensional Bodies," AIAA Paper 89-1970-CP, 1989.
34. Grad, H., "Theory of Rarefied Gases," Rarefied Gas Dynamics, (F.M. Devienne, ed.), Pergamon Press, New York, 1960, pp.100-138.
35. Shidlovskiy, V.P., Introduction to Dynamics of Rarefied Gases, (J.A. Laurmann, ed.), American Elsevier Publishing Company, 1967.
36. Singh, S.N., "Radiation Hypersonic Aerodynamics," to be published, University of Kentucky, Department of Mechanical Engineering, Lexington, Kentucky, 1989.
37. Gökçen, T., MacCormack, R.W., and Chapman, D.R., "Computational Fluid Dynamics Near the Continuum Limit," AIAA Paper 87-1115, 1987.
38. Chrusciel, G.T., Lewis, C.H., and Sugimura, T., "Slip Effects in Hypersonic Rarefied Flows," Rarefied Gas Dynamics: Part II, (Sam S. Fisher, ed.), v.74, AIAA, New York, 1980, pp.1040-1054.
39. Gampert, B., "Velocity-Slip and Temperature-Jump Effects in Similar, Slightly Rarefied Laminar Boundary-Layer Flows Past Surfaces with Incomplete Momentum and Energy Accommodation," Rarefied Gas Dynamics Part II, (Sam S. Fisher, ed.), v.74, AIAA, New York, 1980, pp. 1105-1121.
40. Tsien, Hsue-Shen, "Superaerodynamics, Mechanics of Rarefied Gases," J.A.S., Dec. 1946, pp.653-664.
41. Shorenstein, M.L. and Probst, R.F., "The Hypersonic Leading-Edge Problem," AIAA J., v.6, n.10, Oct. 1968, pp.1898-1906.
42. Candler, G.V. and MacCormack, R.W., "The Computation of Hypersonic Flows in Chemical and Thermal Nonequilibrium," Paper 107, Third National Aero-Space Plane Technology Symposium, June 1987.

43. Scala, S.M. and Sampson, D.H., "Heat Transfer in Hypersonic Flow with Radiation and Chemical Reaction," Report R63SD16, Twenty-First AGARD Combustion and Propulsion Meeting on Supersonic Flow, Chemical Processes, and Radiative Transfer, London, April 1963.
44. Josyula, E. and Shang, J.S., "Numerical Simulation of Nonequilibrium Hypersonic Flows with Wall Catalytic Effects," AIAA Paper 89-0462, 1989.
45. Schlichting, Hermann, Boundary-Layer Theory, McGraw-Hill Book Company, New York, 1979.
46. Viskanta, R. and Grosh, R.J., "Boundary Layer in Thermal Radiation Absorbing and Emitting Media," Int. J. Heat Mass Transfer, v.5, 1962, pp.211-225.
47. Tabaczynski, R.J. and Kennedy, L.A., "Thermal Radiation Effects in Laminar Boundary-Layer Flow," AIAA J., v.5, n.10, Oct. 1967, pp. 1893-1894.
48. Fulkerson, G.D. and Bannerot, R.B., "An Approximation for Combined Heat Transfer in a Radiatively Absorbing and Emitting Gas," AIAA Paper 73-750, 1973.
49. Mengüç, M.P. and Iyer, R.K., "Modeling of Radiative Transfer using Multiple Spherical Harmonics Approximations," J. Quant. Spectrosc. Radiat. Transfer, v.29, n.6, 1988, pp.445-461.
50. Viskanta, R., "Interaction of Heat Transfer by Conduction, Convection, and Radiation in a Radiating Fluid," J. Heat Transfer, v.85, n.4, 1963, pp. 318-328.
51. Siegel, R. and Howell, J.R., Thermal Radiation Heat Transfer, Hemisphere Publishing Corp., New York, 1981.
52. Özişik, M.N., Radiative Transfer and Interactions with Conduction and Convection, Wiley Publishing, New York, 1973.
53. Pai, Shih-I, Radiation Gas Dynamics, Springer-Verlag, New York, 1966.
54. Gupta, R.N., "Navier-Stokes and Viscous Shock-Layer Solutions for Radiating Hypersonic Flows," AIAA Paper 87-1576, 1987.
55. Bloor, M.I.G., "Effect of Radiative Heat Transfer on Hypersonic Shock Layer," AIAA J., v.6, n.10, Oct. 1968, pp.2006-2008.
56. Viskanta, R. and Mengüç, M.P., "Radiation Heat Transfer in Combustion Systems," Prog. Energy Combust. Sci., v.13, 1987, pp.97-160.
57. Deissler, R.G., "Diffusion Approximation for Thermal Radiation in Gases with Jump Boundary Conditions," J. Heat Transfer, v.86, n.2, 1964, pp.240-248.

58. Novotny, J.L. and Yang, Kwang-Tzu, "The Interaction of Thermal Radiation in Optically Thick Boundary-Layers," J. Heat Transfer, v.89, n.4, 1967, pp.309-312.
59. Minin, I.N., "Diffusion of Radiation in a Semi-Infinite Medium in the Case of Anisotropic Scattering. I.," AIAA J., v.1, n.6, June 1963, pp.1486-1491.
60. Aparci, V.S. and Larsen, P.S., "A Thick Gas Model Near Boundaries," AIAA J., v.7, n.4, April 1969, pp.602-606.
61. Wang, L.S. and Tien, C.L., "A Study of Various Limits in Radiation Heat Transfer Problems," v.10, n.10, Oct. 1967, pp.1327-1338.
62. Heaslet, M.A. and Warming, R.F., "Radiative Transport and Wall Temperature Slip in an Absorbing Planar Medium," Int. J. Heat Mass Transfer, v.8, 1965, pp.979-994.
63. Olfe, D.B., "Radiative Cooling in Transparent Shock Layers of Wedges and Cones," AIAA J., v.4, n.10, Oct. 1966, pp.1734-1740.
64. Cess, R.D., "Radiation Effects upon Boundary-Layer Flow of an Absorbing Gas," J. Heat Transfer, v.86, n.4, 1962, pp.462-475.
65. Sampson, D.H., "Choice of an Appropriate Mean Absorption Coefficient for Use in the Grey Gas Equations," J. Quant. Spectrosc. Radiat. Transfer, v.5, n.1, 1965, pp.211-225.
66. Viskanta, R. and Grosh, R.J., "Heat Transfer by Simultaneous Conduction and Radiation in an Absorbing Medium," J. Heat Transfer, v.84, n.1, 1962, pp.63-72.
67. Vincenti, W.G. and Baldwin, B.S., "Effects of Thermal Radiation on the Propagation of Plane Acoustic Waves," J. Fluid Mech., v.12, 1962, pp. 449-477.
68. Mengüç, M.P. and Iyer, R.K., "Modeling of Radiative Transfer using Spherical Harmonics Approximations," J. Quant. Spectrosc. Radiat. Transfer, v.39, n.6, 1988, pp.445-461.
69. Le Sage, L.G., "Application of the Double Spherical Harmonics Method to the One-Dimensional Radiation Transfer Equation," NASA TN D-2589, 1965.
70. Cheng, Ping, "Two-Dimensional Radiating Gas Flow by a Moment Method," AIAA J., v.2, n.9, Sept. 1964, pp.1662-1664.
71. Cheng, Ping, "Dynamics of a Radiating Gas with Application to Flow Over a Wavy Wall," AIAA J., v.4, n.2, Feb. 1966, pp.238-245.

72. Howell, J.R. and Perlmutter, M., "Monte Carlo Solution of Thermal Transfer Through Radiant Media Between Gray Walls," J. Heat Transfer, v.91, Feb. 1964, pp.116-122.
73. Ames Research Staff, "Equations, Tables, and Charts for Compressible Flow," NACA Report 1135, 1953.
74. White, F.M., Viscous Fluid Flow, McGraw-Hill Book Company, New York, 1974.
75. MacCormack, R.W., "Numerical Simulation of the Interactions of a Shock Wave with a Laminar Boundary-Layer," Proceedings of the Second International Conference on Numerical Methods in Fluid Dynamics, (Maurice Holt, ed.), Springer-Verlag, 1970.
76. Vinokur, Marcel, "On One-Dimensional Stretching Functions for Finite-Difference Calculations," NASA Contractor Report 3313, 1980.

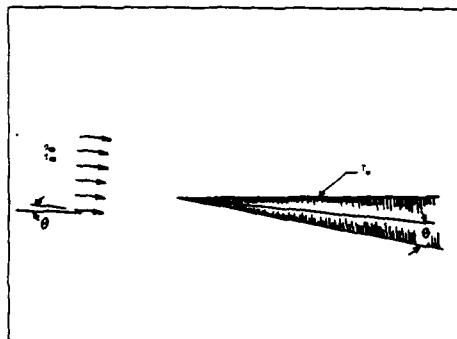


Figure 1: A schematic diagram of the physical flow field configuration.

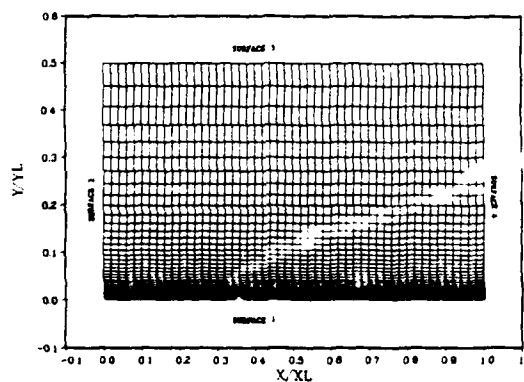


Figure 2: A typical grid (51 X 41) used to model the flow field.

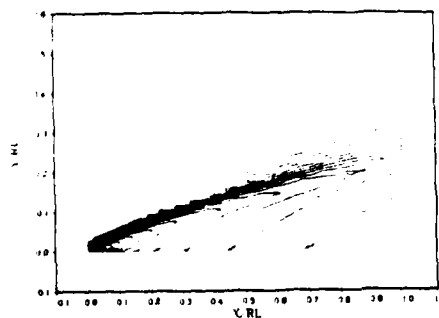


Figure 3: Pressure contours for the converged solution of the no slip, 2° wedge.

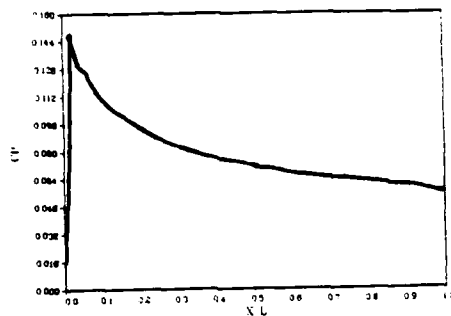


Figure 4: Coefficient of Pressure as a function of streamwise length.

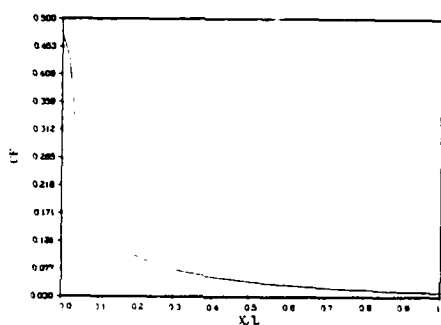


Figure 5: Skin friction coefficient as a function of streamwise length.

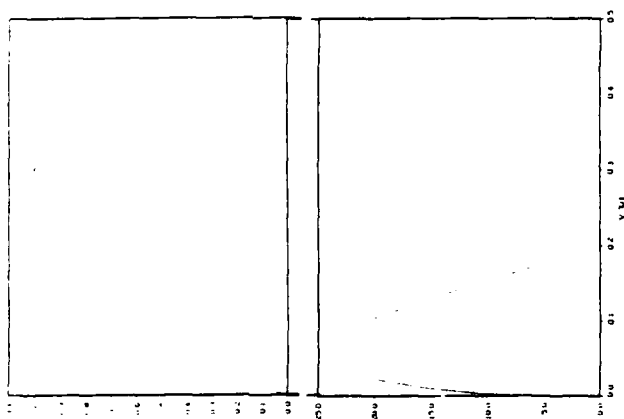


Figure 6: Velocity and temperature profiles at $X/RL=0.5$.

1989 USAF-UES SUMMER FACULTY RESEARCH PROGRAM

GRADUATE STUDENT RESEARCH PROGRAM

Sponsored by the
AIR FORCE OFFICE OF SCIENTIFIC RESEARCH

Conducted by the
Universal Energy Systems, Inc.

FINAL REPORT

VALIDATION SCHEMES

FOR

ACCELERATED CRAZING TESTS

AND

X3D - A FINITE ELEMENT ANALYSIS CODE

Prepared by:	Kerry D. Christopher
Academic Rank:	Graduate Student
Department and University:	Division of Computer Science University of West Florida, Pensacola FL
Research Location:	Aircrew Enclosures Group, Vehicle Subsystems Division, Flight Dynamics Laboratory, WPAFB
USAF Researcher:	Robert McCarty
Date:	September 6, 1989
Contract Number:	F49620-88-C-0053

VALIDATION SCHEMES
FOR
ACCELERATED CRAZING TESTS
AND
X3D - A FINITE ELEMENT ANALYSIS CODE

by
Kerry D. Christopher

ABSTRACT

Aircraft transparency durability is a principle concern of the Vehicle Subsystems Division and efforts are being made to increase the service life of these components. Transparency durability encompasses a range of issues from impact resistance due to birdstrike to optical degradation due to environmental exposure. A durability validation plan is being developed which will enable prediction of the service life of a transparency design based on tests of the building materials at the fabrication stage.

Resistance to birdstrike is considered during the initial design phases. One of the current finite element design analysis tools is MAGNA, Materially And Geometrically Nonlinear Analysis, which uses implicit integration methods. A new finite element analysis tool, X3D, based on explicit integration methods has been delivered to the Aircrew Enclosures Group for evaluation.

Failure modes that necessitate the rejection of the transparencies include scratches, cracks, crazing, coating deterioration and delaminations. The long term service life

validation scheme will consider acrylic crazing because it is the predominate failure mode in transparencies. The F-16 transparency was chosen because of the large amount of data on hand associated with F-16 transparency failures. Once a successful scheme has been devised, additional schemes will be devised for other failure modes of various aircraft transparency systems.

ACKNOWLEDGEMENTS

I wish to thank the Air Force Systems Command and the Air Force Office of Scientific Research for sponsorship of this research.

Special thanks go to Robert McCarty and Mike Gran of the Aircrew Enclosures Group, Vehicle Subsystems Division for their efforts in making my research with them a productive and rewarding experience. I would also like to thank Dr. Nisar Shaikh, University of Nebraska-Lincoln, for his guidance and encouragement.

VALIDATION SCHEMES
FOR
ACCELERATED CRAZING TESTS
AND
X3D - A FINITE ELEMENT ANALYSIS CODE

I. INTRODUCTION

Great cost savings can be realized if the frequency of replacement of aircraft transparency systems can be reduced. At present the acceptance of the parts from a vendor is based largely on their meeting the optical and other performance standards, including birdstrike resistance, with little effective regard to the expected service life. A durability validation scheme is being developed by the Vehicle Subsystems Division that aims to predict the service life of transparencies from various manufacturers, representing different designs, materials and fabrication techniques. When incorporated, such schemes will allow the comparison of alternative transparency designs from different manufacturers based on their service life and thus help determine cost effectiveness. The technique will specify certain tests on coupons from trimmings or a randomly selected transparency from a production batch and predict durability based on this test data.

A. Validating laboratory tests for accelerated crazing

The accelerated crazing test consists of loading a polymethyl-methacrylate (PMMA) specimen exposed to a solvent of known concentration and noting the time of appearance of the craze. The value of strain can be obtained from the strain gages mounted on the specimen. The stress at the location of craze incipience may be calculated from elasticity. These stress results can be compared to results

of a MAGNA solution. The laboratory results may only be compared to MAGNA results prior to the incipience of craze. The onset of crazing will relieve stress in the vicinity of the craze. MAGNA has no way of accounting for the stress relief resulting from the occurrence of crazing.

B. Validation of the X3D code

The X3D finite element analysis code results will be compared to laboratory tests results conducted by the University of Dayton Research Institute (UDRI). The laboratory tests involved loading a cantilever beam and recording strain measurements from strain gauges mounted on the test specimen.

II. OBJECTIVES OF THE RESEARCH EFFORT

At the present time, acrylic crazing is recognized as the principle failure mode for F-16 transparencies. To reduce the cost of ownership, it is necessary to understand the mechanics involved and the root causes of crazing. The Aircrew Enclosures Group is addressing these issues under its durability program.

My assignment was to assist Dr. Nisar Shaikh in conducting laboratory tests to induce accelerated crazing in commercially available PMMA material. Unfortunately, our research periods overlapped for only two weeks. After some preliminary laboratory tests to induce accelerated crazing, Dr. Shaikh had to return to the University of Nebraska-Lincoln. As a follow-on to Dr. Shaikh's work, the laboratory tests were analyzed using MAGNA to show correlation between the test data and predicted values from the finite element analysis code.

Additionally, the Aircrew Enclosures Group has a finite element analysis code, X3D, that requires validation. This project involved using X3D to predict the stresses on a composite cantilever beam of polycarbonate, silicone, and PMMA.

My previous research work has been in the area of Optimal Control Theory and systems integration. This entailed working with applied mathematics in the areas of the calculus of variations, control theory, and Kalman filters. Implementing these concepts involved various programming languages and techniques, real time systems, and embedded systems.

III. VALIDATION OF ACCELERATED CRAZING TESTS

Stress is essential for the induction of craze in plastics. Experiments on stressed specimens taken in dry air and in contact with moisture have shown that the time for growth of craze is significantly accelerated by the presence of solvents, even distilled water. The presence of an organic liquid is found to have a severe effect on the induction of craze in polymethyl-methacrylate (PMMA). The crazing strain is lowered by small molecules of liquid diffusing into the polymer and hence increasing the mobility of the micromolecular chains. In the field, exposure to various solvents has the undesirable effect of reducing the service life of the canopy. In laboratory tests the liquid is used advantageously to reduce the experiment time.

A. Biaxial Test

For the biaxial stress laboratory tests, a rectangular plate of PMMA was held fixed at one edge and left free at the other three edges. Concentrated forces were applied to the side opposite of the fixed edge to simulate a varying biaxial state of stress. Downward forces were applied at the two free corners while an upward force was induced by a support at the middle. By raising or lowering the position of the support, one of the principal stresses can be changed from tension to compression.

B. Test Procedures

Have the fixture made as follows. Two aluminum strips, 8"x2"x0.5", with 3/8" inch diameter holes drilled on one inch centers. The fixture was mounted at the edge of a work table with C-clamps.

First a piece of 10"x8"x0.125" PMMA sheet will be strain gaged and tested. A commercially available acrylic sheet may be used for the test. A variety of sample dimensions and loads may be used, however, the sample size, loads, and middle support displacement should be such that a maximum stress of 2000 psi is induced without excessive deflection. Drill holes at one edge of the PMMA specimen to coincide with that of the fixture so that the edges are flush. A grid should be laid out with felt tipped pen to help locate the strain gages. A clear tape compatible with the strain gauges may be used on the PMMA to help with the grid marking and gage locations. Eight strain gages should be mounted on one side of the plate. They may be mounted on half the surface as symmetry may be assumed. The other side, free from strain gages, will be the top side upon which craze will be induced. A felt sheet soaked with isopropanol (50% concentration in water) will be layed on the top side and covered with a compliant sheet of clear plastic to retard the drying. The incipience and grid location of craze was noted every two minutes for the first ten minutes and every five minutes thereafter. Preferably strain measurements should be taken after each occurrence of crazing, at least in the neighboring regions. The felt sheet should be replenished with solvent as needed to keep the surface wet.

C. Data Analysis

The strain gage readings will be converted to principal strains. The resulting stresses will be compared the results of a MAGNA analysis.

D. Laboratory Test Results

Preliminary tests were conducted at the facilities of the UDRI. A rectangular plate of PMMA was placed under biaxial stress to induce crazing. A 35 percent solution of isopropanol in water was applied to the surface of the test specimen to accelerate the onset of crazing. Strain measurements were obtained from the strain gages mounted on the PMMA test specimen. The induced crazing started at the point of highest stress, near the offset contact point, as expected. Increasing amounts of crazing were observed until the crazing degraded the structural integrity of the PMMA test specimen such that fracture occurred.

Two tests were run using the procedures outlined above.

The first test used 7 pounds of weight at the two free corners with an enforced displacement of $+13/32$ inches at the center edge between the loads. Crazing was noted after approximately 15 minutes. Fracture followed shortly. It is believed that the offset point was the source of an excessive point stress that precipitated the fracture.

In the second test 4 pounds of weight were placed at the two free corners. The point of enforced displacement was moved to the center of the test specimen and set at approximately $3/8$ inches. A compliant pad was used between the offset screw and the PMMA specimen to alleviate the point stress problem of the first test. Crazing occurred in approximately 30 minutes. The crazing was aligned with the principle lines of stress. Crazing progressed for approximately 10 minutes until the test specimen fractured. The premature fracture did not allow us to carry out the planned crazing tests.

E. MAGNA Results

The laboratory test results for strain should only be considered prior to the initial incidence of craze for the purpose of comparison with MAGNA computed strains.

PATRAN was used to model the PMMA test specimen. It was modelled as a hyperpatch with a 13 by 13 by 1 mesh. Each element was designated as HEX/20, a 20 node brick, with the midside nodes suppressed to conform to MAGNA's 16 node brick input requirement. The PATRAN to MAGNA translator, PATMAG, was used to convert the PATRAN neutral file to the input file format required by MAGNA. The preliminary nature of the laboratory tests precludes an indepth analysis, however, the magna results compare favorably with the laboratory results. The Von Mises stress component of the MAGNA analysis results were used to determine the probable areas of craze. This corresponded roughly to those areas with over 2000 psi predicted. Although the Von Mises stress estimates are a conservative measure, the areas of stress concentration matched the areas where crazing occurred in the laboratory test specimens.

IV. X3D VALIDATION

A. PATRAN Modelling

PATRAN was used to model the composite cantilever beam. A patch was created with the overall y-z dimensions and then sectioned into the three composite layers using the BREAK option. A hyperpatch corresponding to each composite layer was created from these patches with the EXTRUDE option. Each hyperpatch was given a 60 by 5 by 5 mesh. Each element was designated as HEX/8, as required by X3D. Next, the EQUIVALENCE option was used to delete duplicate nodes and renumber the remaining nodes. For the nodes that are fixed, boundary conditions must be set. The WINDOWS option was used to look at specific areas containing the fixed nodes. Once these node numbers were determined, the DISPLACEMENT option was used to fix their positions.

B. Preparing X3D Input File

The PATRAN neutral file output was used as the input to the PATRAN to X3D translator, PATX3D. The output from PATX3D requires some editing before it can be used as the input to X3D.

For this particular example, several input blocks were required. They included

- PARAMETERS - Solution control parameters
- PRESSURE - Pressure loading data
- HISTORY - Time history functions for loading data
- MPOST - Request MPOST format output file
- TOLERANCE - Additional solution parameters
- MAT3 - Solid (3-D) material properties

C. X3D Simulations

The X3D simulations to date have been inconclusive. The initial X3D simulations were made with fine mesh beam model. This resulted in an excessively large amount of CPU time for the simulation. A coarser model was developed to reduce the CPU time required for a X3D analysis. The results of the X3D runs with the coarser model still required a large amount of CPU time and the results were uninterpretable. This may be due to the type of solution requested for these analyses. All the analyses thus far have been for a static solution. Even though the laboratory test results were recorded for a static solution, an X3D analysis may require a dynamic analysis with a graduated load history curve. This would alleviate the model from coping with a very large step input at time zero.

V. RECOMMENDATIONS

A. Laboratory tests

An aircraft grade material should be procured and its mechanical properties tested prior to future tests. A more elaborate test fixture should also be designed to induce

strain by prescribed displacements by screws rather than stressing by hanging weights. This will reduce the creep induced effect and make the tests more realistic.

B. X3D validation

The explicit integration methods of X3D do not allow concentrated forces to be placed on nodes. The forces are applied to element faces as pressure loads. In the UDRI laboratory tests the applied force was concentrated at discrete points. In X3D the forces can be modelled by distributing the force over element faces adjacent to the loaded nodes. Alternately, the elements adjacent to the loaded nodes can be joined by deleting the loaded nodes and the force distributed over the newly generated elements. The latter method will increase the stiffness of those new elements, however there should be very little bending in this area and thus the increased stiffness may not affect the overall model behavior. Both methods should be evaluated to obtain the best correlation with the laboratory results.

REFERENCES

1. PATRAN Plus User Manual, Vol. 1 & 2, PDA Engineering, 1987
2. X3D User Information, X3D Version 2.3, University of Dayton Research Institute, 1989

1989 USAF-UES SUMMER FACULTY RESEARCH PROGRAM/

GRADUATE STUDENT RESEARCH PROGRAM

Sponsored by the
AIR FORCE OFFICE OF SCIENTIFIC RESEARCH
conducted by the
Universal Energy Systems, Inc.

FINAL REPORT

Neural Networks and their Role in Visual Object Recognition

Prepared by:	Augustus Morris, Jr., Ph.D. and <u>Nancy Faulkner</u> *
Academic Rank:	Assistant Professor
Department and	*Graduate Student Manufacturing Engineering
University:	Central State University
Research Location:	Flight Dynamics Laboratory, Special Projects, Group
USAF Researcher:	Mangal Chawla, Ph.D.
Date:	September 30, 1989
Contract No:	F49620-88-C-0053

Same Report As
Prof. Augustus Morris
(Report # 109)

1988 USAF-UES SUMMER FACULTY RESEARCH PROGRAM/
GRADUATE STUDENT SUMMER SUPPORT PROGRAM

Sponsored by the
AIR FORCE OFFICE OF SCIENTIFIC RESEARCH
Conducted by the
Universal Energy Systems, Inc.

FINAL REPORT

DAMAGE IN GRAPHITE/EPOXY PLATES SUBJECTED TO LOW VELOCITY IMPACT

Prepared by: Bryan C. Foos
Academic Rank: Graduate Research Associate
Department and University: Civil Engineering Department
The Ohio State University
Research Location: AFWAL/FIBCA
Wright Patterson AFB
OH 45433
USAF Researcher: Dr. R. S. Sandhu
Date: 30 Sep 88
Contract No: F49620-87-R-0004

DAMAGE IN GRAPHITE/EPOXY PLATES SUBJECTED TO LOW VELOCITY IMPACT

by_

Bryan C. Foos

ABSTRACT

Instrumented impact tests on laminated graphite/epoxy panels were conducted using a drop tower. The velocity of the impactor and the load time history were recorded for each specimen tested. In several tests, strains were measured on the back face during the impact event. The depth of surface indentation and the extent of internal damage were measured and correlated with the impact energy. Predicted strains in the outermost ply were compared with experimentally obtained values measured both perpendicular to and in the direction of the outermost fiber. The amount of internal damage and the indentation were found to be dependent upon the energy at impact and to a somewhat lesser degree on the velocity of the impactor. The shape of the damaged area in the specimens tested, was largely dependent upon the thickness of the panel and the location of the supports.

ACKNOWLEDGEMENTS

The author wishes to thank the Air Force Systems Command and the Air Force Office of Scientific Research for sponsorship of this research. Universal Energy Systems administered the project and was very helpful during my summer stay.

I want to thank the administration of the Flight Dynamics Laboratory, AFWAL, for allowing me to participate in the Summer Graduate Student Research Program at their facility and by so doing have the opportunity to work with a very talented laboratory staff. The conversations we had contributed greatly to my understanding of the behavior of composite structures. The assistance of the Materials Laboratory in the evaluation of the levels of post-impact damage is appreciated.

I am particularly grateful to my program monitor, Dr. R. S. Sandhu, and group leader, Mr. G. R. Holderby, who provided the technical background and work environment to make my summer both educational and enjoyable.

I. INTRODUCTION:

The research program described in this report was a continuation of work begun last summer by Graduate student Gregory Schoeppner and his faculty advisor Dr. William E. Wolfe in the Flight Dynamics Laboratory, AFWAL. The experimental studies conducted at that time showed that repeatable low velocity impact tests could be performed on graphite/epoxy laminated composite plates using the instrumented drop tower facility in the Structures Division. Also shown was that a correlation could be made between the impact energy and the extent of internal damage sustained by the composite plate in the form of ply delamination. With the background obtained in the conduct of those tests, the experimental program carried out this year was developed. Target gr/ep plates ranging in thickness from 9 to 96 plies were subjected to different levels of impact energy. The size of the damaged area and a profile of the depth of surface indentation were determined by ultrasonic measurements and Moire methods respectively. The extent of the damage measured in the experiments was compared with the damage zone predicted by a computer program recently received by the Flight Dynamics Laboratory and modified as part of this program.

Last year's tests indicated that the load cell in the instrumented tup tended to vibrate during impact when the target was a graphite/epoxy plate. Because this "ringing" of the load cell makes it difficult to isolate from the total signal, that portion of the load actually being transmitted to the target, a

concern of the investigators during the present testing program was a proper identification of the load time history imparted to the target plate. The necessary measurements were made by positioning strain gages on the back face of the target plate and recording the gage response during the impact event.

II. OBJECTIVES OF THE RESEARCH EFFORT:

The primary objective of this summer research effort was to continue the program begun last summer. That program was designed to determine experimentally, the levels of damage induced in laminated composite plates subjected low velocity impact, and to correlate the damage observed with known properties of the target plate and the impact event. Of particular interest was the identification of the test parameters that would provide us with damage levels consistent with the Air Force and NASA specification for nondetectable damage. That specification states that the limit of nondetectable impact damage is that

damage caused by the impact of a 25 mm (1.0 in) diameter hemispherical impactor with a 135 J (100 ft-lbf) of kinetic energy or that kinetic energy required to cause a dent 2.5 mm (0.10 in) deep, whichever is least. (ASM International, 1987)

Along with the experimental program, the recent literature was reviewed in an expansion of the survey of literature conducted during last summer's effort.

A computer program, only recently received in the Flight Dynamics Laboratory, that predicts the extent of damage in an impacted plate, was investigated. This program allows the user to input the magnitude the impact, the boundary conditions and material properties of the plate, making it possible to simulate our experiments in the computer and thereby to verify the applicability of the model for the material systems currently of greatest interest.

III. REVIEW OF LITERATURE:

The behavior of graphite/epoxy composite systems during impact has been studied extensively over the past twenty years. It has been shown experimentally that interior damage significant enough to reduce overall structural strength by as much as 50% may not be visible on the surface (Cantwell and Morton, 1984 and Ramkumar, 1981). Furthermore, this strength loss may be larger than that resulting from a hole drilled to the same size as the impact and larger than that measured after ballistic tests are performed.

The response of the target has been shown to be a function of specimen thickness. Thin specimens typically fail in flexure, whereas thicker specimens fail in shear. A more thorough review of the existing literature can be found in the report of last year's summer program (Wolfe, 1987).

IV. TEST PROGRAM:

Low velocity impact tests were conducted on composite panels from 9 plies to 96 plies thick using the FIBC Dynatup drop test facility. The impact velocity and time history of force were recorded for all tests. Several panels had strain gages attached to the back face allowing time histories of strain to be recorded as well.

The experimental program was divided into two phases. In phase one, the level of impact energy resulting in just detectable surface damage as defined in Reference was determined. Since the level of impact energy required to cause a detectable dent on the impact face resulted in extensive matrix cracking on the backface, reliable strain measurements could only be made during a second phase of tests in which the impact energy was significantly reduced from the phase one levels. Because the impact energy level was low in the phase two tests, the effect of multiple hits on the response of a target plate could be investigated. This was accomplished by subjecting instrumented 26 and 48 ply plates to repeated low impact energy hits.

V. DISCUSSION OF TEST RESULTS:

A listing of the tests performed in the phase 1 portion of the program is given in Table 1. The impact energy was calculated from the measured velocity at impact. The amount of permanent

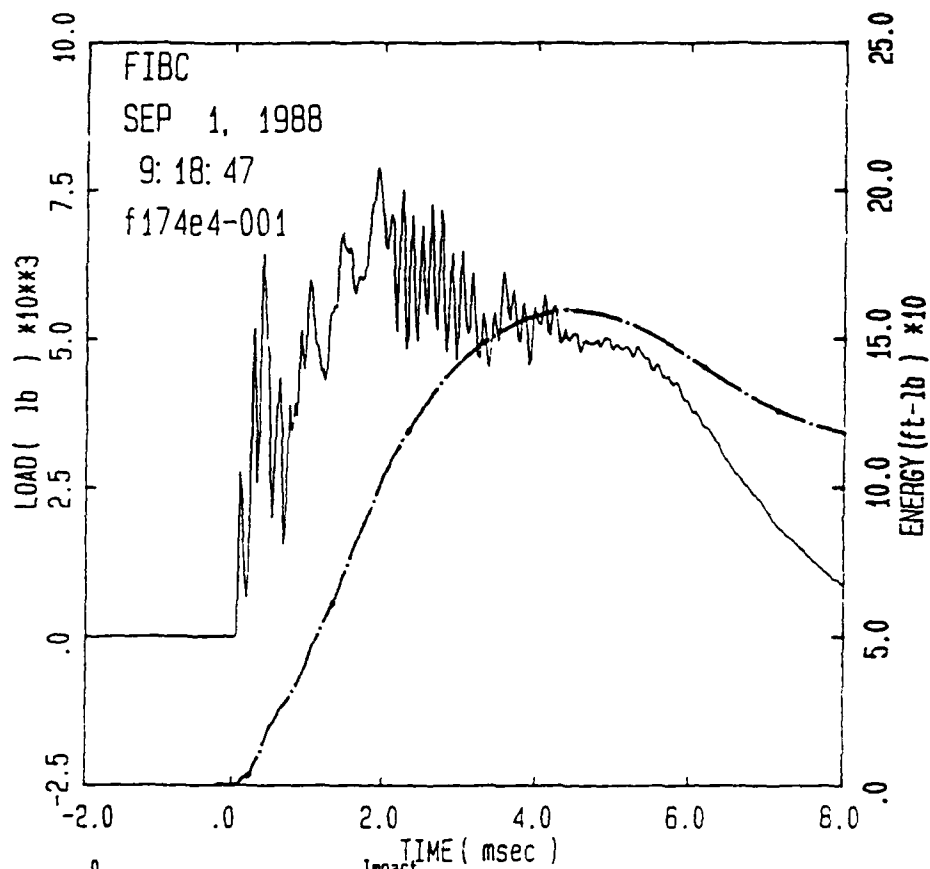
surface indentation was measured for each test using Moire techniques.

An example of typical force and energy time histories (test no. f174e4-001) is shown in Figure 1. Fiber breakage and/or matrix cracking are clearly shown in the figure as a succession of spikes leading up to the maximum load. The maximum load is followed by a series of high frequency spikes which persist for approximately 2 msec. A comparison of the results of the different tests listed in Table 1 is given in Figure 2 in which the ratio of permanent indentation normalized to the thickness of the plate is plotted as a function of impact energy.

An ultrasonic C-scan, was performed on each test panel. The ultrasonic examination showed a significant amount of delamination took place at all phase 1 levels of impact.

TEST NO	THICKNESS in.	DROP HEIGHT in.	HAMMER WEIGHT lbs.	IMPACT ENERGY ft-lbs	SURFACE INDENTATION in.
C3-9E2-001	.0475	6.0	9.315	*	*
C3-9E2-002	.0475	6.0	9.315	4.61	0.008
C3-9E2-003	.0475	9.0	9.315	6.79	0.026
D3-26E3-001	.1365	42.5	9.315	32.72	0.059
D3-26E3-002	.1365	39.0	9.315	30.01	0.051
D3-26E3-003	.1365	36.0	9.315	27.70	0.047
D3-26E4-001	.1365	33.0	9.315	25.44	0.007
D3-26E4-002	.1365	34.0	9.315	26.09	0.022
D3-26E4-003	.1365	35.0	9.315	26.41	0.035
E3-48E4-001	.2520	40.5	30.501	101.80	0.153
E3-48E4-002	.2520	36.0	30.501	90.88	*
E3-48E4-003	.2520	33.0	30.501	82.88	0.060
E3-48E5-001	.2520	34.0	30.501	86.11	0.074
E3-48E5-002	.2520	35.0	30.501	87.80	0.113
E3-48E6-001	.2520	36.0	30.501	90.68	*
E3-48E6-002	.2520	37.0	30.501	92.95	0.118
F2-74E-001	.3885	36.0	53.144	157.46	0.093
F2-74E-002	.3885	38.0	53.144	167.30	0.093
F2-74E-003	.3885	33.0	53.144	144.58	0.084
G2-96E-001	.5046	33.0	77.670	211.40	0.062
G2-96E-002	.5046	38.0	77.670	243.47	0.124
G2-96E-003	.5046	37.0	77.670	237.58	0.091

TABLE 1. SUMMARY OF PHASE 1 TEST RESULTS



Specimen Id	Temp (f)	Veloc. (ft/sec)	Energy (ft-lb)	Time (msec)		Load (lb)		Energy (ft-lb)	
				Max	Total	Max	MaxId	Total	
f174e4-001	70.	13.82	157.82	1.92	10.00	7879.5	98.309	113.513	

Filter No. = 1, No Smoothing.

Comments:

weight 53.144 lbs

drop height 36 inches

FIGURE 1. FORCE AND ENERGY TIME HISTORIES FOR A TYPICAL SAMPLE

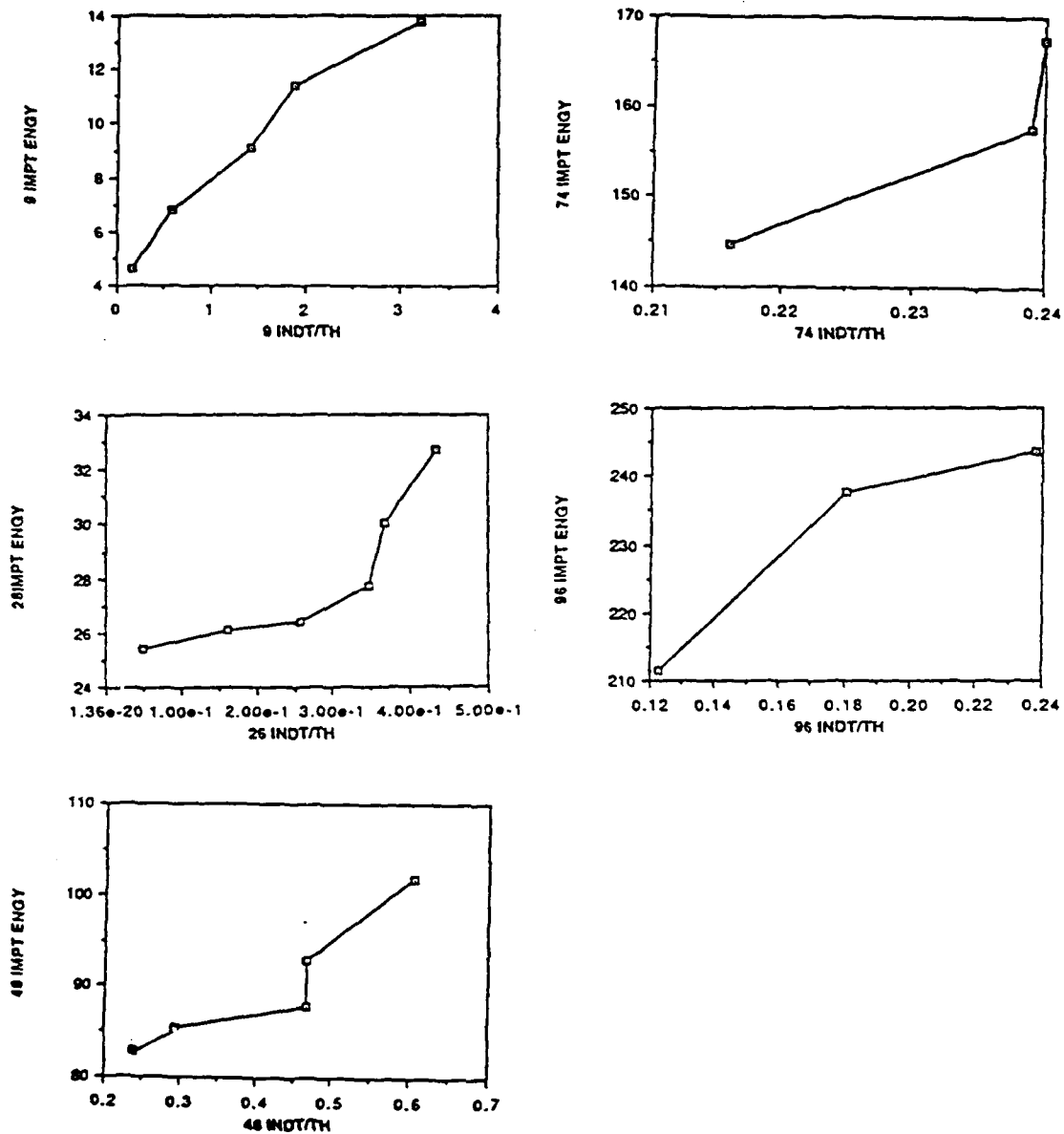


FIGURE 2. PERMANENT INDENTATION VS. IMPACT ENERGY

In order to minimize backface splitting, the magnitude of impact energy was significantly reduced in the phase 2 tests. In addition to measuring the load time history as in phase 1, strain gages were mounted to the backside of the plate and strain time histories were obtained.

TEST NO	THICKNESS in.	DROP HEIGHT in.	HAMMER WEIGHT lbs.	IMPACT ENERGY ft-lbs	INITIAL OR REPEAT HIT
8-10T-001	.1365	9.0	9.315	7.01	initial
8-10T-002	.1365	6.0	9.315		repeat
8-10T-003	.1365	6.0	9.315	6.79	repeat
8-10T-004	.1365	6.0	9.315	4.61	initial
8-10T-005	.1365	6.0	9.315	3.72	repeat
8-10T-006	.1365	6.0	9.315	4.68	repeat
8-10T-007	.1365	6.0	9.315	4.56	repeat
8-10T-008	.1365	6.0	9.315		initial
8-27G-001	.2520	6.0	9.315		initial

TABLE 2. SUMMARY OF PHASE 2 TEST RESULTS

Figure 3 presents the load and two strain time histories for test 8-10T-008. According to Table 2, the target plate used in this test had not been previously impacted. Note that the load time history is very similar in appearance to the load time history presented as Figure 1, i.e. the peak load is followed immediately by a sharp drop in the load. Apparently there is some fiber breakage or matrix cracking even at small energy levels typical of the phase 2 tests. Notice also, that the strains measured on the back face of the panel exhibit the same

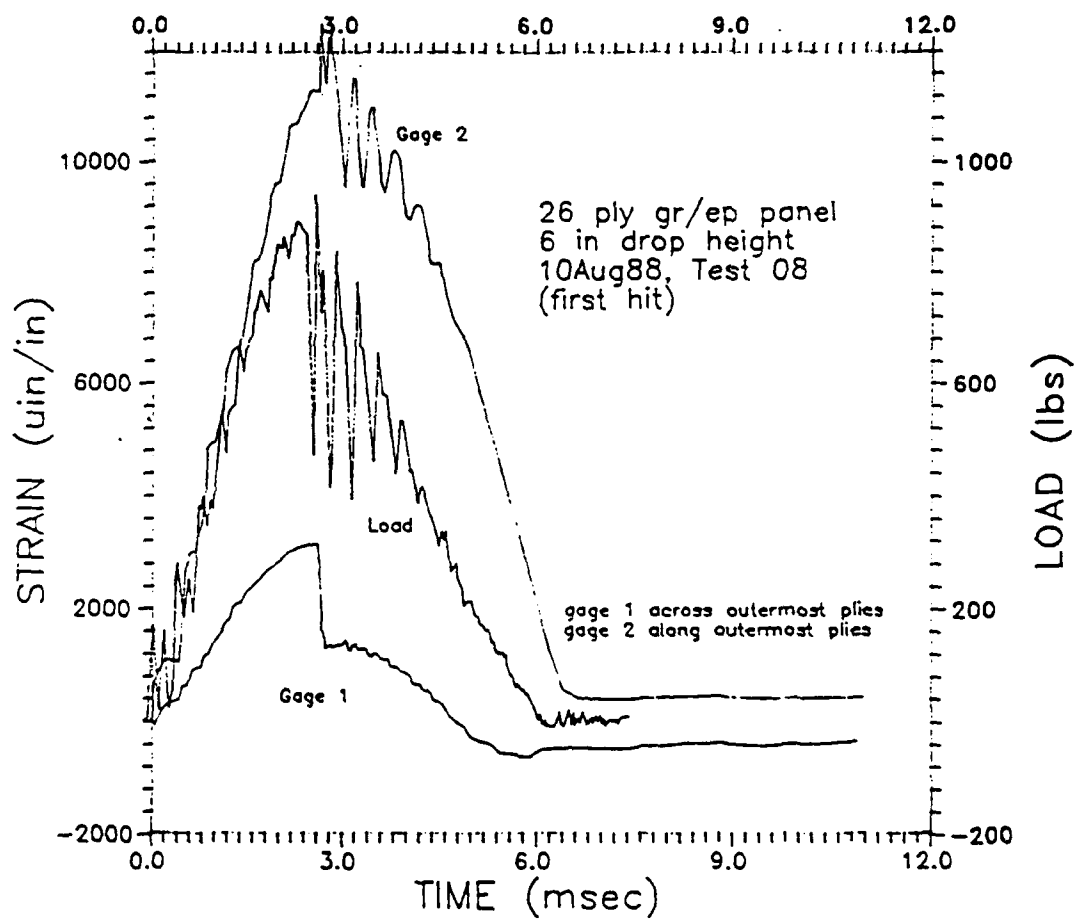


FIGURE 3. PEAK LOAD AND FIBER STRAIN, TEST 8-10T-008

drop that was seen in the load record. Figure 4 presents the load and strain records for a test on a previously impacted panel. Note that there is a significant difference between the behavior observed during an initial impact (Figure 3) and that measured during subsequent tests (Figure 4). These differences in behavior can be clearly seen in the load time history curves presented in Figure 5, which shows three successive impact tests conducted on the same panel. Even at the low load levels employed in this phase, damage occurred during the first test. This damage left the panel less stiff and without the high frequency vibrations which had been typical of the response of the graphite/epoxy composites to impact loads.

Looking again at Figures 3 and 4, it is apparent that the strains measured along the outermost fibers are much larger than those measured across the fiber direction. The program PLATE (Graves and Koontz, 1988) was used to compare the predicted panel strains with these experimentally obtained values. Figure 6 presents a comparison of predicted and observed strains for a 48 ply panel assumed to be simply supported on all four sides. The strains in the direction of the fibers are closely predicted, but present analyses do not adequately predict the strains measured normal to the direction of the fibers.

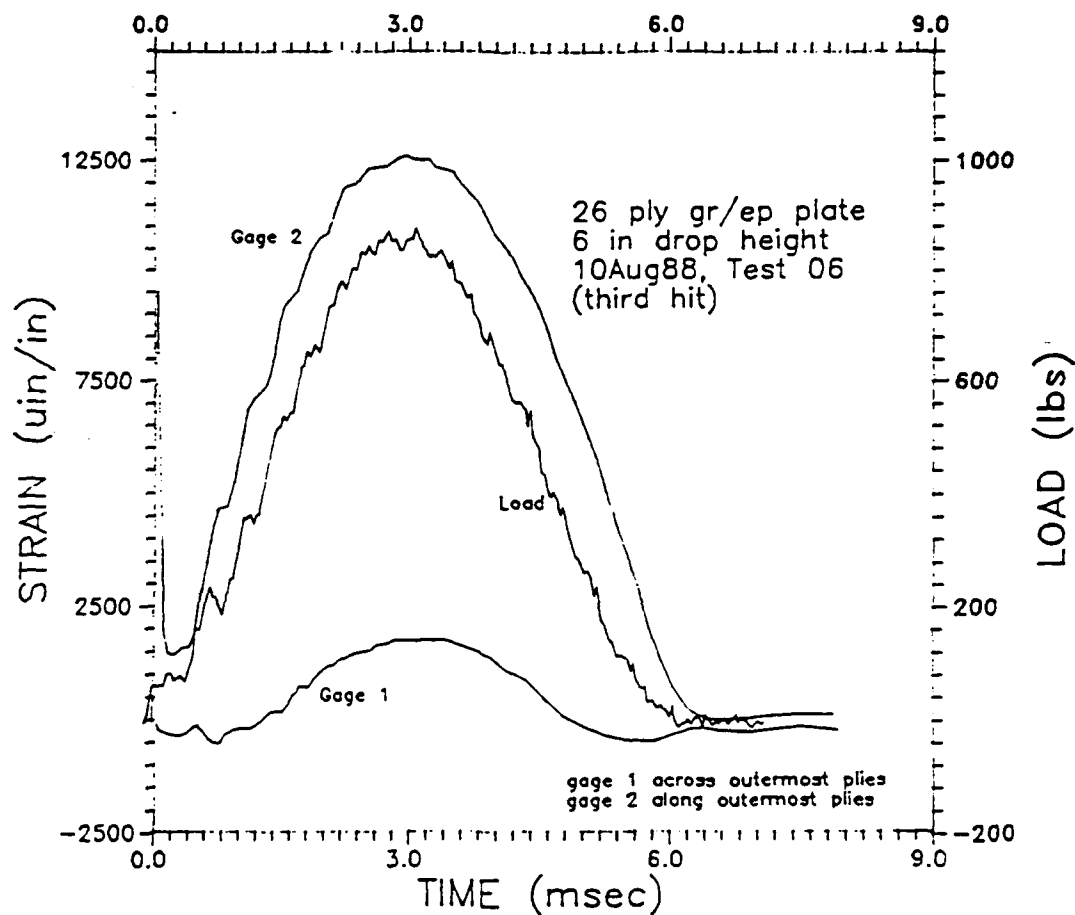
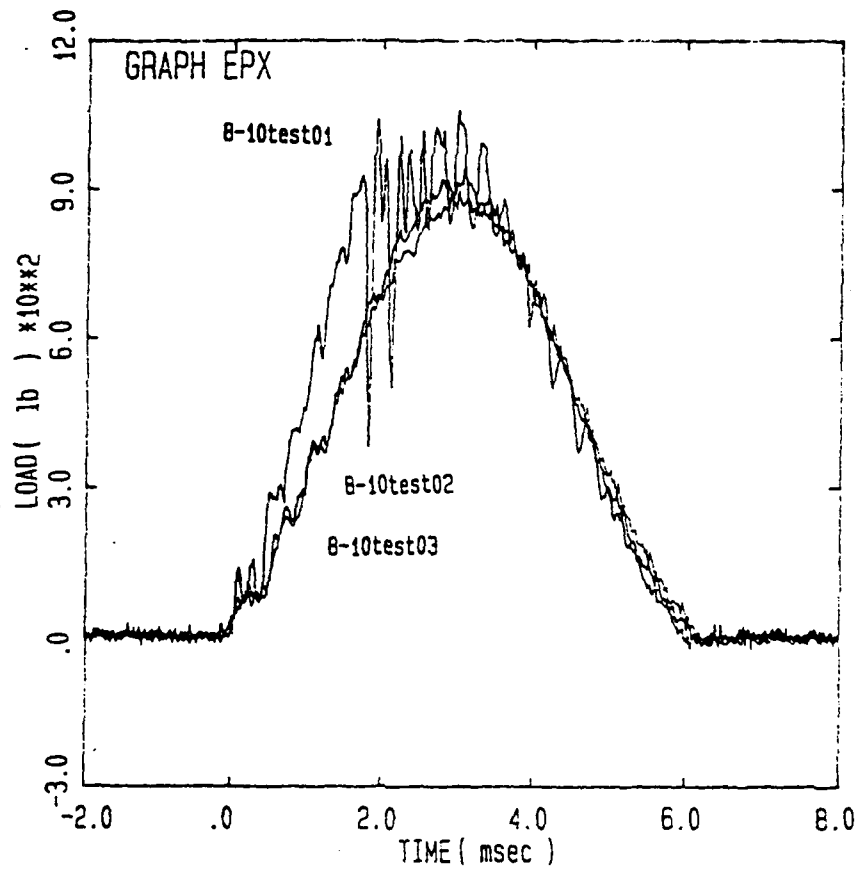


FIGURE 4. PEAK LOAD AND FIBER STRAIN, TEST 8-10T-006



Specimen Id s of Overlaid Curves:
B-10test01 B-10test02 B-10test03

FIGURE 5. COMPARISON OF LOAD VS TIME FOR THREE SUCCESSIVE IMPACTS

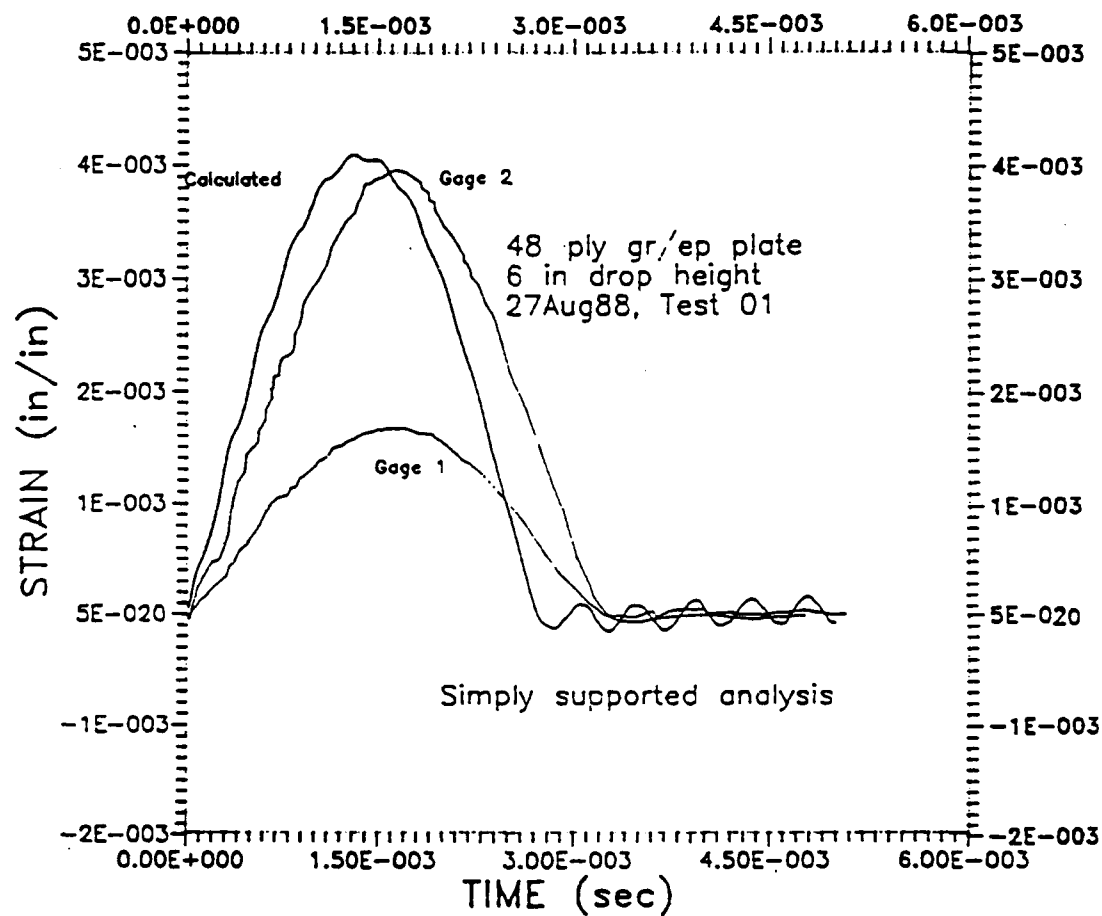


FIGURE 6. COMPARISON OF CALCULATED AND MEASURED STRAIN VS TIME CURVES

VI. RECOMMENDATIONS

The test results presented in the above sections clearly show that the behavior of the test specimen, is dependent on several parameters, impact energy and whether or not the target is subjected to repeated hits. These results combined with compression after impact load tests which still need to be conducted, should form a data base for the development of a method for determining the severity of impact induced damage and the identification of areas requiring repair. Additional tests should be conducted to add to the number of tests in the data base. We propose that additional impact tests be included in a future test program in order to identify the effects of the following on specimen response:

- a) different layup designs maintaining the same energy and velocity
- b) plate thickness on the visible damage on both impact and back faces
- c) support conditions on the levels of damage experienced.

All tests described in this report were performed using the NASA fixture which has a 5in square opening under the impact area. The damage observed in several of our tests extended to the supports and was clearly related to location and fixity of the boundaries. The assumption was made that the NASA fixture provided a fixed condition at the plate boundaries, but our analysis of the response of the test

plate indicates that the boundary conditions are closer to simply supported. The effect of changing boundary fixity needs to be examined.

- d) impactor shape on damage zone. The tests performed to date have all been with hemispherical impactors. The behavior of the composite plate to the hemispherical impactor may be different when the impactor is blunt ended or at the other extreme a sharp corner.

Further tests with the back face of the target plate instrumented need to be conducted. Plates with the same ply orientations studied in this project as well as other orientations need to be studied. Tests in which the deflection of the composite plate is measured without contacting the specimen would complement the strain measurement tests and make it possible to correlate load and strain readings with actual plate deflections.

Tests in which the specimen be impacted is placed under a static load similar to what should be expected to occur in service should be conducted.

REFERENCES

- ASM International, Composites. Engineered Materials Handbook. Volume 1, Metals Park, Ohio, 1987
- Cantwell, W.J. and Morton, J., "Low Velocity Impact Damage in Carbon Fibre Reinforced Plastic Laminates," Proceedings of the Fifth International Congress in Experimental Mechanics, June, 1984, pp. 241-255. pp. 314-319.
- Graves, M.J. and Koontz, J.S., "Initiation and Extent of Impact Damage in Graphite/Epoxy and Graphite/Peek Composites," "AIAA/ASME/ASCE/AHS, 29th Structures, Strucrural Dynamics and Materials Conference, April, 1988, pp. 967-975.

Ramkumar, R.L., "Composite Impact Damage Susceptibility," Final Report, NADC-79068-60, Northrop Corporation, Aircraft Division, Hawthorne CA, January, 1981.

Wolfe, W.E., LOW VELOCITY IMPACT OF GRAPHITE/EPOXY PLATES, Final Report, USAF-UES Summer Faculty Research Program, 1987.

1989 USAF-UES SUMMER FACULTY RESEARCH PROGRAM/
GRADUATE STUDENT SUMMER SUPPORT PROGRAM

Sponsored by the
AIR FORCE OFFICE OF SCIENTIFIC RESEARCH

Conducted by the
Universal Energy Systems, Inc.

FINAL REPORT

STRAIN DISTRIBUTION IN COMPOSITE COUPONS IN TENSION

Prepared by:	William E. Wolfe, Ph.D. and <u>Bryan Foos</u>
Academic Rank:	Associate Professor, Graduate Student
Department and University:	Civil Engineering Department The Ohio State University
Research Location:	WRDC/FIBCA Wright Patterson AFB OH 45433
USAF Researcher:	Dr. R. S. Sandhu
Date:	30 Sep 89
Contract No:	F49620-88-C-0053

Same Report As
Prof. William Wolfe
(Report # 112)

1989 USAF-UES SUMMER FACULTY RESEARCH PROGRAM/
GRADUATE STUDENT RESEARCH PROGRAM

Sponsored by the
AIR FORCE OFFICE OF SCIENTIFIC RESEARCH
Conducted by the
Universal Energy Systems, Inc.
FINAL REPORT

Control System Design Modeling

Prepared by:	Genevieve A. Huston
Academic Rank:	Graduate Student
Department and	Electrical and Computer Engineering
University:	Ohio University
Research Location:	WRDC/FIBGC Wright Patterson Air Force Base Dayton, OH 45433-6553
USAF Researcher:	Major Alan Janiszewski
Date:	25 Aug 89
Contract No:	F49620-88-C-0053

Control System Design Modeling

by

Genevieve A. Huston

ABSTRACT

Accomplishments during the summer research period include learning to construct modal models from finite element data, and studying and practicing residue comparison model reduction techniques. Wright Patterson Flight Dynamics Laboratory has a 12 meter truss which is to be equipped with actuators and sensors for an active control experiment. When this test is completed, data will be collected and used to develop a model. Also during the research period, modal analysis tests were conducted on a radome and F-15 tail section, in order to allow a finite element model to be developed and dynamic characteristics to be studied. In addition, a control circuit was designed and built which will adjust current to a solenoid used for a zero gravity test of the truss.

ACKNOWLEDGMENTS

I wish to thank the Air Force Systems Command, Air Force Office of Scientific Research, and Universal Energy Systems, Inc. for their sponsorship of the Graduate Student Research Program.

Thank you, also, to everyone working at the Structural Dynamics Branch of the Flight Dynamics Laboratory, who have made this a rewarding experience for me. I have learned a great deal from these people.

I. INTRODUCTION:

The design of control systems for large space structures for meeting stringent attitude control and vibration suppression requirements involves several steps: (1) analytical and/or numerical modeling, (2) preliminary control system design and verification by simulation, (3) testing and verification with hardware, (4) system identification after testing, (5) redesign using models from system identification and (6) design fine-tuning. Of course, some iteration is required.

One of the problems in completing step (2) is the production of a model with sufficient fidelity for performing a control system design that achieves satisfactory closed loop performance and with low enough order that numerical problems are avoided in the design process. Fidelity can be measured by comparing frequency responses, and model reduction can be accomplished by eliminating modes that have insignificant effects upon the frequency response.

II. OBJECTIVES OF THE RESEARCH EFFORT:

My plan as a participant in the 1989 Graduate Student Research Program (GSRP) was to perform tasks for aiding in the learning of preliminary control system design , and system identification after testing (steps 2 and 4).

Concerning preliminary control system design and verification, part of the summer's effort was directed towards learning (1) to develop control system design models from finite element data, (2) to generate frequency responses for these models and (3) to develop techniques for model reduction using residue comparison.

In order to complete step (4) mentioned earlier --system identification after testing-- I intended to collect data between control system actuators and sensors using Large Space Structures ground facilities at Wright Patterson Air Force Base to learn various techniques for performing this. Using this data collected during the summer, models would then be extracted upon my return to Ohio University this fall.

III.

a. My efforts toward accomplishing preliminary control system design began with a presentation on model reduction given by my advising professor, Dr. Jerrel Mitchell. I studied the construction of modal models from finite element data, and, using typical data, I practiced the method.

I also studied the technique for model reduction in which mode residues are compared, and those that do not peak above the straight line approximation of the system frequency response are eliminated. The philosophy is to reduce the model in such a way that there are insignificant differences between the frequency response of the reduced-order model and the frequency response of the full-order model.

b. Wright Patterson Flight Dynamics Laboratory has, as a part of its Large Space Structures Technology Program (LSSTP), a 12 meter truss which is to be used for the experimental evaluation of active and passive vibration control approaches. Control forces input to the truss will come from linear momentum exchange type actuators, while truss response is measured using 8 control accelerometers. An Onosokki spectrum analyzer will be used for real-time sampling and generation of time and frequency response data from the accelerometers. A control

computer will record and analyze control sensor response signals and actuator commands. I intended to gather data from this test, as stated in the objective.

Unfortunately, the schedule for the truss testing is running later than expected. There have been difficulties with the control computer. I have spent some time assisting with the computer control system. There remain, however, problems with the software, and the testing will not commence until I have returned to school.

c. Also during my research period at Wright Patterson Air Force Base, I became involved in several modal analysis tests performed on a radome , and on an F-15 tail section. The radome test involved exciting the radome with a white noise signal, and recording response from accelerometers on the radome. The results will be used to adjust a finite element model of the radome. Tests on the tail section consisted of excitation and recording of response in an undamaged, damaged, and repaired tail. The modal test will compare the dynamic characteristics of the various states of the tail, and will be used to verify the effectiveness of damage repair techniques.

d. In addition, I was assigned by one of the engineers, a project appropriate for someone with a background in electrical engineering such as I have. It consisted of

designing and building a circuit to control current to a solenoid which, along with and attached mass, will be used to impart a force to the 12 meter truss on a zero-gravity test. The solenoid requires full power to completely activate, then a reduction in power which allows the solenoid to hold the mass in place without overheating. This must be accomplished without the need for manual adjustments to the dials on the power supply during the test. Originally, I designed an electronic timing and switching circuit which would allow full power for a calculated time, then switch current through a resistor to reduce power to the solenoid. Finally, however, I decided to use a manual switch design, which was simpler, and had less opportunity to malfunction.

IV. RECOMMENDATIONS:

I have requested that a set of data be sent to me upon completion of the truss active control experiment. I will then use the techniques I have learned for system identification to develop a model from this data.

REFERENCES

Anton, Howard. Elementary Linear Algebra. John Wiley & Sons,
New York, 1984.

Golub, G.H., C.F. Van Loan. Matrix Computations. The John
Hopkins University Press, Baltimore, 1983.

Gordon, Robert. 12 Meter Truss Active Control Experiment.
WRDC Test Plan, April 1989.

Horn, R.A., C.A. Johnson. Matrix Analysis. Cambridge
University Press, Cambridge, 1985.

Klema, V.C., A.J. Laub. "The Singular Value Decomposition:
Its Computation and Some Applications," IEEE Transactions
on Automatic Controls. 1980, Vol. AC-25, pp 164-176.

1989 USAF-UES FACULTY RESEARCH PROGRAM/
GRADUATE STUDENT RESEARCH PROGRAM

Sponsored by the
AIR FORCE OFFICE OF SCIENTIFIC RESEARCH

Conducted by the
Universal Energy Systems, Inc.

FINAL REPORT

ACCESSING THE COMPUTER AUTOMATED DESIGN DATABASE(CADDB)
THROUGH CADS- A COMPUTER AIDED DESIGN SYSTEM

Prepared by:	Richard A. Swift
Academic Rank:	Ph.D. student/research assistant
Department and	Aerospace and Mechanical Engineering
University:	University of Notre Dame
Research Location:	WRDC/FIBRA Wright-Patterson AFB Dayton, Ohio 45433
USAF Researcher:	Captain Robert A. Canfield
Date:	9-14-89
Contract No:	F49620-88-C-0053

Accessing the Computer Automated Design Database (CADDDB)
Through CADs - A Computer Aided Design System

by

Richard A. Swift

ABSTRACT

CADDDB (the Computer Automated Design Database) allows a flexible environment for the retrieval and manipulation of ASTROS (the Automated Structural Optimization System) database information. There are currently a limited number of software packages which can directly access this database information. CADs (a Computer Aided Design System), which is used regularly for the pre- and post-processing of NASTRAN, ANALYZE, and OPSTAT analyses, was chosen for use with CADDDB. It was desired to enhance CADs so that it could read data from CADDDB. This would allow for the plotting and manipulation of the ASTROS finite element and aerodynamic models, as well as allowing for the post-processing of specific ASTROS analysis results (i.e., displacement, stress, etc.).

Acknowledgements

I wish to thank the Air Force Systems Command and the Air Force Office of Scientific Research for sponsorship of this work. I would also like to thank Universal Energy Systems for their help in the administration of this research program.

I would like to thank the following Air Force personnel for their assistance in this work: Captain R. A. Cantfield, Mrs. V. Tischler, Mr. R. Kolonay, and Dr. V. Venkayya. Their assistance has been greatly appreciated.

I. INTRODUCTION:

ASTROS (the Automated Structural Optimization System) is a finite element analysis and optimization package for the preliminary structural design of complex aerospace structures. ASTROS may be represented in a simplified manner as an executive system with a scientific database structure supported by six engineering modules:

1. Structures and Dynamics
2. Airloads
3. Aeroelasticity
4. Sensitivity Analysis
5. Optimization
6. Control Response

One limitation of ASTROS is that it has no pre- or post-processing capabilities. It would be advantageous to develop tools for ASTROS pre- and post-processing.

My research interests are in the area of effective finite element modeling of complex structures at the preliminary design stage. Simplified models are always desirable to minimize analysis requirements, but maintaining an effective and representative model of the structure and aerodynamics becomes challenging. My present work involves using ASTROS as the analysis package for research into these modeling difficulties. Developing a background into the database structures of CADDB and CADS will aid in this research.

II. OBJECTIVES OF THE RESEARCH EFFORT:

In order to enhance the capabilities of ASTROS, it is desired to extend a current pre- and post-processing package for use with ASTROS. One software package which has been used extensively for NASTRAN applications is CADS. Because of the high degree of compatibility between the bulk data formats of ASTROS and NASTRAN, CADS has been used effectively for the creation and display of ASTROS finite element models. The use of CADS with ASTROS has been limited to these two functions.

My assignment as a participant in the 1989 Graduate Student Researchers Program (GSRP) was to determine the feasibility of allowing CADS to directly access the ASTROS database, CADDDB. By directly reading the database, the finite element model information, aerodynamic model data, and certain analysis results would be available for plotting or other manipulation by CADS. In order to accomplish this goal, it was decided to create a "READ ASTROS" module for installation into CADS.

A series of objectives for construction of this module were set out at the beginning of the research period. These objectives were defined as follows:

1. Read the Basic Grid Point Data Table from CADDDB. The following information is of interest; internal node numbers, external

node numbers, and nodal coordinates. Also, read the Element Summary Tables (EST's) for all of the major ASTROS finite element types from CADDB. The information of interest are the element numbers, element connectivities, and element properties. All of this data should then be converted to the equivalent CADS database format and stored.

2. Read the aerodynamic model information from CADDB and manipulate it into a form compatible with CADS for plotting purposes.

3. Read specific analysis results from CADDB (i.e., displacements, stresses, etc.) for post-processing in CADS.

4. Read in pressures from CADDB for post-processing in CADS (plotting of pressure distributions on the aerodynamic models).

Objectives 1. and 2. were determined to be realistically obtainable within the ten week research period. Objectives 3. and 4. were to be attempted if any additional time became available.

During my 1989 GSRP, objectives 1 and 2 were completed and the final version of the "READ ASTROS" module was installed into CADS. The most important benefit from this work is the availability of ASTROS aerodynamic models for plotting.

III. FINITE ELEMENT MODEL CONVERSION FROM CADDDB TO CADS

The Computer Aided Design Database (CADDDB), developed as part of the Automated Structural Optimization System (ASTROS), provides a flexible medium for the storage of complete finite element model information. As described by Herendeen, CADDDB stores this information as a collection of related data groups termed entities. Three types of entities comprise the CADDDB database:

Relational Entities

Matrix Entities

Unstructured Entities

A relational entity may be considered as a table of data; CADDDB refers to the rows of the table as entries and the columns as attributes.

Matrix entities are stored in CADDDB using a data compression technique to minimize storage requirements. Only nonzero terms are stored.

Unstructured entities are a means of internal data representation used within ASTROS; they are collections of data "with only a local and transient purpose" (Herendeen).

The CADS program uses a pair of random access files to store model geometry information and analysis results (Less). This summer's

work has dealt with no analysis results, therefore only the geometric database will be discussed.

The geometric database is laid out in the format of a master record which points to header records, which in turn point to the actual data records. Each record of the database is limited to 990 words. The records are not stored in any particular order, thus allowing a degree of flexibility in the creation scheme to be employed.

The hierarchy of the CADs database structure is as follows:

1. Geometric Model Header
2. Node Data Header Record
3. Element Header Record
4. Node Data Records
5. Element Data Records
6. Property Data Records
7. Material Data Records

The first objective of the READ ASTROS module was to access the finite element model data (grid point coordinates, element connectivities, etc.) from CADDB and convert this information into an equivalent CADs database.

An algorithm was developed to access the Basic Grid Point Data Table, retrieve those attributes of interest, modify the format of

these attributes to meet the requirements of CADS, and then write these files to the CADS database. In pseudocode, the procedure employed is as follows:

```
OPEN  the appropriate CADDB database
IF BGPDT status is EXIST THEN
    READ  internal and external node numbers, and
          nodal coordinates from BGPDT
    WRITE external node numbers to a sequential set of
          990 word CAD data records
    WRITE nodal coordinates to a sequential set of 990 word
          CAD data records
ELSEIF BGPDT status is NOTEXIST THEN error and RETURN
ENDIF
```

A second algorithm was developed to read the Element Summary Tables (EST's). In pseudocode the algorithm is as follows:

```
DO 10 I=1, number of ASTROS finite element types
IF EST(I) status is EXIST THEN
    READ  element numbers, connectivities, and properties
          from EST(I)
ELSEIF EST(I) status is NOTEXIST THEN GOTO 10
ENDIF
WRITE  element numbers to a sequential set of 990 word CAD
       data records
CALL SORT  to obtain the element connectivities in terms of the
           external node numbers
WRITE  element connectivities to a sequential set of 990 word
       CAD data records
```


WRITE element properties to a sequential set of 990 word CAD
data records

10 CONTINUE

No size limitation is imposed by this procedure, and models as large as approximately 12000 nodes may be considered (a CADs limitation).

In order to minimize the complexity of the read module, only a single major property is read for each element type. This allows for a much simpler coding since similarities in element attributes between element types can be taken full advantage of.

As each record is written to the CADs database, a record number is assigned. These record numbers are then used for the formulation of the geometric model header record, node header record, and element header record. Each header is also constrained by the 990 word record length.

The information which has thus been retrieved from CADDB and placed in a CADs database format may now be plotted or further manipulated using the preprocessing capabilities of CADs.

IV. AERODYNAMIC MODEL CONVERSION FROM CADDB TO CADs

The next phase in the development of the read module involved the incorporation of procedures to develop an aerodynamic model

plotting capability. Because CAD\$ handles only finite element model information, the aerodynamic model must be treated as a finite element group or a set of finite element groups. This imposes no unreasonable difficulties in terms of coding implementation or plotting in CAD\$. Fortunately, CAD\$ handles a large number of finite element types (specifically, quadrilaterals which can be readily employed as analogies to the aerodynamic panels for plotting purposes). One inconvenience that was encountered is that there is no single attribute in CADDB which stores the aerodynamic model geometry information. Only basic geometric parameters are stored in the CAERO1, CAERO6, AIRFOIL, and AEFACT entities. These various parameters, which define the planforms for the steady and unsteady lifting surfaces, as well as the panelling geometry, must be used to determine a set of nodes, nodal coordinates, panel numbers, panel connectivities, and element groups for processing by CAD\$. Because of time limitations, aerodynamic bodies were not considered in this development.

Pseudocode for the generation of the aerodynamic models is as follows:

```
C   Read in all steady aerodynamic lifting surfaces
    IF CAERO6 status is EXIST AND AIRFOIL status is EXIST THEN
      READ  lifting surface planform parameters from CAERO6,
            AIRFOIL, and AEFACT entities
    ENDIF
C   Read in all unsteady aerodynamic lifting surfaces
```

IF CAERO1 status is EXIST THEN

READ lifting surface planform geometry parameters from
CAERO1, and AEFACT entities

ENDIF

Generate node numbers and nodal coordinates for each lifting
surface

Generate element numbers and element connectivities for each
set of lifting surface panels

END

This process reads all steady and unsteady aerodynamic lifting surfaces, and generates a group of finite elements representing the panel geometry of each lifting surface. These element groups may then be plotted using the present capabilities employed in CADs.

V. SOFTWARE DESCRIPTION

The final version of the read module consists of three subroutines. RDAST is the main subroutine and is responsible for reading in all data from CADDB. RDAST calls the subroutine PNW, which packs the data and writes it to a sequential set of CADs database records. The final subroutine is UCADDB, which opens the CADDB database.

The incorporation of the read module into CADs is straight-forward; only two of the CADs subroutines need to be modified, and these modifications involve the addition of only 10-15 lines of code.

The "READ ASTROS" option has been demonstrated in the current version of CADs, and the read module is now awaiting final installation into the most recent version of CADs.

VI. RECOMMENDATIONS:

The implementation of the "READ ASTROS" module for installation into CADS has been described. The module allows CADS to directly access the ASTROS database, CADDB. Currently, only the basic finite element model information and aerodynamic lifting surface data is read. Aerodynamic bodies are not supported, and this would be the next logical extension of the read module.

In order to obtain the aerodynamic body panelling information in a form compatible with CADS, a procedure similar to that used for the lifting surfaces is required. That is, node numbers and coordinates, panel numbers and panel connectivities must be generated from the basic geometric information supplied in certain CADDB entities. Because of the 3-dimensional nature of the aerodynamic bodies, the required coding becomes more complex but it is not overly difficult.

A second enhancement to the read module would involve the ability to access specific analysis results for post-processing in CADS. This involves retrieving the data of interest from the appropriate CADDB entities, and manipulating the data into a format compatible with CADS. This would prove a valuable addition for interpretation of ASTROS analyses.

REFERENCES

Herendeen, D.L., M.R. Ludwig, "Interactive Computer Automated Design Database (CADDDB) Environment User's Manual", AFWAL-TR-88-3060, Flight Dynamics Laboratory, Wright-Patterson Air Force Base, Ohio

Less, M.C., Susan Manuel, "CADS - A Computer Aided Design System Volume III - Program Maintenance Manual", AFWAL-TR-85-3066 Volume III, Flight Dynamics Laboratory, Wright Patterson AFB, Ohio

1989 USAF-UES SUMMER GRADUATE STUDENT RESEARCH PROGRAM

Sponsored by the
AIR FORCE OFFICE OF SCIENTIFIC RESEARCH

Conducted by the
Universal Energy Systems, Inc.

FINAL REPORT

Dislocations in René N4+ with Respect to Orientation and Temperature

Prepared by:	David Allen Alden
Academic Rank:	graduate student
Department and	Materials Science and Engineering
University:	University of Cincinnati
Research Location:	Wright-Patterson Air Force Base, Materials Laboratory, MLLN
USAF Researcher:	Dr. Ted Nicholas
Date:	Tuesday, September 19, 1989
Contract No:	F49620-88-C-0053

Dislocations in René N4+ with Respect to Orientation and Temperature

by

David Allen Alden

ABSTRACT

Oriented single crystals of the nickel-base superalloy René N4+ which had been mechanically tested in tensile and double-tensile tests were examined in a transmission electron microscope in an attempt to correlate mechanical response and dislocation type. The crystals had strikingly different mechanical responses with respect to orientation and temperature, and it was found that they existed quite different dislocation types as well, which correlated well with each other.

ACKNOWLEDGMENTS

I would like to thank the Air Force Systems Command, the Air Force Office of Scientific Research, and the Materials Laboratory of Wright-Patterson Air Force Base for sponsorship of this research. I would also like to thank Universal Energy Systems for their assistance in all of the administrative aspects of this program.

I am grateful to my dissertation advisor, Professor N. Jayaraman, of the University of Cincinnati, and to Dr. Ted Nicholas, of the Materials Laboratory, for their guidance in my research program. Thanks are also due to Dr. Vijay Vasudevan of the University of Cincinnati, Scott Apt of SRL and Lou Henrich of UES for all of their help and assistance.

I. INTRODUCTION

Nickel-base superalloys have some anomalous yield strength versus temperature properties due the existence of ordered precipitates with the L1₂ crystal structure. The degree of anomalous behavior is dependent upon both the orientation of the crystal and the test temperature. The reason for the orientation and temperature dependencies are due to the different slip systems which are active. Both the normal FCC octahedral slip systems as well as cube slip systems may be active in nickel-base superalloys

A few studies of nickel-base superalloys have noted an interesting yield phenomenon, that of serrated yielding for some orientations at temperatures below about 760°C. Some other intriguing yield phenomena have been noticed in tests during research already conducted as part of a research program at the University of Cincinnati.

The Materials Laboratory at Wright-Patterson Air Force Base(WPAFB) is involved with many different studies of high temperature materials and has transmission electron microscope(TEM) facilities necessary for such research. My dissertation research involves extensive TEM studies and. my dissertation advisor has been on sabbatical at WPAFB for the past year and so knew of the facilities available there. It is for this reason that I was assigned to the Materials Laboratory

II. OBJECTIVES OF THE RESEARCH EFFORT

For the research it was planned to further examine the yield phenomena which occur during both tensile and 'double tensile' testing of René N4+ single crystals. A double tensile test consists of: loading the sample until some plastic strain has occurred, unloading the sample and holding at zero load for two minutes, and then reloading the sample at a second strain rate.

The examination will be accomplished by doing detailed transmission electron microscopy studies of the dislocations in each of the samples.

The types of dislocations present will be determined as a function of temperature, orientation and strain rate.

This research will lead to a better understanding of the mechanisms of deformation occurring in the material, allowing engineers to better design the jet engine components which are composed of this and other similar materials.

III.

a. For this study I there were 14 René N4+ single crystal specimens which had been mechanically tested in either tensile or double-tensile tests. Eight specimens were tested at 760°C and six at 982°C. The specimens tested at 760°C were of five different nominal orientations (some tests were run on specimens with equivalent nominal orientations): [0 0 1], [0 1 1], [0 1 2], [1 1 1] and [1 2 3]. The tests undertaken at 982°C utilized specimens of four different nominal orientations: [0 0 1], [0 1 1], [1 1 1] and [1 2 3]. While all of the double-tensile tests done at 982°C were with a first strain rate six times slower than the second strain

rate, two of the double-tensile tests done at 760°C were with the first strain rate six times faster than the second strain rate.

Five disks were sliced from each of the fourteen specimens. The slices were made perpendicular to the tensile axis. Each of these slices was ground down to a disk 3mm in diameter. The disks were then sanded down to between 2 and 3 mils thick using 320, 400 and 600 grit emery paper.

Each of these disks was then electrochemically thinned in a Fischione jet thinning apparatus until perforated. The electrolyte employed was: 60% methanol, 35% butyl cellosolve and 5% perchloric acid. The electrolyte was maintained at a temperature of approximately -40°C. The thinning was done at approximately 25V and 12mA for 10-15 minutes.

One good foil from each of the fourteen specimens was studied in a JEOL 100cx transmission electron microscope, with an accelerating voltage of 100kV (two foils were, however, studied at 120kV.)

b. The mechanical response of the specimens, as indicated by the stress-strain curves obtained, differed greatly with respect to orientation and temperature. There were four different forms for the stress-strain curves obtained:

- i. specimens which had serrated yield behavior, and very elastic-plastic stress-strain curves, with no strain rate dependence on the yield stress and no relaxation during the two minute hold time,
- ii. specimens which didn't have serrated yielding, and had strain hardening, a strain rate dependence on the yield stress and relaxation during the two minute hold time,
- iii. specimens which didn't have serrated yielding, and had strain hardening, but no strain rate dependence on the yield stress and no relaxation during the two minute hold time, and

iv. specimens which had serrated yield behavior, strain hardening and relaxation during the two minute hold time, but no strain rate dependence on the yield stress.

The dislocation types present in the foils from specimens with these four different types of mechanical behavior were also different:

foils from specimens with mechanical behavior types i and iii had many dislocations and some dislocation pairs, but no stacking faults,

foils from specimens with mechanical behavior type ii had many stacking faults, with some dislocations and pairs of dislocations, and

foils from specimens with mechanical behavior type iv had some stacking faults, and some dislocations and pairs of dislocations.

IV. RECOMMENDATIONS

b. The exact nature of the dislocation and fault types must still be determined, before a more complete understanding of the operative deformation mechanisms in this material can be realized.

I also feel that it would be interesting to study more double-tensile tests at 760°C with the fast strain rate first, since there does appear to be some differences in the material response as compared to tests with the slow strain rate first. If there were to indeed be a difference it would of interest to vary the strain rates to see at what strain rates, or strain rate ratio, the change occurred.

REFERENCES

- Gabb, T.P., J. Gayda and R.V. Miner, *Met. Trans.*, **17A**, March 1986, 497-505.
- Gabb, T.P., R.V. Miner and J. Gayda, *Scripta Met.*, **20**, 1986, 513-518.
- Gabb, T.P. and G.E. Welsch, *Scripta Met.*, **20**, 1986, 1049-1054.
- Gabb, T.P., G. Welsch and R.V. Miner, *Scripta Met.*, **21**, 1987, 987-992.
- Gevers, R., A. Art and S. Amelinckx, *Physica Status Solidi*, **3**, 1963, 1563-1593.
- Kear, B.H., J.M. Oblak and A.F. Giamei, *Met. Trans.*, **1**, Sept. 1970, 2477-2486.
- Milligan, W.W. and S.D. Antolovich, NASA CR 4215, 1989.
- Miner, R.V., T.P. Gabb, J. Gayda and K.J. Hemker, *Met. Trans.*, **17A**, March 1986, 507-512.
- Miner, R.V., R.C. Voigt, J. Gayda and T.P. Gabb, *Met. Trans.*, **17A**, March 1986, 491-496.
- Oblak, J.M. and B.H. Kear, in Proceedings of the Fifth International Symposium "The Structure and Properties of Materials - Techniques and Applications of Electron Microscopy," G. Thomas, R.M. Fulrath and R.M. Fisher eds., University of California, Berkeley, September, 1971, 566-616.

1989 USAF-UES SUMMER FACULTY RESEARCH PROGRAM/
GRADUATE STUDENT RESEARCH PROGRAM

Sponsored by the
AIR FORCE OFFICE OF SCIENTIFIC RESEARCH

Conducted by
Universal Energy Systems, Inc.

FINAL REPORT

AN APPROXIMATE ANALYTICAL SOLUTION OF THE NONLINEAR
DIFFUSION EQUATION AND A PRELIMINARY INVESTIGATION OF
NONLINEAR OPTICS

Prepared by:	Darwin L. Boyd
Academic Rank:	Graduate Student
Department and	Physics Department
University:	Kent State University
Research Location:	WRDC/MLPO WPAFB Dayton OH 45433
USAF Researcher:	Dr. Patrick M. Hemenger
Date:	August 11, 1989
Contract No.:	F49620-88-0053

AN APPROXIMATE ANALYTICAL SOLUTION OF THE NONLINEAR
DIFFUSION EQUATION AND A PRELIMINARY INVESTIGATION OF
NONLINEAR OPTICS

by

Darwin L. Boyd

ABSTRACT

An approximate analytical solution of the nonlinear diffusion equation was applied to two special cases of concentration dependence of diffusivity. Zeroth and first order corrected dopant profiles were calculated for the cases $D = D_0 C^V$ and $D = D_0 \exp(kC)$. Good agreement was found between the first order corrected profiles and profiles obtained by a direct numerical integration using a forward time centered space differencing of the nonlinear diffusion equation. Additional work on the analytical solution produced results that allowed the initial dopant peak position and concentration at the surface to be accurately specified. These results would be essential to actual use of the analytical solution in tracking dopant profiles. Finally a preliminary investigation was made into nonlinear optics concentrating on surface electromagnetic waves at a plane boundary between BaTiO_3 and other optical materials.

ACKNOWLEDGEMENTS

I would like to thank the Air Force Systems Command, Air Force Office of Scientific Research, and the Wright Research and Development Center / Materials Laboratory where I worked for sponsorship of this research. I would also like to thank Universal Energy Systems for a well run and administered program.

Thanks to Dr. David Uhrich my advisor and the Physics Department of Kent State University for allowing me the time to complete this work. A special thanks to everyone at the materials laboratory who helped me, Dr. Patrick Hemenger for helping in many ways and always making sure I had what I needed, Ron Perrin for all his assistance and expertise with the computers, and Tom Kensky for helping me with the Macintosh. Finally a very special thanks to Dr. David Moroi for his help, guidance, and patience throughout this work and for the many times we went fishing.

I. INTRODUCTION

When semiconductor wafers are ion-implanted with dopant there results an initial dopant profile. These wafers are then annealed. During the annealing process the dopant diffuses into the wafer resulting in a final dopant concentration profile. Since the process may display "concentration-enhanced" diffusivity¹, the appropriate mathematical tool to describe the diffusion is the nonlinear diffusion equation where the diffusivity is some function of the concentration. In order to control the electrical properties of these devices it is necessary to have a clear understanding of the diffusion process. Optimization of the characteristics of these devices is important to the materials laboratory of the Wright Research and Development Center at Wright Patterson Air Force Base which has an interest to their application to infra-red detectors.

The study of nonlinear optics is very important in a diverse range of phenomena associated with the interaction and propagation of laser beams, phase conjugation, distortion free transmission of data, and many other interesting optical phenomena². The materials laboratory is increasing its emphasis on nonlinear optics and hence theoretical understanding of such processes is of fundamental importance.

My background in solid state physics as well as experience with computers and programming proficiency contributed to my assignment to this project.

II. OBJECTIVES OF THE RESEARCH EFFORT

A broad goal of this research effort was to shed light onto a mathematical method of solution to parabolic partial differential equations and then to apply such a solution to the nonlinear diffusion equation. While dopant profiles can be obtained through

straightforward numerical integration of the nonlinear diffusion equation, the cost in computer time can be very high. Recent work by Moroi and Hemenger³ has produced an approximate analytical solution which is much more efficient in obtaining dopant profiles. My assignment as a participant in the 1989 Summer Graduate Student Research Program involved obtaining dopant profiles using the analytical solution and comparing them with profiles obtained by direct numerical integration of the nonlinear diffusion equation. This work is a continuation of work begun while a participant in the 1988 Summer Graduate Student Research Program⁴.

Work in nonlinear optics was directed at finding analytical solutions to the Maxwell equations first concentrating on surface electromagnetic waves at a plane boundary between BaTiO₃ and other optical materials. The eventual goal would be to develop computer code using the analytical solutions and compare results with more direct numerical calculations.

III. APPROXIMATE ANALYTICAL SOLUTION OF THE NONLINEAR DIFFUSION EQUATION

We start with the one dimensional nonlinear diffusion equation and the initial and boundary conditions

$$\frac{\partial C}{\partial t} = \frac{\partial}{\partial z} \left(D \frac{\partial C}{\partial z} \right) \quad z, t \geq 0 \quad (1)$$

$$\left. \frac{\partial C}{\partial z} \right|_{z=0} = 0 \quad (2)$$

$$C(\infty, t) = 0 \quad (3)$$

$$C_0(z) = C(z, 0) \quad (4)$$

where $C(z, t)$ is the concentration at position z , time t , and $D[C(z, t)]$ is the diffusivity which may be an arbitrary function of the concentration.

By introducing new variables defined by

$$\zeta = \zeta(z, t) = \int_0^z \varphi[C(z', t)] D^{-1}[C(z', t)] dz' \quad (5)$$

$$\tau = \tau(z, t) = \int_0^t \varphi^2[C(z, t')] D^{-1}[C(z, t')] dt' \quad (6)$$

$$\Gamma = \Gamma(\zeta, \tau) = \beta \int_0^{C(z, t)} \varphi(C') dC' \quad (7)$$

Moroi and Hemenger have been able to transform Eqs. (1)-(4) into

$$\frac{\partial \Gamma}{\partial \tau} - \frac{\partial^2 \Gamma}{\partial \zeta^2} = \epsilon \quad (8)$$

$$\Gamma_0(\zeta) = \Gamma(\zeta, 0) = \beta \int_0^{C_0(z)} \varphi(C') dC' \quad (9)$$

$$\left. \frac{\partial \Gamma}{\partial \zeta} \right|_{\zeta=0} = 0 \quad (10)$$

$$\Gamma(\infty, \tau) = 0 \quad (11)$$

where β is a constant scaling factor and ϵ is given by

$$\epsilon = \epsilon(\zeta, \tau) = \frac{\partial \Gamma}{\partial \tau} \frac{D}{\varphi} \frac{\partial}{\partial z} \left[\frac{D}{\varphi} \frac{\partial \tau}{\partial z} \right] - \frac{\partial \Gamma}{\partial \zeta} \frac{D}{\varphi^2} \frac{\partial \zeta}{\partial t} + 2 \frac{\partial^2 \Gamma}{\partial \tau \partial \zeta} \frac{D}{\varphi} \frac{\partial \tau}{\partial z} + \frac{\partial^2 \Gamma}{\partial \tau^2} \left[\frac{D}{\varphi} \frac{\partial \tau}{\partial z} \right]^2 \quad (12)$$

The functional form of $\varphi(C)$ considered was

$$\varphi = a\sqrt{D} \quad (13)$$

By setting

$$\Gamma = \Gamma^{(0)} + \Gamma^{(1)} \quad (14)$$

they were able to use a standard perturbation method to get an approximate solution to Eq. (8).

In Eq. (14) $\Gamma^{(0)}$ and $\Gamma^{(1)}$ are the zeroth and first order terms in the perturbation and satisfy the following equations

$$\frac{\partial \Gamma^{(0)}}{\partial \tau} - \frac{\partial^2 \Gamma^{(0)}}{\partial \zeta^2} = 0 \quad (15)$$

$$\frac{\partial \Gamma^{(1)}}{\partial \tau} - \frac{\partial^2 \Gamma^{(1)}}{\partial \zeta^2} = \epsilon^{(0)} \quad (16)$$

with appropriate initial and boundary conditions. The $\epsilon^{(0)}$ is given by

$$\epsilon^{(0)}(\zeta, \tau) = \epsilon(\zeta, \tau)|_{\Gamma \rightarrow \Gamma^{(0)}} \quad (17)$$

The solution to Eq. (15) satisfying the initial and boundary conditions is

$$\Gamma^{(0)}(\zeta, \tau) = \frac{1}{\sqrt{4\pi\tau}} \int_0^\infty \left\{ \exp\left(-\frac{(\zeta-\zeta')^2}{4\tau}\right) + \exp\left(-\frac{(\zeta+\zeta')^2}{4\tau}\right) \right\} \Gamma_0(\zeta') d\zeta' \quad (18)$$

The solution to Eq. (16) satisfying the initial and boundary conditions is

$$\Gamma^{(1)}(\zeta, \tau) = \int_0^\tau \int_0^\infty G(\zeta, \tau | \zeta', \tau') \epsilon^{(0)}(\zeta', \tau') d\zeta' d\tau' \quad (19)$$

where $G(\zeta, \tau | \zeta', \tau')$ is the Greens function and is given by

$$G(\zeta, \tau | \zeta', \tau') = \frac{1}{\sqrt{4\pi(\tau-\tau')}} \left\{ \exp\left(-\frac{(\zeta-\zeta')^2}{4(\tau-\tau')}\right) + \exp\left(-\frac{(\zeta+\zeta')^2}{4(\tau-\tau')}\right) \right\} \quad (20)$$

The concentration in real space time is

$$C(z, t) = C^{(0)}(z, t) + C^{(1)}(z, t) \quad (21)$$

where $C^{(0)}$ and $C^{(1)}$ are determined by Eq. (9)

$$\Gamma^{(0)}(\zeta, \tau) = \beta \int_0^{C^{(0)}(z, t)} \varphi(C') dC' \quad (22)$$

and

$$\Gamma^{(1)}(\zeta, \tau) = \beta \int_{C^{(0)}(z, t)}^{C(z, t)} \varphi(C') dC' \approx \beta C^{(1)}(z, t) \varphi[C^{(0)}(z, t)] \quad (23)$$

With $\varphi = a\sqrt{D}$ Eqs. (5)-(7) and (12) become

$$\zeta = a \int_0^z D^{-1/2} [C(z', t)] dz' \quad (24)$$

$$\tau = a^2 t \quad (25)$$

$$\Gamma = a\beta \int_0^{C(z, t)} D^{1/2} [C'] dC' \quad (26)$$

$$\varepsilon^{(0)} = - \frac{\partial \Gamma^{(0)}}{\partial \zeta} \frac{\partial \zeta}{a^2 \partial t} \quad (27)$$

The inverse of Eq. (24) is given by

$$z = z(\zeta, \tau) = a^{-1} \int_0^\zeta D^{1/2} \{ C[\Gamma(\zeta', \tau)] \} d\zeta' \quad (28)$$

The initial dopant distribution in the transformed variables is chosen to be a truncated Gaussian.

$$\Gamma_0(\zeta) = \Gamma_m \exp \left[- \frac{(\zeta - \zeta_0)^2}{2\sigma^2} \right] \quad (29)$$

where Γ_m , σ , and ζ_0 are constants to be determined later. Note that because of the relationship between ζ and z the profile will not be a truncated Gaussian in real space.

Substituting Eq. (29) into Eq. (18) and integrating over ζ' we obtain

$$\Gamma^{(0)}(\zeta, \tau) = \frac{\Gamma_m}{2\sqrt{\frac{4\tau}{2\sigma^2} + 1}} \left\{ \exp(-w^{(+)}) \operatorname{erfc}(\xi^{(+)}) + \exp(-w^{(-)}) \operatorname{erfc}(\xi^{(-)}) \right\} \quad (30)$$

where

$$w^{(\pm)} = \frac{(\zeta \pm \zeta_0)^2}{(4\tau + 2\sigma^2)} \quad (31)$$

$$\xi^{(\pm)} = \frac{1}{\sqrt{2}\sigma} \frac{\pm 2\sigma^2 \zeta - 4\zeta_0 \tau}{\sqrt{4\tau(4\tau + 2\sigma^2)}} \quad (32)$$

and erfc is defined by

$$\operatorname{erfc}(\xi) = \frac{2}{\sqrt{\pi}} \int_\xi^\infty \exp(-x^2) dx \quad (33)$$

We now apply the calculations to two specific cases. For the first case we choose the diffusivity to depend on a power of the concentration.

$$D = D_v C^v \quad (34)$$

where D_v and v are constants. Eqs. (24)-(27) become

$$\zeta = \frac{a}{\sqrt{D_0}} \int_0^z C^{(v/2)}(z', t) dz' \quad (35)$$

$$\tau = a^2 t \quad (25)$$

$$\Gamma^{(0)}(\zeta, \tau) = A C_m^{(v/2)} \quad (36)$$

$$\epsilon^{(0)} = \Gamma^{(0)}\left(\frac{v}{v+2}\right) \frac{\partial \Gamma^{(0)}}{\partial \zeta} \int_0^\zeta \frac{\partial}{\partial \tau} [\Gamma^{(0)}(\zeta', \tau)] \left(\frac{v}{v+2}\right) d\zeta' \quad (37)$$

where

$$A = \frac{2a\beta\sqrt{D_v}}{v+2} = \frac{\Gamma_m}{C_m \left(\frac{v+2}{2}\right)} \quad (38)$$

Here C_m is the maximum initial dopant concentration in real space at $z=z_0$. Eq. (28)

becomes

$$z = z(\zeta, \tau) = a^{-1} \sqrt{D_v} A \left(\frac{v}{v+2}\right) \int_0^\zeta [\Gamma(\zeta', \tau)] \left(\frac{v}{v+2}\right) d\zeta' \quad (39)$$

We can obtain Γ_m in terms of C_m from Eq. (36)

$$\Gamma_m = A C_m \left(\frac{v+2}{2}\right) \quad (40)$$

and z_0 in terms of ζ_0 from Eq. (39)

$$z_0 = \sqrt{\frac{\pi(v+2)}{2v}} \sigma \left(\frac{\sqrt{D_v C_m^v}}{a} \right) \left[1 - \operatorname{erfc} \left(\sqrt{\frac{v}{v+2}} \frac{\zeta_0}{2\sqrt{\sigma}} \right) \right] \quad (41)$$

σ was determined by choosing $C(z=0, t=0)$ and using Eqs. (29) and (36).

$$\sigma = \zeta_0 \left[\frac{-1}{2 \ln \left(\frac{A}{\Gamma_m} C(0,0) \left(\frac{v+2}{2}\right) \right)} \right]^{\frac{1}{2}} \quad (42)$$

It is seen that with $C(0,0)$ held constant z_0 is directly proportional to ζ_0 .

For the second case we choose the diffusivity to depend exponentially on the concentration.

$$D = D_e \exp(kC) \quad (43)$$

Eqs. (23)-(26) become

$$\zeta = \frac{a}{\sqrt{D_e}} \int_0^z \exp\left(-\frac{kC(z,t)}{2}\right) dz' \quad (44)$$

$$\Gamma^{(0)}(\zeta, \tau) = B \left[\exp\left(-\frac{kC(z,t)}{2}\right) - 1 \right] \quad (45)$$

$$\varepsilon^{(0)} = \frac{1}{[\Gamma^{(0)} + B]} \left(\frac{\partial \Gamma^{(0)}}{\partial \zeta} \right)^2 \quad (46)$$

where

$$B = \frac{2a\beta\sqrt{D_e}}{k} = \frac{\Gamma_m}{\left[\exp\left(\frac{kC_m}{2}\right) - 1 \right]} \quad (47)$$

Eq. (28) becomes

$$z = z(\zeta, \tau) = \frac{\sqrt{D_e}}{a} \left[\zeta + \frac{1}{B} \int_0^\zeta \Gamma(\zeta', \tau) d\zeta' \right] \quad (48)$$

as before Γ_m in terms of C_m is obtained from Eq. (36)

$$\Gamma_m = B \left[\exp\left(\frac{kC_m}{2}\right) - 1 \right] \quad (49)$$

and z_0 in terms of ζ_0 from Eq. (39)

$$z_0 = \frac{\sqrt{D_e}}{a} \left\{ \zeta_0 + \sqrt{\frac{\pi}{2}} \sigma \left[\exp\left(\frac{kC_m}{2}\right) - 1 \right] \left[1 - \operatorname{erfc}\left(\frac{\zeta_0}{\sqrt{2}\sigma}\right) \right] \right\} \quad (50)$$

σ again comes from Eqs. (29) and (36)

$$\sigma = \zeta_0 \left[\frac{-1}{2 \ln \left(\frac{A}{\Gamma_m} \left[\exp\left(\frac{kC(0,0)}{2}\right) - 1 \right] \right)} \right]^{\frac{1}{2}} \quad (51)$$

Results of the calculations are plotted in Figs. 1 - 6. Zeroth order profiles are shown in Figs 1 (a) - 6 (a), first order corrected profiles in Figs 1 (b) - 6 (b) and numerical profiles in Figs. 1 (c) - 6 (c). In each case the dopant profile is shown at j s intervals to 20 s ($t_0 = 0$ s, $t_1 = 5$ s, $t_2 = 10$ s, $t_3 = 15$ s, $t_4 = 20$ s). Figs. 1 and 2 show results for the case $D = D_0 C^v$ with $v = 1$ and $v = 2$ respectively while Figs. 3 - 6 are for the case $D = D_0 \exp(kC)$ with $k = 1/2, 1, 2, 4$. In all cases the first order corrected profiles are significantly closer to the numerical profiles than are the zeroth order profiles over most of the depth range of interest indicating the validity of the analytical approach.

IV. A PRELIMINARY INVESTIGATION OF NONLINEAR OPTICS

We start with the source-free Maxwell equations for electromagnetic fields in nonlinear anisotropic optical media.

$$\nabla \times \mathbf{E} + \frac{1}{c} \frac{\partial \mathbf{B}}{\partial t} = 0 \quad (52)$$

$$\nabla \times \mathbf{H} - \frac{1}{c} \frac{\partial \mathbf{D}}{\partial t} = 0 \quad (53)$$

$$\nabla \cdot \mathbf{D} = 0 \quad (54)$$

$$\nabla \cdot \mathbf{B} = 0 \quad (55)$$

And the constitutive equations.

$$\mathbf{D} = \epsilon \mathbf{E} = \mathbf{E} + 4\pi \mathbf{P} \quad (56)$$

$$\mathbf{B} = \mu \mathbf{H} = \mathbf{H} + 4\pi \mathbf{M} \quad (57)$$

We have used the C.G.S. system of units and we assume that μ , the permeability of the medium, is isotropic and constant. Eliminating \mathbf{B} from Eq. (52) using Eq. (57) and taking the curl of the result we obtain

$$\nabla \times \nabla \times \mathbf{E} + \frac{\mu}{c} \frac{\partial}{\partial t} (\nabla \times \mathbf{H}) = 0 \quad (58)$$

Eliminating \mathbf{D} from Eq. (53) using Eq. (56), using the result to eliminate $\nabla \times \mathbf{H}$ from Eq. (58), and with

$$\epsilon = \epsilon^{(L)} + 4\pi\chi^{(NL)} \quad (59)$$

and

$$\mathbf{P}^{(NL)} = \chi^{(NL)} \mathbf{E} \quad (60)$$

we obtain

$$\nabla \times \nabla \times \mathbf{E} + \frac{\mu \epsilon^{(L)}}{c^2} \frac{\partial^2}{\partial t^2} \mathbf{E} = - \frac{4\pi\mu}{c^2} \frac{\partial^2}{\partial t^2} \mathbf{P}^{(NL)} \quad (61)$$

We denote \mathbf{E}_j the electric field associated with the j^{th} harmonic of the original angular frequency ω .

$$\omega_j = j\omega \quad (j = 1, 2, 3, \dots) \quad (62)$$

$$\mathbf{E}_j = \mathbf{E}^{(j)}(\mathbf{x}) e^{i\varphi_j} \quad (63)$$

$$\varphi_j = \int_{\mathbf{x}} \mathbf{k}^{(j)}(\mathbf{x}') \cdot d\mathbf{x}' - \omega_j t \quad (64)$$

where $\mathbf{k}^{(j)}(\mathbf{x})$ is the local wavevector of the j^{th} harmonic. The total electric field is then given by

$$\mathbf{E} = \sum_j \mathbf{E}_j \quad (65)$$

Similarly for the nonlinear polarization

$$\mathbf{P}^{(NL)} = \sum_j \mathbf{P}_j^{(NL)} \quad (66)$$

$$\mathbf{P}_j^{(NL)} = P_j^{(NL)}(\omega_j) e^{i\varphi_j} \quad (67)$$

$$P_j^{(NL)}(\omega_j) = P_j^{(2)}(\omega_j) + P_j^{(3)}(\omega_j) + P_j^{(4)}(\omega_j) + \dots \quad (68)$$

plugging this into Eq. (61)

$$\nabla \times \nabla \times (\mathbf{E}^{(j)}(\mathbf{x}) e^{i\varphi_j}) + \frac{\mu \epsilon^{(L)}}{c^2} \frac{\partial^2}{\partial t^2} (\mathbf{E}^{(j)}(\mathbf{x}) e^{i\varphi_j}) = - \frac{4\pi\mu}{c^2} \frac{\partial^2}{\partial t^2} (P_j^{(NL)}(\omega_j) e^{i\varphi_j}) \quad (69)$$

$$\frac{\partial^2}{\partial t^2} (\mathbf{E}^{(j)}(\mathbf{x}) e^{i\phi_j}) = -\omega_j^2 (\mathbf{E}^{(j)}(\mathbf{x}) e^{i\phi_j}) \quad (70)$$

$$\frac{\partial^2}{\partial t^2} (P_j^{(NL)}(\omega_j) e^{i\phi_j}) = -\omega_j^2 (P_j^{(NL)}(\omega_j) e^{i\phi_j}) \quad (71)$$

$$\nabla \times (\mathbf{E}^{(j)}(\mathbf{x}) e^{i\phi_j}) = \begin{vmatrix} \hat{x} & \hat{y} & \hat{z} \\ \frac{\partial}{\partial x} & \frac{\partial}{\partial y} & \frac{\partial}{\partial z} \\ E_x^{(j)} e^{i\phi_j} & E_y^{(j)} e^{i\phi_j} & E_z^{(j)} e^{i\phi_j} \end{vmatrix} \quad (72)$$

$$\begin{aligned} &= \hat{x} \left[\frac{\partial}{\partial y} (E_z^{(j)} e^{i\phi_j}) - \frac{\partial}{\partial z} (E_y^{(j)} e^{i\phi_j}) \right] \\ &+ \hat{y} \left[\frac{\partial}{\partial z} (E_x^{(j)} e^{i\phi_j}) - \frac{\partial}{\partial x} (E_z^{(j)} e^{i\phi_j}) \right] \\ &+ \hat{z} \left[\frac{\partial}{\partial x} (E_y^{(j)} e^{i\phi_j}) - \frac{\partial}{\partial y} (E_x^{(j)} e^{i\phi_j}) \right] \end{aligned} \quad (73)$$

$$\frac{\partial}{\partial y} (E_z^{(j)} e^{i\phi_j}) = E_z^{(j)} \frac{\partial}{\partial y} (e^{i\phi_j}) + e^{i\phi_j} \frac{\partial}{\partial y} (E_z^{(j)}) \quad (74)$$

$$\frac{\partial}{\partial y} (e^{i\phi_j}) = i e^{i\phi_j} \frac{\partial}{\partial y} (\phi_j) \quad (75)$$

$$\frac{\partial}{\partial y} (\phi_j) = \frac{\partial}{\partial y} \left(\int_{\mathbf{x}} \mathbf{k}^{(j)}(\mathbf{x}') \cdot d\mathbf{x}' - \omega_j t \right) = k_y^{(j)} \quad (76)$$

$$\frac{\partial}{\partial y} (E_z^{(j)} e^{i\phi_j}) = e^{i\phi_j} \left[i E_z^{(j)} k_y^{(j)} + \frac{\partial}{\partial y} (E_z^{(j)}) \right] \quad (77)$$

With similar relationships for the other components. Then

$$\nabla \times (\mathbf{E}^{(j)}(\mathbf{x}) e^{i\phi_j}) = e^{i\phi_j} [\nabla + i\mathbf{k}^{(j)}] \times \mathbf{E}^{(j)}(\mathbf{x}) \quad (78)$$

Now

$$\nabla \times \nabla \times (\mathbf{E}^{(j)}(\mathbf{x}) e^{i\phi_j}) = \nabla \times [e^{i\phi_j} [\nabla + i\mathbf{k}^{(j)}] \times \mathbf{E}^{(j)}(\mathbf{x})] \quad (79)$$

Using the vector identity⁵

$$\nabla \times \psi \mathbf{a} = \nabla \psi \times \mathbf{a} + \psi \nabla \times \mathbf{a} \quad (80)$$

Eq. (79) can be written as

$$\nabla \times [e^{i\phi_j} [\nabla + i\mathbf{k}^{(j)}] \times \mathbf{E}^{(j)}(\mathbf{x})] = \nabla e^{i\phi_j} \times [\nabla + i\mathbf{k}^{(j)}] \times \mathbf{E}^{(j)}(\mathbf{x}) + e^{i\phi_j} \nabla \times [\nabla + i\mathbf{k}^{(j)}] \times \mathbf{E}^{(j)}(\mathbf{x}) \quad (81)$$

and

$$\nabla e^{i\phi_j} = e^{i\phi_j} i\mathbf{k}^{(j)} \quad (82)$$

So we have

$$\nabla \times \nabla \times (\mathbf{E}^{(j)}(\mathbf{x}) e^{i\phi_j}) = e^{i\phi_j} [\nabla + i\mathbf{k}^{(j)}] \times [\nabla + i\mathbf{k}^{(j)}] \times \mathbf{E}^{(j)}(\mathbf{x}) \quad (83)$$

plugging Eqs. (70), (71), and (83) into Eq. (69), a factor of $e^{i\phi_j}$ comes out and we have

$$[\nabla + i\mathbf{k}^{(j)}] \times [\nabla + i\mathbf{k}^{(j)}] \times \mathbf{E}^{(j)}(\mathbf{x}) - \frac{\omega_j^2 \mu \epsilon^{(L)}}{c^2} \mathbf{E}^{(j)}(\mathbf{x}) = \frac{4\pi\omega_j^2 \mu}{c^2} \mathbf{P}_j^{(NL)}(\omega_j) \quad (84)$$

This is the wave equation for which we seek solutions in the form of a spatially varying electric field $\mathbf{E}^{(j)}(\mathbf{x})$ for each harmonic. Wave interaction gives rise to the nonlinear polarization $\mathbf{P}_j^{(NL)}(\omega_j)$.

V. RECOMENDATIONS

The program CA, used to produce all the dopant profiles is presented in the appendix along with the required input file CA_IN.DAT. The program is written in FORTRAN77 and is documented to provide guidance for its use and modification. All runs were done on a Microvax III.

Before the analytical approach can actually be used for tracking dopant profiles the best functional form to use for $D(C)$ must be determined. Also an analysis of how well real dopant profiles can be fit with the initial profile is necessary. Ghetz et. al.¹ have determined that real profiles can be accurately fit with truncated Gaussians. Although the

initial profiles obtained with the analytical approach are not truncated Gaussians they differ primarily in the tail regions at low concentrations and hence may adequately describe real profiles in the region of interest.

The work in nonlinear optics was only a beginning and much remains to be done before actually writing computer code. Work could be extended to crystals other than BaTiO_3 and eventually from surface waves to waves in bulk material and more complicated geometries.

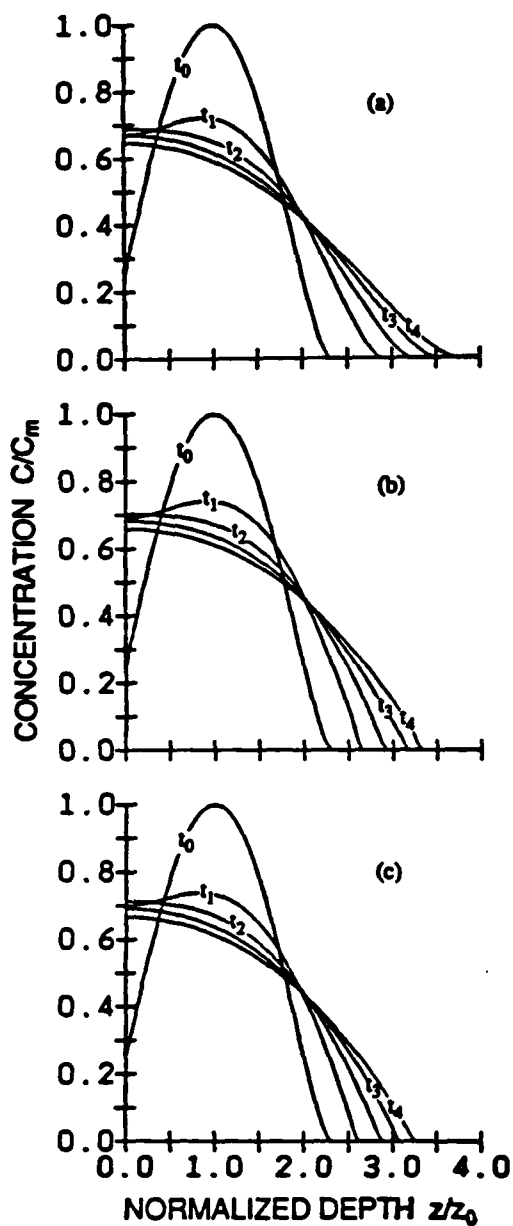


FIG. 1. Time development of dopant profile for $D = D_v C^v$ with $v = 1$: (a) zeroth order, (b) first order, (c) numerical.

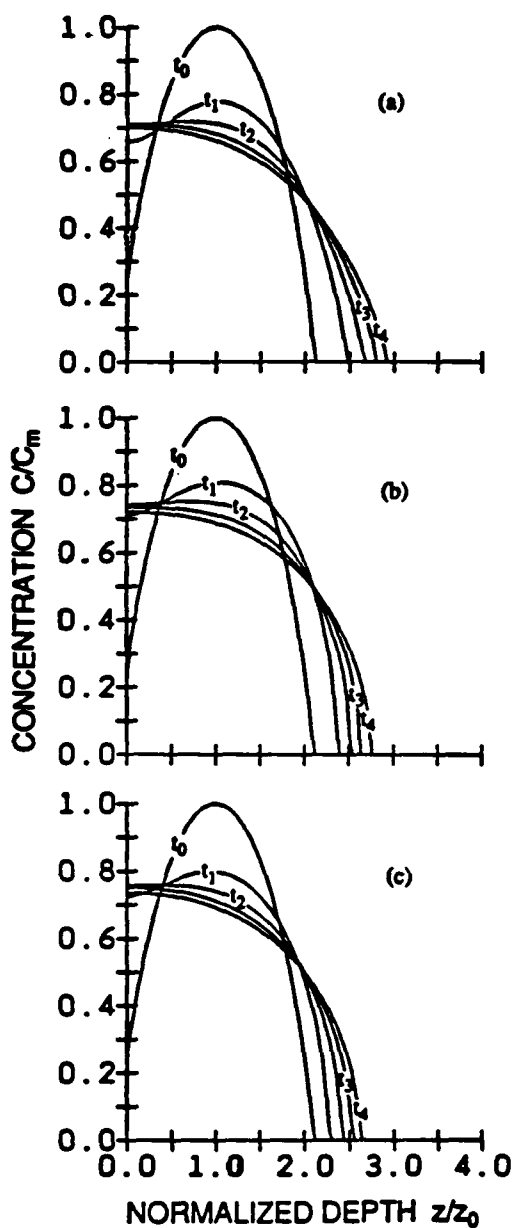


FIG. 2. Time development of dopant profile for $D = D_v C^v$ with $v = 2$: (a) zeroth order, (b) first order, (c) numerical.

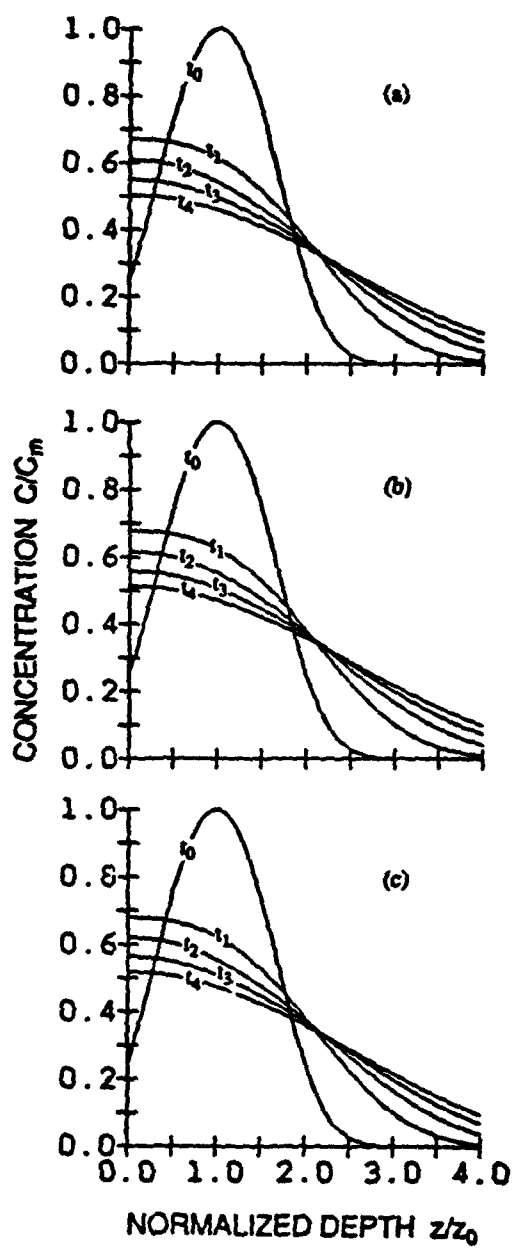


FIG. 3. Time development of dopant profile for $D = D_e \exp(kc)$ with $k = 1/2$: (a) zeroth order, (b) first order, (c) numerical.

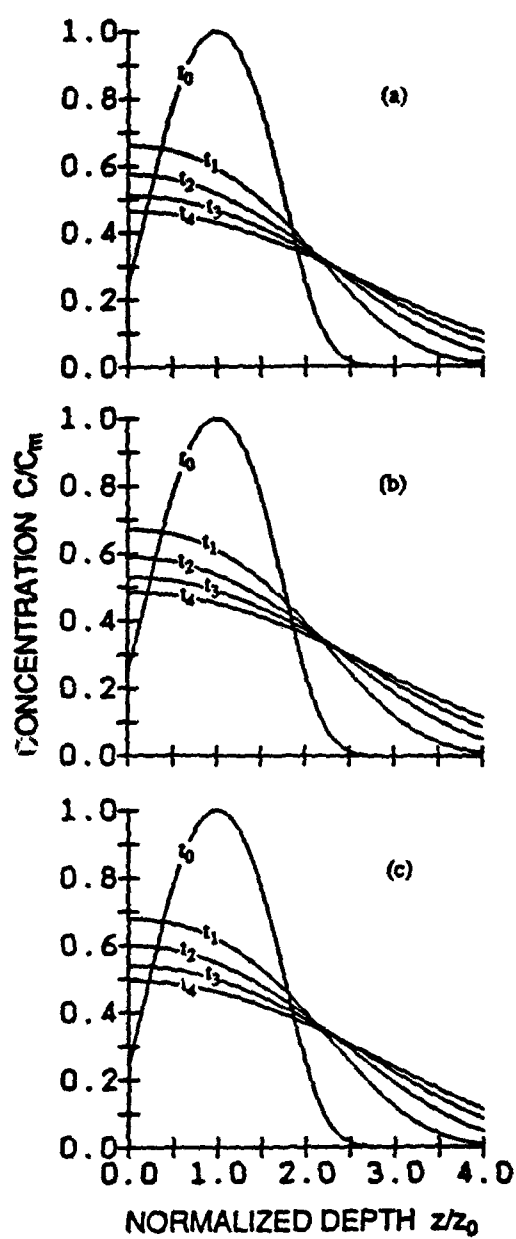


FIG. 4. Time development of dopant profile for $D = D_e \exp(kc)$ with $k = 1$: (a) zeroth order, (b) first order, (c) numerical.

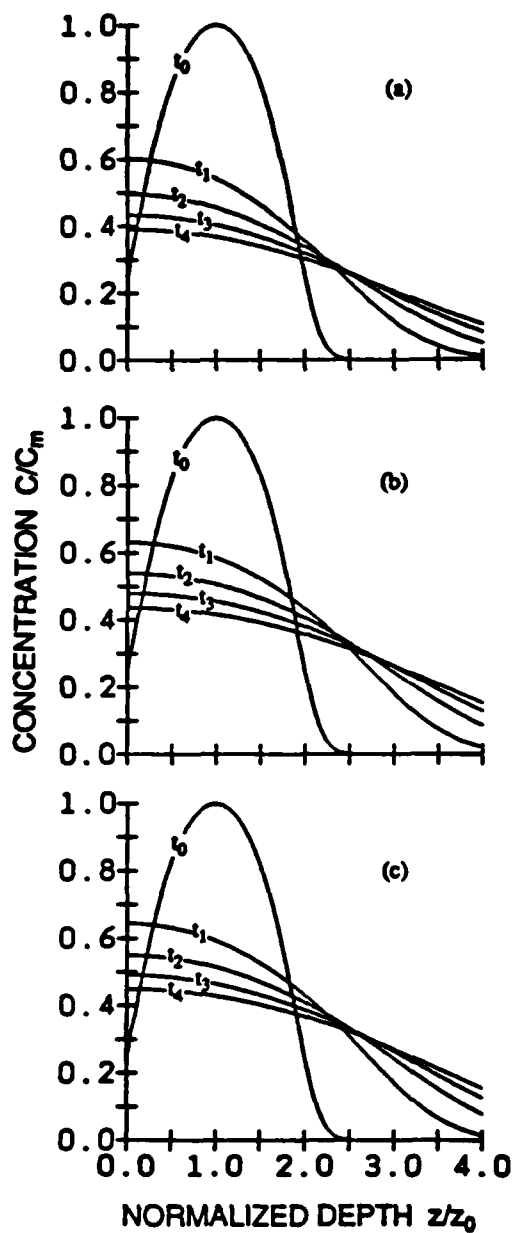


FIG. 5. Time development of dopant profile for $D = D_e \exp(kc)$ with $k = 2$: (a) zeroth order, (b) first order, (c) numerical.

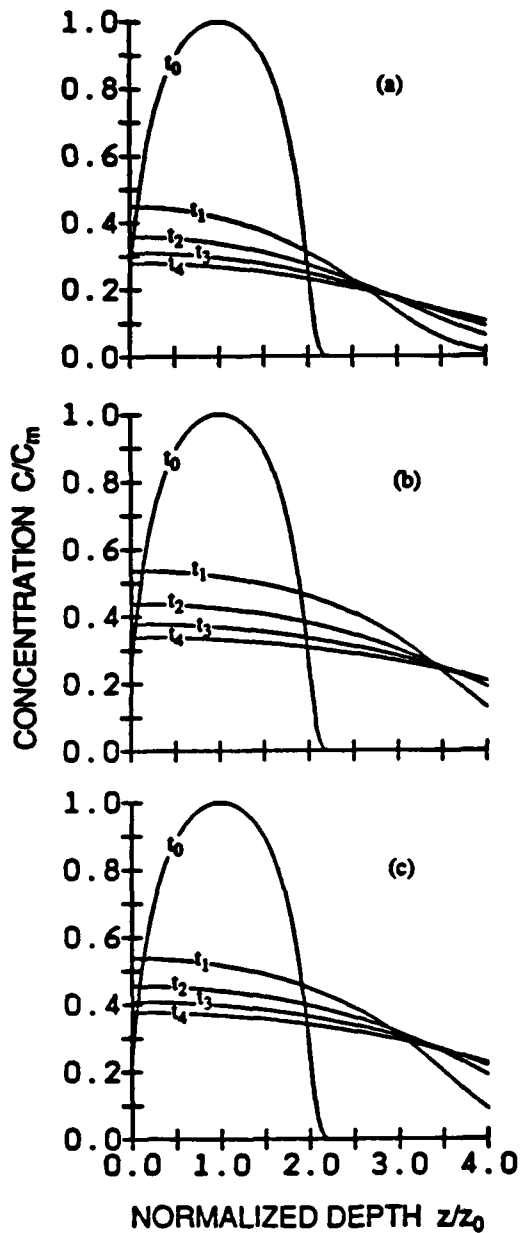


FIG. 6. Time development of dopant profile for $D = D_e \exp(kc)$ with $k = 4$: (a) zeroth order, (b) first order, (c) numerical.

REFERENCES

- ¹R. Ghez, G. S. Oehrlein, T. O. Sedgwick, F. F. Morehead, and Y. H. Lee, "Exact Description and Data Fitting of Ion-implanted Dopant Profile Evolution During Annealing", *Applied Physics Letters* 45, 881 (1984).
- ²Y. R. Shen, The Principles of Nonlinear Optics, New York, John Wiley and Sons, 1984.
- ³D. S. Moroi and P. M. Hemenger, "Perturbation Method for Solution to Nonlinear Diffusion Equation", to be published.
- ⁴D. L. Boyd, "Analytical and Numerical Solutions of the Nonlinear Diffusion Equation", final report to USAF-UES summer faculty research program/graduate student research program, 1988.
- ⁵J. D. Jackson, Classical Electrodynamics, second edition, New York, John Wiley and Sons, 1975.

APPENDIX

MAY BE OBTAINED FROM AUTHOR OR UNIVERSAL ENERGY SYSTEMS, INC.

1989 USAF-UES SUMMER FACULTY RESEARCH PROGRAM/

GRADUATE STUDENT RESEARCH PROGRAM

Sponsored by the

AIR FORCE OFFICE OF SCIENTIFIC RESEARCH

Conducted by the

Universal Energy Systems, Inc.

FINAL REPORT

INVESTIGATION OF THE THERMOMECHANICAL RESPONSE OF A TITANIUM ALUMINIDE
METAL MATRIX COMPOSITE USING A VISCOPLASTIC CONSTITUTIVE THEORY

Prepared by: James A. Sherwood, Ph.D.
Academic Rank: Assistant Professor

Prepared by: Marcia J. Boyle
Academic Rank: Graduate Student

Department and University: Mechanical Engineering
University of New Hampshire

Research Location: WRDC/MLLN
Wright-Patterson AFB, OH 45433

USAF Researcher: Theodore Nicholas, Ph.D.

Date: 22 September 89

Contract No: F49620-88-C-0053

Same Report As
Prof. James Sherwood
(Report # 122)

1989 USAF-UES SUMMER FACULTY RESEARCH PROGRAM
GRADUATE STUDENT RESEARCH PROGRAM

Sponsored by the
AIR FORCE OFFICE OF SCIENTIFIC RESEARCH

Conducted by the
Universal Energy Systems, Inc.
FINAL REPORT

Synthesis of Model Benzothiazoles

Prepared by: Charles E. Gray
Academic Rank: Graduate Student
Department and University: Department of Chemistry
Wright State University
Research Location: Materials Laboratory, Nonmetallic
Materials Division, Polymer Branch
Wright Patterson Air Force Base,
Dayton Ohio
USAF Researcher: Dr. Fred E. Arnold
Date: 9-27-89
Contract No: F49620-88-C-0053

SYNTHESIS OF MODEL BENZOTHAZOLES

by

Charles E. Gray

ABSTRACT

Two benzothiazole models were prepared. The first model was prepared by reacting DABT monomer with 2-(1-propanesulfonic acidbenzimidazole) benzoic acid in polyphosphoric acid to give the corresponding 2,5-disubstituted dibenzothiazole. This model was prepared to determine stability of the monomer at polymer reaction conditions. The second model was prepared by reacting DABT monomer with formic acid neat. The resulting unsubstituted dibenzothiazole will be used to study non-linear optical properties of polybenzothiazoles.

ACKNOWLEDGEMENTS

I would like to thank the Air Force Systems Command and Office of Scientific Research for sponsorship of the G.S.R.P. program. In addition Universal Energy Systems should be recognized for making the administrative process most convenient.

The group of people at the Materials lab Polymer Branch at W.P.A.F.B. deserve more credit than I can Give them for there ensight and friendliness. The assistance of Thuy Dhang is most appreciated and also that of Dr. Fred E. Arnold whose ideas made everything possible. I would also like to thank Dr. James J. Kane my research advisor at Wright State U. who prepared me for the summer appointment and initially encouraged me to apply.

I. INTRODUCTION:

The synthesis of novel rigid-rod polybenzothiazoles with increased mechanical properties as well as thermal stability has been of much interest in aerospace research as possible replacements for the more dense metallic materials.

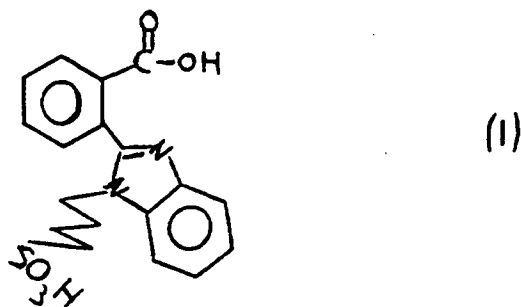
The Polymer Branch of the Materials laboratory at W.P.A.F.B. is currently investigating the synthesis and analysis of conducting polybenzothiazoles for such applications.

My masters thesis and research has been in the synthesis of benzimidazole models with benzothiazole pendants and has thus aided my summer effort.

II. OBJECTIVES OF THE RESEARCH EFFORTS:

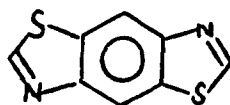
The area of conducting polymers branches more rapidly as new data accumulates and therefore the future of this project may take many different routes. Some possible aeronautical applications for conducting polybenzothiazoles may be as insulators semi-conducting devices or wiring depending on the degree of conductivity.

My immediate goals of the Graduate Student Research Program were to synthesize the following polymer end capper and to determine if it would be stable at polymerization conditions of 190 deg. celsius in polyphosphoric acid:



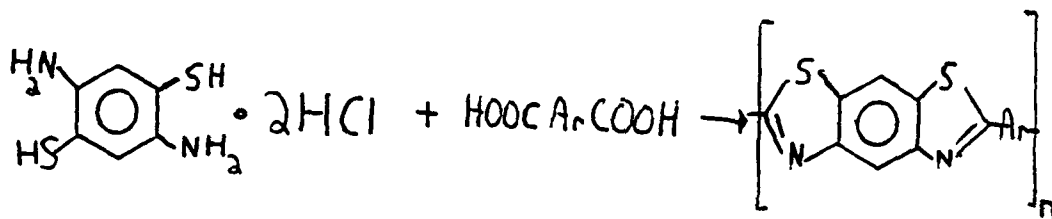
Time did not allow for any polymerization reactions but the end capper was produced. Compound (I) was determined to be non stable at these conditions.

In addition the following model compound was desired and produced for future determination of its non-linear optical properties because it is the basic unit of P.B.T.'s.



III. RESULTS AND DISCUSSION

Polybenzothiazoles are made by reacting DABT monomer with the appropriate diacid as shown in figure 1.



These polymers are meant to have applications at high temperatures. If the polymer is not end capped it is possible that cross-linking and additional polymerization can occur at temperatures higher than that of the reaction conditions. So a monoacidic end capper can terminate a polymerization by leaving non active sites at the end of the polymer chain eliminating a varience of physical properties due to cross-linking and additional polymerization at application temperatures. In addition it is hoped that compound 1 will show pendant interaction between side chains through the sulphonic acid functionality, resulting in side chain protonation and intrinsic conduction(1). Conductivity measurements will be done in the future.

IV. EXPERIMENTAL:

O(2-BENZIMIDAZOLY)BENZOIC ACID(III)

10.00 grams of phthalic anhydride was dissolved in 100 ml. of D.M.F. and transferred to a 500 ml. three necked R.B. flask equipped with a nitrogen inlet outlet and a mechanical stirrer. To this solution was added 7.30 grams of o-phenylenediamine in 100 ml. of D.M.F. This solution was heated to reflux overnight and upon cooling the next day the product fell out of solution. The white precipitate was filtered and washed with methanol in a Soxhlet extractor overnight. Filtering and drying gave a 14.20 g of material 88% yield m.p above 300 deg. C.

1-PROPANESULFONIC ACID,2-oBENZOIC ACIDBENZIMIDAZOLE(IV)

250 ml. of spec grade D.M.S.O. was purged under nitrogen for 15 min. in a 500 ml. 3-necked r.b flask equipped with a mechanical stirrer. To this was added 1.70 grams of 60% NaH in oil and this mixture was heated to 60 deg. Celsius for 1 hour. This was then cooled to 40 deg. and 5.00 grams of (III) was added. This mixture was heated to 70 deg. for 1 hour and then cooled to 40 deg. To this mixture was added 2.55 grams of 97% 1,3 propane sultone. This was heated to 70 deg. overnight. The next morning the solution was cooled to r.t. and poured into about 2000 ml. of T.H.F. This solution was stirred for several hours to complete precipitation and to allow unreacted sultone to dissolve. The white material the disodium salt of (IV) began to melt and turn yellow in the air presumably because it is very hygroscopic. This material was then transferred to a 250 ml. flask and 10% HCl solution was added at B.P. until solid just dissolved (approximately 100ml.). Upon cooling a white solid fell out of solution. This was filtered to give 3.2 grams of diacid %yield =42.3, M.P. 300-305.

DIBENZOTHIAZOLE(V)

1.0 Grams of DABT monomer was added to about 70 ml. of 98% formic acid in a 200 ml. r.b.f. equipped with a mechanical stirrer and under a nitrogen atmosphere. This mixture was heated to reflux for 5 hours. Upon cooling a white precipitate formed and this material was filtered and recrystallized from ethanol to give 0.48 grams of (V) =74% yield M.P.=258-260

MODEL COMPOUND OF (I)

1.00 gram of (I) and 0.34 of DABT monomer was placed in a 100 ml. R.B.F. and 20 grams of P.P.A. was added. The flask was set up under a nitrogen inlet/outlet and equipped with a mechanical stirrer. This mixture was heated overnight at 80 deg. C to drive off the HCl from the DABT. The next day the mixture was heated slowly to 190 deg C. The mixture started to darken at about 160 deg.C. When the temp. reached 190 deg. C it was allowed to stay there for about 2 hours. It was then poured into water to give an off white material after filtering M.P. above 300 deg. C. This material was sochlet extracted with water overnight to completely remove the P.P.A.. Purification of this material was not achieved but FTIR shows no indication of a carbonyl peak or an NH₂ peak.

V. RECOMMENDATIONS

The less than quantitative yield of the synthesis of model compound I together with the darkening of the P.P.A. solution at about 160 deg. C indicates partial decomposition of the monomer. Future polymerizations may be more effective if they are done at lower temperatures. More conjugated pendant groups on the end capper may also result in increased conductivity for example replacement of the propane sulfonic acid function with a propene sulfonic acid function.

REFERENCES

Textbooks:

1. Seawor, Donald, Electrical Properties of Polymers
Academic Press 1982

1989 USAF-UES SUMMER FACULTY RESEARCH PROGRAM/
GRADUATE STUDENT RESEARCH PROGRAM

Sponsored by the
AIR FORCE OFFICE OF SCIENTIFIC RESEARCH
Conducted by the
Universal Energy Systems, Inc.
FINAL REPORT

State of the Art Sensors for In-Situ
Monitoring of Composite Cure

Prepared by :	Dean R. Hofmann
Academic Rank :	Graduate Student
Department and	Department of Chemical And
University :	Materials Engineering
	University of Dayton
Research Location :	USAF
	Wright-Patterson AFB
	Dayton, Ohio 45440
USAF Researcher :	Dr. Tony Saliba
Date :	July 17, 1989
Contract Number :	F49620-88-C-0053

State of the Art Sensors for In-Situ

Monitoring of Composite Cure

by

Dean R. Hofmann

ABSTRACT

This paper surveys those sensors presently in commercial use or under development for the application toward in-situ composite cure monitoring. Five categories of in-situ sensors are presented: electrical properties, acoustic, optical, eddy current and direct. Theory and practice are discussed and a critical review of those sensors which are standard, hardened and currently used in industry is presented.

Acknowledgements

I wish to thank the Air Force Systems Command and the Air Force Office of Scientific Research for the sponsorship of this research. For their help in all the administrative and directional aspects of this program my thanks goes out to the people at Universal Energy Systems. My special thanks goes out to Dr. Tony Saliba, Frances Abrams and Major Steve Leclair whose support and guidance made this summer program both enjoyable and a learning experience.

I. INTRODUCTION:

As the use of composite parts and structures become more and more prevalent in today's society, so does the need to improve upon the quality and ease of production of these pieces. The need to achieve higher degrees of tolerance, both dimensionally and mechanically, in the production of composite structures is forcing industry to develop systems to optimally process composite materials. The "eyes and ears" of any system are sensors. Placed within or upon the layup, these sensors monitor what is taking place during the cure process.

Heat Transfer, resin flow, chemical reaction, physical changes and void formation are the physical and chemical phenomena that take place during the cure of a typical composite material. Ideally, a sensor would be available to monitor a parameter directly related to each of the aforementioned phenomena.

Heat transfer in a curing composite depends upon bagging and tooling materials, surrounding atmosphere, as well as the type of composite material being processed. Temperature distributions as a function of position and time are essential to determine cure conditions. Thermocouples are the sensors used in temperature measurement. However, new developments in fiber optics may soon replace the thermocouple.

Resin flow is essential in order to eliminate voids and provide a well bonded matrix. However, too much flow results in a resin starved laminate, severely limited in its structural integrity. Too little resin flow also effects the structural properties of the laminate as well as its dimensional aspects by not allowing the laminate to consolidate and compact. Resin flow cannot be sensed in-situ. However, by combining several sensors, it may be possible to infer the degree of resin flow.

The kinetics of each reaction taking place during a cure cycle is unique. The ability to monitor the kinetics of a curing resin can reveal valuable information about viscosity and void formation. Monitoring the rate and degree of cure provides information that can

be used to optimize temperature and pressure cycles, resulting in lower process times and improved structural properties.

Due to trapped gases in the laminate and the production of volatiles during the cure, voids are formed within the laminate. Pressure gradients, diffusion, and thermal expansion govern void size, distribution, and movement.

The final dimensions of the composite materials are determined by the compaction rate and residual stresses. Residual stresses result in warpage/shrinkage of the laminate. With consolidation and residual stress sensors tight tolerances on the dimensions of the composite structure could be attained and post cure modifications kept to a minimum.

Although, not all the properties mentioned above can be monitored directly, it is essential to develop sensors which can monitor directly or indirectly all the parameters that are necessary to produce a mechanically and physically sound product.

For the successful implementation of an expert system controller or, more simply, the ability to monitor the layup in order to manually manipulate the temperature and pressure, it is necessary to understand the simple theory behind in-situ sensors, their limitations, and the meaning of their output. A survey of five categories of sensors is presented. They include: electrical properties, acoustic, optical, eddy current and direct.

II. OBJECTIVES OF THE RESEARCH EFFORT:

Currently, there is no available single source which describes the latest available technology in in-situ composite cure monitoring sensors. A survey of available technology in this area was deemed necessary in order to create a knowledge base which could be referred to in the event that the application of a certain sensor was in question, or a specialty sensor, or basic theory behind a certain sensor was needed. Temperature and pressure sensors are well established in the composite industry and except for novel approaches will not be covered in this paper.

My assignment as a participant in the 1989 Summer Research Program was to compile theoretical background, typical operation, and mechanical/physical limitations of state-of-the-art in-situ composite cure monitoring sensors.

III. ELECTRICAL PROPERTIES SENSORS:

As the polymeric matrix material undergoes reaction during the curing process, complex chemical and physical changes take place as the material is transformed from a liquid to a glassy solid. Due to these chemical and physical changes, the polymeric material also undergoes large changes in its electrical properties due to the presence of molecular dipoles within the resin.

Several methods of monitoring cure based on the variation of electrical properties in time have been devised, including: iongraphing, phaseometry, and dielectric analysis.¹ Because dielectric analysis is the most widely used technique, it will be discussed indepth; the other techniques will be mentioned briefly.

IONGRAPHING

Due to the presence of ions in the matrix, either from impurities, reaction products, or initial reactants, the technique of iongraphing plots ionic mobility with respect to time. Initially the ions are frozen in place due to the highly viscous nature of an uncured B-staged resin. However, as the temperature increases so does the mobility of the ions in the matrix. Due to this mobility, the DC conductivity increases. Figure 1 is a simple schematic of an iongraphing system. Further heating causes the matrix to undergo transition into a glassy solid which causes the ion mobilities to again decrease and the DC conductivity to follow this decline.² However, the output signal is reduced as the thickness of the laminate

increases, making it difficult to monitor thick laminates with the iongraphing technique.

PHASEOMETRY

In this technique the resin sample is used as a resistive circuit element. An electronic schematic is shown in Figure 2. By imparting an AC signal through a reference resistor in series with the resin, one can monitor the changes in phase angle (across the resistor), which are related to similar changes within the resin.³ These changes are analogous to those described in the iongraphing technique. Like the iongraphing technique, phaseometry has the same difficulty in monitoring thick laminates.

DIELECTROMETRY

Dielectric analysis measures the two fundamental electrical characteristics of a material, capacitance and conductance, as a function of time, frequency and temperature.⁴ Capacitance is a measure of a material's ability to store electric charge and conductance is a measure of a material's ability to transfer electric charge.

There are three different types of devices used to perform dielectric analysis, including parallel plate, comb electrodes, and microdielectrometry. These devices and their relationship to each other are pictured in Figure 3.

Using parallel plate electrodes, the thickness of the laminate changes, causing the plate spacing to change during the cure. Because the capacitance and conductance is dependent upon the plate spacing, it is not possible to determine the permittivity and loss factor separately. As a result, the ratio of the loss factor to the permittivity, called the loss tangent, is measured. Calibration of parallel plate electrodes is independent of plate spacing when measuring the loss tangent. However, the loss tangent does not reveal as much information about the cure process as does the permittivity and the loss factor.

Comb electrodes do provide fixed values of the permittivity and loss factor because the dimensional quantities of the electrodes

remain constant throughout the cure. However, the comb electrode device is much less sensitive to the changes in electrical properties than is the parallel plate. While the microdielectrometer has essentially become the standard due to its ease of location, sensitivity, and its independence of laminate thickness.

Locating the microdielectrometer in the laminate requires two important considerations. The sensor must be in intimate contact with the resin and must not be in contact with any conducting fibers. Wrapping the sensor in a bleeder cloth and assuring good resin contact are solutions to these problems. A microdielectric sensor produced by Micromet is shown in Figure 4.

The procedure used to track a curing composite is as follows. After obtaining values of the capacitance C , and conductance G , the measured permittivity ϵ'_m , and loss factor ϵ''_m , are calculated by⁵,

$$\epsilon'_m = \frac{C}{C_o} \quad (1)$$

$$\epsilon''_m = \frac{G}{C_o 2\pi f} \quad (2)$$

where,

f - frequency

C_o - capacitance of air

The actual permittivity ϵ' , represents the amount of alignment of the dipoles to the electric field. Figures 5 and 6 show dipole arrangement before and after application of an electric current. The permittivity is low for polymers at low temperatures as well as highly crosslinked resins due to the fact that the molecules are locked in place and the dipoles cannot move to align themselves with the electric field.⁶

The actual loss factor ϵ'' , is a measure of the amount of energy required to align dipoles or move ions. Ionic conduction does not become significant until the polymer becomes fluid, thus allowing the ions to become mobile. For this reason, ion conductivity can be directly correlated with viscosity or degree of cure.⁷

The actual permittivity ϵ' , and loss factor ϵ'' are related to the relaxed ϵ_r , and unrelaxed ϵ_u permittivity and the ionic conductivity σ , by⁸

$$\epsilon' = \epsilon_u + \frac{\epsilon_r - \epsilon_u}{1 + (\omega\tau)^2} \quad (3)$$

$$\epsilon'' = \frac{\sigma}{\omega\epsilon_o} + \frac{(\epsilon_r - \epsilon_u) \omega\tau}{1 + (\omega\tau)^2} \quad (4)$$

where,

ω - $2\pi f$, angular frequency

τ - dielectric relaxation (time required for a polarization to appear or disappear)

ϵ_o - permittivity in free space

The relaxed permittivity measures the maximum dipolar alignment that can be achieved at a given temperature and chemical state and the unrelaxed permittivity is the permittivity measured well below the T_g and at all frequencies has a constant value.

Because ions build up at the electrode surface without discharging, electrode polarization occurs. This results in a charged layer that acts as a large capacitor. Electrode polarizations cause the permittivity to be measured higher and the loss factor to be measured lower. Thus, correction factors may be used to relate the measured values to the actual values using,

$$\epsilon'_m = \epsilon'(EP1) \quad (5)$$

$$\epsilon''_m = \epsilon''(EP2) \quad (6)$$

As previously mentioned the ionic conductivity is of primary interest because it can be correlated to the properties of viscosity and degree of cure. Using the Kranbuehl Method⁹ as an example, frequencies are found at which electrode polarization and dipole effects are negligible and ionic effects dominate.¹⁰ Thus, $EP2 = 1.0$ rearranging equations 4 and 6 we have,

$$\epsilon'_m \omega = \frac{\sigma}{\epsilon_o} + \frac{(\epsilon_r - \epsilon_u) (\omega^2 \tau)}{1 + (\omega\tau)^2} \quad (7)$$

Assuming that the ionic effects dominate then equation 7 becomes,

$$\epsilon'_m \omega \approx \frac{\sigma}{\epsilon_o} \quad (8)$$

and the ionic conductivity can then be calculated. Once the ionic conductivity is calculated, the ionic viscosity can be calculated by

taking the reciprocal of the ionic conductivity. A plot of ion viscosity versus time correlates well with the actual viscosity.

It must be recognized that frequencies at which ionic effects dominate are not known, a priori. Thus, a wide range of frequencies must be scanned in hopes that at least two will give the same value of the product of $\epsilon'_m \omega$.

A typical, although rather idealized, response for a thermosetting resin monitored using a dielectrometer operating at a fixed frequency is shown in Figure 7. Due to high internal friction at the beginning of the cure cycle, the molecules are essentially locked in place. As the temperature increases, the viscosity of the resin decreases, allowing the polar groups and ion impurities to become mobile. This causes an increase in capacitance. At some point the resin reaches a minimum, causing the capacitance to reach a maximum. As the temperature increases due to the reaction of the solidifying resin, the capacitance decreases.¹¹

Results presented by Ciriscioli and Springer¹² show that although dielectric measurements yield useful information about the cure process, they do not provide a direct indication of the viscosity or degree of cure during the entire cycle. The ionic conductivity data does indicate the time at which the viscosity is minimum and the time at which the cure is near completion ($d\sigma/dt \rightarrow 0$). (see Figure 8). Furthermore, the interlaminar location of a microdielectrometer in a thick composite structure is possible only at the expense of losing some of the structural properties of the laminate.

IV. OPTICAL SENSORS:

Fourier Transform Infrared Spectroscopy

Fourier transform infrared spectroscopy used in-situ to monitor composite cure was first reported in September 1988.¹³ The arsenic, germanium, selenide chalcogenide optical fiber used has a transmission range of 1250cm^{-1} to 3300cm^{-1} . The ability to use FTIR to monitor cure has been made possible through the development of low loss optical fibers. These fibers allow the sample to be left outside of the spectrometer itself during analysis.

The heart of the FTIR spectrometer is the Michelson Interferometer (see Figure 9). A monochromatic light source is split at the beam splitter. One part of the light reflects off of the fixed mirror and the other portion of the light beam is passed to a movable mirror and then reflected back to the beam splitter which recombines the two light beams. If the mirror is continuously moved, the signal produced by the recombined light source will oscillate from strong to weak for each one-quarter wavelength λ of movement, producing a cosine wave or interferogram. Using a broad-line spectral input, the output will be the sum of all cosine oscillations caused by the optical frequencies of the source.

An interferogram can be represented mathematically as,¹⁴

$$I(x) = \int_{-\infty}^{+\infty} B(\nu) \cos(2\pi\nu x) d\nu \quad (9)$$

where,

$I(x)$ - interferogram intensity at the detector

x - mirror displacement

$B(\nu)$ - intensity of the source as a function of frequency λ

This equation is one-half of the cosine Fourier transform pair,

$$B(\nu) = \int_{-\infty}^{+\infty} I(x) \cos(2\pi x \nu) dx \quad (10)$$

These two equations relate the spectrum $B(\nu)$ and the interferogram $I(x)$. A computer performs the transformation and produces an IR spectrum (Figure 10a).¹⁵

The uniqueness of the FTIR is evident. Most other sensors monitor secondary effects, ie. dielectric properties, acoustic attenuation, and then infer the pure resin chemistry from this data. FTIR monitors the vibration of the atoms and molecules associated with the dissociation and formation of the chemical bonds. This allows the monitoring of certain spectra bands, watching for the appearance/disappearance of certain bands indicative of degree of cure (Figure 10b). Shown in figure 10a at 1535cm^{-1} an amide band is present and indicative of an uncured resin (LaRC-TPI). Notice in Figure 10b this band has disappeared, indicating a cured sample. However, because

of expense, delicate fibers and a small transmission range the applications of infrared transmitting fibers are limited.¹⁶

Fiber Optic Temperature and Pressure Sensors

The Fiber Optic Sensor Probes presently being tested for use in monitoring composite cure were developed by Metricor. Metricor Coloroptic measurement technique is unique to fiberoptic sensing. This technique depends upon color changes, not light intensity.¹⁷ Via an LED light source, light is supplied to the sensor, modified at the sensor tip and reflected back along the fiber to a detector. The spectral makeup of the reflected light is then modified in proportion to the parameter being measured.¹⁸ Douglas Aircraft Company studies¹⁹ show negligible impact on the mechanical performance of the composites with the fiber optic sensor running parallel to the carbon fiber reinforcements. A 14% reduction in compressive properties was found when the optical fibers were embedded perpendicular to the carbon fibers. The fiber optic density in the latter case was 0.33. Although the optic fibers are relatively nonobtrusive and can be used to monitor the properties of the cured matrix in its working environment, the expense of the sensors may inhibit their widespread use in the near future.

Acoustic Source

This method requires the layup of a two-dimensional grid of optical fibers within the sample. The monitoring of the attenuation and longitudinal velocity of an acoustic transmission could locate voids.²⁰ At this time, little research has been done in this area.

Refraction Technique

Basically, light propagates in a fiber with minimal loss as long as the refractive index of the surrounding medium is less than that of the fiber and the angle of incidence exceeds the critical angle according to:²¹

$$\sin(\theta_i) > \frac{n_m}{n_f} \quad (11)$$

where,

n_m and n_f - refractive indices of the medium and fiber

θ_i - angle of incidence

The angle ϕ that the incident light makes with the normal to the front surface of the fiber is given by:²²

$$\phi < \sin^{-1}(n_f^2 - n_m^2)^{.5} \quad (12)$$

Assuming that the excitation light, propagating in the air, $n=1$, enters the fiber through a surface that is normal to the fiber and resin interface.²³

By sandwiching a cured polymer fiber, of the same material as the composite being processed, between two glass fibers, the index of refraction is monitored. When the index of refractions are equal, light will no longer be transmitted down the optical fiber, giving zero output and indicating a sufficiently cured product.²⁴

Not only can this technique be used as a degree of cure sensor, but with certain modifications, it can also be used to sense degree of consolidation²⁵ and viscosity changes.²⁶

Fluorescence Technique

This technique is based on the combination of fiber optic fluorometry and a viscosity/degree of cure dependence of epoxy resin fluorescence.²⁷

Fluorescence is the emission of electromagnetic radiation, usually in the form of visible light, which occurs only during the absorption of radiation from another source. Fiber optic waveguides are used to deliver excitation energy to the fluorescing media. Fiber optics are also used to carry the emitted fluorescence back to a detector or a spectrometer. There are basically two types of fluorescence sensors being used for in-situ cure monitoring: evanescent wave and distal end sensors. A evanescent wave sensor collects fluorescent light emitted from chromophores lying near the optic surface. These chromophores are initially excited by the evanescent wave of the guided light. A distal end sensor collects fluorescent light from a sampling volume which is illuminated by the guided light.²⁸

Fluorescence may be produced either by a particular type of resin or from organic dyes added to the polymeric matrix.²⁹ According to Fanconi³⁰, an effective probe molecule should be chemically inert with respect to both the resin and optical fibers, easily dispersed in the resin, and absorb and fluoresce in a spectral region free of interferences from either the resin or the optic fiber.

Results³¹ show that changes in the fluorescence maximum wavelength reveal the minimum viscosity and gelation point and also the degree of cure during the latter stages of the cure cycle. Further results³² using the fluorescent and refractive properties of a curing resin indicate the degree of consolidation of the polymeric matrix.

V. ULTRASONIC ACOUSTIC SENSORS:

Ultrasonic acoustic sensors operate by transmitting an ultrasonic wave through a laminate and measuring the attenuation of the transient elastic stress wave exiting the material. The ultrasonic wave is produced by applying a voltage across a piezoceramic crystal. The resulting compression wave is received by another piezoceramic crystal which generates a voltage when is it disturbed from its resting state.³³ The difference between the output voltage and the input voltage of the piezoceramic transducers is indicative of the condition of the material and thus can be correlated to viscosity or degree of cure.

The absorption of sound in a material was attributed to heat conduction and internal friction by Stokes³⁴ and Kirchoff³⁵ with the development of the following equation,

$$2\alpha = \frac{4\pi^2 f^2}{c^3 \rho_0} \left[\frac{4}{3}\eta + \frac{(k-1)}{C_p} \kappa \right] \quad (13)$$

The quantity 2α is the intensity absorption coefficient of a plane wave as defined by,

$$I = I_0 e^{-2\alpha x} \quad (14)$$

where,

- c - velocity of sound
- Cp - specific heat at constant pressure
- Cv - specific heat at constant

- temperature
- f - frequency of the wave
- I₀ - intensity at time equals zero
- k - Cv/Cp
- η - viscosity
- κ - thermal conductivity
- ρ₀ - mean density

The following equation defines the loss of energy and the ultrasonic attenuation of an ultrasonic wave propagating in the z-direction.³⁶

$$A = A_0 e^{-\alpha' z} \cos(kz - \omega t) \quad (15)$$

where,

- A - final wave amplitude
- A₀ - initial wave amplitude
- k - propagation constant, $2\pi/\lambda$
- α' - attenuation (absorption) coefficient
- ω - radian frequency, $2\pi f$

As an ultrasonic wave propagates through a medium it may be absorbed or scattered. The attenuation coefficient α', is a measure of these processes. When a wave is scattered, its energy is redistributed into many other waves. This process is continued until the wave is absorbed; that is, dissipated directly as heat. Otherwise, the wave is transmitted through the medium. Studies show³⁷ that the attenuation coefficient is affected by many physical phenomena. Therefore, monitoring the attenuation coefficient is a means of monitoring the changes in certain physical phenomena.

As a wave propagates through a viscoelastic material³⁸ it will attenuate such that,

$$A_f = A_i e^{-\alpha' h} \quad (16)$$

where,

- A_f - final amplitude of the waveform
- A_i - initial amplitude of the waveform
- h - material thickness
- α' - attenuation coefficient

An increase in viscosity would increase the intensity absorption coefficient 2α (see equation 11). Because,

$$\alpha' = \frac{2\alpha}{2} \quad (17)$$

The increase in viscosity would result in a lowered final wave amplitude A_f , (see equation 14). Thus, the acoustic ultrasonic output would increase. Figure 11 shows a typical setup of an acoustic sensor and a typical output.

As with dielectric monitoring, acoustic sensors do not provide a direct indication of viscosity during the entire cure cycle. However, the ultrasonic acoustic sensor is nonobtrusive because it is not located in the layup itself; rather, it is placed on top of the layup. Furthermore, with knowledge of the speed of sound as a function of cure time or viscosity of the resin, the sensor could serve a dual purpose as a viscosity sensor and a thickness sensor.

VI. EDDY CURRENT SENSORS:

An eddy current sensor system has been developed by Douglas Aircraft Company and NDT Instruments, Inc. The system setup is shown in Figure 12. The sensor measures the thickness of the curing composite by monitoring the gap between the probe and the caul plate.³⁹ The initial thickness of the composite layup must be known using this setup.

Within the sensor a coil generates a time varying electromagnetic field that induces an electric current in the caul plate (see Figure 13). In form, these currents resemble the eddies in flowing streams of turbulent water, thus the name eddy currents. The electrical conductivity of the test object (here the caul plate), and the frequency and amplitude of the applied electromagnetic field determines the amount of electrical current flowing in the eddies.⁴⁰ The eddy currents created in the test specimen, in turn, create their own electromagnetic field, which may be sensed due to the fact that this field directly opposes the field generated by the coil.

Maintaining that the permeability of the test specimen is constant, only changes in the electrical conductivity of the test specimen or the gap distance can effect the output of the sensor.

By using phase analysis⁴¹, a separation of the changes in electrical conductivity and gap distance can be accomplished due to the fact that the effects of these two changes occur out of phase.

Phase analysis is based on the fact that the current(I) is out of phase with voltage(V) when a coil is connected across a voltage generator. Inductance is the measure of the property that opposes a change in current. A coil is an inductor whose current lags its voltage by less than 90 degrees. If a coil's magnetic field is interfered with, then a change in its inductance will take place. This in turn changes the lag between the current and the voltage. The coil's resistance and reactive inductance($X_L = 2\pi fL$) is represented graphically in Figure 14. Where Z is the impedance, as the coil impedance changes, the phase angle (see Figure 15) changes. Three properties effect the phase angle: conductivity, permeability, and dimensional changes. By using phase analysis, keeping permeability constant, separation of the conductivity and dimensional effects are possible because conductivity changes parallel resistance in the coil and dimensional changes parallel the inductive reactance (see Figure 16).

VII. DIRECT SENSORS:

Figure 17 shows the setup used by Kim and Jun to measure the thickness and compaction rate of a curing composite.⁴² The compaction rate is related to the strain imposed upon a strain gage located in the measuring block. Although, this setup is suitable for flat laminates, it does not seem readily adaptable to curved surfaces. Nor could it be located within a material without cutting a hole at the point of application.

VIII. SUMMARY:

This report reviewed the basic theory behind the latest technology in in-situ sensors. Table 1 lists the advantages and limitations of the most promising sensors.

Table 1

Method	Advantages	Limitations
Electrical Properties		
Longraphing	simple application	thick laminates
Phaseometry	nonobtrusive	present problems
Dielectrometry		
Parallel Plate	simple, nonobtrusive	change in plate spacing
Comb Electrodes	simple	sensitivity
Microdielectrometry	sensitivity, economical	obtrusive in interlaminar applications (see ultrasonic)
Optical		
FTIR	can be left in laminate for future use, nonobtrusive	expensive
Fiberoptic	" "	expensive
Fluorescent	" "	expensive
Ultrasonic	sensitivity, nonobtrusive	no direct correlation with viscosity
Eddy Current	nonobtrusive	fixture and initial spacing needed

Sensors capable of measuring the degree of cure and viscosity within a curing composite are the most extensively developed. However, it is possible only to correlate these sensors output to the viscosity or degree of cure. Other sensors suffer from this very same problem and more research in the area of sensor development is needed. New sensors need to be developed which enable the user to obtain accurate measurements of voids, residual stress, and thickness, in turn, allowing the production of a much higher quality, less labor intensive product.

REFERENCES

1. Carlin, D.M., "Dielectric Monitoring in Material Quality and Process Control," University of Dayton, November 1986, pp. 1-2.
2. Carlin, D.M., p. 2.
3. Lawless, G.W., " Dielectric and Phaseometric Monitoring of Adhesives," Adhesives Age, April 1981, pp. 26-27.
4. Dupont, product literature on the 2970 Dielectric Analyzer.
5. Ciriscioli, P.R., Springer, G.S., "Dielectric Cure Monitoring - A Critical Review," 34th International SAMPE Symposium, May 1989, pp. 313-314.
6. Dupont, product literature on the 2970 Dielectric Analyzer.
7. Dupont, product literature on the 2970 Dielectric Analyzer.
8. Ciriscioli, P.R., Springer, G.S., "Dielectric Cure Monitoring - A Critical Review," 34th International SAMPE Symposium, May 1989, pp. 314-315.
9. Ciriscioli, P.R., p. 315.
10. Ciriscioli, P.R., p. 315.
11. Carlin, D.M., p. 9.
12. Ciriscioli, P.R., p. 317.
13. Young, P.R., Druy, M.A., Stevenson, W.A., Compton, D.A.C., "In-situ Composite Cure Monitoring Using Infrared Transmitting Optical Fibers," SAMPE Journal, Vol. 25, April 1989, pp. 11-16.
14. Young, P.R., Chang, A.C., "FTIR Characterization of Advanced Materials," SAMPE Quarterly, Vol. 17, July 1986, p. 33.
15. Chang, A.C., p. 33.
16. Fanconi, B., "Monitoring Consolidation of Reinforcement Plies in Polymer Matrix Laminates," SAMPE Journal, Vol. 25, July/August 1989, p. 37.
17. Metricor, product literature on fiber optic sensors.
18. Metricor, product literature on fiber optic sensors.
19. "Advanced Composite Processing Technology Development," First Quarterly Interim Technical Report, McDonnell Douglas Corp., U.S. Air Force Contract F33615-88-C-5455, p. 15.
20. McDonnell Douglas, p. 5.
21. Fanconi, B., p. 37.
22. Fanconi, B., p. 36.
23. Fanconi, B., p. 36.
24. McDonnell Douglas, p. 7.
25. Fanconi, B., p. 36.
26. Fanconi, B., p. 36.
27. McDonnell Douglas, p. 13.
28. Fanconi, B., p. 37.
29. Fanconi, B., p. 40.
30. Fanconi, B., p. 40.
31. McDonnell Douglas, p. 15.
32. Fanconi, B., p. 41.
33. Saliba, S.S., Saliba, T.E., Lanzafame, J.F., "Acoustic Monitoring of Composite Materials During the Cure Cycle," 34th International SAMPE Symposium, May 1989, pp. 397.

34. Stokes, G.G., Phil. Trans, Vol. 8, p. 287, 1845.
35. Kirchoff, G., Pogg. Ann., Vol. 134, p. 177, 1868.
36. Mason, W.P., Thurton, R.N., Physical Acoustics Principles and Methods, Vol. 12, Academic Press, New York, New York, pp. 277-307, 1976.
37. Saliba, S.S., Saliba, T.E., Lanzafame, J.F., "Acoustic Monitoring of Composite Materials During the Cure Cycle," 34th International SAMPE Symposium, May 1989, pp. 397-406.
38. Applied Polymer Technology, Inc., "Ultrasonic Determination of Storage and Loss Moduli of Solid Propellents," Small Business Innovative Research Program, 1985.
39. McDonnell Douglas, p. 5.
40. "Nondestructive Testing: A Survey," NASA SP-5113, 1973, p. 102.
41. "Nondestructive Testing: Eddy Current Testing," General Dynamics, Vol. 1, 1967, pp. 5-30 - 5-115.
42. Kim, T.W., Jun, E.J., "Compaction Behavior of Thick Composite Laminates During Cure," 34th International SAMPE Symposium, May 1989, pp. 15-19.

***** Because of limited space the figures that accompany this paper were intentionally left out. Copies are available by contacting the author.

1988 USAF-UES FACULTY RESEARCH PROGRAM/
GRADUATE STUDENT RESEARCH PROGRAM

Sponsored by the
AIR FORCE OFFICE OF SCIENTIFIC RESEARCH

Conducted by the
Universal Energy Systems, Inc.

FINAL REPORT

DATA REDUCTION OF PHOTOREFLECTANCE FROM CAPPED
ALUMINUM GALLIUM ARSENIDE STRUCTURES

Prepared by:	Neal Jahren
Academic Rank:	B.A.
Department and	Physics Dept.
University:	Univ. of Mn. Duluth
Research Location:	AFWAL/MLPO Wright-Patterson AFB Dayton Ohio 45433
USAF Researcher:	William Mitchel
Date:	11 Aug 89
Contract No:	F49620-88-C-0053

DATA REDUCTION OF PHOTOREFLECTANCE FROM CAPPED
ALUMINUM GALLIUM ARSINIDE STRUCTURES

by

Neal Jahren

ABSTRACT

Photoreflectance is used to estimate the composition and doping levels of $\text{Al}_x\text{Ga}_{1-x}\text{As}$ epilayers capped with GaAs. We have analyzed data from our experiment by fitting it with Aspnes' third derivative functional form and electro-optic function. We have also used an indirect method developed by Bottka et al. to estimate doping levels.

ACKNOWLEDGEMENTS

Everyone at the Materials Lab did their best to accomodate and support our work there. People who deserve special mention include Ron Perrin, William Mitchel, Patrick M. Hemenger, Frank Szmulowicz, David Moroi, and Darwin Boyd. My reasearch advisor, Michael Sydor, not only made his experience and expertise available to me, but provided his encouragement and enthusiasm, and also helped me facilitate my off-base arrangements.

This research was supported by the Air Force Office of Scientific Research through a contract with Universal Energy Systems.

I. INTRODUCTION:

Photoreflectance (PR) can be used as an effective tool for quick evaluation of the quality of AlGaAs¹ and GaAs² material. It also provides an accurate method for measurement of the band gap energies and doping concentrations in GaAs.²⁻⁴ We consider here the extension of PR to measurements of doping levels and composition of Al_xGa_{1-x}As layers in epi-structures capped with GaAs. The Materials Laboratory of the Air Force Wright Aeronautical Laboratory at Wright-Patterson Air Force Base is particularly interested in characterizing both AlGaAs and GaAs/AlGaAs structures grown by Molecular Beam Epitaxy (MBE). There is a need for nondestructive testing of AlGaAs/GaAs structures before they are used in manufacturing of electronic devices.

My research interests are in theoretical physics, and I have been responsible for carrying out numerical computations in most of the research teams I have worked with to date.

II. OBJECTIVES OF THE RESEARCH EFFORT:

Current methods for evaluating the characteristics of samples grown by the Wright Research and Development Center's MBE group are lengthy and often destructive. Photoreflectance offers a quick, nondestructive way to achieve the same ends. Our main objective was to reduce the data from our photoreflectance experiment to a form useful to other researchers, and to find a process that would allow us to do so quickly.

My assignment as a participant in the 1989 Graduate Student Research Program (GSRP) was to assist Professor Michael Sydor in the construction of a PR station. Once completed, we used the equipment to study various samples grown by the MBE group. We analyzed the data on various computer systems in the Materials Lab. Data was collected on a Zenith Z-100 microcomputer interfaced with a Keithley 199 digital voltmeter and running a ZBASIC program. Data was analyzed on a small DEC VAX mainframe. Programming for the VAX was coded in either RPL, a language for the data-handling package RS/1, or in FORTRAN 77. These programs were either developed by us or modified from pre-existing codes. We plotted data on an Apple Macintosh II running Cricket Software's GRAPH.

III. RESULTS

This section will be devoted to presenting examples of results we obtained by following the customary methods established for analysis of PR data from GaAs.³⁻¹⁰ For undoped samples of AlGaAs and when the FKO are absent in the PR data, the band gap energy can be determined¹ through the use of Third Derivative Functional Fits (TDFF) to the PR signal. The TDFF provide a fit to the photorefectance $\Delta R/R$ according to:⁷

$$\Delta R/R = \text{Re}\{C e^{i\theta} (E - E_g + i\Gamma)^{-n}\} \quad (1a)$$

where E is the energy of the probe beam, Γ is a broadening parameter for E_g , the critical point energy, and n refers to the type of critical point in question; $n = 2, 2.5$, or 3 for an exciton, a three-dimensional band-to-band, or a two-dimensional band-to-band transition, respectively. C and θ are an amplitude and a phase factor that both vary slowly with E and determine the amplitude and the asymmetry of the PR signal.

Rewriting (1a) in terms of all real expressions gives:

$$\Delta R/R = C |E - E_g + i\Gamma|^{-n} \cos\{\theta - n \cos^{-1}[(E - E_g)/|E - E_g + i\Gamma|]\} \quad (1b)$$

Eq. (1) is generally applicable for low electric field conditions typified by the absence of Franz-Keldysh Oscillations (FKO), usually when $\Delta R/R < 10^{-4}$. An example of a TDFF to data taken on our equipment is shown in Fig. 1. This fit was obtained using the FIT FUNCTION command in RS/1.¹¹

When the AlGaAs is doped or when the unintentional impurities exceed 10^{16} cm^{-3} , the FKO become prominent, so the TDFF should not be used.¹ The general solution for high field condition yields the oscillatory behavior for $\Delta R/R$ in terms of the electro-optic function:⁸⁻¹⁰

$$\Delta R/R = \alpha_{lh} G[(E_g - E)/\hbar\theta_{lh}] + \alpha_{hh} G[(E_g - E)/\hbar\theta_{hh}] \quad (2a)$$

where $G(x)$ is given by the Airy functions and their derivatives according to:

$$G(x) = A_i'(x)B_i'(x) - xA_i(x)B_i(x) \quad , \quad (2b)$$

and

$$(\hbar\Theta_{ih})^3 = e^2\hbar^2\mathcal{E}^2/2\mu_{ih} \quad , \quad i = l \text{ or } h \quad , \quad (2c)$$

where \mathcal{E} is the electric field, and μ_{lh} and μ_{hh} are the reduced effective masses for the light and heavy holes, respectively. Most fits require that the broadened $G(x)$ functions be used.⁹ Fig. 2 shows an electro-optic function fit to PR data for a doped AlGaAs sample. This fit was accomplished with standard regression techniques;¹² the Airy functions were evaluated numerically.¹³

An indirect method for the determination of the band gap energy and estimation of doping concentrations from PR data was given by Bottka et al.³ For large \mathcal{E} , Eq. (2) takes on the asymptotic form:⁸

$$\Delta R/R \equiv \cos\{(2/3)[(\mathcal{E} - E_g)/\hbar\Omega]^{3/2} + \pi(d-1)/4\} \quad , \quad (3)$$

where d is the dimensionality of the critical point. AlGaAs with $x < 0.3$ should have a direct band to band transition, so we take $d = 3$. If we neglect the amplitude factor in Eq. (3), the position of the FKO extrema can be approximated by:³

$$E_j = \hbar\Omega F_j + E_g \quad , \quad j=1,2,\dots \quad , \quad (4A)$$

$$F_j = [3\pi(j-1/2)/2]^{2/3} \quad . \quad (4B)$$

$\hbar\Omega$ is a characteristic energy associated with the critical point. It is related to the electric field \mathcal{E} by:

$$\hbar\Omega = (\mathcal{E}^2 e^2 \hbar^2 / 8m)^{1/3} \quad , \quad (5)$$

where m is the interband reduced mass.

As indicated by Eq. (4), a plot of E_j vs. F_j is a straight line with slope $\hbar\Omega$, and intercept E_g . The label i denotes successive FKO extrema following the main PR peak at

the band edge. The slopes of the lines from Eq. (4) depend only on the carrier concentrations, independent of temperature fluctuations, the laser energy, its intensity, and the sample preparation.^{2,3} The intercept E_g usually falls close to the band gap energy determined by PL measurements. Using the generalized Schottky equation and Eq. (5), Bottka et al.³ have shown that the carrier concentration N , and the built-in surface potential V_b are related through ϵ by:

$$\epsilon = [2eN(V_b - V_p - kT/e)/\kappa\epsilon_0]^{1/2} \quad , \quad (6)$$

where V_p is the quasi-equilibrium photovoltage of the laser, kT/e is a thermal term, and $\kappa\epsilon_0$ is the dielectric constant times the permittivity of free space. V_p is determined from Eq. (6) by using calibrated samples where N is known. Taking $\Delta V = (V_b - V_p - kT/e)$, we obtain :

$$(\Delta V)N \propto (E_2 - E_1)^3 \quad , \quad (7)$$

where $(E_2 - E_1)$ is in eV and E_2 and E_1 refer to the energies of the second and the first FKO, respectively.

Similarly, using the PR signal zero cross-over points, we obtain from Eq. (3):

$$E_m = E_0 + \hbar\Omega \quad (3m\pi/2)^{2/3} \quad , \quad m=0,1,2,\dots \quad , \quad (8)$$

where E_0 corresponds to $m = 0$, the first zero PR cross-over point past the main PR peak at the band edge. Using Eqs. (5), (6), and (8), we obtain a relationship for the cross-over points equivalent to Eq. (7):

$$N = C_0 (\Delta E)^3 \quad , \quad (9)$$

where C_0 is an experimentally determined constant and ΔE is the energy difference between the two zero cross-over points $m = 0$, and $m = 1$. The zero base line for the PR can be obtained from the signal well beyond the AlGaAs band gap energy. A plot of ΔE vs. N provides a convenient graph for estimating carrier concentration in doped AlGaAs.

Fig. 3 shows the calibration curve for determination of doping levels in AlGas as observed in our experiment.

IV. RECOMMENDATIONS:

PR has been shown to be a viable method for quick characterization of samples, including GaAs, AlGaAs, and layered structures involving both materials. It can be used to help improve the quality of the samples grown by the MBE group.

REFERENCES

- ¹D. Huang, G. Ji, U. K. Reddy, H. Markoç, F. Xiong, & T. A. Tombrello, J. Appl. Phys. 63, 5447 (1988).
- ²M. Sydor, J. Angelo, W. Mitchel, T. W. Haas, & Ming-Yuan Yen, J. Appl. Phys. 66, 156 (1989).
- ³N. Bottka, D. K. Gaskill, R. S. Sillmon, R. Henry, & R. Glosser, J. Electron. Materials 17, 161 (1988).
- ⁴L. Peters, L. Phaneuf, L. W. Kapitan, & W. M. Theis, J. Appl. Phys. 62, 4558 (1987).
- ⁵O. J. Glembocki, B. V. Shanabrook, N. Bottka, W. T. Beard, & J. Comas, SPIE 524, 86 (1985).
- ⁶J. L. Shay, Phys. Rev. B 2, 803 (1970).
- ⁷D. E. Aspnes, Surf. Science 37, 418 (1973).
- ⁸D. E. Aspnes, Phys. Rev. 147, 554 (1966); 153, 972 (1967). D. E. Aspnes & A. A. Studna, Phys. Rev. B 7, 4605 (1973):
- ⁹Joel Grover, Stephen Koeppen, & Paul Handler, Phys. Rev. B 4, 2830 (1971).

¹⁰C. Van Hoof, K. Deneffe, J. De Boeck, D. J. Arent, & G. Borghs, Appl. Phys. Lett. 54, 608 (1989).

¹¹RS/1 User's Guide: Statistical Tools Release 4, Cambridge, MA, BBN Software, 1988.

¹²Philip R. Bevington, Data Reduction and Error Analysis for the Physical Sciences, New York, McGraw-Hill, 1969.

¹³See the formulas and algorithms in Jerome Spanier & Keith B Oldham, An Atlas of Functions, Washington, Hemisphere, 1987.

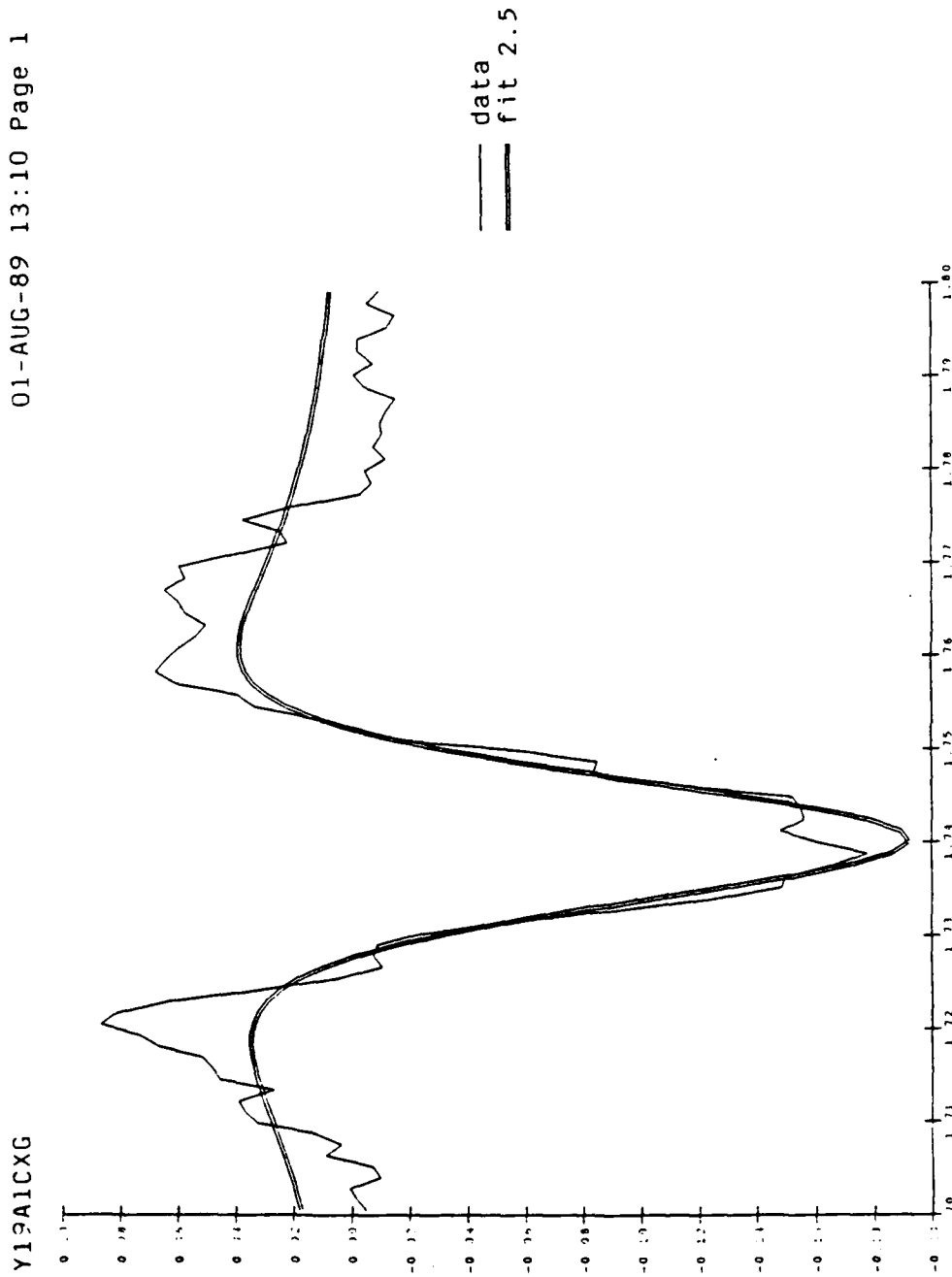


FIG. 1: The single line shows PR data from AlGaAs. The double line shows a TDFF according to Eqn. (1), with $n = 2.5$ and $E_g = 1.75$ eV.

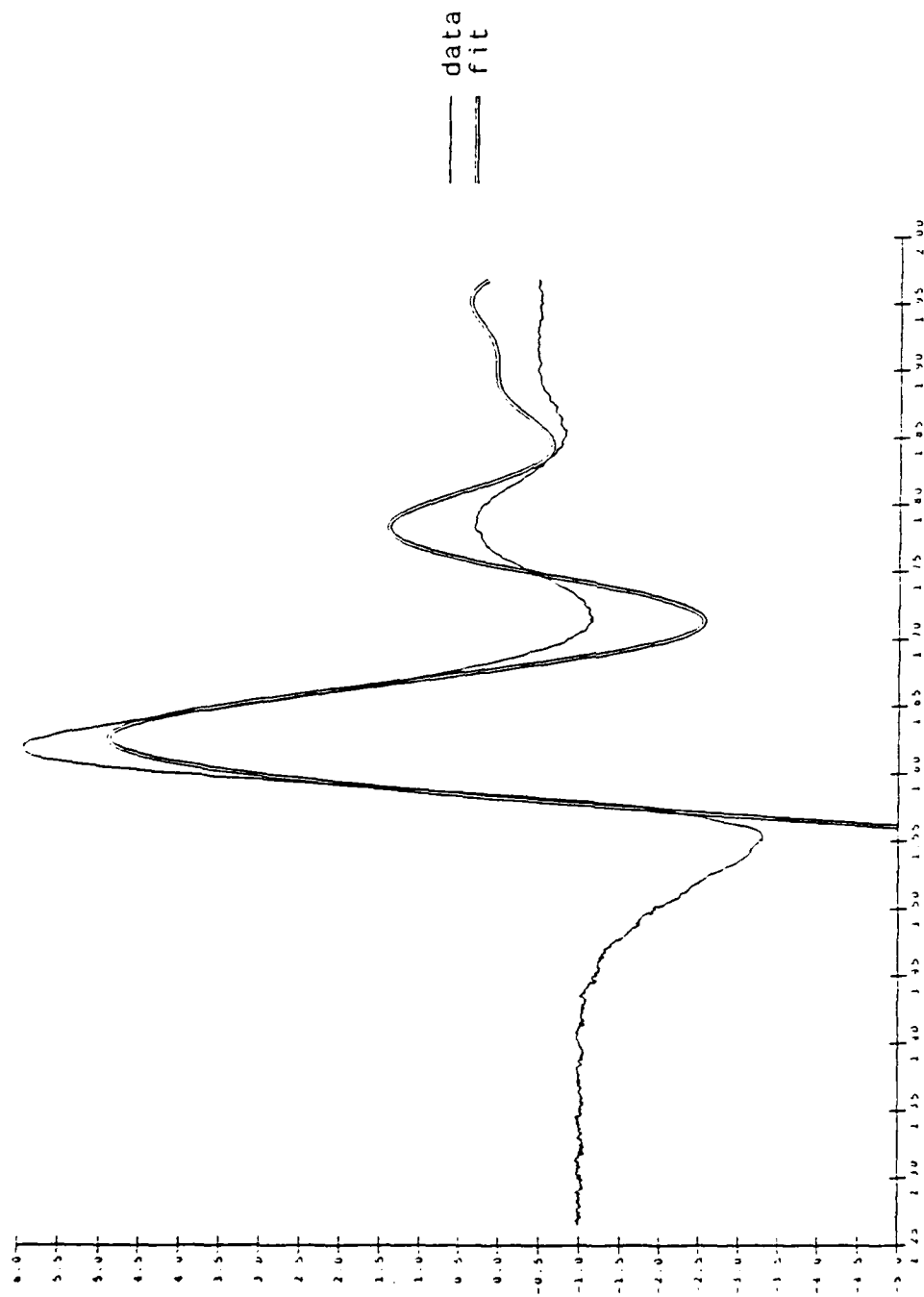


FIG. 2: The single line shows PR data from doped AlGaAs. The double line shows a fit according to Eqn. (2), with $E_g = 1.54$ eV.

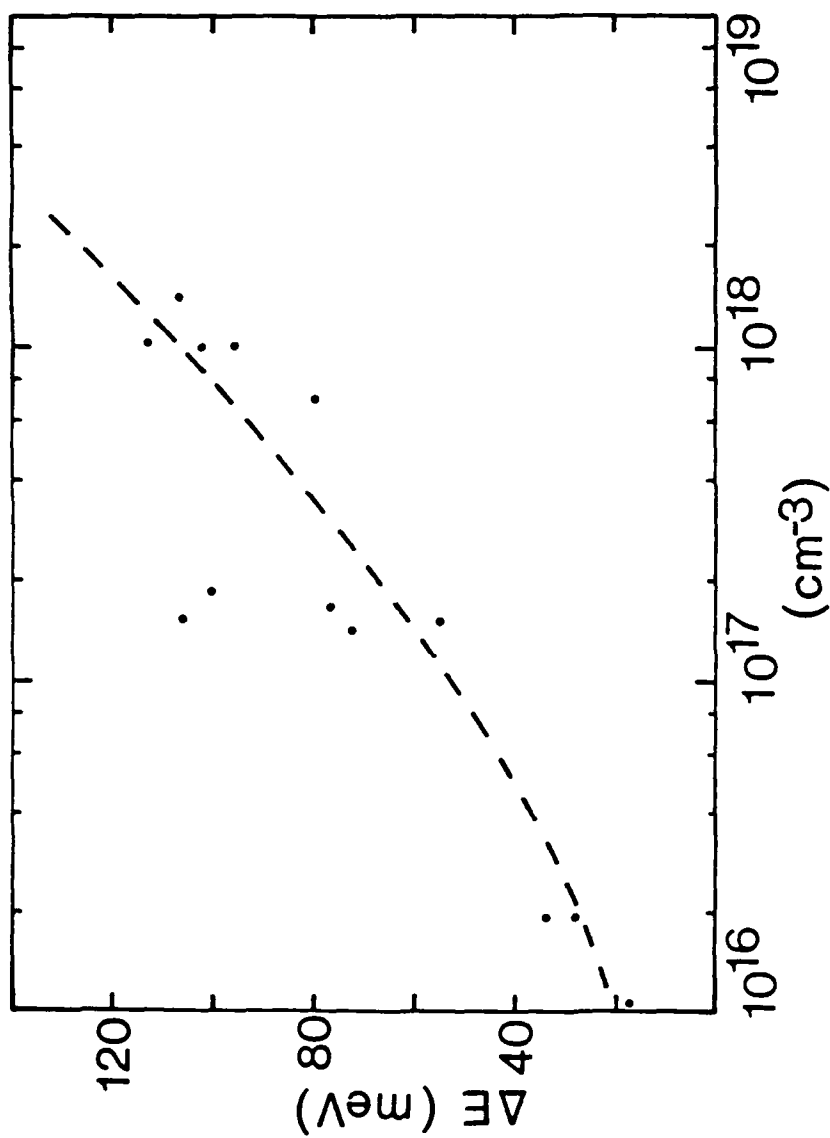


FIG. 3: Points show our data for ΔE (the difference in energy between the first two crossover points after the band-edge peak) vs. doping concentration N . The broken line shows a fit according to Eqn. (9).

1989 USAF-UES FACULTY RESEARCH PROGRAM/
GRADUATE STUDENT RESEARCH PROGRAM

Sponsored by the
AIR FORCE OFFICE OF SCIENTIFIC RESEARCH

Conducted by the
Universal Energy Systems, INC.

FINAL REPORT

SCANNING TUNNELING MICROSCOPY AND
BALLISTIC-ELECTRON-EMISSION SPECTROSCOPY

Prepared by:	Rex D. Ramsier
Academic Rank:	Graduate Student
Department and	Physics
University:	The University of Akron
Research Location:	WRDC/MLBM (Bldg. 652) Wright-Patterson AFB WPAFB, OH 45433-6533
USAF Researcher:	T. W. Haas, Ph. D.
Date:	11 Aug 89
Contract No:	F49620-88-C-0053

SCANNING TUNNELING MICROSCOPY AND
BALLISTIC-ELECTRON-EMISSION SPECTROSCOPY

by

Rex D. Ramsier

ABSTRACT

A scanning tunneling microscope from the Department of Physics at The University of Akron has been configured to image surfaces and Schottky-barrier heterostructures of electronic devices fabricated in the Materials Laboratory of Wright-Patterson AFB. Computer code has been written in Microsoft C for: a) adjusting the tip-sample distance, b) acquiring data for topographic images of surfaces, c) acquiring ballistic-electron-emission spectra, and d) data processing for image enhancement. Electronic circuits have been designed and fabricated for: a) obtaining images of metal and semiconductor surfaces at constant tunneling current, and b) measurement of collector currents from the base metal electrode into the semiconductor as a function of tip-to-base bias voltage. The latter is a high-sensitivity (gain= 10^{11} V/A), low-impedance current amplifier. Topographical images with atomic resolution of highly oriented pyrolytic graphite have been obtained.

ACKNOWLEDGEMENTS

I wish to thank the Air Force Systems Command and the Air Force Office of Scientific Research for sponsorship of this research, and Universal Energy Systems for guidance in administrative aspects of the program. In particular, I want to thank Col. Claude Cavender, Jr. of AFOSR, and Milton Danishek, Rodney Darrah, and Ross Morgan of UES for their concern and guidance.

Special appreciation is due Dr. T. Walter Haas of the Materials Laboratory Surface Studies Group at WPAFB for suggesting this particular problem and for his encouragement throughout the summer. The technical assistance and support of Larry Grazulis and Jim Hierholzer with electronics, and David Tomich with computer programming has been invaluable to the research. Help from all members of the Surface Studies Group and their willingness to provide space in a crowded laboratory is greatly appreciated.

I. INTRODUCTION

Despite decades of intensive study, a complete understanding of the electronic structure of metal-semiconductor interfaces is still lacking (Henisch 1984). Of particular interest has been the metal-semiconductor Schottky-barrier (SB) interface, because of its importance in determining electrical properties of electronic devices. SB formation is complicated by several parameters such as interface defect formation and reconstruction, electrode interdiffusion, and chemical reaction; all of which may produce structural inhomogeneities affecting the electronic properties of heterojunction structures. These inhomogeneities, and the fact we are dealing with a buried interface, compound the problem when attempting to ascertain band structure information employing conventional surface analytical techniques. When used, conventional methods yield a complicated average of SB properties if structural inhomogeneities exist in the interfacial plane.

Recently, Kaiser and Bell (1988) developed ballistic-electron-emission microscopy (BEEM), which utilizes a scanning tunneling microscope (STM) for investigation of SB systems, semiconductor heterojunctions, and other interfaces. For the first time, this technique allows investigation and imaging of the electronic structure of buried interfaces, and does so with high spatial resolution.

Figure 1 is a schematic illustration of the electron energy levels of a BEEM experiment when the tunnel tip is positioned within tunneling distance of the base metal of a S-B heterojunction. When the base electrode is no thicker than 100 Angstrom, some of the tunneling electrons travel ballistically through the metal, reaching the interfacial region with no attenuation and with little lateral divergence. With the base grounded, electrons reaching the semiconductor (collector) can be detected as a collector current which can be measured as a function of tip bias relative to the grounded electrode. The resulting collector current versus tip bias spectrum provides a direct probe of the buried interface electronic structure. From the schematic it can be seen that the collector current remains zero until the tip bias (V) is equal to the SB barrier height (V_b). Thus, the onset of collector current provides a direct measure of S-B height.

High spatial resolution is a result of being able to place the tunnel tip over the surface with great precision, and conservation of transverse momentum of the ballistic electrons upon entering the semiconductor. These effects result in a lateral resolution of 10 Angstroms for a 100 Angstrom thick base layer, and allows one to obtain spatial images of buried interfacial electronic structures while scanning the tunnel tip over the heterostructure. A simultaneous topographic image of the base electrode can be obtained for comparing geometric features of the surface with electronic features of the subsurface.

II. OBJECTIVE OF RESEARCH EFFORT

The overall objective of the SFR program was to develop facilities for BEEM investigations of SB heterojunctions. For this purpose the following equipment and materials were needed: 1) an STM for positioning and scanning the tunnel tip over the surface of the base electrode, 2) an electronic circuit for driving the STM in a constant current mode to obtain topographic images of the base electrode, 3) electronic circuitry for measuring collector currents as low as 1 pA with 0.1 pA resolution, 4) software for driving the STM, for data acquisition, and for displaying both topographic and BEEM images, and 5) techniques for tip and SB heterojunction preparation.

Prior to this project no STM facilities existed in the Materials Laboratory of Wright-Patterson AFB. After ten weeks of effort, considerable progress has been made in both instrumentation and software development. To complete the project several additional months of effort will be required at WPAFB, and hopefully will be continued under the auspices of a faculty improvement leave from The University of Akron, an AFOSR University Resident Research Program, and an AFOSR Mini Grant. The progress made thus far will be delineated in the following section.

III. ACCOMPLISHMENTS

A. SOFTWARE

Eight programs have been written for setting scanning parameters, data collection, image display, and data manipulation. All programs were written in Microsoft C.

1. "ADJUST" is used in positioning the tip within tunneling range. This program is initiated by entering the bias voltage to be used in subsequent scans. The tip-to-sample distance is then adjusted with specified bias voltage applied to tip. During adjustment, two sets of numbers are being displayed: "z-offset" which is proportional to extension of z-piezoelectric tube, and "current" which is proportional to tip-to-surface distance.
2. "SCAN" acquires x-, y-, and z-position data, allows limited data manipulation, displays a topographical image, and allows one to do voltage spectroscopy at a particular point.
3. "SCAN2" allows one to acquire data for two topographic images simultaneously; one image is obtained while the tip is scanning from left-to-right, the other while the tip is scanning in the opposite direction. A comparison of images provides information on tip quality.
4. "LINE SCAN" allows one to retrieve a stored image and obtain a plot of a particular horizontal or vertical line of the image, i.e., a particular row or column of data array.

5. "SEE" recalls and displays any topographical image which has been stored in the data files, and allows one to do data smoothing by weighting each point, its nearests and next nearest neighbors.
6. "BEEM" simultaneously acquires topographic and collector-current images and displays them sequentially. The program addresses two data files, and topographic and collector-current data are acquired at each position of the tip during a scan.
7. "BEEM2" is a routine similar to BEEM, however, in this case both images are displayed side-by-side for simultaneous visual comparison.
8. "SEEBEEM" allows one to recall and display a particular BEEM image in a manner similar to SEE.

B. ELECTRONICS

The original electronics for controlling the STM were designed to provide topographical images while maintaining constant conductance between tip and sample. With this design the STM could be used in an inelastic-electron-tunneling mode for obtaining vibrational spectra of adsorbed molecules. Such a design is not appropriate for BEEM investigations, thus two additional circuits were required which have been designed and fabricated.

1. CONSTANT CURRENT ELECTRONICS consist of a preamplifier with a feedback loop which maintains a constant current from tip to sample, a low pass filter which blocks high frequencies beyond the preamplifier, and an active bias circuit which controls the tip bias.

2. CURRENT PREAMPLIFIER consisting of an electrometer grade operational amplifier, filters, and additional amplification for collector current measurements.

Both circuits have been constructed and tested for optimal performance, and analog noise levels have been reduced by installing shielded cables and improving grounding techniques.

C. TIP PREPARATION

The quality of images obtained with an STM is directly related to the quality of the tip used in scanning the surface. Ideally, one would like a very sharp tip with tunneling always being from one particular atom. All tips used thus far have been prepared by electrochemically etching 0.01 in. diameter tungsten wire in 4 molar solution of KOH using about 30 V ac. Tungsten provides relatively good and inexpensive tips, and etching techniques and parameters are easily varied until one learns to consistently produce satisfactory tips.

D. TOPOGRAPHIC IMAGES OF HIGHLY-ORIENTED PYROLYTIC GRAPHITE

HOPG consists of planes of carbon atoms forming a hexagonal net. The planes are stacked such that every other atom around a

hexagon is located directly above (or below) an atom in adjacent planes, and the remaining atoms are located above (or below) the center of hexagons in adjacent planes. This arrangement causes the electric potential of alternate atoms around the hexagon to be different. Potentially equivalent carbon atoms in the surface plane are separated by 2.456 Angstroms and are clearly visible as the darkest regions in Figs. 2 and 3, which are STM images of HOPG obtained during this appointment. A portion of the hexagonal net is indicated in Fig. 2. The asymmetry of the hexagons is due to lack of symmetry about the cylindrical axis of the piezoelectric scanner which moves the tip across the surface. Lines connecting adjacent equivalent atoms, which are separated by 2.456 Angstrom, are drawn in Fig. 3.

IV. RECOMMENDATIONS

BEEM is a promising new technique for characterizing the electronic structure of metal/semiconductor interfaces. Results of BEEM measurements can depend sensitively on the quality of the interface between the semiconductor and deposited metal. To ensure characterization of quality SB devices, metal deposition be done in ultrahigh vacuum to keep the interface free of unwanted adsorbates, and measurements made in an inert atmosphere to prevent unwanted oxidation and contamination which may cause deterioration.

An STM specifically for BEEM investigations is being designed which includes several feature to reduce noise and sharpen band

edge and barrier height measurements. The design will includes a new tip holder assembly, a Macor body to reduce thermal effects, improved electronics for data acquisition and driving the STM, and a scanning mechanism and preamplifier which can be submerged in liquid nitrogen.

As mentioned earlier, image quality is improved by using good tips. In the future, gold tips will be used since they are less susceptible to oxidation and contamination, and will reduce electrical noise at low collector currents. Techniques for etching and preparing tips will be of major concern.

In summary, meticulous care in sample preparation, working in an atmosphere of dry nitrogen, and electronics with sensitive low-level signal detection, good filtering and minimal noise levels are necessary for BEEM measurements. These features will be incorporated in continued research.

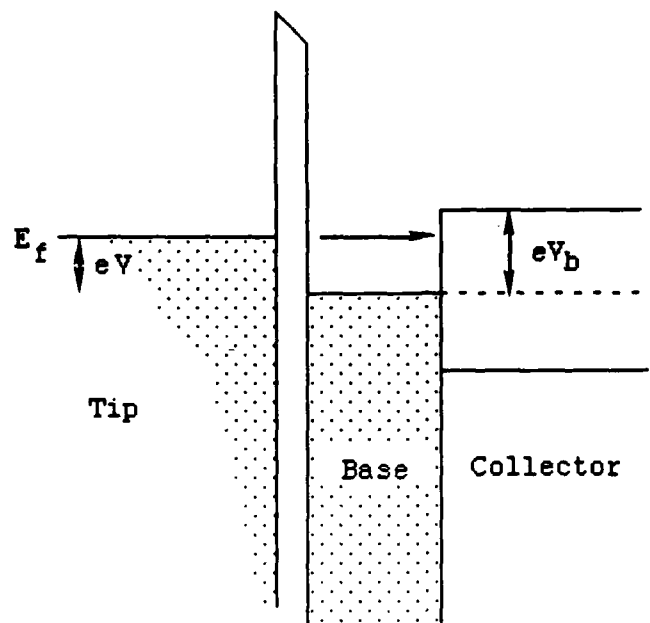


FIGURE 1

Schematic energy-band diagram for three-terminal BEEM measurement. The tip is separated by a vacuum barrier from the base metal. Ohmic contacts are made to the tip, base, and semiconductor collector. Shown is the case for tunnel bias less than the barrier voltage, $eV < eV_b$

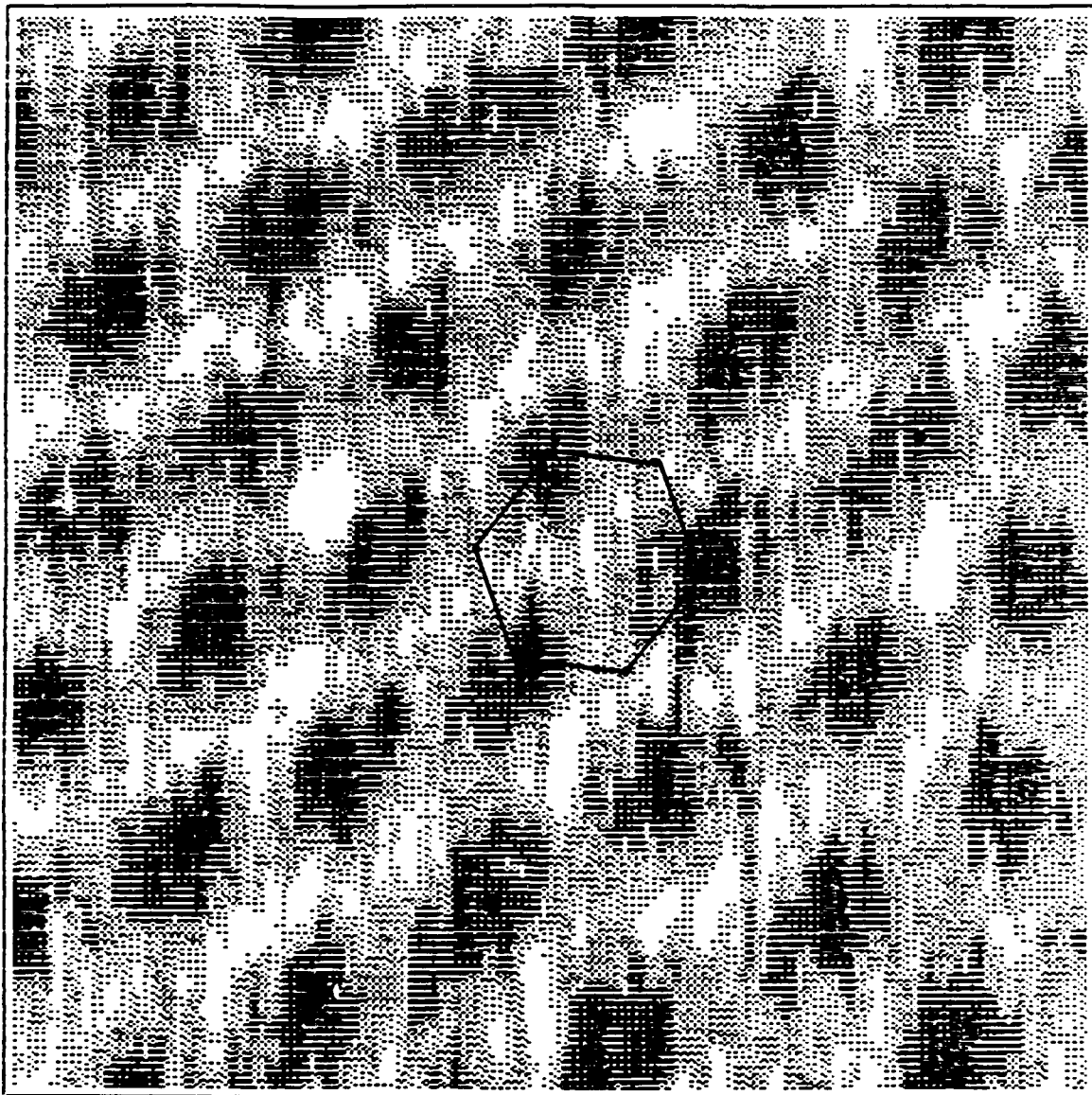


FIGURE 2

Topographical image of HOPG. Dark regions correspond to higher points and white to lower points on surface. In the hexagonal illustration, dark corners represent atoms which are directly above atoms in adjacent planes, while circles indicate atoms located above centers of hexagons in adjacent planes.

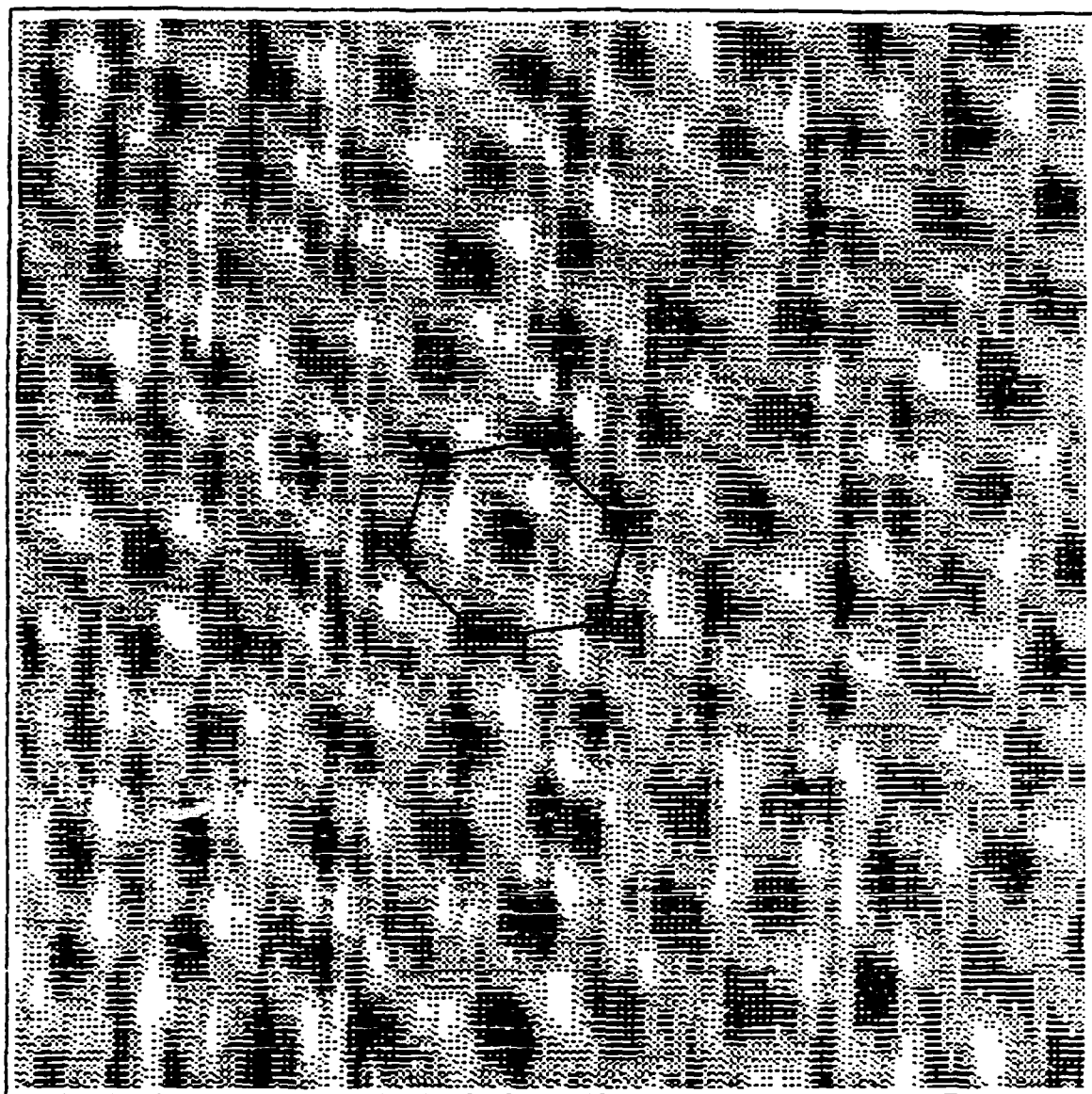


FIGURE 3

Hexagonal array formed by carbon atoms located directly above atoms in adjacent array. The nearest neighbor distance between similar atoms in an array is 2.456 Angstroms. The length of each side of the figure is about 24 Angstroms.

REFERENCES

Journal Publications:

1. W. J. Kaiser and L. D. Bell, "Direct Investigation of Subsurface Interface Electronic Structure by Ballistic-Electron-Emission Microscopy", Physical Review Letters, Vol 60, pp. 1406-1409, 4 April 1988.
2. L. D. Bell and W. J. Kaiser, "Observation of Interface Band Structure by Ballistic-Electron-Emission Microscopy", Physical Review Letters, Vol. 61, pp, 2368-2371, 14 Nov 1988.

Textbooks:

3. Henisch, Heinz K., Semiconductor Contacts: An Approach to Ideas and Models, Oxford, England, Clarendon Press, 1984.

**1989 USAF-UES SUMMER FACULTY RESEARCH PROGRAM/
GRADUATE STUDENT RESEARCH PROGRAM**

**Sponsored by the
AIR FORCE OFFICE OF SCIENTIFIC RESEARCH**

**Conducted by the
Universal Energy Systems, Inc.**

FINAL REPORT

**EVALUATION OF CR-SI ALLOYS FOR AEROSPACE
STRUCTURAL APPLICATIONS**

Prepared by:	Joseph W. Newkirk , <u>James Sago</u>
Academic Rank:	Assistant Professor , Graduate Student
Department and University:	Department of Metallurgical Engineering University of Missouri-Rolla
Research Location:	Wright Research and Development Center High Temperature Materials Branch
USAF Researcher:	Dennis M. Dimiduk
Date:	26 September 1989
Contract No.:	F49620-88-C-0053

Same Report As
Prof. Joseph Newkirk
(Report # 119)

USAF-UES SUMMER FACULTY RESEARCH PROGRAM/
GRADUATE STUDENT RESEARCH PROGRAM

Sponsored by the
AIR FORCE OFFICE OF SCIENTIFIC RESEARCH
conducted by the
Universal Energy Systems, Inc.
FINAL REPORT

An Intelligent Neural Model for Recognition of
Input/Output Patterns for a Molecular Beam Epitaxy Process

Prepared by:	George H. Tompkins
Academic Rank:	Graduate Research Assistant
Department and	Department of Industrial Engineering
University:	Kansas State University
Research Location:	Materials Laboratory WRDC/CA-M Building 653 Wright-Patterson AFB, OH 45433
USAF Researcher:	Major Steven R. LeClair, Ph.D., P.E.
Date:	02 Aug 89
Contract No:	F49620-88-C-0053

An Intelligent Neural Model for Recognition of
Input/Output Patterns for a Molecular Beam Epitaxy Process

by

George H. Tompkins

ABSTRACT

This paper discusses the problem of pattern recognition as applied to the rapid characterization of a Molecular Beam Epitaxy (MBE) process. The MBE process is a complex and difficult process to control, typically resulting in low production yields. The characterization of new materials may take months before the process can produce quality, repeatable results. This paper reviews the application of neural networks to recognize patterns within the input/output relationship of MBE process variables. The objective is the ability to self-improve process knowledge and thereby decrease the time necessary to find acceptable ranges for producing quality parts. Further research is suggested in order to incorporate the concepts of neural networks into a Qualitative Process Automation (QPA) philosophy that will make the MBE process both "self-directed" and "self-improving".

Acknowledgements

I would like to thank the Air Force Systems Command and the Air Force Office of Scientific Research for providing the financial support which has allowed me to initiate this research. I would also like to thank UES, Inc. for the administrative help which they provided throughout the summer.

I am particularly grateful to the people of the Materials Laboratory, who worked with me this summer. Major Steven LeClair provided invaluable guidance and motivation during the entire project for which I am very grateful. Captain Oliver Patterson was also extremely helpful in acting as a liaison between myself and the personnel of WUD 50. Finally, I would like to express my deepest gratitude to Dr. Ken Currie who supervised this project and provided valuable guidance and suggestions.

I. INTRODUCTION:

Molecular Beam Epitaxy (MBE) is a state of the art technique for growing thin film epitaxial layers for semiconductor devices in the microwave/digital and opto-electronic areas. Several optical and microwave devices have already found specific military applications. The MBE process is a very complex and unique process for growing epitaxial layers that conventional processes are unable to produce.

MBE utilizes advances in vacuum technology to create an implosion of a vaporous compound upon a rotating substrate at the molecular level. The result is a high degree of control of film thickness and surface morphology between layers. Another advantage of MBE is the capability of making surface and beam analyses, if not directly then indirectly, while the growth is in process. However, there are stumbling blocks to the widespread use of MBE as a production tool such as contamination and lack of precise process control, resulting in low yields. Typically, the empirical characterization of the process takes several months to produce a single, new material type that achieves the desired optical, electrical, and molecular properties.

The Materials Laboratory of the Wright Research Development Center at Wright-Patterson Air Force Base is interested in several facets of the MBE process. Research is being conducted in device type characteristics, computer modeling of the atomic interactions, control of process related variables, and an intelligent model to aid in the rapid characterization of operating parameters for new materials. The latter research area is the focus of this report.

My research interests are in the identification of trends or patterns in data that aid in the simplification of a complex task. There are several techniques for pattern recognition

including statistical, fuzzy clustering, and more recently using neural models. It is my interest in the advances of neural modeling that contributed to my selection by the Materials Laboratory for this assignment.

II. OBJECTIVES OF THE RESEARCH EFFORT:

As stated in the introduction the empirical characterization of the MBE process takes several months to produce a single, new material type that achieves the desired optical, electrical, and molecular properties. The interaction of several of the process variables along with a non-linear input/output relationship make this a non-trivial task.

My assignment as a participant in the 1989 Graduate Student Research Program (GSRP) was to develop an intelligent neural model that would aid in the rapid characterization of the MBE process for new materials. Using a neural network software package called NNET (a trademark of AIWARE) a neural network model was constructed to identify patterns and trends of input/output relationships. The model was to determine a "recipe" of initial set points for operation of the MBE machine given a set of input parameters for growing a thin layer material(s), with the desired material characteristics. Historical process information was used as a knowledge base for training the network to associate input cues to a corresponding output pattern.

Historical data was thought to have existed that would aid in the characterization of the neural model, however the data available was too limited and too difficult to obtain within the ten week period. In the absence of sufficient historical data to model the MBE process, the project objectives were changed to develop a proof of concept neural network utilizing simulated data assuming a variety of underlying causal input/output effects. The secondary

objective was to define a plan for incorporation of the neural network output to improve control of the MBE process.

III. PATTERN RECOGNITION AND NEURAL NETWORKS:

The problem of pattern recognition as applied to the MBE process is one of recognizing trends and response surfaces of multivariate input data, and predicting an estimate of an output pattern of variables. In his book on adaptive pattern recognition, Pao [1] classifies the subject into two basic methods. The first method is to classify multivariate patterns as a member of a specific class of patterns. The second method is to estimate output attribute values given a particular mapping of an input pattern.

There are several approaches available for identifying class membership using statistical models for clustering and discriminant analysis [2, 3, 4]. There are also fuzzy clustering techniques when underlying assumptions about the population are unknown or vague [5,6]. More recently the use of neural networks for pattern discrimination has shown a great deal of promise without (the conventional) limiting assumptions [7,8,9]. The free form of neural nets is particularly helpful when dealing with numeric data as is the case in the MBE process. This class of network is also referred to as an auto-associative network and uses unsupervised learning. Unsupervised learning refers to the absence of a training set of patterns in order for the network to classify a new input pattern.

When using statistical models to predict input/output causal effects, distributional assumptions about the input values are critical to the success of the model. Neural networks are capable of establishing very complex mappings from the input space to the output space such that the output space is linearly separated by hyperplanes. Distributional restrictions are not a problem in neural networks, and their ease of application is a definite

advantage over applicable statistical methods. Two particular neural network architectures have provided a measure of success in identifying attribute estimates from a given input pattern; the backward propagation net [10] and the functional link net [11] (Figure 1(a) and 1(b) respectively). Both networks use a delta learning rule, however the back propagation network has a hidden layer thus requiring the use of the generalized delta rule. The functional link requires a functional enhancement of the inputs that helps to identify the proper dimension in which to map the inputs onto the output space. The back propagation allows the hidden layer to search over all combinations of the input nodes in which to find a satisfactory dimension in which to map the input space onto the output space. By apriori inserting a functional enhancement the time necessary to train the model is significantly reduced since the functional link net is not preoccupied with finding the appropriate dimensional structure.

IV. PROOF OF CONCEPT:

Due to a lack of any actual MBE process data a series of experiments was conducted using simulated data to test the feasibility of neural networks for pattern recognition. The neural network package used to facilitate these experiments was NNET 210 a trademark of AI WARE. The reason for selecting this particular software was the availability of both functional link and back propagation networks along with an unsupervised learning (clustering) algorithm.

The data used to test the various neural networks was simulated using the same variables used to model the MBE process. The range of input values was allowed to fluctuate randomly between prescribed limits and a single output was calculated using one of the following functions to combine input variables:

1) Linear $f(x) = a * x_1 + b * x_2$

2) Polynomial $f(x) = a * x_1^2 + b * x_2^3 + c * x_3$

3) Discontinuous (Linear over half the range and Polynomial over the other half)

A typical network is shown in Figure 2 with the functional enhancements used to create a functional link network for the polynomial case. Several trials were made using various network architectures with some useful observations. It was found that the addition of a hidden layer increased the training time substantially without adding any apparent predictor value. That's not to say that a back propagation network is useless, simply that in the trials that we ran, given the circumstances the back propagation net merely inhibited training. Another valuable insight was the decomposition of the output pattern into a recursive set of networks with only a single output. The accuracy of prediction and the speed of training was significantly improved as opposed to a multivariate output pattern. The unsupervised learning network in NNET was very weak in terms of providing an easy and accurate means of clustering patterns of data. Table 1 is a summary of the key parameters of those networks which successfully trained and provided a reasonable prediction of the output variable.

The linear data set assumed all inputs to be linearly combined according to a prescribed equation to predict a single output value. Several enhancements were tested, and the network with the shortest training time and most accurate prediction of the output was a single layer network with no functional enhancements. To test the robustness of the NNET neural network a single variable that comprised approximately 5% of the variability in the output was omitted from the network. The network was still able to predict the output value to within an average of 1% error. When a pattern was tested that fell outside the range of output values within the training set, the error was only 0.325%.

The **polynomial** function was used to generate the simulated data included linear, quadratic, and cubic terms of the original input variables, but no interaction terms. More patterns were necessary to adequately predict the polynomial function. Two different functional enhancements were tried and both were extremely successful. It was observed that the more complex the pattern, the greater number of enhancements and training time is required to accurately predict the output.

The **discontinuous** data set was trained using the same type of functional enhancements as the polynomial , but required less training patterns to achieve similar prediction results. There appears to be an increase in the prediction error as values of the output variable approach the point of discontinuity, but only slightly.

V. "SELF-IMPROVING" MBE PROCESS CONTROL:

The Materials Laboratory at Wright-Patterson AFB has conducted highly successful research with "self-directed" process control of autoclave curing of composite materials. The technique used for "self-directed" control is a philosophy termed Qualitative Process Automation (QPA)[12]. QPA has resulted in time savings of over 70% in curing of composites. Central to the QPA philosophy is the creation of a knowledge base with process specific goals. In applying QPA to the MBE process the knowledge base is currently undefined. QPA requires that the knowledge about the process remain relatively static. If the process changes significantly causing changes in the rules and conditions by which goals are achieved and prevented then the knowledge base must be modified. By coupling QPA with neural networks, discovery of trends and patterns within the processing information creates a "self-improving", "self-directed" control scheme for the MBE process. The neural network will encode the knowledge of the MBE process in the network by adjusting the weights to account for the strength of the relationship between

input and output variables. As new materials are characterized or as the process parameters shift the network will be able to include the new processing information to create an improved knowledge base. In-situ "self-directed" control of the MBE process will still be carried out by QPA, however the knowledge base will be dynamically changing as new materials are characterized, and as ex-situ material properties confirm process trends and patterns.

The overall schematic of how QPA and a neural network interface will work together to self-direct and self-improve the MBE process is illustrated in Figure 3. The control is still left in the hands of the MBE operator, with suggestions from past runs and a predicted "recipe" from the neural network. The operator will input the processing knowledge about the specific run, and QPA will dynamically develop the knowledge bases to perform self-directed control.

Within the neural network interface, both types of pattern recognition methodologies, classifying pattern membership and attribute estimation, will be used in characterizing the MBE process as illustrated in Figures 4(a), (b), and (c). Figure 4(a) shows the input pattern as represented by a multivariate vector of features which are passed through a filter. The function of the filter will be to cluster or discriminate among a historical database of patterns those patterns similar to the input pattern. The resultant output of the filter is a class of patterns relatively similar to the new input pattern which is used to create a transparent mapping for pattern recognition and estimation of the feature attribute values (Figure 4(b)). By using a class of similar patterns as the training set the construction of the transparent mapping and the accuracy of the estimation of attribute values is significantly improved due to the reduced variability of the input features. The final step (Figure 4(c)) is to use the transparent mapping formed in Figure 4(b) to estimate the appropriate attribute values given a specific input pattern vector.

VI. RECOMMENDATIONS:

To utilize neural networks in intelligently characterizing the MBE process it is imperative that data be collected on any and all variables that have a significant role in mapping the input to output patterns. The minute amount of historical data available during this project, demonstrated that critical information about the process is lacking. Therefore, it is suggested that an automated data acquisition system be developed to monitor process variables throughout the run. By automating this function the critical role of the operator to monitor the process can be accomplished without interruption for recording data.

There is also a need to customize a neural network interface between the operator and the QPA Language (QPAL). Using the NNET 210 software a user interface can be created which will allow for accessing a database in which data from previous runs may be stored and accessed for knowledge acquisition.

REFERENCES

- [1] Pao, Yoh-Han, Adaptive Pattern Recognition and Neural Networks, Addison-Wesley Publishing Co., Inc., Reading, MA, 1989.
- [2] Anderberg, M. R., Cluster Analysis for Applications, Academic Press, New York, New York, 1973.
- [3] Goldstein, M. and W. R. Dillon, Discrete Discriminant Analysis, John Wiley & Sons, New York, New York, 1978.
- [4] Dillon, W. R. and M. Goldstein, Multivariate Analysis Methods and Applications, John Wiley & Sons, New York, 1984.
- [5] Kandel, A., Fuzzy Techniques in Pattern Recognition, Wiley-Interscience, New York, 1982.
- [6] Bezdek, J. C., "A Convergence Theorem for the Fuzzy ISODATA Clustering Algorithms", IEEE Transactions on Pattern Analysis and Machine Intelligence, Vol. 2, 1980, pp. 1-8.
- [7] Carpenter, G. A. and S. Grossberg, "Category Learning and Adaptive Pattern Recognition, a Neural Network Model", Proc. Third Army Conference on Applied Mathematics and Computing, ARO Report 86-1, 1985, pp. 37-56.
- [8] Kohonen, T., "Adaptive, Associative, and Self-Organization Functions in Neural Computing, Applied Optics, Vol. 26, 1987, pp. 4910-4918.

- [9] Lippman, R. P., "An Introduction to Computing With Neural Nets", IEEE ASSP Magazine, Vol. 4, 1987, pp. 4-22.

- [10] Rumelhart, D. E., G. E. Hinton, and R. J. Williams, "Learning Internal Representations by Error Propagation" in D. E. Rumelhart and J. L. McClelland (Eds.), Parallel Distributed Processing: Explorations in the Microstructures of Cognition. Vol. 1: Foundations, MIT Press, Cambridge, MA, 1986, pp. 318-362.

- [11] Pao, Yoh-Han, "Functional Link Nets: Removing Hidden Layers", AI Expert, April, 1989, pp. 60-68.

- [12] Abrams, F. L., T. L. Lagnese, S. R. LeClair, and J. B. Park, "Qualitative Process Automation for Autoclave Curing of Composites", Air Force Wright Aeronautical Laboratories Technical Report 87-4083, November, 1987.

**1988 USAF-UES SUMMER FACULTY RESEARCH PROGRAM/
GRADUATE STUDENT RESEARCH PROGRAM**

**Sponsored by the
AIR FORCE OFFICE OF SCIENTIFIC RESEARCH**

**Conducted by the
Universal Energy Systems, Inc.**

FINAL REPORT

**HIGH RESOLUTION SCANNING ELECTRON MICROSCOPY
OF PITCH-BASED CARBON FIBER**

Prepared by:	Deborah L. Uezie
Academic Rank:	Graduate Student
Department and	Dept. of Chemical, Bio, and Materials Eng.
Location:	Arizona State University, Tempe, AZ
Research Location:	AFWAL/MLBP, Wright-Patterson AFB, OH
USAF Researcher:	Dr. W. Wade Adams
Date:	30 Sept 1988
Contract No:	F49620-88-C-0053

HIGH RESOLUTION SCANNING ELECTRON MICROSCOPY
OF PITCH-BASED CARBON FIBER

by

Deborah L. Hezie

ABSTRACT

New technology has created the demand for the development of high performance polymers to replace natural or metallic materials. In particular, the Air Force is investigating new polymer materials that have high tensile strength and modulus, and are thermally stable and environmentally resistant for structural use in airplanes and spacecraft. A problem with these polymers, however, is an inherently low compressive strength.

Due to their wide range of mechanical properties, carbon fibers are being investigated as a means to gain insight into what mechanisms control compressive strength of fibers. Once these mechanisms are understood, improvements in the compressive strength of high performance polymer fibers can be made.

High resolution, low voltage scanning electron microscopy was used to determine structure-property correlations of pitch-based carbon fibers. Sheet-like structures were seen in all fibers. Lower compressive strength, higher modulus fibers had more oriented sheets, whereas higher compressive strength, lower modulus fibers showed less oriented sheets, which corresponds to wide angle x-ray diffraction studies.

Acknowledgements

I would like to thank the Air Force Systems Command and the Air Force Office of Scientific Research for sponsorship of this research. I would also like to thank Universal Energy Systems for their concern and helpfulness in all administrative and directional aspects of this program.

Many thanks go to Dr. Wade Adams of AFWAL/MLBP for his constant support, encouragement, and guidance. I would also like to thank Dr. Steve Krause of Arizona State University and Dr. David Joy of the University of Tennessee for their help with this project.

I. INTRODUCTION:

The Polymer Branch of the Materials Laboratory of the Air Force Wright Aeronautical Laboratories is investigating and developing new polymer materials that are high tensile strength, high modulus, thermally stable, and environmentally resistant for structural use in aircraft and spacecraft. A problem with these materials is, however, an inherently low compressive strength that limits their range of structural use. In order to improve the compressive strength of these polymers, some correlation between fiber structure, mechanical properties, and processing conditions must be determined. Due to their wide range of mechanical properties, the structure-property correlations of carbon fibers are being investigated as a means to gain insight into what mechanisms control compressive strength. Once these mechanisms are understood, improvements in the compressive strength of high performance polymers can hopefully be made.

My research interests are in the area of the study of the morphology and structure-property correlations of high performance polymers, particularly rigid-rod polymers. Transmission electron microscopy, scanning electron microscopy, and wide angle x-ray scattering are three techniques I am currently using to conduct my research. In this study, a series of pitch-based carbon fibers with varying processing conditions and mechanical properties was studied using high resolution, low voltage scanning electron microscopy. For each fiber the liquid nitrogen fracture surface morphology was studied to reveal the internal structure of the fibers.

II. OBJECTIVES:

The goal of this study was to provide a comparative survey of a variety of pitch-based carbon fibers to determine if there were significant differences in structural features that could be correlated to differences in mechanical properties and processing conditions. Structure-property correlations with respect to compressive strength were of particular interest. High resolution, low voltage scanning electron microscopy was used to image the internal structure of

uncoated carbon fibers. Also, comparisons of microscope performance were made between the JEOL 840 and the Hitachi S-900 scanning electron microscopes.

III. EXPERIMENTAL METHODS:

Fibers were tensile fractured in liquid nitrogen to reduce ductility. Uncoated fracture surfaces were imaged with a Hitachi S-900 scanning electron microscope at an accelerating voltage of 2.0 keV and at magnifications ranging from 10,000 X to 100,000 X. Fracture surfaces were also imaged on a JEOL 840 scanning electron microscope at an accelerating voltage of 5.0 keV and at magnifications ranging from 5,000 X to 25,000 X. Lower magnifications were used with the JEOL 840 due to the resolution limits of this microscope. All images were recorded on Polaroid P/N 55 film.

IV. RESULTS:

The fibers examined in this study are mesophase pitch-based carbon from Amoco (Union Carbide). Mesophase pitch is a liquid crystalline carbon phase of partially pyrolysed pitch that allows orientation of the carbon lamellar structure through low temperature spinning. Fibers of mesophase pitch can then be heat treated at elevated temperatures to form a three dimensional graphitic structure in the fiber.

Five types of mesophase pitch-based carbon fiber were studied; their mechanical properties are given in Table 1. Certain trends are obvious from examination of the mechanical properties and are summarized as follows:

1. Compressive strength is inversely proportional to the elastic tensile modulus.
2. Compressive strength increases as the density decreases.
3. Compressive strength decreases and elastic tensile modulus increases as heat treatment temperature increases (P-25 has the lowest heat treatment temperature and P-120 has the highest heat treatment temperature).

Table 1: Mechanical Properties of Pitch-Based Carbon Fiber

Fiber	Compressive Strength (ksi)	Tensile Modulus (Msi)	Tensile Strength (ksi)	Density (g/cc)
P-25	167	23	200	1.90
P-55	123	55	275	2.00
P-75	100	75	300	2.04
P-100	70	105	325	2.15
P-120	65	120	325	2.18

Figures 1 and 2 are high magnification fracture surface images of core and edge regions, respectively, of P-25 fiber. The fiber is round and measures 11 microns in diameter. The graphitic sheets seen in these images are very rounded and wavy. The sheets appear not only to be curved in the horizontal direction but also in the vertical direction along the fiber axis. The graphite sheets in the core region are disordered and randomly oriented, whereas the sheets in the edge region are radially oriented. There is no definite delineation between the core and edge regions, but a gradual transition between these regions. The radial region extends approximately 3 microns from the surface toward the center of the fiber. The smallest measureable sheet thickness is approximately 50 Angstroms.

Figures 3 and 4 show high magnification fracture surface images of core and edge, respectively, of P-55 carbon fiber. The fiber is round and 10 microns in diameter. The graphitic sheets are still very wavy, but there are a few kinked, angular sheets, also. The sheets appear to be more aligned along the fiber axis when compared to the P-25 fiber. As in the P-25 fiber, the sheets are randomly oriented in the core region and radially oriented in the edge region of the fiber. The smallest measureable thickness of the sheets is 50 Angstroms.

High magnification fracture surface images of core and edge regions of P-75 carbon fiber are shown in Figures 5 and 6, respectively. The fibers here are also round and 10 microns in diameter. The sheets are more angularly bent and folded around one another than in the P-55 fiber. Some of the sheets have very curled ends. The sheets are more densely packed than in the P-55 fiber and appear to be more vertically aligned along the fiber axis. Again, there is the appearance of randomly oriented core and a radially oriented edge regions. The smallest measureable sheets are 50 Angstroms.

Figure 7 is a high magnification fracture surface image of the core region of a P-100 carbon fiber. The sheets here are very densely packed and folded in and around one another. The sheets are extremely bent and angular in nature, and in some cases form almost 180 degree bends. The P-100 fiber also had a radially oriented edge region and a randomly oriented core region with a gradual transition between the two regions. The fiber is round with a 10 micron diameter, and 100 Angstrom thick sheets. Figure 8 shows a folded graphite sheet or multisheets that have been pulled out of the internal structure of the fiber. Folds in the sheet can be seen, but no measurements can be made of the dimensions of the sheet due to the angle of the image.

A high magnification, very highly tilted image of P-120 carbon fiber can be seen in Figure 9. The graphite sheets are interfolded and fractured in "steps". The observed stepped fracture corresponds to the fractures seen in the other pitch-based fibers. The brighter sheets seen in Figures 1-7 are "higher" steps and the darker sheets are "lower" steps. The width of the graphite sheets in Figure 9 could not be measured due to the high angle of tilt.

Figures 10a and 10b are images of uncoated P-25 carbon fiber taken at the same magnification. Figure 10a was taken on a Hitachi S-900 SEM and Figure 10b was taken on a JEOL 840 SEM. These images are indicative of images taken of a large number of fibers on both microscopes. The difference in these images is quite striking. Figure 10a shows much more detail and much more surface topography than

Figure 10b. The image from the JEOL 840 appears to be much flatter and does not show the void structure that the S-900 image does.

V. DISCUSSION:

To the author's knowledge, this is the first time that a pitch-based carbon fiber morphology has been so clearly visualized. The results of this research are quite an improvement over SEM studies previously done, as will be discussed later when comparing microscope performance. Several conclusions can be made about the morphology and structure-property correlations of the pitch-based carbon fiber examined in this study and are as follows:

- 1. All fibers were round, approximately 10 microns in diameter, and had a graphite sheet-like structure.**
- 2. All fibers had a disoriented core region and a radially oriented edge region.**
- 3. There was no evidence of a thin skin structure as reported by others.**
- 4. When comparing the whole series of P-25 to P-120 fiber (low to high heat treatment), the graphite sheets become more aligned with respect to the fiber axis at higher heat treatments, which corresponds to x-ray diffraction data. As the heat treatment temperature is increased, the crystallite size becomes larger, and as the graphite sheets become larger they must align more to fit into the structure.**
- 5. When comparing the whole series of P-25 to P-120 fiber, the graphite sheets become more densely packed with higher heat treatment, which also corresponds to x-ray diffraction data. The higher heat treatment fibers approach the theoretical density of graphite.**

The comparison of microscope performance can be summarized as follows:

- 1. The JEOL 840 image appeared flat with curly edged sheets. The S-900 image showed wavy sheets with voids in between the sheets.**

2. The S-900 obviously gives better resolution at lower voltages as shown by the more detailed structure in Figure 10a.
3. The difference in resolution of the microscopes is due to the actual design of the microscopes and the accelerating voltage used to obtain the optimum image. With the JEOL 840, a higher accelerating voltage (5keV) must be used to get a respectable image. In this case the electron penetration depth was greater than in the S-900, resulting in the appearance of a flatter looking image.
4. The results of the S-900 images must be interpreted with caution at this point due to the lack of understanding of the behavior of electron image formation at low voltages. At low voltages, "what you see" may not be "what you get" as with SEM imaging at higher voltages.

VI. RECOMMENDATIONS:

There appears to be a direct correlation between changes in the sheet-like structure in pitch-based fiber, fiber processing, and mechanical properties. This preliminary study has given some insight as to what those correlations might be, but more extensive studies must be done to get the complete picture. All samples in this study were imaged perpendicular to the fiber axis, but questions still remain as to what the structure looks like parallel to the fiber axis. A possible means to addressing this question would be to mount, polish, and then etch the samples parallel to the fiber axis. Transmission electron microscopy studies could also prove useful.

REFERENCES

1. Adams, W.W., and Eby, R.K., High-Performance Polymer Fibers, Materials Research Society Bulletin.
2. Joy, D.C., Low Voltage Scanning Electron Microscopy, to be published.
3. Eby, R.K., private communication.
4. Watt, W., and Perou, B.U., Strong Fibers, Elsevier Science Publishers, New York, 1985.



Figure 1: SEM micrograph of core region of P-25 carbon fiber.



Figure 2: SEM micrograph of edge region of P-25 carbon fiber.



Figure 3: SEM micrograph of core region of P-55 carbon fiber.



Figure 4: SEM micrograph of edge region of P-55 carbon fiber.



Figure 5: SEM micrograph of core region of P-75 carbon fiber.



Figure 6: SEM micrograph of edge region of P-75 carbon fiber.

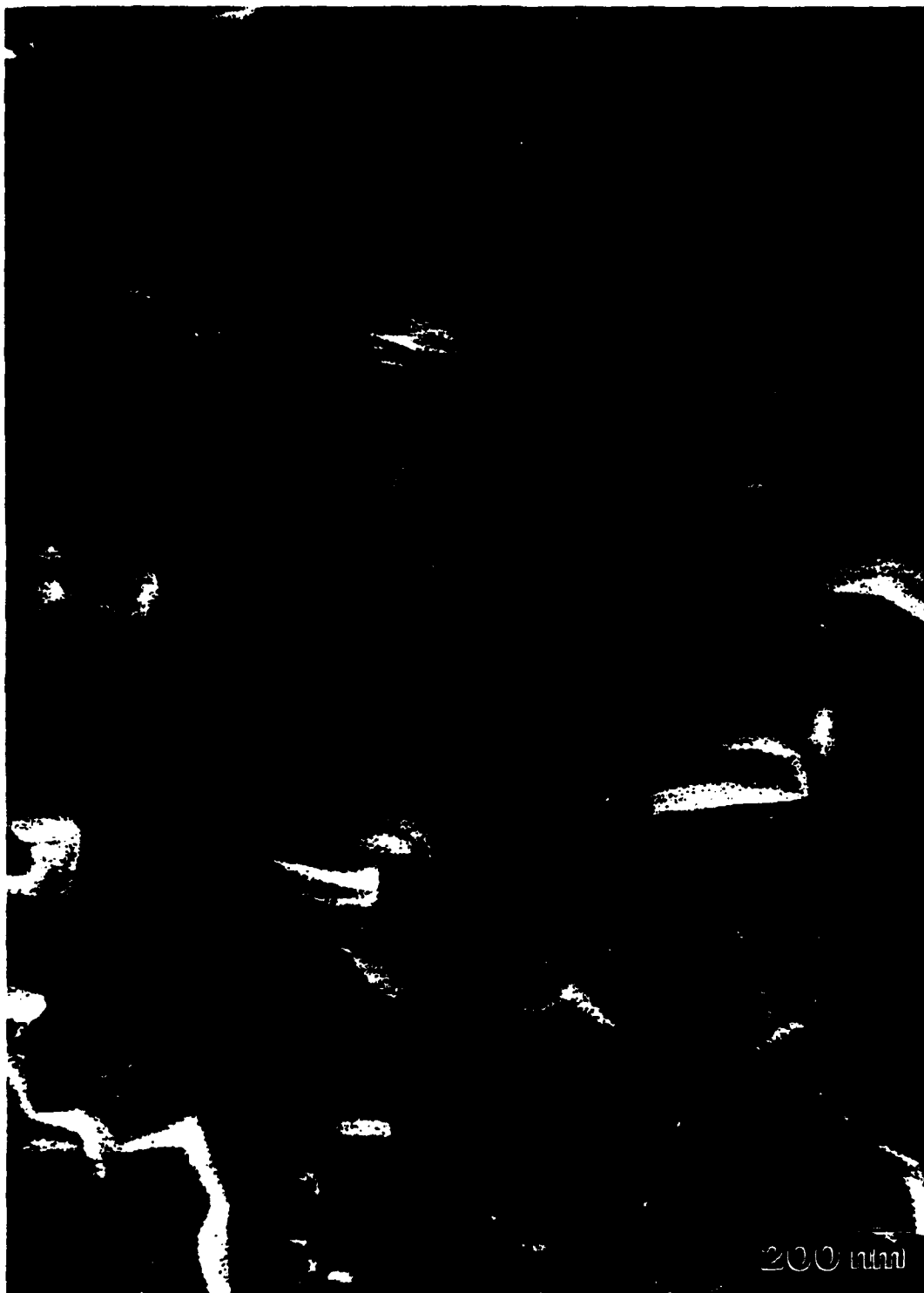


Figure 7: SEM micrograph of core region of P-100 carbon fiber.

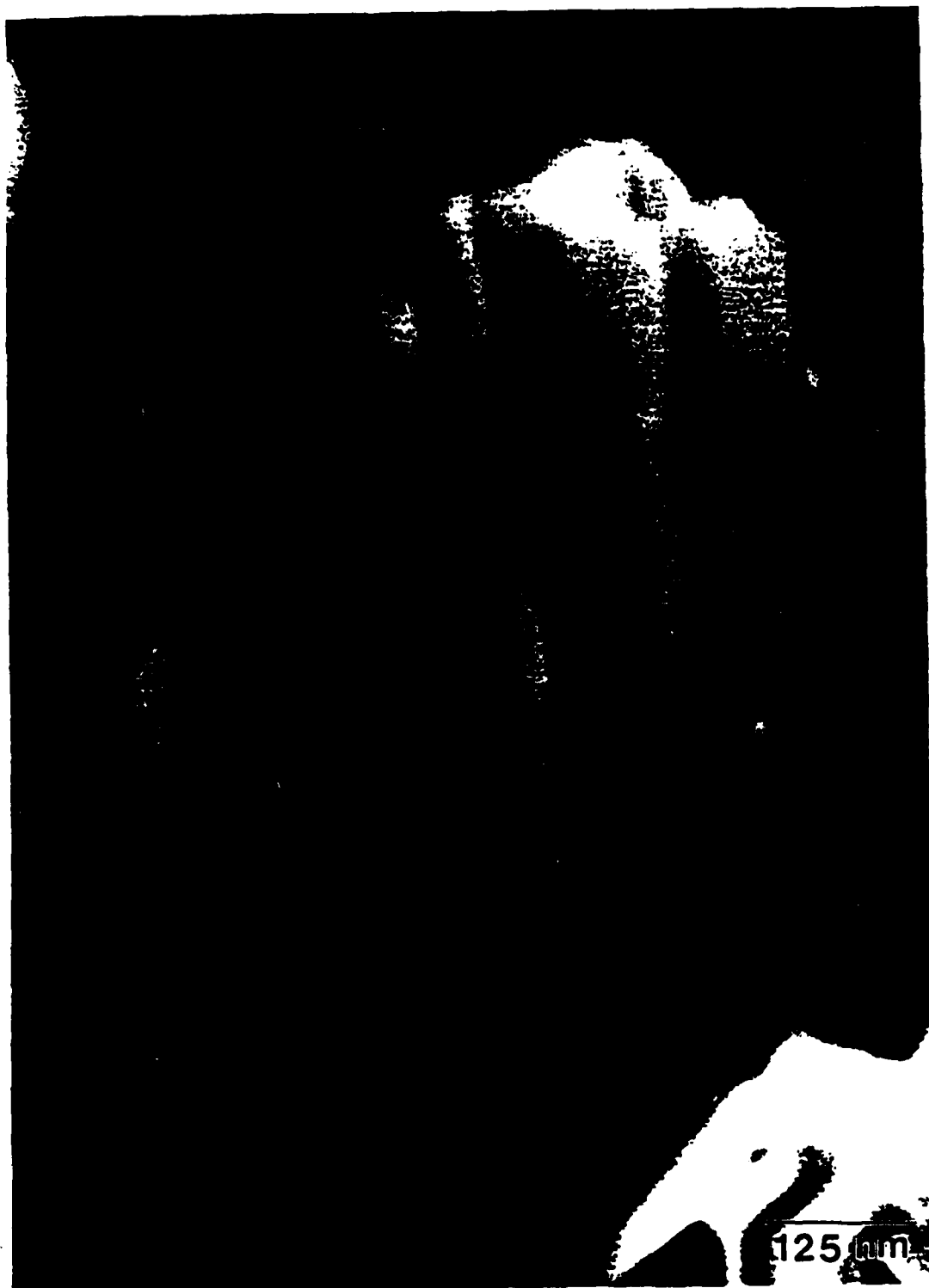


Figure 8: SEM micrograph of pulled out sheet in P-100 carbon fiber.



Figure 9: Highly tilted SEM micrograph of P-120 carbon fiber.



Figure10: SEM micrographs of P-25 carbon fiber from a) Hitachi S-900 SEM, and b) JEOL 840 SEM.